Design and Analysis of Pulse tube Refrigerator

A Thesis Submitted for Award of the Degree of

Doctor of Philosophy

Sachindra Kumar Rout

Mechanical Engineering Department
National Institute of Technology
Rourkela 769008

Dedicated to my

PARENTS

&

TEACHERS

NATIONAL INSTITUTE OF TECHNOLOGY

ROURKELA, INDIA

Ranjit Kr Sahoo
Professor
Mechanical Engg. Department
NIT Rourkela

Sunil Kr Sarangi
Director
NIT Rourkela

CERTIFICATE

Date:

This is to certify that the thesis entitled "**Design and Analysis of Pulse tube Refrigerator**", being submitted by **Sri Sachindra Kumar Rout** for the award of the degree of **Doctor of Philosophy** in Mechanical Engineering, is a record of bonafide research carried out by him at Mechanical Engineering Department, National Institute of Technology, Rourkela, under our guidance and supervision. The work incorporated in this thesis has not been, to the best of our knowledge, submitted to any other university or institute for the award of any degree or diploma.

(Ranjit Kr Sahoo) (Sunil Kr Sarangi)

Acknowledgement

The research through my Ph.D. study would not have been complete without the help and support of many individuals who deserve my appreciation and special thanks.

At First, I would like to express my deep sense of gratitude and respect to my supervisors Prof. R. K. Sahoo and Prof. S. K. Sarangi for their excellent guidance, suggestions and constructive criticism. I feel proud that I am one of their doctoral students. I will always remember their helping hands and moral support in my good and evil day during this period. I would also like to express my sincere gratitude to the Head of the Department of Mechanical Engineering Prof. S. S. Mahapatra for his timely help during the entire course of my research work.

Very special thanks to my family members for their consistent support and faith shown upon me. Their love and patience made this work possible and their encouragement immensely helped me in my work for this thesis. I am also thankful to all those who have directly or indirectly helped during my research period.

I am extremely thankful to my research colleagues Dr. Balaji Kumar Choudhury, Vutukuru Ravindra , Pankaj Kumar, Ajay kumar Gupta for their friendship during my stay at NIT Rourkela and for making the past few years more delightful.

Finally, but most importantly, I am thankful to Almighty, my Lord for giving me the will power and strength to make it this far.

(January 30, 2015) Sachindra Kumar Rout

Abstract

After decades of rapid development, the absence of moving parts in the cold head, low vibration, long lifetime and high reliability, pulse tube refrigerators are the most promising cryo-coolers. Because of these momentous advantages, they are widely used in Superconducting Quantum Interference Devices (SQUIDs), cooling of infrared sensors, low noise electronic amplifiers, missiles and military helicopters, superconducting magnets, liquefaction of gases, gamma ray spectrometers, liquefaction of gases, X-ray devices and high temperature superconductors etc. It has also got wide applications in preservation of live biological materials as well as in scientific equipment.

It is essential to accurate modelling of the pulse tube cryocooler and predicts its performance, thereby arrive at optimum design. At the current stage of worldwide research, such accurate models are not readily available in open literature. Further, the complexity of the periodic flow in the PTR makes analysis difficult. Although different models are available to simulate pulse tube cryocoolers, the models have its limitations and also range of applicability. In order to accurately predict and improve the performance of the PTR system a reasonably thorough understanding of the thermo fluid- process in the system is required. One way to understand the processes is by numerically solving the continuum governing equations based on fundamental principles, without making arbitrary simplified assumptions. The recent availability of powerful computational fluid dynamics (CFD) software that is capable of rigorously modelling of transient and multidimensional flow and heat transfer process in complex geometries provides a good opportunity for analysis of PTRs.

Performance evaluation and parametric studies of an Inertance tube pulse tube refrigerator (ITPTR) and an orifice pulse tube refrigerator (OPTR) are carried out. The integrated model consists of individual models of the components, namely, the compressor, after cooler, regenerator, cold heat exchanger, pulse tube, warm heat exchanger, inertance tube or orifice, and the reservoir.

In the first part of the study, the commercial CFD package, FLUENT is used for investigating the transport phenomenon inside the ITPTR. The local thermal equilibrium and thermal non-equilibrium of the gas and the matrix is taken into account for the modelling of porous zones and the results are compared.

The focus of the second part of the study is to establish the most important geometrical dimension and operating parameters that contribute to the performance of ITPTR and OPTR.

The numerical investigation procedure for these investigations is conducted according to the Response surface methodology (RSM) and the results are statistically evaluated using analysis of variance method. Finally a multi-objective evolutionary algorithm is used to optimize the parameters and for an optimized case the phasor diagram is discussed.

Contents

List of Figures

Page No.

List of Tables

Page No.

Nomenclature

a	Piston displacement [m]
a_0	Amplitude [m]
A_g	Free flow cross sectional area of regenerator,[m^2]
A_{rg}	Cross sectional area of regenerator,[m^2]
C_p	Specific heat at constant pressure,[J/kg-K]
C	Inertial resistance factor, [m^{-1}]
C_v	Specific heat at constant volume,[J/kg-K]
C_d,C_{di},C_1	Constants
d	Diameter, [m]
d_o	Outer diameter of screens,[m]
d_h	Hydraulic diameter of screen,[m]
d_w	Wire diameter of screen, [m]
E	Energy,[J/kg]
f	Operating frequency,[Hz]
g	Gravity acceleration, [m/s^2]
h	Local enthalpy,[W]
h	heat transfer coefficient
$\dot{H}$	Enthalpy ,[W]
I	Unit (Identity) tensor
I_m	Current
k	Thermal conductivity, [W/m-K]
K_P	Darcy permeability
l	Mesh distance,[m]
L	Length, [m]

$\dot{m}$	Mass flow rate, [kg/s]
$\dot{m}_c$	Mass flow rate at cold end section ,[kg/s]
$\dot{m}_h$	Mass flow rate at hot end section ,[kg/s]
m	Mesh size, [per inch]
n	Total number of screens used to pack the regenerator
P,p	Pressure, [N/m^2]
P_0	Average pressure, [N/m^2]
P_1	Pressure amplitude, [N/m^2]
P_d	Dynamic pressure, [N/m^2]
P_t	Pressure inside the pulse tube,[N/m^2]
P_h	High pressure, [N/m^2]
P_l	Low pressure, [N/m^2]
P_m	Mean pressure, [N/m^2]
P_{cp}	Pressure at compressor,[N/m^2]
P_r	Pressure at reservoir,[N/m^2]
q	Heat flux,[W/m^2]
$\dot{Q}$	Heat rate ,[W]
r	Radial coordinate
r_h	Hydraulic radius of the screen matrix,[m]
Re	Reynolds number
R	Ideal gas constant, [J/kg-K]
s	Pitch,[m]
t	Time,[sec]
t_s	Screen thickness,[m]
T	Temperature, [K]
T_{ac}	Temperature at after cooler,[K]

T_{cold}	Temperature at cold end heat exchanger,[K]
T_{cp}	Gas temperature at the compressor,[K]
T_h	Gas temperature at hot end heat exchanger,[K]
T_{rg}	Gas temperature at the regenerator,[K]
T_o	Temperature of the ambient,[K]
U	Internal energy,[J]
v	Physical velocity, [m/s]
V	Volume, [m^3]
$\dot{V}$	Volumetric velocity,[m^3/s]
V_s	Compressor cylinder stroke volume ,[m^3]
V_t	Pulse tube volume,[m^3]
W	Mechanical work,[W]
W_{ac}	Acuastic power, [W]
$\dot{W}$	Power,[W]
W_{comp}	Input compressor power [W]

Greek symbols

α	Permeability, [m^2]
β	Opening area ratio of screen
γ	Ratio of specific heat
μ	dynamic viscosity, [kg/m-s]
ν	kinematic viscosity, [m^2/S]
ρ	Density, [kg/m^3]
λ	ratio of specific heats [dimensionless]
ω	Angular frequency, [rad/s]
θ	phase between pressure and mass flow

υ	Specific volume,[m^3/kg]
ϕ	Porosity
φ	Generic variable
σ	Area density,[m^{-1}]
τ	Stress tensor
ς	Period of the cycle,[sec]
ψ	Diffusion flux
ξ	Capacitance
∇	Gradient operator
∇p	Pressure drop
Γ	Exchange coefficient
E	Compliance
Ω	Resistance
Z	Impedance
L	Inductance
$\rightarrow$	Vector Form
$\langle\ \rangle$	Cycle average quantity
$\oint$	Cyclic integral

Subscripts

amp	Amplitude of piston displacement
ac	After cooler
avg	Average value
chx	Cold end heat exchanger
c	Cold end
comp	Compressor

eff	Effective
f	Fluid
h	Hot end
j	Summation
loss	Losses
o	Orifice
p	Constant pressure
pt	Pulse Tube
pv	PV work
r	Radial direction
reg	Regenerator
refrig	Refrigeration
reject	Rejection
s	Solid
x	Axial direction

Abbreviations

AFTC	After cooler
ANOVA	Analysis of variance
BPTR	Basic pulse tube refrigerator
CHX	Cold end heat exchanger
CV	Control volume
COMP	Compressor
COP	Coefficient of performance
DC	Direct flow
DF	Degrees of freedom
DIPTR	Double inlet pulse tube refrigerator

DOE	Design of experiment
GM	Gifford Mc-Mahon
HHX	Hot end heat exchanger
HP	High pressure
ITPTR	Inertance tube pulse tube refrigerator
LP	Low pressure
OPTR	Orifice pulse tube refrigerator
PT	Pulse tube
PTR	Pulse tube refrigerator
REG	Regenerator

Chapter 1

INTRODUCTION

1.1 Cryogenic refrigeration

The precise meaning of "cryogenics" is production of icy cold or low temperature. It comes from two Greek words, "kyros" (meaning icy cold or freezing) and "gen" (meaning to produce). Cryogenics is the branch of science which deals with the study of phenomena occurring below a temperature of 123 K (-150°C) and incorporates numerous areas like production of low temperatures, and behaviour and properties of materials at very low temperatures. In particular, this includes refrigeration, liquefaction, storage and transport of cryogenic fluids, cryostat design and the study of phenomena that occur at these temperatures.

Cryogenic refrigerators or cryocoolers are the devices which generate cryogenic temperatures. All cryocoolers mainly operate with a working cycle. Cryocoolers with minimum number of moving parts are being studied extensively because they have many advantages over the existing cryocoolers based on the mechanisms like piston-displacer or a conventional piston-cylinder. The advantages are reliability, low cost, low mechanical vibrations, low magnetic interference and long life. Such coolers are greatly preferred in the industry, due to the scope for compactness. Within the last few years, there have been impressive developments in cryocoolers, especially in the field of pulse tube refrigerators (PTRs). The PTR has become one of the most important cryocoolers and its efficiency is being raised towards that of the Stirling cooler. Multistage PTR units are also developed by adding extra modules to the first stage. Both single and multistage pulse tube cryocoolers are used in military applications for cooling infrared detectors, thermal imaging circuits, night vision cameras, etc. In the medical field, the cryocoolers are used in cryobiology and cryo-surgery.

1.2 Classification of cryocooler

The cryocooler are categorized into many types from different approaches. From the viewpoint of operating gas flow pattern Matsubara [1] classified cryocoolers into two different groups: Circulating flow cryocooler and Oscillating flow cryocooler as illustrated in Figure 1.1.

Circulating flow cryocooler

The Circulating flow cryocoolers are composed of a turbo expander or a low temperature valved reciprocating expander with counter flow heat exchanger. In this type of cryocoolers, the function of each component, such as a compressor, a counter flow heat exchanger, an expander or a JT valve are rather independent of each other. Joule-Thomson cryocooler and Brayton cryocooler is based on circulating flow.

Oscillating flow cryocooler

The oscillating flow cryocooler consists of the valve less expander and a regenerator. So it is compact in size and has a wide range of application. The function of regenerator for oscillating flow type cryocoolers has a strong dependency on other components. Stirling, GM, Solvay and Vuillemier cycle and pulse tube cryocoolers are based on Oscillating flow.

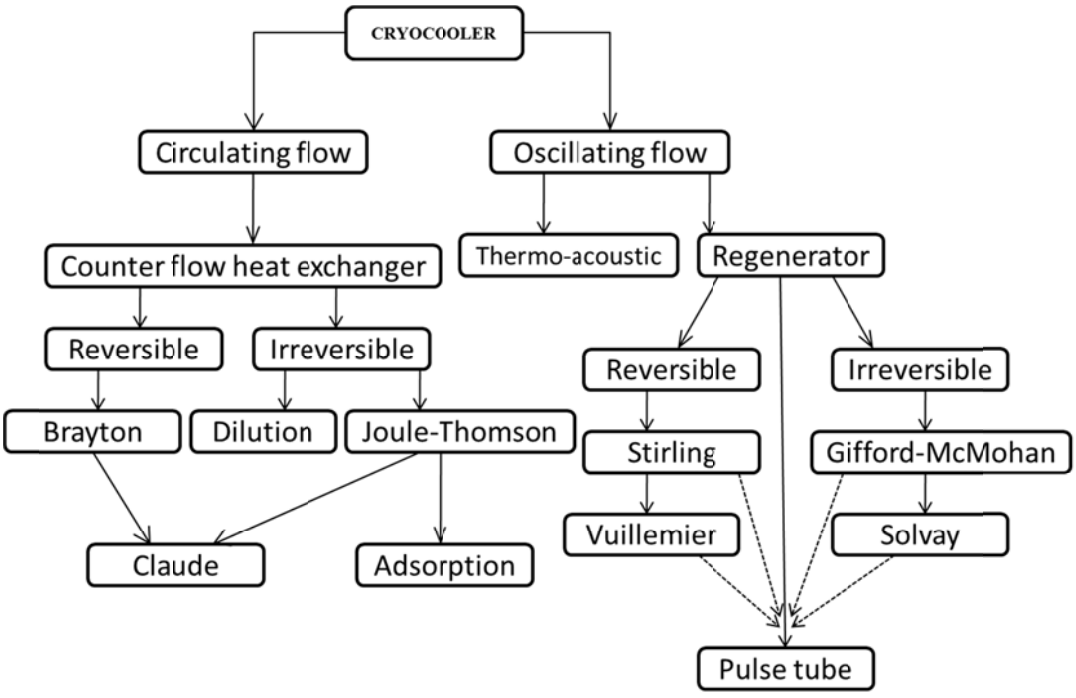

Figure 1.1 Classification of cryocoolers.

Depending on the working cycle, Radebaugh [2] classified the crycoolers into two groups: open cycle and closed cycle cryocoolers.

Open cycle

The gaseous medium undergoes various cooling processes and is finally liquefied. Makeup gas is supplied in a quantity that balances the liquefaction rate. This type of cryocoolers includes those working on boiling of cryogens or Joule-Thomson expansion of highly pressurized gases.

Closed cycle

The cryocoolers can be described as a closed system with the working gas undergoing cyclic processes, with no inflow or outflow to the medium across the system. Cryocoolers operating on closed cycles include Solvay, Gifford-McMahon, Vuilleumier, etc.

On the basis of use of regenerative or recuperative heat exchangers, cryocoolers are classified by Radebaugh [2] into two types: recuperative type crycoolers (Figure 1.2) and regenerative type Cryocoolers (Figure 1.3). In recuperative heat exchangers, the hot and cold fluids are separated by a continuous wall, across which heat transfer occurs. In regenerative heat exchangers, the same flow passage is alternately working by hot and cold fluids. Figure 1.4 shows the schematics of both types of heat exchangers. Regenerators are used as devices for thermal energy storage and release. The processes of storage and release occur during different phases in a cycle, the thermal inertia being provided by an intermediate porous matrix inside the regenerator. For the regenerator matrix, it is desirable to have a large thermal storage capacity, larger contact surface (or heat transfer) area and minimal hydraulic resistance for lower pressure drop. The regenerator temperature profile at any point is a function of space and time. The regenerator attains a periodic state of operation if the temperature at any point in the system remains same after successive cycles of operations.

1.3 Pulse Tube Refrigerator

The most important feature of the pulse tube cryocooler over other types of cryocoolers is the absence of moving parts in the cold end. This advantage of pulse tube cryocooler makes it long life, low vibration, highly reliable, simple and efficient. The concept of pulse tube cryocooler was proposed by Gifford and Longsworth [3] of Syracuse University in 1963. This device consists of a hollow cylindrical tube with one end closed and the other end open. Both ends are connected with heat exchanger. The open end is subjected to an oscillating pressure through a regenerator, causing the

open end to cool while the closed end is exposed to an ambient temperature heat exchanger. This device latter named as the basic pulse tube refrigerator (BPTR) is shown in Figure 1.5. The working principle of BPTR is based on surface heat pumping [4], which is caused by heat exchange between the working fluid and the pulse-tube walls.

The BPTR can produce a minimum temperature of 124 K using single stage and can reach up to 79 K using multi stage. There are several drawbacks associated with BPTR. The phase difference between the mass flow rate and pressure wave is the major one. There is a phase difference of 90^0 between the pressure and the mass flow rate in a BPTR. This can be explained as follows, when the mass flow rate becomes the maximum, the pressure becomes minimum at the hot end of the pulse tube.

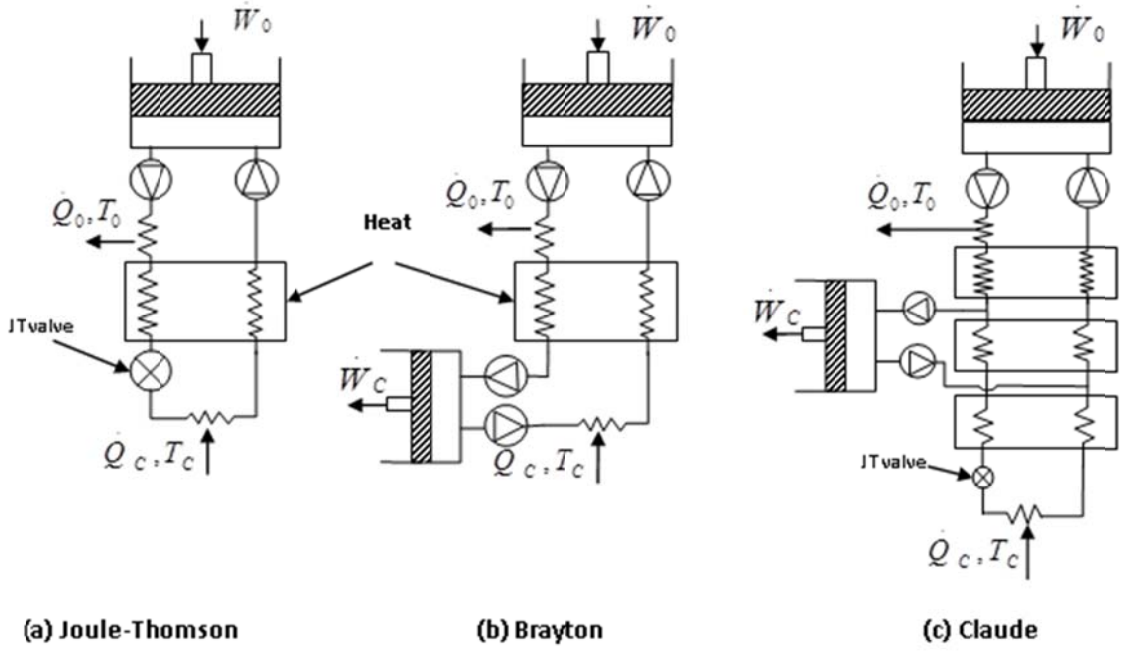

Figure 1.2 Recuperative type Cryocoolers

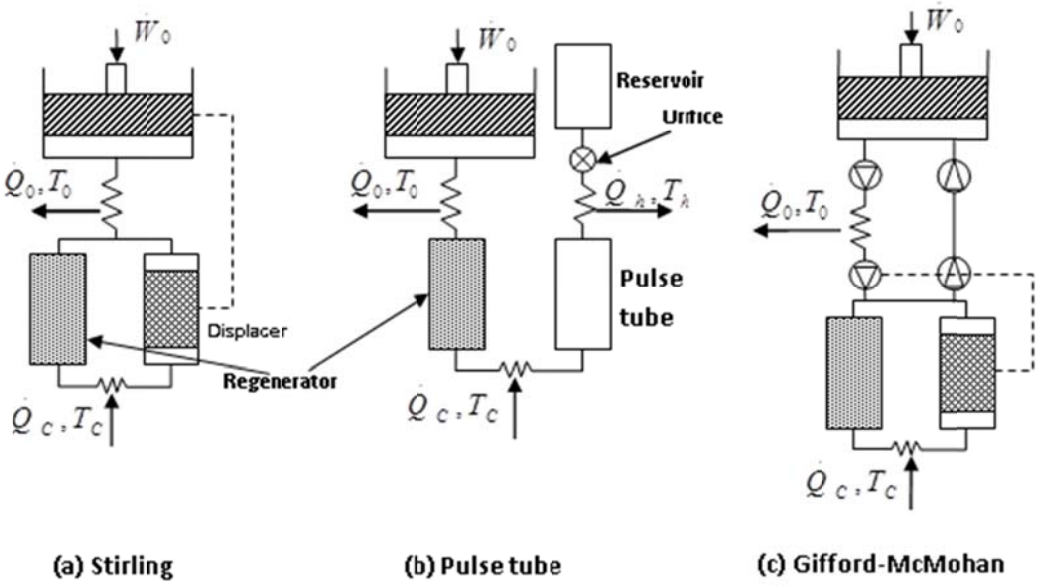

Figure 1.3 Regenerative type Cryocoolers

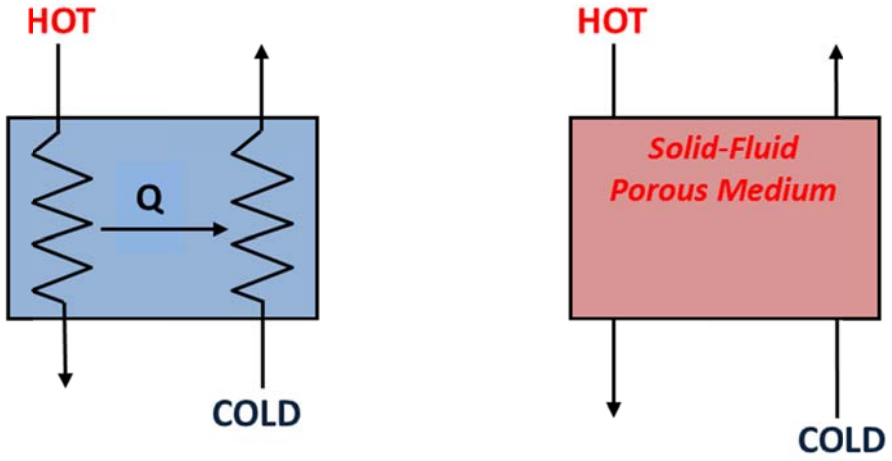

Figure 1.4 Schematic diagram of recuperative (left) and regenerative (right) heat exchangers.

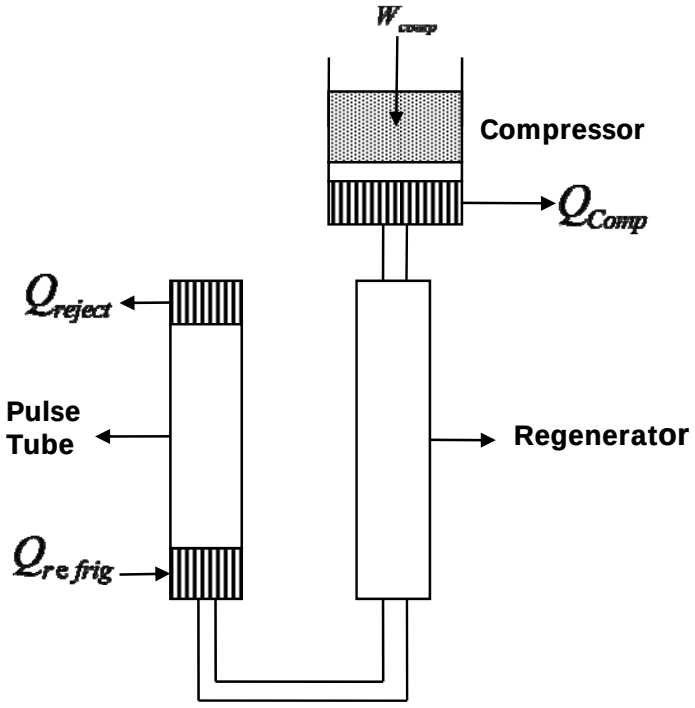

Figure 1.5 Schematic diagram of basic pulse tube refrigerator

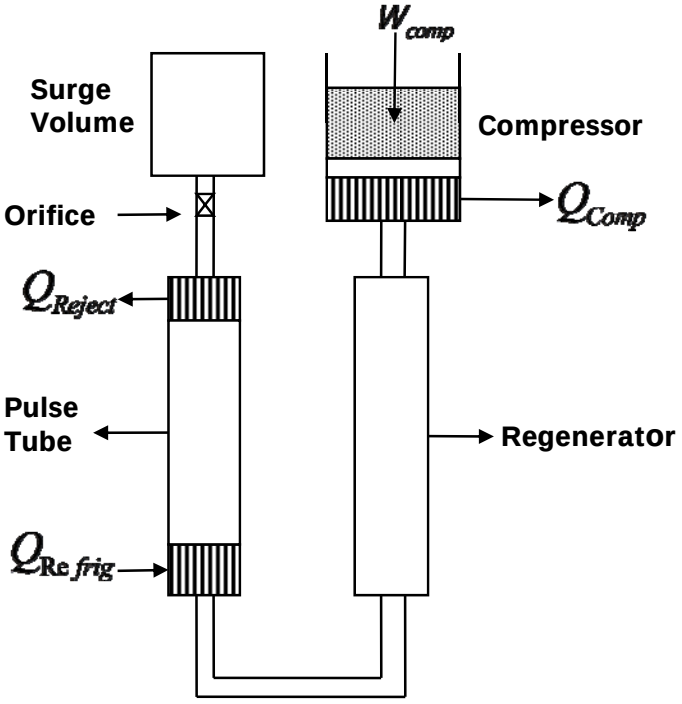

Figure 1.6 Schematic diagram of orifice pulse tube refrigerator

To reduce this phase difference between the pressure and the mass flow rate to a value below 90^{o}, it needs an orifice valve and a reservoir after the hot end of pulse tube. This innovative concept was proposed by a Russian researcher Mikulin et. al. [5] in 1984. He added an orifice valve and a buffer volume after the hot end of pulse tube of the BPTR and named it Orifice Pulse Tube Refrigerator (OPTR) as shown in Figure 1.6. This device produced a better favorable phase difference than BPTR, subsequently a much lower temperature and higher COP was achieved. A lower temperature of 60 K in single stage and 20 K in multi stage was achieved using OPTR. There also few limitations associated with OPTR. The major one is the mass flow rate always lead the pressure in the limiting case, the mass flow rate and pressure wave may be in phase with one another. This limitation does not allow the optimal phase to be achieved in which the pressure would lead the mass flow rate at the inlet to the expansion space. One more major limitation is that the large volume of gas without cooling effect flows through the regenerator into pulse tube. This was well discussed by Zhu et al. [6] and also suggested that this unwanted mass flow at the hot end of the pulse tube is very small compared to that at the cold end, so the gas at the hot end does almost the maximum work and the mass at the cold end does not do the maximum work which was contrary to the desired set-up. To solve this problem a bypass was connected from hot end of pulse tube to inlet of regenerator and it was able to increase the refrigeration power per unit mass flow rate through the regenerator. This type of pulse tube refrigerator was named as double inlet pulse tube refrigerator (DIPTR) as shown in Figure 1.7. A lower temperature of 41 K was achieved using the DIPTR model compared to the OPTR model and also the rate of temperature drop in the DIPTR model is higher than that of OPTR.

There found a slow oscillation of the cold end temperature by several minutes in a DIPTR. This temperature instability at the cold end was due to circulating gas flow through the regenerator and pulse tube, the so-called DC gas flow.

The orifice valve of the OPTR was replaced by a long thin tube called the inertance tube by Kanao et al. [7], shown in Figure 1.8. An inertance tube is simply a long and narrow tube that imposes a hydraulic resistance and causes a basically adjustable delay between the pressure responses of the pulse tube and the reservoir. By employing an electrical analogy, Roach and Kashani [8], and Iwase et al. [9] have described the inductance added by the inertance tube allows for an improved power transfer in the pulse tube.

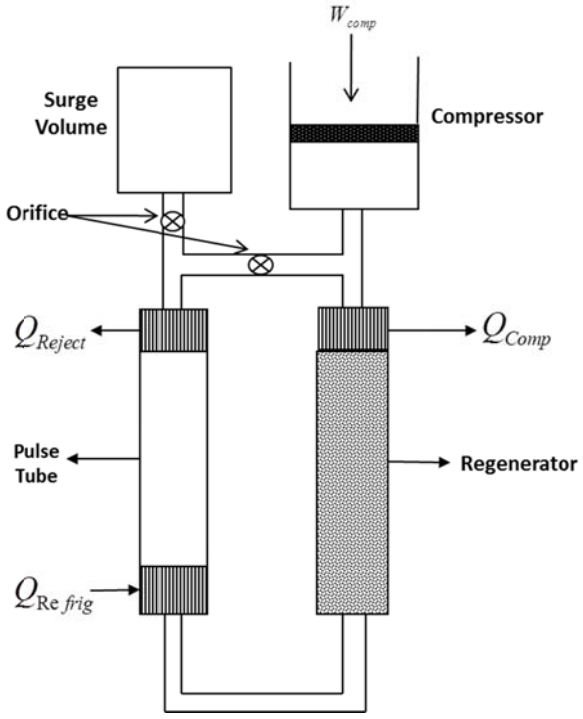

Figure 1.7 Schematic diagram of double inlet pulse tube refrigerator

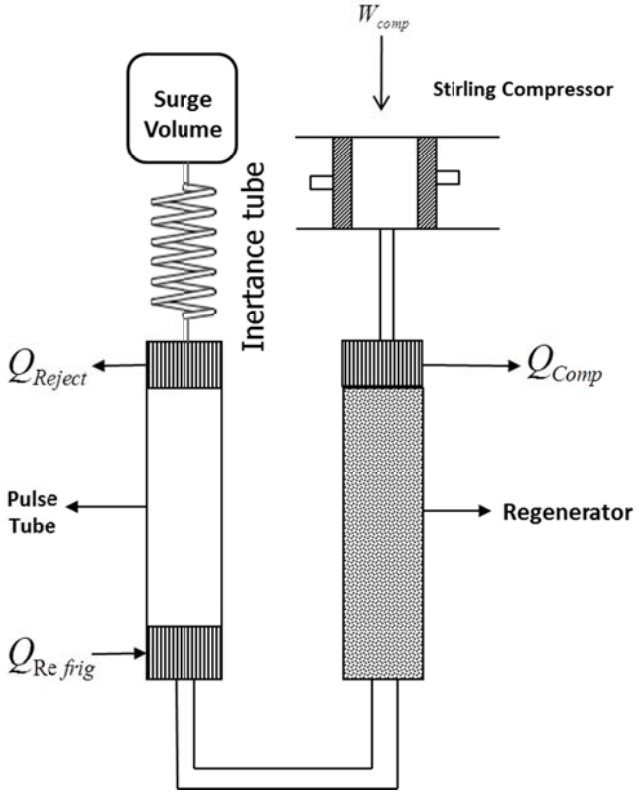

Figure 1.8 Schematic diagram of the inertance tube pulse tube refrigerator

Analogous to inductance in an electrical circuit, the inertance tube offers reactive impedance that allows the phase relationship between the pressure and mass flow to be widely adjusted. This flexibility offers the potential to maximize the pressure and mass flow phase relationship and achieve a higher cooling efficiency.

1.4 Classification of Pulse Tube Refrigerator

Pulse tube refrigerators can be categorized from many approaches. On the basis of pressure wave generation, pulse tube refrigerators are classified into two broad groups; Stirling type or GM type. The Stirling type pulse tube refrigerator as shown in Figure 1.9 (a), consists of a piston cylinder apparatus is directly coupled to the hot end of the regenerator so that the pressure oscillation can directly generated by the piston movement. There is no valve in this type of refrigerator. It operates at high frequency.

The G-M type pulse tube refrigerator distributes pressure oscillation by the use of a rotary valve that switches between high and low pressure sources into the pulse tube and other components as shown in Figure 1.9 (b). Generally a rotary valve or solenoid valve is used in G-M type cryocooler. It operates at low frequency.

- *Based on nature of pressure wave generator:*

i. Stirling type PTR (valve less)
ii. Gifford McMahon type PTR (with valve)

- *On the way of development:*

i. Basic pulse tube refrigerator (BPTR)
ii. Orifice pulse tube refrigerator (OPTR)
iii. Double inlet pulse tube refrigerator (DIPTR)
iv. Inertance type pulse tube refrigerator (IPTR)
v. Multiple inlet pulse tube refrigerator
vi. Multi stage pulse tube refrigerator
vii. Thermoacoustic pulse tube refrigerator
viii. Active buffer pulse tube refrigerator

- *According to geometry or shape:*

i. In-line type pulse tube refrigerator
ii. U type pulse tube refrigerator
iii. Coaxial type pulse tube refrigerator
iv. Annular pulse tube refrigerator

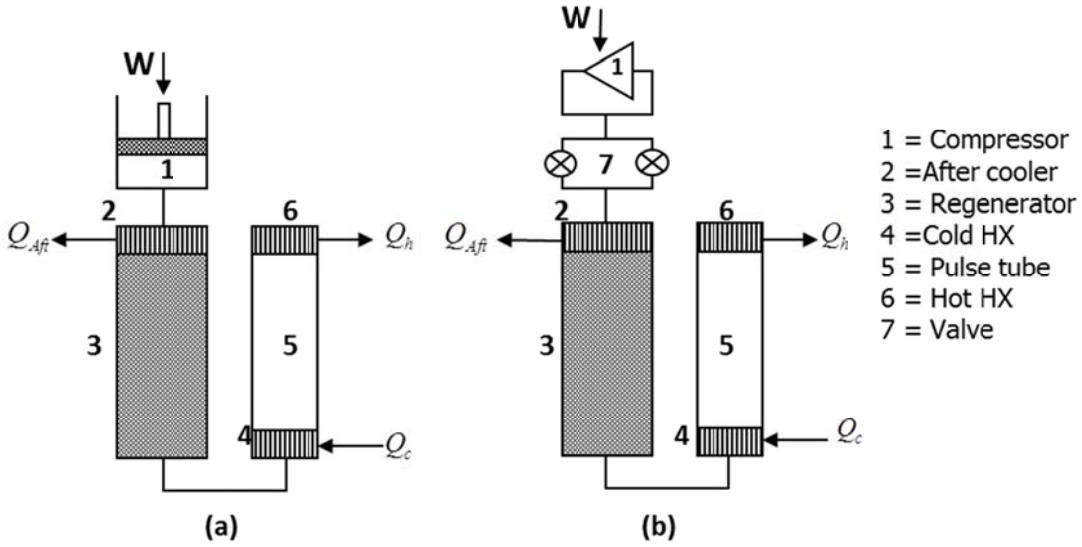

Figure 1.9 Schematics of basic pulse tube refrigerator (a) Stirling type (b) G-M type.

Pulse tube refrigerators may also be classified according to the way of development as follows:

1.4.1 Basic Pulse Tube Refrigerator (BPTR)

Figure 1.5 shows the main components of Stirling type BPTR. It is composed of six components: compressor, after cooler, regenerator, cold heat exchanger, pulse tube and warm heat exchanger. The advantage of BPTR is its simplicity, ease of fabrication and reduced vibration at the cold end. The phase angle between the mass flow rate and temperature is an important factor determining the overall performance.

1.4.2 Orifice Pulse Tube Refrigerator

Figure 1.6 shows the main components of orifice pulse tube refrigerator (OPTR). The schematic configuration of an OPTR can be viewed as the addition of an orifice and a reservoir in series at the hot end heat exchanger of a BPTR. The reservoir volume is added such that the mass flow into and out of the reservoir have no effect on the pressure. Radebaugh [10] theoretically explained the phenomenon of energy transfer in an OPTR with the help of phase relations between mass flow rate and temperature.

1.4.3 Double Inlet Pulse Tube Refrigerator

Figure 1.7 shows the main components of Stirling type DIPTR. In a DIPTR, hot end of the pulse tube is connected with the entrance (hot end) of the regenerator by a

secondary orifice adjusted to an optimal value. The secondary orifice allows a small fraction (about 10%) of the gas to pass directly between the compressor and the warm end of the pulse tube, thereby bypassing the regenerator. This bypass flow is used to compress and expand the portion of the gas at the warm end of the pulse tube that always remains at warm temperature. The bypass flow reduces the flow through the regenerator, thereby reducing the regenerator loss.

1.4.4 Inertance Tube pulse tube Refrigerator

Lastly invented PTR is the inertance tube pulse tube refrigerator (ITPTR) as shown in Figure 1.8. In this type of PTR, the orifice valve is replaced by a long, thin inertance tube having a very small internal diameter and adds reactive impedance to the system. The implementation of the inductance phenomenon generates an advantageous phase shift in pulse tube and produces an improved enthalpy flow. Studies show that use of the inertance tube is significantly beneficial for large-scale pulse tubes operating at higher frequencies.

On the way of geometrical shape and arrangement of components of pulse tube refrigerators are classified into three types. They are linear type PTR; U type PTR and coaxial type PTR. The details about these three major single stage PTRs configurations are discussed below.

1.4.5 Linear type PTR

In a linear type or inline configuration PTR as shown in Figure 1.10 (a), all the components starting from the regenerator to the reservoir are placed in a straight line. Since the absence of curve path flow losses is minimum in this type of configuration, hence this type of PTR is often preferred where high performance is required. The limitation associated with this configuration is that the cold end is situated in the middle of the assembly, which makes it difficult to access, and also it requires more space. The best arrangement for mounting the PTR in the vacuum chamber is with the hot end of the tube, where heat is released to the environment.

1.4.6 U-shape type PTR

The U-type configuration of PTR is compact in size and allows easy access to the cold end of the PTR. U-type configuration PTR, shown in Figure 1.10 (b) is made by bending the PTR at the cold end of the regenerator and the pulse tube. Both hot ends

can be mounted on the flange of the vacuum chamber at room temperature. Due to the U-bend at regenerator end the performance of the U-type configuration PTR decreases as compared to inline configuration.

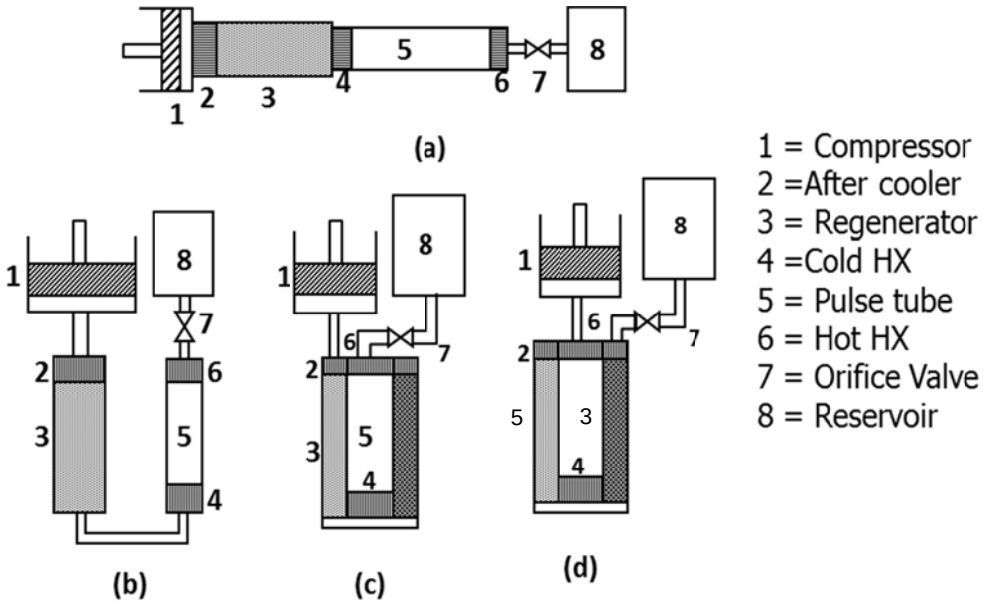

Figure 1.10 Schematic diagram of pulse tube geometry (a) Linear, (b) U-type, (c) Coaxial (d) annular

1.4.7 Coaxial type PTR

Coaxial pulse tube refrigerators are very compact in size. PTR can be constructed in a coaxial way so that the regenerator becomes a ring shape space surrounding the pulse tube as shown in Figure 1.10 (c). This leads to the degradation of regenerator performance. The major limitation of the coaxial arrangement is the presence of large heat transfer between the pulse tube and the regenerator. Generally the temperatures of the two components may differ. In order to overcome this difficulty, a thin layer of insulation material is used between the regenerator and the pulse tube, although this increases the overall outer diameter of the refrigerator.

1.4.8 Annular PTR

In annular type PTR, the regenerator is kept inside the pulse tube whereas, the pulse tube is placed inside the regenerator in a coaxial PTR. The pulse tube wall and

regenerator walls are separated by providing a thermal insulation between them. Figure 1.10 (d) shows the all components of an annular PTR.

1.4.9 Four valve and five valve PTR

In four valve pulse tube refrigerator there is no reservoir at the hot end. The low pressure and high pressure from the compressor by valves are directly connected to the hot end, which are opened and closed by a timing mechanism and adjusted for optimum performance. Figure 1.11 (a) shows the schematic diagram of the four valve pulse tube refrigerator. The opening and closing times of the orifice at the hot end of the tube are synchronized with the pressure wave in the tube and adjusted for optimum performance of the system. In five valve pulse tube refrigerator (Figure 1.11 (b)) there is a reservoir added at the hot end through an extra valve in a four valve PTR. These types PTR can be able to diminish the DC flow. The five valve pulse tube refrigerator can produce higher cooling power than other single stage G-M configuration. But the limitation associated with the valves life period and, it also very complex in configuration and operation.

1.4.10 Active Buffer PTR

The Figure 1.12 (Zhu et al. [11]) shows the schematic diagram of the active buffer pulse tube refrigerator (ABPTR) with 'n' numbers of buffers. It is generally used to increases the efficiency. Two or more buffers are connected, to decrease the loss through the high pressure valve and the low pressure valve at the warm end of the pulse tube through on/off valves. The ABPTR contains a regenerator, a pulse tube, a low pressure valve, a high pressure valve, on/off valves and buffers. The high pressure valve and the low pressure valve are connected to the high pressure side and the low pressure side of the compressor simultaneously. In the Figure 1.12 the heater at cold end is used for heat load measurments. The cooler at hot end refers to water cooling measurements.

The gas in the buffers lets the pressure in the pulse tube increase to near the high pressure before the high pressure valve is opened. After the high pressure valve is closed, the gas in the pulse tube expands adiabatically to near the low pressure. Then the low pressure valve is opened. So the irreversible loss through the high pressure valve and the low pressure valve decreases significantly compared to previous pulse tube refrigerators.

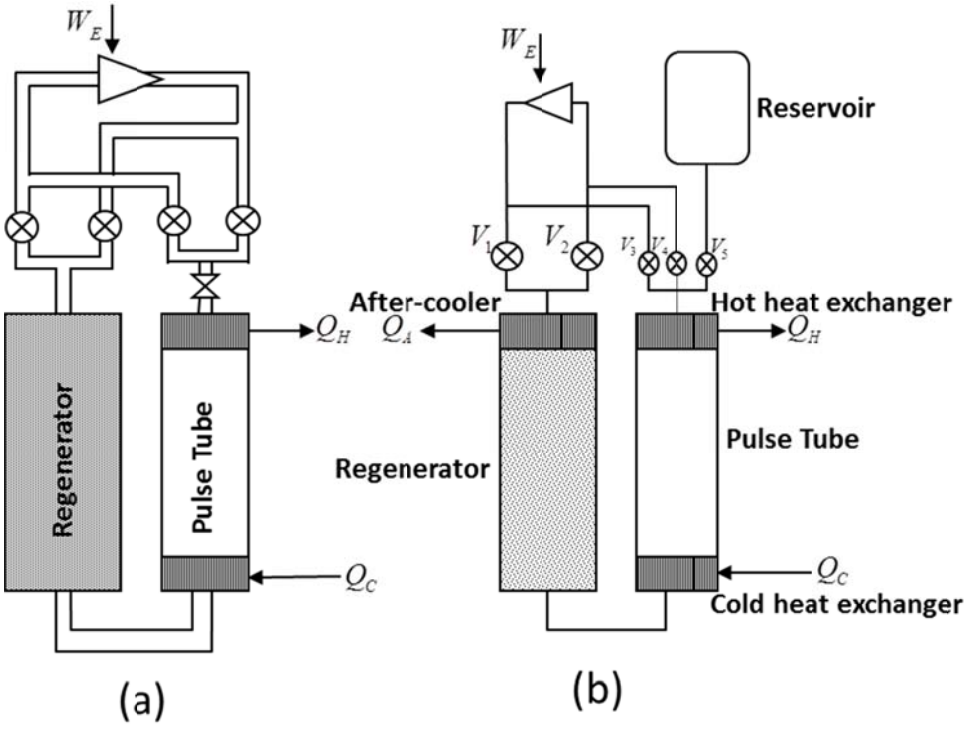

Figure 1.11 Schematic diagram of single stage, (a) four valve (b) five valve pulse tube refrigerator

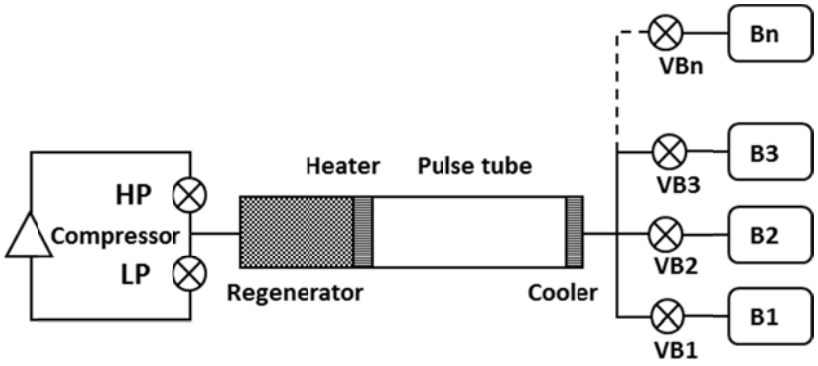

Figure 1.12 Schematic diagram of the Active-buffer PTR [11]

1.4.11 Multiple-inlet type PTR

In this type of PTR a bypass tube and an orifice connect the middle of the regenerator and the pulse tube as shown in Figure 1.13. The mass flow from or to the pulse tube owing to the pressure drop in the regenerator controlled by the orifice. The flow resistance of the linking must be matched with the flow resistance of the

regenerator. This type of PTR improves the performance due to similar distribution of temperature along the length of both regenerator and pulse tube.

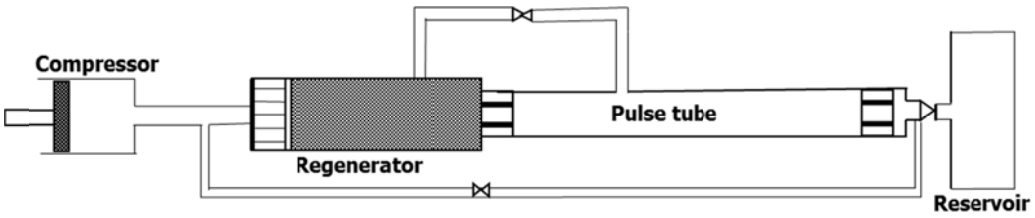

Figure 1.13 Schematic diagram of Multiple-inlet PTR

1.4.12 V-M type pulse tube refrigerator

The advantage of V-M type pulse tube refrigerator over other type pulse tube refrigerator is that, it does not require a mechanical compressor. It uses a thermal compressor which generates pressure oscillation by making use of temperature difference. The schematic diagram of a V-M type pulse tube refrigerator is shown in Figure 1.14. The V-M type PTR consists of displacer, expander, work transfer tube, three regenerator parts, pulse tube, heat exchanger immersed into liquid nitrogen. The main phase shifter at the pulse tube hot end is an expander. Inside this V-M side, displacer, work transfer tube and first regenerator serve as thermal compressor.

1.4.13Multi stage Pulse tube refrigerator

To achieve low temperature below liquid helium temperature it is not possible in a single stage PTR. Hence multi staging method of pulse tube refrigerator is required to achieve liquid helium temperature. One PTR is used to pre-cool for the input for next stage. Figure 1.15 (a) shows the schematic configuration of a double-stage PTR and Figure 1.15 (b) shows the schematic configuration of a three stage PTR. In this arrangement the cold end of the first stage regenerator becomes the warm end of the second stage regenerator. The minimum temperature can be found at cold head of second stage of two stage PTR, and at third stage of three stage PTR. The PTRs are staged by two methods; thermal coupling and fluid coupling.

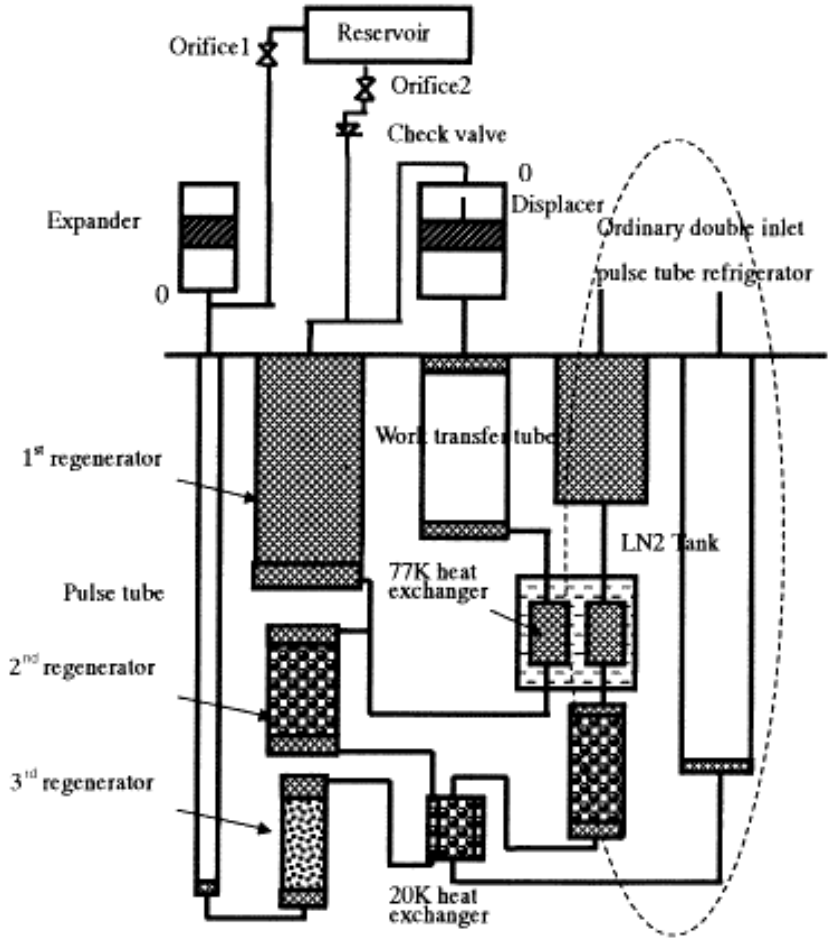

Figure 1.14 Schematic diagram of V-M type pulse tube refrigerator [12]

In thermal coupling the two stages concurrently exist and a special thermal bus connection is made between the cold heat exchanger of the first stage and the aftercooler of the second stage. The second stage has a pre-cooling regenerator between the compressor end and the aftercooler of the second stage. This regenerator produces heat that must be absorbed by the first stage, hence the first stage have a heat life capacity larger than that the amount that must be absorbed from the precooling regenerator. This coupling scheme allows for the second stage warm temperature to be that of the first stage cold temperature.

In fluid coupling the flow of working fluid literally splits, for example: flow between the cold heat exchanger and corresponding pulse tube gets split where a portion of the mass flow travels to the pulse tube and the remaining mass flow visits another regenerator, which is the entrance of the second stage.

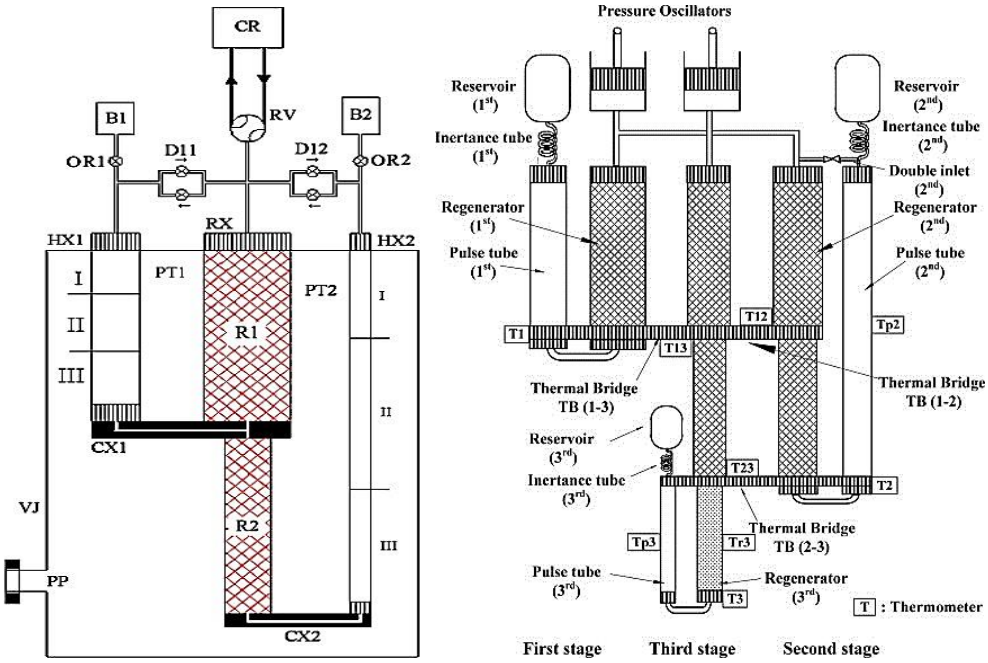

Figure 1.15 Multi-stage PTR (a) two Stage [13], (b) three stage [14].

1.4.14 Pulse tube refrigerator with 'L' type pulse tube

The 'L' type pulse tube can simplify the cold end structure and increase the symmetry of the PTR. The limitation of this type PTR is due to the relatively large wall thickness of the 'L' type pulse tube at the cold end affect the cold end temperature of the system. The Figure 1.16 shows the schematic diagram of the 'L' type pulse tube PTR.

1.4.15 DIPTR with a diaphragm configuration

The double-inlet pulse tube refrigerators with a diaphragm configuration can able to suppress DC gas flow. It is composed of two flanges with a cone-shaped hollow and a circular diaphragm made of polyethylene film. The size of diaphragm controls the gas displacement volume. Diaphragm configuration suppresses DC gas flow and increases the cooling performance of the refrigerator. Figure 1.17 shows the schematic diagram of DIPTR with a diaphragm configuration.

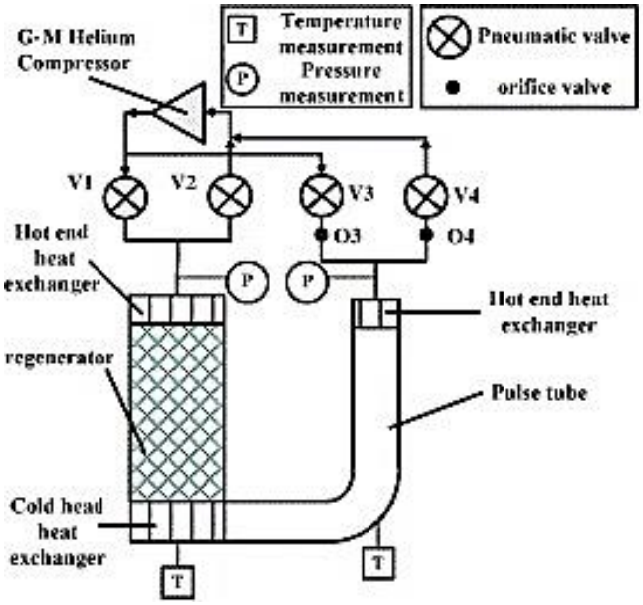

Figure 1.16 Schematic diagram of an 'L' type pulse tube and two orifice valves [15]

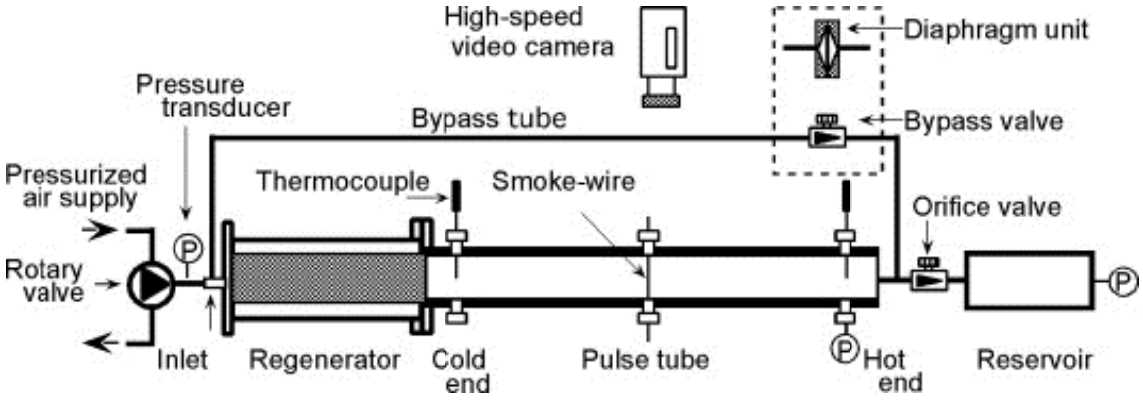

Figure 1.17 Schematic of DIPTR with a diaphragm configuration [16]

1.5 Basic theories for the Pulse Tube Refrigerator

To understand the working principle of a pulse tube refrigerator, efforts have been made by many researchers. However some conceptual theories are proposed to demonstrate the working principle of this type of refrigerator as discussed here.

1.5.1 Surface heat pumping theory

Surface heat pumping theory also called shuttle heat transfer. This mechanism was explained by Gifford and Longsworth [4]. In an oscillatory flow, due to presence of

a temperature gradient, there is a heat transfer between gas and the wall which is called surface heat pumping. It is the basic working principle of a BPTR.

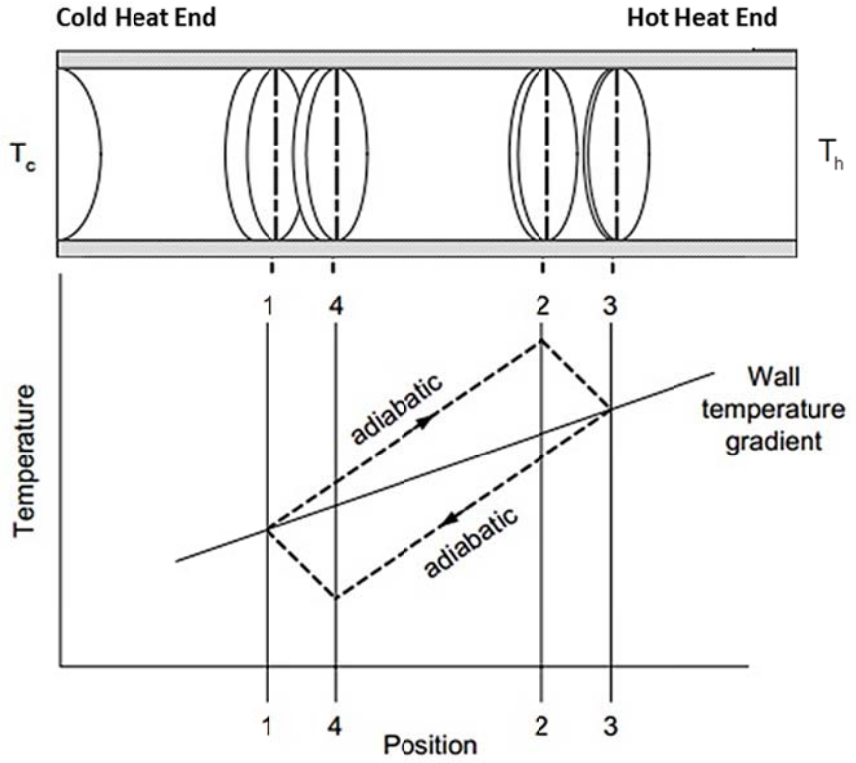

Figure 1.18 Surface heat pumping cycle.

The surface heat pumping cycle is shown in Figure 1.18. The left side of the system is connected to an oscillating pressure wave generator through a regenerator and the right side is closed. It undergoes four steps to complete a single cycle due to periodic pressurization and depressurization of gas inside the regenerator and hollow tube.

1. Initially, the gas parcel is at point 1 at low pressure and temperature as shown in Figure 1.18. The gas parcel undergoes adiabatic compression and moves to the point 2 on right side. Due to the adiabatic compression, the temperature of gas parcel increases.

2. The gas parcel at hot end stops moving and gets adequate time for thermal interaction with the wall of the hot heat exchanger, and cools the gas in the hot heat exchanger with a decrease in temperature, and the cycle moves from point 2 to point 3.

3. During depressurisation the gas parcel undergoes adiabatic expansion and moves towards the cold heat exchanger from point 3 to point 4 in the cycle. The temperature of gas parcel decreases.

4. The parcel becomes stationary at the cold end. The wall transfers heat to the gas parcel at the left side cold end with an increase in gas parcel temperature and the cycle moves from point 4 to point 1.

However, the heat is transferred from the cold end to hot end (left side to right side). The process of surface heat pumping happens at all points between the hot heat exchanger and the cold heat exchanger synchronously and the heat is pushed from the cold heat exchanger to the hot heat exchanger.

1.5.2 Enthalpy flow model

The enthalpy flow theory can easily applied to different components in a pulse tube refrigerator individually. The cyclic averaged enthalpy flows at different locations along the pulse tube can be calculated by an integration of the governing equations. Using enthalpy flow model Radebaugh et al. [10] compared different types of pulse tube refrigerators. In this model, time-averaged enthalpy flow in the pulse tube and the resultant refrigeration effect are calculated. This theory was developed to explain the cooling performance in orifice pulse tube refrigerator. It was proposed that the phase shift between pressure and velocity plays an important role in the cooldown, while the surface heat pumping is minimal in the orifice pulse tube refrigerator. Phasor analysis was developed based on this theory, depending on the first law of thermodynamics to explain the effect of the various parameters on the performance.

1.5.3 Thermoacoustic theory

In thermoacoustic devices work flow, heat flow and their mutual conversion is possible. A prime mover converts heat flow to work flow and the refrigerator converts work flow to heat flow. The thermoacoustic device basically contains two media, fluid and solid. The fluid is oscillating in nature and the solid is the matrix of a regenerator or wall of a pulse-tube or plate. If there is a large temperature gradient inside a tube closed at one end, the gas inside the tube starts oscillating. Similarly an oscillating gas inside a closed tube will produce a temperature gradient across the ends. The compressor is considered as a device to generate time-averaged work flow towards the

pulse tube and hence there is a time average enthalpy flux in the pulse tube. The amount of work flow transferred from pulse tube, the same amount of heat is transported from the cold end to the hot end of the regenerator. This is based on thermoacoustic theory to explain performance of a pulse tube refrigerator with the help of an enthalpy flow model [17].

1.6 Main Components of a Pulse Tube Refrigerator

- ✓ **Compressor**

The compressor generates high and low pressure oscillation in a PTR. It uses electric energy as input power and converts it into equivalent mechanical work to generate pressure fluctuation. The efficiency of compressor is very important on the performance of PTR. For Stirling model reciprocating compressor is used. For high frequency systems, moving coil type linear motor driven compressors are chosen. For GM type system the compressed gas is controlled by a rotary valve.

- ✓ **Regenerator**

The heart of a pulse tube refrigerator is a regenerator. In a regenerator the two streams flow alternately. Heat transferred from the hot fluid is stored in the matrix, making its temperature rise, and is subsequently given up to the cold fluid during the return stroke, causing its temperature to fall. It is made of a porous matrix consisting of stacked wire screens. This porous matrix of the regenerator increases the heat transfer area and permits the working fluid to pass through it. In thermally equilibrium condition the regenerator assumes effectiveness of 100% and the time averaged enthalpy flow in the regenerator is zero. This is called an ideal or perfect regenerator. The specific heat capacity of matrix material decreases at cryogenic temperatures so it is very difficult task to handle regenerators operating at cryogenic temperatures compared to those operating at room temperature.

- ✓ **Heat exchangers**

In a pulse tube refrigerator system heat exchangers are also playing a vital role. After compressor a heat exchanger (after cooler) for cooling the compressed gas temperature from the compressor, at the cold end of the pulse tube one heat exchanger for supplying cooling load and at hot end of pulse tube a hot heat exchanger are coupled. These are consisting of porous media of wire mesh or sintered metal. The after cooler heat exchanger and hot heat exchanger are generally provided by water

cooling or air cooling. Due to the porous nature, such heat exchangers allow easy passage of the working gas for heat removal. The cooling load is given at the cold heat exchanger.

- ✓ **Pulse Tube**

Pulse tube is a hollow cylindrical tube made up of stainless steel in which enthalpy flows from the cold end to the hot end in the form of heat. It is situated after the regenerator cold end.

- ✓ **Phase shifter**

To get on favorable phase shift between mass flow rate and the pressure wave, various types of phase shifters are used, such as orifice valve and inertance tube. These are placed between the hot end heat exchanger of pulse tube and reservoir. By adjusting the orifice diameter or the inertance tube length and diameter, the required phase relationship can be achieved. The inertance tube is a long thin cylindrical tube whereas orifice valve is a needle valve type.

- ✓ **Surge volume**

The surge volume or reservoir is situated at the hot end side after the phase shifter. Its volume is adjusted in such a way that the pressure and mass flow fluctuation inside it is very negligible.

- ✓ **Rotary valve**

The rotary valve is one of the important components of a GM type pulse tube refrigerator. The schematic diagram of a rotary valve is shown in Figure 1.19. It is used to switch high and low pressure from the compressor to the pulse tube system. The high and low pressure of compressor is connected to the rotary valve through the quick disconnect couplings. The rotary valve has a rulon part which is made to rotate with the help of a synchronous motor against an aluminum block with predefined passages connecting the high and low pressures from the compressor. The rotational frequency of the synchronous motor is controlled using an inverter drive.

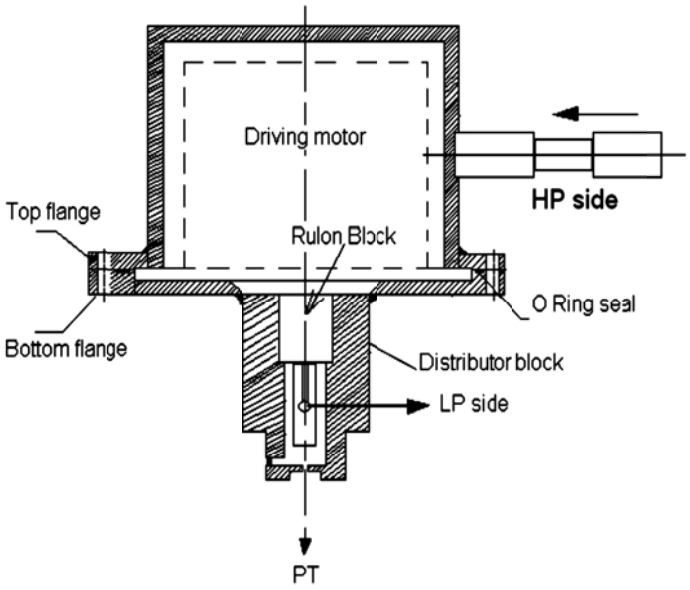

Figure 1.19 Schematic diagram of rotary valve.

1.7 Losses in Pulse Tube Refrigerator

In actual practice, there are number of losses associated with pulse tube refrigerator. These are responsible for determining the performance of a pulse tube refrigerator. Some of the losses are discussed here.

- **DC flow loss**

The double inlet bypass constructs a closed loop flow path through regenerator and pulse tube and therefore opens up the possibility of a circulating gas flow, the so called DC gas flow. DC flow varies from negative to positive. If the flow is from the pulse tube hot end of the regenerator inlet through the double inlet valve then this is known as negative DC flow. If the flow is from the regenerator inlet to the hot end of pulse tube through double inlet valve then it is called positive DC flow as shown in Figure 1.20. A suitable negative DC flow increases the performance where as positive DC flow diminishes the performance of cryocooler and also affects the stability of refrigeration temperature. Due to DC flow loss the cold end temperature would slowly oscillate by several degree with periods of several minutes or more.

There are various methods to overcome the DC flow loss. (i) A tapered tube known as a jet pump method. (ii) Different version of second orifice [18] (iii) Multi bypass [19] (iv) Membrance suppression method.

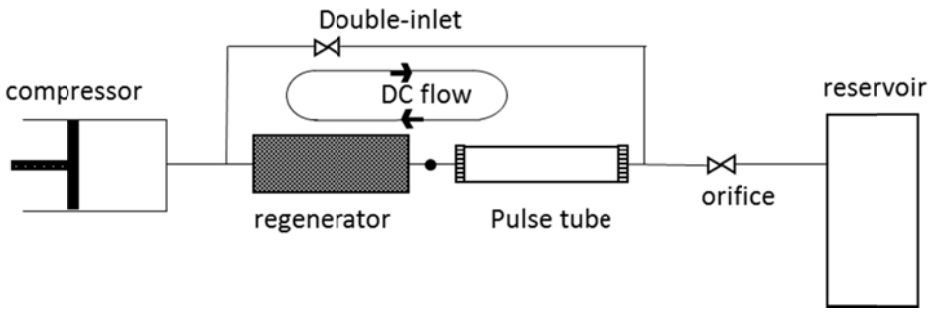

Figure 1.20 DC flow direction in a DIPTR [18]

❖ **Hot end loss**

The hot end loss was theoretically as well as experimentally introduced by Gerster et al. [20]. It occurs due to the regenerative effect of the hot heat exchanger. Most pulse tube refrigerators need an additional heat exchanger at the hot end of the working space in contrast to other refrigerators with regenerators. There is a periodic, alternate gas flow, which passes through this hot heat exchanger. Due to this fact the hot heat exchanger has to be considered not only with a desired recuperative effect but also with a regenerative effect. This regenerative effect of the hot end heat exchanger acts as a loss. This loss is called as hot end loss. This hot end loss has been described by means of the enthalpy flow model. As the heat exchanger at the hot end of the pulse tube is not needed by a four valve pulse tube refrigerator, the hot end loss can be avoided.

❖ **Work Loss**

There is a loss in spite the DC flow loss, the work loss [21] associated with the bypass of the double-inlet pulse tube refrigerator. The work loss is also known as double-inlet work loss. The mass flow rate through the bypass is caused by the pressure drop through the regenerator. It includes two components. One is in phase with the pressure wave, the other is in a 90° phase with a pressure wave. The component of the mass flow rate in the 90° phase with the pressure wave is useful for adjusting the phase angle between the mass flow rate and pressure wave at the cold end of the pulse tube. The component of the mass flow rate in phase with the pressure wave is the work loss.

❖ **Regenerator Loss**

The regenerator losses are found in two types [22]: the thermal losses, which raise the refrigeration temperature, T_c and the pressure drop losses that lowers pressure, P_4 as shown in Figure 1.21.

These losses are described as:

- Regenerator thermal losses associated with the regenerator inefficiency. This is due to the longitudinal thermal conduction loss through the matrix material and regenerator housing.

- Regenerator pressure losses are due to a reduction in the expansion space pressure amplitude caused by the pressurization and depressurization of the regenerator void volume

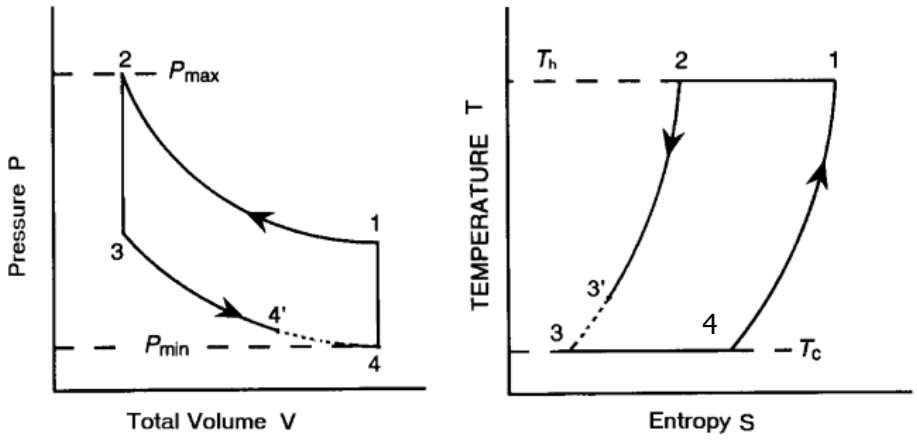

Figure 1.21 P-V diagram and T-S diagram of a Stirling cycle, indicating the pressure drop loss and thermal loss.

❖ **Shuttle loss and pumping loss**

The shuttle loss and pumping loss are resulting from the oscillating flow inside a hollow tube. The movement of gas piston is very similar to the actual cold piston in PTR. The gas piston length itself could keep unchanged, but the piston is constantly changing. The heat is transferred from low temperature to high temperature gradually according to wall and gas piston contact. This loss in Stiriling refrigerator is large and important.

Another is pumping gas loss. This loss is to consider the effect of the gap or clearance between gas piston and the wall. Due to viscosity this gas gap adheres to tube wall and cannot move like gas piston. Then some more gas will go into this gap from cold end or the gas piston during compression and be released during expansion. This loss is smaller in Stirrling or GM refrigerator.

Boundary layer thickness in the pulse tube may be very thick compared to the acting piston. The above features will result in a small shuttle loss and a large pumping loss. It is important that independent of thick and thin boundary layer thickness, the sum of the shuttle loss and pumping loses will be an important loss in the PTR.

- **Enthalpy flow loss**

The existence of steady large scale mass streaming within the pulse tube causes enthalpy flow from the hot end heat exchanger to the cold end heat exchanger. This can be a major loss mechanism of the pulse tube refrigerators. The mass streaming reduces net cooling power. Tapering the pulse tube reduces both the steady mass flux and the steady component of the second-order temperature, which results in a decrease of streaming-driven enthalpy flow loss.

- ***Streaming***

The term 'streaming' refers to a steady mass flux or velocity, usually of second order, that is superimposed on the larger first-order oscillating flow. In a simplified view of the working principle of the pulse tube refrigerator, the gas in the pulse tube pushes pressure and velocity fluctuations from the cold heat exchanger to the hot heat exchanger. The gas inside the pulse tube must thermally insulate the cold heat exchanger from the high temperature of the hot heat exchanger. But due to convective heat transfer within the pulse tube it is ruined, which carries heat from the hot heat exchanger to the cold heat exchanger and thereby reduces the net cooling power.
The convection inside the pulse tube considers being due to drive by streaming. In the context of the pulse tube, this driving can occur in the oscillatory boundary layer at the side wall of the pulse tube; in this layer, both viscous and thermal phenomena are dominated. When a gas parcel in the viscous boundary layer moves in one direction, it will have a different temperature than when it moves back. As a result, the drag it experiences is different too. Hence, there is a net displacement of the gas parcel.

Because the total mass flow over the tube cross section should be zero, a mass flux in the boundary layer must be compensated by a mass flux in the center of the tube. The result is a torus-like vortex as shown in Figure 1.22. The streaming mass flux depends on several parameters. Pressure amplitude, velocity and temperature in the boundary layer play an important role. Because the thickness of the thermal boundary layer and viscous boundary are about equal, the above mentioned surface heat pumping effect will also influence the streaming.

The enthalpy flow associated with the secondary streaming could be a major loss mechanism. The tapered pulse tube concept can solve the streaming effect.

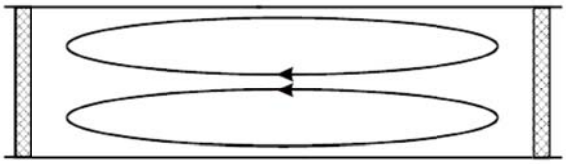

Figure 1.22 Torus shape vortex formation inside the pulse tube due to viscous drag in the boundary layer

1.8 Application of Pulse Tube Refrigerator

After decades of rapid development, due to the absence of moving parts in the cold head, low vibration, long lifetime and high reliability, pulse tube refrigerators are the most promising cryo-coolers. Because of these momentous advantages, they are widely used in Superconducting Quantum Interference Devices (SQUIDs), cooling of infrared sensors to about 80^0 K for night vision capability of the military, low noise electronic amplifiers, missiles and military helicopters, superconducting magnets, liquefaction of gases, gamma ray spectrometers, liquefaction of oxygen on Mars, x-ray devices and high temperature superconductors, mine sweeping magnets, magnetic resonance imaging (MRI), maser amplifiers, superconductor in wireless communication bases, storage of medical specimens, cryosurgery,

PTRs are used in conditions where small liquid helium baths need a temperature around 4 K. It is possible to reach zero boil-off by means of a PTR. PTCs are generally used in refrigeration systems with small heat loads, in the range of a few watts, at very low temperatures. A details list of cryocooler applications in different industries is listed below [2].

- ✓ **Military**
  - (1) Infrared sensors for missile guidance & night vision
  - (2) Infrared sensors for surveillance (satellite based)
- ✓ **Police and security**
  - (1) Infrared sensors for night-security and rescue
- ✓ **Environmental**
  - (1) Infrared sensors for atmospheric studies (satellite)
  - (2) Infrared sensors for pollution monitoring
- ✓ **Commercial**
  - (1) Cryopumps for semiconductor fabrication
  - (2) Superconductors for cellular-phone base stations
  - (3) Superconductors for voltage standards
  - (4) Semiconductors for high-speed computers
  - (5) Infrared sensors for NDE and process monitoring
  - (6) Industrial gas liquefaction
- ✓ ***Medical***
  - (1) Cooling superconducting magnets for MRI
  - (2) SQUID magnetometers for heart and brain studies
  - (3) Liquefaction of oxygen for hospital and home use
  - (4) Cryogenic catheters and cryosurgery
- ✓ ***Transportation***
  - (1) LNG for fleet vehicles
  - (2) Superconducting magnets in maglev trains
- ✓ ***Energy***
  - (1) LNG for peak shaving
  - (2) Superconducting power applications (motors, transformers, etc.)
  - (3) Infrared sensors for thermal loss measurements
- ✓ ***Agriculture and Biology***
  - (1) Storage of biological cells and specimens

1.9 Aim of the Present Study

All pulse tube refrigerators are working in a closed system. There is no mass exchange between the environment and pulse tube system. In PTR no moving part present at the cold end. The only moving component present at the compressor is to

generate the oscillating pressure inside the system. Due to lower critical temperature and high thermal conductivity helium is chosen as working fluid.

The optimum design and fabrication of pulse tube refrigerator is a topic of concern in the current era of cryocooler research field. There is no open literature readily available to describe the designing and modelling of the pulse tube refrigerator. To analyse the transport phenomenon, fluid flow and heat transfer in the PTR there are various models available. But the models have its own limitations and also range of applicability.

The exhaustive literature review reveals that ITPTR is least explored out of many Cryocoolers. In this direction, present work emphasizes on the ITPTR functionality to understand the multiple interacting phenomena involved with this process and make it reliable and predictable using the powerful computational fluid dynamics (CFD) software. It can analyse the transient multidimensional flow and heat transfer process in complex geometries of ITPTR. In next part comprehensive investigation on the effect of operating parameters and geometrical parameters on cold end temperature and input power for ITPTR and OPTR are investigated using the ANOVA method.

Based on these guiding principles, the objective of the present research is as follows:

- The simulation of PTR using a commercial CFD software, FLUENT to study the flow phenomena and heat transfer characteristics in the pulse tube refrigerator system.
- Analysis of numerical results generated with the help of 1-D simulation code SAGE for ITPTR and OPTR, using statistical methods.
- Determination of relationship between operating parameters and responses.
- Optimum parameter selection for overall improvement in part quality.

1.10 Thesis outline

The present thesis is organized into seven chapters.

- The present chapter (Chapter 1) describes an introduction about cryocoolers, classification of cryocoolers, their working principles, general applications, comparisons and a brief description of different types of pulse tube refrigerators along with their components.
- The Second chapter provides an overview of the subjects and review of the literatures on pulse tube refrigerators with related technologies.

- The third chapter describes different methods of pulse tube refrigerator analysis such as surface heat pumping, enthalpy flow theory, phasor diagrams for different PTR models. Also step by step design procedure for pulse tube refrigerator is discussed.
- The fourth chapter detailed CFD simulation using commercial software Fluent describes the inertance tube pulse tube refrigerators (ITPTR) derivation of governing equations for fluid flow and heat transfer in pulse tube and regenerator. For regenerator which is modelled as porous medium, the methods are discussed to calculate porous media parameters with emphasis on wire mesh regenerators. Also the step by step procedures for CFD simulations are presented.
- The fifth chapter emphasises on comprehensive investigation on the effect of process parameters on cold end temperature and input power for ITPTR.
- The sixth chapter emphasis on comprehensive investigation on the effect of process parameters on cold end temperature and input power for OPTR.
- The final chapter reflects salient points and concluding remarks on the results and adopted methodology on previous chapters. Some recommendations have also been highlighted for further investigation.

Chapter 2

REVIEW OF LITERATURE

2.1 Introduction

An introduction to the pulse tube refrigerator was proposed in 1963 by Gifford and Longsworth [3] and it was latter named as the basic pulse tube refrigerator (BPTR). The working principle of BPTR was based on the concept of "surface heat pumping". It reached a minimum temperature of 124 K with single stage BPTR and 79 K in two stage from room temperature. A significant improvement was made by Mikulin et al. [5] by adding an orifice and a reservoir at the hot end and this is called the orifice pulse tube refrigerator (OPTR). It attained a minimum temperature of 105 K with single stage and below 4 K in multi stage from room temperature. Zhu et al. [23] achieved a new constructional improvement by adding a by-pass between the hot end of pulse tube and hot end of regenerator, and this is known as the double inlet pulse tube refrigerator (DIPTR). It was able to achieve a minimum temperature of 42 K in a single stage, with significantly improved refrigeration performance. The latter improvement modification is the design of inertance tube pulse tube refrigerator (ITPTR) which substitutes the orifice of OPTR with an inertance tube, a long narrow tube which provides necessary phase shift between temperature and mass flow rate. There are several innovations of pulse tube refrigerators by several researchers such as multi-stage, multi-bypass, four-valve, active buffer, work recovery phase shifter, double orifice, diaphragm insert, etc. After decades of rapid development, the absence of moving parts in the cold head, low vibration, long lifetime and high reliability, pulse tube refrigerators are the most promising cryo-coolers. Because of these momentous advantages, they are widely used in Superconducting Quantum Interference Devices, cooling of infrared sensors, low noise electronic amplifiers, missiles and military helicopters, superconducting magnets , liquefaction of gases , gamma ray spectrometers, liquefaction, x-ray devices and high temperature superconductors. An extensive review related to the pulse tube refrigerator has been reported in literature [24-27].

2.2 Basic Pulse Tube Refrigerator

In the year 1963 Gifford and Longsworth [3] from Syracuse University developed the fundamental idea of innovative type cryocooler, a new method of achieving

cryogenic temperature having no moving parts at the cold end region unlike the Stirling cryocooler. This cryocooler was based on the heat shuttle effect on the wall. They reported the first experimental set up design, result and comparison with other refrigeration model in their next paper in the year 1964 [28].

The concept of cooling in pulse tube refrigerator was described as "the pressurization and depressurization of a constant volume system due to unsymmetrical heat transfer of heat and refrigeration may lead to the build up of large temperature differences within the volume". The initial design was based on a slender, thin walled cylindrical tube with one end open and the other end closed. The closed end was attached with a water cooled heat exchanger and the open end was connected to a regenerator through a heat exchanger. As a result of the oscillatory flow field caused by periodic pressurization and expansion formed by the compressor, the open end was subjected to an oscillatory pressure from the regenerator, causing the open end to cool. This refrigerator was later named as basic pulse tube refrigerator (BPTR). It consists of a compressor, aftercooler, regenerator, cold heat exchanger, pulse tube and a hot heat exchanger.

The compressed gas from compressor during the compression process moves towards the close end of the pulse tube. As the compression process inside the pulse tube under goes adiabatic compression, hence there is a temperature rise of the working fluid and there is a temperature exchange between the boundary layer and the tube wall. The heat exchanger attached at the closed end cools the hot wall. During the corresponding adiabatic expansion process during expansion of compressor, the depressurized gas moves towards the cold heat exchanger and causes temperature drop. The wall discharges heat to the working fluid. The net heat transfer between the gas and the pulse tube wall, thus shuttles heat from the cold end to the warm end. However the net amount of heat transferred is relatively small and disappears when the temperature gradient in the wall becomes sufficiently large to match the temperature excursions developed in the gas during the compression and expansion processes. This is the so-called 'surface heat pumping theory' that explains the cooling mechanism of the BPTR [4].

Gifford and Kyanka [29] investigated the working principle of a reversible pulse tube refrigerator and its problem, and also compared the operation with that of a valved pulse tube refrigerator. It was reported that the refrigeration capacity of a reversible pulse tube refrigerator is inferior to that of valve type while rest parameter and operating condition kept constant. de Boer [30] developed a non-liner model to

calculate the coefficient of performance and net work done per cycle in terms of pressure ratio and non-dimensional length of heat exchangers at the closed end of BPTR without a regenerator, by taking into account the gas motion during the cooling and heating process. In his next paper [31] he extended the previous work by attaching a heat exchanger at the hot end of regenerator. The pressure was considered uniform during the entire cycle. The performance of the BPTR presented in terms of heat removed per cycle, coefficient of performance and regenerator efficiency were presented as a function of the temperature ratio of the heat exchangers, using control volume method. Bauwens [32] numerically studied the performance of BPTR using near isothermal theory. The author calculated the entropy flux of the system which enables to divide the enthalpy flux into heat and work at the boundaries of the tube, generating a complete performance representation.

Lee et al. [33] claimed an existence of secondary flow inside the BPTR configurations which causes a measure loss due to the enthalpy flow associated with secondary streaming. The secondary flow inside a BPTR configuration with finite temperature gradient has been explained analytically by Jeong [34]. The axial temperature gradient is inversely proportional to the length of pule tube, hence for the same volume of pulse tube secondary flow and enthalpy flow associated with secondary streaming could be minimized by the use of short tube of large diameter rather than a long tube of smaller diameter. Koshimizu et al. [35] numerically analysed the movement of gas particles and heat transfer between gas particles and wall of the BPTR, and also explained the mechanism of surface heat pumping. The system performance characteristics of the BPTR were experimentally investigated by Huang and Tzeng [36]. Experiments were carried out with different regenerators to find out the time constant of the regenerator and the pulse tube wall. It was found that the cool down time is dominated by the time constant of the pulse tube wall.

However, there are many limitations associated with the basic pulse tube refrigerator. The phase relation between the mass flow rate and pressure wave plays a vital role. The phase difference between the pressure and the mass flow rate in a basic pulse tube refrigerator is 90^{o}. In other words, when the pressure becomes the maximum, the mass flow rate becomes zero at the warm end of the pulse tube. Hence phasor analysis is considered to be one of the most effective methods for designing and optimising the pulse tube configurations. This method provides a simple means for finding the optimum phase shift between mass flow and pressure wave for PTRs. There are various types of phase shifter proposed by researchers such as the orifice, the

inertance tube and the double inlet arrangement. A clear understanding of phase shift between pressure wave and mass flow rate for different types of pulse tube refrigerators was described by Hofmann and Pan [37] using phasor diagrams based on volume flow rates. This methodology was applied for both ideal systems with no losses and also for the systems by taking account of irreversible losses caused by friction as well as heat conduction and heat transfer. The ideal case results were compared with experimental data of single-stage and two-stage pulse tube refrigerators. They indicated that, the phase shift calculation for the pulse tube was quite easier, whereas there was more divergence for the regenerator. The analysis can be extended to the design of multistage systems without much modification.

2.3 Basic concept of Pulse Tube Refrigerator

To increase the performance of the pulse tube refrigerator, a phase shifter is required in between the hot end and reservoir. There are various types of phase shifter used by different researchers such as orifice, double inlet, multi bypass, two pistons, four valve, inertance tube, active buffer inter phasing and double orifice. The concept phase shifting mechanism as well as the transport phenomenon of pulse tube refrigerator is theoretically as well as experimentally investigated by researchers.

The analytical model proposed by Richardson [38] illustrated the method of predicting optimum pulse rate. He reported that in pulse tube refrigeration the transient radial heat transfer is one of the significant parameter. The importance of surface heat pumping in different cryocoolers was summarized. The thermodynamic loss of rotary valve and the COP of GM type pulse tube refrigerator have been investigated by Ju [39] using the first and second laws of thermodynamics. A standard correlation for COP for GM type PTR has been formulated based on two types of pressure profile. The sinusoidal wave inside the pulse tube and the step wave at the compressor side are compared with that of Stirling type PTR.

Kasuya et al. [40] described the importance of heat exchange between the working gas in the pulse tube and the tube wall inside a pulse tube refrigerator. Experimental investigations were conducted to analyse the work flow going through the pulse tube without heat exchange, by mounting a piston at the hot end of the pulse tube. It was reported that the refrigeration power increases when the work flow reaching the hot-end piston increases. Hence the work flow has more importance for the increase in the refrigeration power. An analytical model for the ideal OPTR, DIPTR

and Modified PTR have been developed by Maréchal et al. [41] taking into account the pressure drop and the capacity of the regenerator, and for a supplied mass flow rate delivered by the compressor.

A mathematical model has been proposed by Smith [42], using systems of partial differential equations for the pulse tube refrigerator to understand the heat and mass transfer inside the system. The cooling mechanism was described, considering the equation for conservation of momentum, as the pressure is a known function of time. Liang et al. [43] performed a theoretical as well as experimental studies to visualize the thermodynamic non-symmetry effect on the pulse tube refrigerator, which is responsible for the production of refrigeration power at the cold end of the pulse tube to much lower temperatures. The gas elements enter the cold end of the pulse tube at the wall temperature of the cold end heat exchanger but return back to the cold end of the pulse tube at much lower temperatures and this is termed as thermodynamic non-symmetry effect by the authors. The thermodynamic non-symmetry significantly affects the performance of a pulse tube refrigerator. The same group published two more papers. In one paper [44] they reported that the temperature and viscosity influences of the pulse tube wall and proposed the concept of a thermal viscous layer in the pulse tube, on which the compound pulse tube model is based and taking into account the principal losses of cooling, including regenerator inefficiency loss and solid conduction loss. In another paper [45] they performed the experimental investigation to validate the previous published two theoretical models. The experimental results were found to be in good agreement with the theoretical predictions. Kittel et al. [46] introduced a simple 1-D model to analyse the qualitative behavior of the pulse tube refrigerator. Using this method the concept of entropy flow and Gibbs free energy flow has been well described and the different losses associated with the pulse tube refrigerator have been calculated. To correlate between the mass flow rate and the pressure wave, an alternative phasor model was proposed.

The term cooling power of a cryocooler was well defined by Waele [47]. It is defined as the work done by the compressor and the entropy generated due to the irreversible processes in different components of the system. For the design and analysis of the cryocoolers a general relationship for the entropy production in the components of pulse tube refrigerators was proposed by the author. The losses like heat exchanger losses, orifice and valve loss, viscous loss and regenerator losses were well described in this work. The author also discussed the dynamic behaviour of the temperature profiles inside the regenerator, hot and cold ends of the pulse tube

elaborately [48]. The effect of a single-orifice and double inlet valve were presented using general thermodynamic relations.

Olson and Swift [49] demonstrated the acoustic streaming inside a tapper tube with axially changing temperature, in the vicinity of the boundary layer. This investigation leads to give an appropriate pulse tube shape to eliminate the streaming. They conducted experiments and suggested that the conical pulse tube of optimum cone angle could eliminate streaming and increase the cooling power than a cylindrical pulse tube. To calculate the enthalpy flow rate along the pulse tube in a pulse tube refrigerator Zhu and Chen [50] formulated an integration formula assuming mass flow rate and pressure fluctuation as sinusoidal using the Lagrange method. To evaluate the volume of the pulse tube in ideal OPTR and DIPTR, it is simplified to polynomial functions. Instead of the orifice the mechanism of the symmetry nozzle was proposed and studied experimentally by Yang et al. [51]. A better cooling was found in symmetry-nozzle pulse tube refrigerator compared to the other ideal pulse tube refrigerator when the pressure ratio and mass flow amount are same.

Baek et al. [52] proposed a two dimensional model for tapered pulse tube model and applied the linearized conservation equations of mass, momentum and energy. In the first analysis they investigated the effect of operating frequency, taper angle, displacement volume ratio and velocity phase angle between the ends of the pulse tube on net energy flow. Proceeding with the similar numerical approach in their next part [53] the effects of the taper angle and frequency on the steady mass flux and the enthalpy flow loss associated with the steady mass streaming were discussed. The effects of the operating frequency and the taper angle on the unsteady components of the second-order mass flux and temperature were investigated by Park et al. [54]. They found that the unsteady second-order mass flux and the time-averaged enthalpy flow by the unsteady second-order mass flux increases as the second-order displacement volume at the cold end increases.

The most influencing parameter in a GM type pulse tube refrigerator is timing of the rotary valve, which is responsible for the relationship between intake and exhaust processes. A parametric experimental study of valve timing effects on cooling performance of a two-stage 4 K PTR were conducted by Qiu and Thummes [55]. It could be seen that the optimization of valve timing can significantly improve the cooling performance for both stages. Will et al. [56] worked on rotary valve of the GM PTR to reduce wear and torque requirement. They developed two types of valves, which have balanced forces on the rotor. In the first valve the rotor and the stator make no

mechanical contact. The second type is a contact valve, but the forces on the rotor are balanced in a different way. Therefore, these valves are less liable to wear, and the torque needed to rotate the valves is small. This type of valve has a small internal leak, and relatively easy to fabricate.

Lu and Cheng [57] experimentally investigated the dynamic pressures of the viscous compressible flow fluctuating at different locations in a GM type PTR operating in cyclic steady states. They found that at the hot end of the regenerator the oscillating amplitude of the pressure was largest while in the reservoir the cycle-averaged pressure was the smallest. They reported that at low frequencies, the cycle-averaged pressure of the compressible flow oscillating in a tube increases from the compressor toward the reservoir. They also discussed the effect of the cycle-averaged pressure on the refrigeration performance. De Boer [58] developed a linearized model of pulse tube refrigerator to calculate the maximum attainable non-dimensional rate of refrigeration assuming the regenerator to be thermally perfect and has negligible dead volume. Yang [59] performed several experiments with a high frequency tapered pulse tube cryocooler in order to improve the performance of PTR. It was reported that PTCs with tapered pulse tube, degrade the performance of PTCs, but if the PTC was tapered from two directions, i.e. larger diameter at two ends and smaller diameter at middle (like converging-diverging nozzle), then performance could be improved marginally by about 1.5 K at minimum temperature and 3% on the cooling power.

2.4 Orifice Pulse Tube Refrigerator

Orifice pulse tube refrigerator was introduced in 1984 by Mikulin et al. [5]. The invention of the simple OPTR is regarded as a milestone in the development of pulse tube refrigerator.

2.4.1 Analytical and numerical studies

The numerical modeling of an OPTR with a valve less compressor was presented by Wu and Zhu [60] assuming the pressure drop inside the regenerator as negligible. Lee and Dill [61] considered the pulse tube as a nodal regenerator and the effect of residual gas velocity on the heat transfer mechanism of the orifice pulse tube. De Boer [62] developed a thermo dynamical model to investigate the heat pumping mechanism that covers the operation of an OPTR, and highlighted the important role of the regenerator for this type of pulse tube refrigerator, as compared with the BPTR. The

results are presented in terms of the heat removed per cycle, the coefficient of performance, and the refrigeration efficiency as a function of the compression ratio and the expansion ratio. In his next paper [63], he used a nonlinear thermodynamic model to calculate the heat removal rate inside the orifice pulse tube, for the compressor-driven and the linear-motor-driven cases, considering the leakage of gas to and fro from the pulse tube to orifice. The results from the analysis were compared with experiments and found to be in good agreement. Transient radial heat transfer is the dominating effect inside the PTR as reported by Richardson [64]. He developed an analytical model to study the optimum pulse rate and also verified it by conducting experiments. The relevance of surface heat pumping to the non-ideal behaviour inside the pulse tube refrigerator has been highlighted. A lower temperature below 70 K was achieved at the cold end in a single stage. The pulse tube used in the experiment was having seamless stainless steel of 15 mm diameter with 0.25 mm wall thickness and 300 mm length.

For better understanding of the refrigeration process and behaviour of the orifice pulse tube refrigerator an analytical model was developed by Storch and Radebaugh [65]. The results were presented in terms of average enthalpy flow assuming ideal gas and sinusoidal pressure variation inside the system. A vector representation of the temperature, pressure and mass flow rate waves were presented for phasor analysis. They claimed that the refrigeration power is proportional to the average pressure, frequency, mass flow rate and the square of the dynamic pressure ratio. Razani et al. [66] proposed a numerical model to investigate the exergy flow inside an OPTR and reported that in an ideal OPTR the exergy destruction is equivalent to the refrigeration power resulting in a second law efficiency. The exergy flow and irreversibility of different processes inside the regenerator are calculated using the developed correlation for pressure drop and thermal analysis in the regenerator. Godshalk et al. [67] designed the world's first 350 Hz thermo acoustic driven orifice pulse tube refrigerator. This could measure the phase of the mass flow rate and pressure wave at all key locations of the system. The results were presented in terms of velocity and pressure phase, pressure amplitude and enthalpy flow which showed good agreement with the simulations. Zhang et al. [68] presented a thermodynamic analysis to analyze the effect of reservoir volume on the thermodynamic performance of various components in an OPTR using linearized model. The reservoir volume significantly affects the entropy production in various components if the reservoir volume to the pulse tube volume ratio is below 5. The process and performance of OPTR was theoretically investigated by Wu et al. [69]

by using the method of characteristics and an introductory comparison with experimental results was explained. This paper is very useful and convenient for understanding of the process and design of the OPTR. Rawlins et al. [70] conducted an experiment for OPTR and compared the result in the form of enthalpy flow with analytical model. Time averaged entropy flow and time averaged hydrodynamic work flow inside the pulse tube is also presented in this paper.

For better understanding of the physical process like fluid flow and heat transfer phenomena occurring inside the pulse tube refrigerator and determining the parameters affecting the refrigeration power and efficiency, an improved numerical method was suggested by Wang et al. [71] which takes into account the heat transfer, aerodynamic friction and material properties. It was reported that due to phase and amplitude difference in pressure inside regenerator there exists a gas flow resistance. The assumptions in the model included one dimensional flow, ideal gas and negligible axial conduction. The model successfully predicts the property profiles inside the pulse tube.

A theoretical, comparative study between OPTR and Stirling hybrid pulse tube refrigerator was presented by Nika [72]. An orifice pulse tube refrigerator without a reservoir volume was numerically analysed and experimentally verified by Wang et al. [73]. The theoretical results show that the reverse phase of the pressure in the crankcase could be used instead of steady pressure in the reservoir to appropriately shift the flow velocity at the hot end of the pulse tube. A small increase in refrigeration power was found using MOPTR comparing to OPTR. The loss due to interface inside the small amplitude OPTR Model was investigated by Bauwens [74] using linearized model analysis. This loss is due to the abrupt transition between the cold end and pulse tube. It was reported that the loss is strongly dependent upon the pressure amplitude and of the cosine of the phase angle.

Kittel [75] presented a theoretical investigation for the efficiency of an ideal OPTR analogy to the Stirling refrigerator. An analytical model of the ideal OPTR has been developed by David et al. [76]. The heat flow mechanism at the tube ends were described as the result of the hysteretic process of the elements of gas entering and leaving the tube. The motion of the buffer gas was deduced by numerical integration and the energy balance equation for the heat flow at the hot and cold exchangers was established. The numerical data obtained from the model was found to be in good agreement with the experimental data. There were reported an insignificant difference in results compared to the theory. An isothermal model for an OPTR was established by

Zhu and Chen [77] due to advantages over nodal analysis. A comparison between the isothermal model and the nodal based analysis were also presented. The main assumptions of the isothermal model were that the gas in the middle part of the pulse tube is adiabatic and the gas in the other parts was isothermal.

A theoretical model was developed by Roach and Kashani [78], which solved all the components of an orifice pulse tube cooler. Separately, one dimensional thermodynamic equation for regenerator was solved assuming all mass flows, pressure oscillations and temperature oscillations were small and sinusoidal. A comparative analysis were also presented with the results of available REGEN 3 from NIST and Delta-E from Los Alamos National Lab for low amplitudes where there is no turbulence, and reported that they are in good agreement. They claimed that their model was easier to use than other available models because of its simple graphical interface and the fact that no guesses are required for the operating pressures or mass flow. In addition, the model only required a minute of running time, allowing many parameters to be optimized in a reasonable time.

A linear flow network model, and a new type of approach for the operational analysis of an OPTR was introduced by Huang and Chuang [79]. The pressure was considered as the electrical voltage and the mass flow was considered as the electric current in this flow network analysis. A sinusoidal signal analysis has been used to calculate the thermal performance by solving the equivalent circuit of the OPTR. The gas elements were divided into three parts inside the pulse tube of an OPTR. The middle part of the gas element generated the higher specific cooling capacity. For a fixed mass the overall cooling capacity of the OPTR was increased by increasing ratio of the gas elements in the middle portion, while the side portion was decreased. This innovative approach was theoretically studied by Xu et al. [80], using the method of characteristics.

To explain the distortion of mass flow rate and temperature oscillation curves Kuriyama and Radebaugh [81] theoretically illustrated the connection among the curves of temperature, mass flow rate and pressure as a function of time in an OPTR. The mass flow rate and temperature oscillations were expressed in terms of fundamental oscillations and harmonics, the time-averaged enthalpy flow rate and other energy flow rates were described in terms of the amplitude and phase of the fundamental oscillation of the mass flow rate through the orifice. De Boer [82] presented an optimization investigation for OPTR in two different conditions. In the first case the reservoir volume

was infinitely large and the regenerator volume was zero while in second case infinite reservoir volume and regenerator volume was considered for numerical analysis. The results were presented in the terms of enthalpy flux, pressure amplitude, mass rate amplitude and phase angle between mass flow rate and pressure as a function of orifice conductance and frequency. The optimized parameters considered were amplitude of driving pressure, and driving power amplitude of the piston. A correlation also developed for the enthalpy loss calculation due to the finite regenerator ineffectiveness.

Beside mathematical calculation there were very limited works that had been done to investigate the OPTR performance using software packages. A detailed list of software used to analyse the different type of pulse tube refrigerator is listed in Table 2.1. A two-dimensional axis-symmetric computational fluid dynamic simulation of a GM-type simple OPTR has been performed by Zhang et al. [83] to obtain results for the phase difference between velocity and pressure at cold end, the temperature profiles along the wall and the temperature oscillations at cold end with different heat loads. The multidimensional flow and heat transfer inside the pulse tube under conditions of oscillating pressure were highlighted. A swirling flow pattern in the pulse tube was observed and the mechanism for its formation was analysed elaborately. They found that the swirl causes undesirable mixing in the thermally stratified fluid and is partially responsible for the poor overall performance of the cooler, such as unsteady cold end temperature. Antao and Farouk [84] studied the effect of operating frequency on the performance of an OPTR and showed the presence of streaming in the pulse tube of the OPTR . They also studied the possibility of acoustic streaming suppression in the pulse tube region by tapering the pulse tube by a small angle [85].

Neveu and Babo [86] considered two analytical models, an ideal model and a time dependent model to investigate the performance of OPTR. The ideal model predicts that the refrigeration load could be connected to an entropy flow. From the dynamic simulation of second law it was reported that the existing device optimisation required higher permeability for the regenerator. To solve the complicated fluid flow and heat transfer characteristics inside the PTR system a new modeling approach which combines one-dimensional and two dimensional models together was proposed by He et al. [87]. The numerical results presented that the 1-D and 2-DCC (two-dimensional combined computational) model were reliable and practical, which could be used to explore the physical mechanism of the thermodynamic processes of the PTR system and design optimization of the PTR system and its components.

Table 2.1 Summary of the investigations of cryocoolers using various commercial software packages

Reference		Year	Software	Model type
(Jahanbakhshi et al. 2013)	[88]	2013	Sharif PTR	DIPTR
(Antao and Farouk 2013)	[89]	2013	CFD-ACE+	OPTR.
(Antao and Farouk 2011)	[85]	2011	CFD-ACE+	OPTR
(Farouk and Antao 2012)	[90]	2012	CFD-ACE+	co-axial PTR
(Gu et al. 2012)	[91]	2012	FLUENT	ITPTR
(Arablu et al. 2013)	[92]	2013	FLUENT,	stirling-type 2-stage
(Huang and Caughley 2012)	[93]	2012	FLUENT, SAGE	diaphragm pressure wave generator
(Boroujerdi et al. 2011)	[94]	2011	MATLAB	ITPTR
(Ashwin et al. 2010)	[95]	2010	FLUENT	ITPTR
(Dietrich and Thummes 2010)	[96]	2010	SAGE	two-stage PTR
(Banjare et al. 2010)	[97]	2010	FLUENT	GM type DIPTR
(Zhang et al. 2008)	[98]	2008	FLUENT	IPPTC
(Zhang et al. 2007)	[83]	2007	FLUENT	OPTR
(Paek et al. 2007)	[99]	2007	Delta-E	standing-wave
(Cha et al. 2006)	[100]	2006	FLUENT	ITPTR
(Dodson et al. 2009)	[101]	2009	FLUENT, REGEN	ITPTR
(Cao et al. 2009)	[102]	2009	SAGE, REGEN 3.2	single-stage stirling-type PTC
(Sobol et al. 2011)	[103]	2011	SAGE	In line PTC
(Hofmann 2005)	[104]	2005	FZKPTR	2-stage 4K PTC
(Mitchell and Bauwens	[105]	2002	MS∗2	Pulse tube cryocooler
(Roach and Kashani 1997)	[106]	1996	ARCOPTR	OPTR

2.4.2 Experimental studies

As mentioned earlier in the introductionary OPTR can reach up to 105 K [5] whereas a lowest temperature of 60 K was found experimentally at cold end by Radebaugh et al. [10] with a single stage OPTR. By improving the regenerator, the hot end heat exchanger and the insulation of the low temperature sections a temperature of 49 K at no load condition and 77 K at 12 W was achieved experimentally by Liang et al. [107] with a single stage OPTR. The results were presented in the form of ratio of regenerator volume to pulse tube volume and minimum temperature. Baks et al. [108] performed an experiment to verify the analytical results for orifice pulse tube refrigerator at ambient temperature. At this condition the regenerator losses are

negligible. The cooling power of a pulse tube refrigerator was correlated in terms of average enthalpy flow through the pulse tube and regenerator loss. It was also reported that enthalpy flow through the pulse tube is dependent on the amplitudes of the pressure variation inside the pulse tube and the volume flow through the orifice. Huang and Yu [109] experimentally investigated the design of single stage OPTR. A correlation was developed from experimental result for the performance of OPTR in terms of operating condition and dimensions of OPTR on net cooling capacity. A single stage linear OPTR was designed, fabricated and tested by Ishimura and Bodegom [110] and calculated the cooling power based on the experimental data. To calculate the cooling power, a simple discrete model of the pulse tube was developed.

Kral et al. [111] designed, fabricated and tested an OPTR. A hydraulically actuated diaphragm compressor was used to drive the refrigerator. Obtained experimental results were compared to analytic results. The working principle of the waiting time of the OPTR was discussed numerically by Zhu et al. [112] and verified by experiments. The pressure differences across the high-pressure valve and the low-pressure valve are decreased by long waiting times. Thus, the cooling capacity and efficiency are increased, and the no-load temperature is decreased. From experimental result it was reported that at cooling capacity 0 W, 45 W and 58 W the lowest temperature achieved are 40.3 K, 80 K and 80 K respectively while the waiting time were 90° , 1° and 60 ° respectively.

Antao and Farouk [89] performed both experimental and numerical investigation to study the performance of the OPTR at various values of the mean pressure of helium (0.35 MPa - 2.2 MPa), amplitudes of pressure oscillations, frequencies of operation and sizes of orifice opening. Watanab et al. [113] designed and tested a new concept of superfluid OPTR. They reached a temperature of 0.64 K at cold end.

Huang and Sun [114] performed an experimental investigation to study a variable orifice pulse tube refrigerator. The valve was designed resemble to a high-speed solenoid valve used in automobile engines. By changing the frequency and periods of ON and OFF through an electronic device, the flow resistance could be changed. This provides a possibility for an orifice pulse tube to be controlled on line during operation. They claimed that variable orifice type could able to achieve on-line control by the regulation of the degree of valve opening or frequency. The thermal losses were shown to be much less compared to a conventional orifice. The interaction between the phase angle of piston motion and the minimum temperature of on OPTR was investigated by Kasuya et al. [115]. The analysis also focused on how the

performance of pulse-tube refrigeration affected by the phase angle between pressure oscillation and gas displacement. It was reported that the optimum phase angle of piston motion in the range of 90°-180° is restricted to an OPTR between 0° and 90°. Hence OPTR cannot achieve the optimum phase angle. The authors suggested that this optimum phase angle (beyond 90°) could be achieved using DIPTR. A high frequency (50 Hz), U shaped at cold head type OPTR was fabricated and tested by Kanao et al.[7]. The authors reported a no load minimum attainable temperature of 98 K with 60 W input and 119 K at 214 mW cooling load with 60 W input power.

2.5 Double Inlet Pulse Tube Refrigerator

An important improvement in the development of pulse tube refrigerator was suggested by Zhu et al. [23]. The new modification to OPTR was proposed to control the extra mass flow through regenerator and hence increase the cooling capacity per unit mass of working gas. This new modification consisted of a bypass provided at the hot end of the pulse tube connecting to the input of regenerator. This was named as double inlet pulse tube Refrigerator (DIPTR). The author demonstrated theoretical as well as experimental results presenting an improved performance of DIPTR over OPTR. The new design of DIPTR could reduce the mass flow through the regenerator hence the refrigeration power per unit mass flow rate through the regenerator was greatly increased.

2.5.1 Analytical and numerical studies

Ying-wen and Ya-ling [116] investigated the mechanism of improvement on the performance of a DIPTR with tapered regenerator, based on the enthalpy flow theory. They reported that there exists an optimum cone angle for tapered regenerator. When the cone angle is close to a certain value, the pulse tube refrigerator with convergent type regenerator can improve the performance. But the divergent type regenerator deteriorates the performance. In order to understand the physical process like heat transfer and fluid flow occurring inside the pulse tube refrigerator and predicting the effect of orifice and double inlet valve on the refrigeration and efficiency of the DIPTR was investigated using an improved numerical model by Ju et al. [117]. Simulation results were compared with the experimental results and found to be in good agreement. Wang et al. [118] developed a numerical model to study the internal

process occurring inside the DIPTR. They reported that the bypass valve in the DIPTR considerably affects on the amplitude and the phase of the dynamic parameters and also reported that DIPTR could obtain higher refrigeration power with lower PV work than the conventional orifice version.

An analytical model was proposed by Mirels [119] to study the performance of a DIPTR using a stepped piston compressor. The performance was presented as a function of the area ratio of the stepped piston and was also reported that the refrigeration power could be increased at the cost of reduced thermal efficiency in a DIPTR than the corresponding single inlet device. The work loss through the bypass by solving an analytic equation of the mass flow rate through the bypass of the DIPTR was presented by Zhu et al. [21] taking account of the pressure drop in the regenerator. They claimed that the work loss decreases due to two conditions (1) with increase of the void volume ratio of the regenerator over the pulse tube, (2) with increase in temperature ratio of the ambient temperature over the refrigeration temperature, and it increases with the increase in double-inlet factor. The work loss ratio at 80 K was calculated for different void volume ratio of the regenerator over the pulse tube. Also the analytical results were compared with numerical results and found to be in good agreement. Iskandar and Tiow [120] mathematically studied the effect of pulse tube length, diameter and different working gas on refrigeration effect of the DIPTR.

Nika and Yannick [121] theoretically illustrated the design and the optimization of a miniature DIPTR. The hydrodynamic and thermal behaviours of the BPTR were predicted by using two different methods: a classical thermodynamic model and an electrical analogy model. The thermodynamic study takes into account the thermal gradients in the pulse tube wall. The performance of the system decreases due to the axial heat conduction in the pulse tube wall. In the next part, a new PTC model with an optimization scheme based on an electrical analogy was proposed by Bailly and Nika [122]. The model was capable of taking into account of effects such as pressure drop due to geometrical discontinuities and internal flows. The thermal behaviour of the regenerator was studied and the model was also verified against experimental results.

Using the thermo acoustic theory developed for regenerative cryocoolers by Xiao et al. [123] a miniature DIPTR was designed and experimentally tested. A lowest temperature of 78 K was achieved with a filling pressure of 12 bar, operating frequency of 48 Hz and a swept volume of 4 cm^3. The lowest temperature achieved in DIPTR was about 23 K lower compared with OPTR. Using the first law and second law of thermodynamics He et al. [124] investigated the performance of both OPTR and DIPTR.

The authors developed an exergy loss method to analyze each component in the PTR and calculated the performance coefficients. Using this exergy loss method, it was reported that the exergy losses in the regenerator and orifice were significantly larger than that of other components of the PTR system. They also reported that the performance coefficient of the DIPTR was 9 % higher than OPTR and the exergy efficiency of DIPTR was 4.91 % higher than that of OPTR. A linearized one-dimensional model was developed by de Boer [125] to study the performance of DIPTR, which account for the void volume of the regenerator. They compared the results of the DIPTR with corresponding OPTR results and found a large improvement in performance obtained with the DIPTR over the OPTR. The maximum rate of refrigeration is expressed as a function of frequency, with the regenerator void volume as an independent parameter.

The process of improvement in refrigeration power for DIPTR compared to OPTR has been explained using a proposed phasor diagram by Chokhawala et al. [126]. The phasor diagram for DIPTR was presented in terms of mass flow through orifice, double inlet valve etc. Effects of pulse tube diameter and length, frequency, pressure difference and flow coefficient for double inlet valve on phase angle and mass flow rate at cold end was also studied for DIPTR and OPTR. Banjare et al. [127] performed a two-dimensional computational fluid dynamic simulation of a Gifford–McMahon type DIPTR, operating under a variety of thermal boundary conditions. The results such as the cool down behaviours of the system, phase relation between mass flow rate and pressure at cold end and refrigeration load for different boundary conditions of the system were presented. The results display that there is a good agreement between CFD simulation results and experimental results. In their next paper they followed same boundary condition and simulation procedure for a 3-D model [97] of DIPTR. The result shows that the use of the DIPTR configuration for 40% DI valve opening and 60% orifice valve opening gives a better possibility of higher performance and efficiency compared with other values of valve openings.

For understanding the dynamic performance and physical processes occurring inside the pulse tube refrigerator, and calculating the effect of the orifice and double-inlet valve on the cooling power and efficiency of the DIPTR, Ju et al. [128] developed an improved numerical model. The numerical model solves the conservation of mass, energy, and momentum for compressible oscillating flow including the pressure viscous, inertia, gradient and convection terms. The numerical results are compared with experimental data and found to be in good agreement. Dash et al. [129] performed the

exergy analysis of a DIPTR using phasor analysis. They studied the pulsating mass flow considering the effect of different parameters such as frequency, cold end temperature, valve coefficients of orifice valve and double inlet valve, average pressure of the system and initial phase angle of compressor outlet pressure. They concluded that when operating below the critical frequency of a DIPTR, there was no cooling and increase in system average pressure improves the system performance. Arablu et al. [92] investigated the accuracy of local energy loss correlations in simulation of abrupt expansion or contraction joints under oscillating flow conditions of pulse tube cryocoolers using a 1-D code and also FLUENT software. The results were compared for 2-D and 1-D simulations, and reported that steady friction factors do not possess sufficiently accurate predictions of losses under oscillating flow.

2.5.2 Experimental studies

A theoretical as well as experimental analysis of double-inlet reversible pulse tube refrigerator was illustrated by Wang et al. [130] . They stated that the swept volume of the auxiliary piston and the phase difference between the two pistons considerably effects the performance of the DIPTR. Results also revealed that the performance of a pulse tube refrigerator could significantly be enhanced by using the DIPTR. Cai et al. [131] experimentally investigated the phase shift mechanism in a DIPTR. They also discussed the effects of varying the amplitudes and phase difference of the pressure oscillation and mass flow.

Gan et al. [132] conducted an experimental study on multi-phase helium and nitrogen mixtures in a DIPTR. They found from the experiment that both coefficient of performance and cooling power could be improved to some extent at above 70 K with less than 25 % of the nitrogen fraction in the mixture. Using this mixture model they reached a minimum temperature of 63.14 K at cold end. The internal working process of a DIPTR was experimentally studied by Zhou et al. [133]. The effects of some significant parameters such as by-pass valve and orifice opening, operating frequency and mean pressure on the amplitude shift and phase shift of three dynamic pressures at the hot end of the regenerator, pulse tube and reservoir were illustrated in this work. The effect of conjugate heat transfer between pulse tube and regenerator was also experimentally presented and stated that, the heat transfer degrades the performance of the pulse tube refrigerator. Tanaka et al. [134] constructed a DIPTR and drew a lissajous figure using the measured gas temperature and pressure in the tube from the experiment. They found that the shapes of lissajous figure depend on the location in the

pulse tube and is very sensitive to the opening of the needle valves. A comparative study between BPTR, OPTR and DIPTR was experimentally presented by Ravex et al. [135]. The lowest temperature of 28 K has been achieved in a single staged DIPTR. Due to the permanent flow in DIPTR, DC flow could significantly decreases the performance. This was experimentally investigated by Charles et al. [136] for low and high frequency and also tried to improve the performance.

2.6 Inertance Tube Pulse Tube Refrigerator

The term "inertance" was well defined by Gardner and Swift [137], which means an acoustics term connecting both inertia and inductance, because it is due to inertial effects of moving gas and acoustic is analog of electrical inductance. For large gross cooling power, the use of an inertance is significantly beneficial. It was also reported that using of inertance tube larger-volume pulse can be implemented, which could provide higher efficiencies than OPTR.

2.6.1 Analytical and numerical studies

de Boer [138] stated that the rate of cooling of the inertance pulse tube is a function of the relevant parameters. In the simplified case of infinite volume of the reservoir and zero dead volume of the regenerator, these parameters are the dimensions of the inertance tube, volume of the pulse tube, conductance of the regenerator, driving pressure, and the frequency. A simple turbulent flow model was introduced to calculate the effective conductance of the inertance tube and reported that the performance of the ITPTR was higher to that of the OPTR over a limited range of frequencies. The improvement is explained in terms of the pressure amplitude in the pulse tube, the flow rate between the regenerator and the pulse tube and the phase angle between these parameters. This analysis could be extended to the case of finite reservoir and regenerator volumes.

Chen et al. [139] numerically investigated the thermodynamic cycles in an ITPTR using CFD simulation software FLUENT. In different sections of ITPTR the working gas parcels experience different thermodynamic cycle. It was also reported that under different frequencies of piston movement, the gas parcels working in the same part of the system experience the same type of thermodynamic cycles. A comparison of thermodynamic cycle between CFD simulation and theoretical analysis was performed and found to have a similar trend of qualitative results. To simulate the ITPTR, Zhu and

matsubara [140] introduced a nodal based analysis method. Implicit control volume method was used in this model to solve continuity equation, momentum equation and energy equation of gas and energy equation of solid. Ashwin et al. [95] proposed a thermal non-equilibrium model in the porous media (heat exchangers and regenerator) and considered a finite wall thickness for the various components of the ITPTR. The effect of a finite wall thickness was found to increase in the steady-state temperature at the cold end of the pulse tube due to the heat conduction along the walls of the pulse tube from the hot end to the cold end.

Cha et al. [100] studied two ITPTR systems based on the geometry of the pulse tube (for two values of L/D ratio) using CFD simulation software FLUENT. They reported the formation of instantaneous vortical structures in the pulse tube for the small L/D case which had a negative effect on the cooling performance of the ITPTR due to the mixing of flow in the pulse tube. A numerical model was developed by Kirkconnell and Colwell [141] to solve the one-dimensional, nonlinear governing equations for heat and mass flow in a pulse tube. The governing equations were solved for frequencies above 60 Hz. Using the method of lines approach the governing nonlinear time-dependent equations were solved. A parametric investigation was conducted to study the effect of various parameters on the solution.

The refrigeration effect in pulse tube refrigerator was explained in terms of time dependent phase shifting between the oscillations of pressure and mass flow rate at the cold end of the pulse tube by Chen et al. [142]. They solved a linear ordinary differential equation of the second order with variable coefficients to define the time-dependent phase shifting effect due to variable frictional coefficient. The resistance coefficient of the inertance tube was expressed as a function of time frequency and other parameters, which are deduced from momentum and mass differential equations of the working gas. It was found that the phase shifting angle provided by the interance tube varies with time. By integrating over one cycle, the average phase angle was found to agree with previously published results.

Wei et al. [143] proposed that connecting an inertance tube without buffer can provide proper phase relationship. An experimental investigation was performed by the authors to compare the results and found that a thermo-acoustically driven pulse tube cooler without reservoir yields results close to those of a system with reservoir in terms of the cold end temperature and both gave better performance than that of an orifice

with reservoir. So without buffer the system becomes more compact in size and shape. Cha [144] have employed a numerical model for pulse tube cryocoolers that solves the full set of compressible conservations equations under the assumption of axis-symmetry using the commercially available CFD package FLUENT. Luo et al. [145] illustrated a thermo acoustic turbulent-flow model to solve the turbulent flow inside the inertance tube. This model accounts both turbulent-flow and heat transfer effects. The inertance tube was modelled with a distributed parameter model. The results obtained from these models were compared with experimental findings. The authors also suggested the modelling of inertance tube with CFD, which is much more complicated, compared to electrical analogy, but can yield more accurate results.

2.6.2 Experimental studies

Ko et al. [146] optimised the pulse tube dimensions which is affected by the dynamic behaviour of linear compressor as well as the cooling performance of a pulse tube refrigerator. Ju et al. [147], experimentally measured the flow resistance and flow inductance of inertance tubes at high acoustic amplitudes for four different inner diameters, namely, 0.6, 1.0, 1.5 and 2.0 mm, for various tube lengths ranging from 100 to 1500 mm, at frequencies of 30, 40, 50, 60 and 70 Hz. These experiments were carried out under an operating mean pressure of 20 bar at ambient temperature. The experimental data were compared with the explicit solution to the linear momentum equation for small acoustic amplitudes. The data were fitted with the modification of coefficients in terms of the operating frequency and Reynolds numbers characterized by the amplitude of gas velocities. From these experimental results the difference of the flow resistance and flow inductance of inertance tubes at high and low acoustic amplitudes could be more clearly seen. Such analyses are very helpful for designing high frequency inertance tube systems.

Experimental results of an in-line type ITPTR were analysed by Park et al. [148]. They analysed the characteristics of in line type inertance tube pulse tube refrigerator in order to identify the main factors influencing the performance. The design parameters of the in-line IPTR are discussed by ARCOPTR program. The analysis includes the net cooling of IPTR with volume of the regenerator and the volume ratio of the regenerator to the pulse tube. The optimal conditions of in-line type IPTR, cool down characteristics according to the variations of the charging pressure, inertance tube volume, regenerator volume and pulse tube volume are measured by the experiment. By varying

the length and diameter of the regenerator and pulse tube, they have tested several ratios of V_{reg}/V_{pt}. The general conclusion is that as the volume of the regenerator is increased, the performance of the lowest temperature, cooling capacity and COP is improved. Cooling capacity is the highest at a charging pressure of 32 bar with 5W at 72 K. On the other hand, the COP of the in-line type IPTR has become the highest at the charging pressure of 21 bar with 0.018 W at 77 K.

Performance evaluation and parametric studies of an IPTR are carried out for different length-to-diameter ratios, with the Computational Fluid Dynamics (CFD) package FLUENT by Ashwin [149]. The study was extended to other types of PTRs, namely, the Orifice type Pulse Tube Refrigerator (OPTR), Double inlet type pulse tube refrigerator (DIPTR) and a PTR with parallel combination of inertance tube and orifice (OIPTR).

2.7 Co axial Pulse Tube Refrigerator

An experimental investigation of a coaxial pulse tube refrigerator was proposed by Xu et al. [150]. The pulse tube was 50 mm in length and 5 mm in inner diameter with an effective tube volume of about 0.4 cm^3. At no load a lowest temperature of 159.4 K with operating frequency of 11 Hz and a filling pressure of 11.9 bar was reported. To reduce the heat transfer between the pulse tube and the surrounding regenerator, nylon tube was used. Dang [151] developed a high-capacity single-stage coaxial pulse tube cryocooler. It produced 4.06 W at 60 K with the input power of 180 W. The larger pulse tube diameter of 14.2 mm was used and the evident orientation sensitivity was observed in the range of 55–65 Hz.

A high-power coaxial pulse tube refrigerator has been designed, fabricated and tested by Haruyama et al. [152] to meet the requirements of liquefaction and re-condensation of xenon gas for a large liquid xenon calorimeter. A feature of this pulse tube refrigerator is that a cylindrical regenerator is placed inside the pulse tube for space saving and easy fabrication. It provides a cooling power of 70 W at 165 K by using a 2.2 kW GM-type compressor. The cooling power performance of up to 120 W using a much larger compressor was also tested. The details of experimental design and fabrication of a compact co-axial type orifice pulse tube refrigerator was described by Richardson [153]. This could be integrated into many systems with less difficulty than a Stirling or G-M cryocooler. The performance of this design is analogous with that of a

'conventional' pulse tube of similar size. The influence of viscosity on the surface heat pumping mechanism also illustrated and claimed that miniaturization of the pulse tube is quite feasible provided the effect of viscosity is appreciated. Wang et al. [154] experimentally tested a liquid nitrogen precooled co-axial pulse tube refrigerator and reported a no load lowest temperature of 20 K at cold end. They also found that, the increase in the average pressure and the frequency could not improve the performance of the DIPTR. A multi bypass coaxial pulse tube refrigerator was designed, fabricated and tested to study the influence of DC flow on the refrigeration performance by Liang et al. [155]. Using a linear pressure wave generator of 1.06 cm^3 maximum swept volume, 81 K lowest temperature was achieved at 200 mW net cooling power with 28.4 W input power. Ding et al. [156] experimentally obtained the influencing factors on the lowest cooling temperature of a miniature co-axial pulse tube refrigerator. They reported that 16.7 Hz was the optimum operating frequency and also concluded that below 2% of the mole fraction of hydrogen the lowest refrigerating temperature could be achieved.

2.8 Multi stage Pulse Tube Refrigerator

Tanaka et al. [157] designed and tested a two stage pulse tube refrigerator fitted with two rotary valves. The performance was investigated by changing regenerator parameters. A lowest temperature of 20 K was achieved at the second stage cold end. For the cooling of the superconducting magnet a three staged pulse tube refrigerator has been fabricated and tested by Matsubara and Gao, [158] and a lowest no load temperature of the third stage, second stage and first stage pulse tube of 3.6 K, 47 K and 85 K respectively was achieved with the operating frequency of 2 Hz and the mean pressure of 15 bar. Experiments were performed by Gao and Matsubara [159] on several types of single-stage pulse tube refrigerators coupled with a Gifford-McMahon cryocooler to reach 4 K temperature. They claimed that it could possible to reach 4 K using a three stage pulse tube in which the phase shifter for each stage is located at room temperature.

Matsubara and Gao [160] illustrated the experimental design and operation of a three-stage pulse tube refrigerators with novel staging configuration. A valve compressor was used to generate pressure oscillation. A lowest temperature of 3.6 K and a cooling capacity of 119mW at 4.9 K were reported by this system. Tanida et al. [161] fabricated and tested a three-staged pulse tube refrigerator controlled by the

four-valve method. The minimum temperature reached at first stage was 115 K, at second stage was 29.5 K and at third stage was 2.75 K with the cycle frequency of 2 Hz. The optimum valve timing for the mass flow at the hot end of each stage pulse tube was also discussed. A 15 W at 70 K inertance pulse tube refrigerator based on cyclic simulation was designed and tested by Narayankhedkar and Gawali [162]. Different losses on refrigerating effect and power were incorporated to arrive at the net refrigeration effect and gross power requirements.

A two-stage pulse tube refrigerator was experimentally investigation by Wang et al. [163] using a rotary valve and a valved compressor. It was shown that a minimum no load temperature of 11.5 K and a cooling capacity of 1.3 W at 20 K were found at cold head at an operating frequency of 4.2 Hz and operating pressure of 15 bar. Using the numerical analysis Wang et al. [164], designed and constructed a two-stage DIPTR for cooling below 4 K. A lowest temperature of 2.23 K and cooling powers of 370 mW at 4.2 K and 700 mW at 5 K were observed using a three-layer second stage regenerator occupied with $ErNi_{0.9}Co_{0.1}$, ErNi and lead spheres while the average working pressure was 15.5 bar, the operating frequency was 1.0 Hz and the pressure ratio at the main inlet was 2.0. The authors claimed that the obtained cooling powers were satisfactory for several applications. In their next work [165] they designed, fabricated, tested and compared four configurations of two-stage pulse tube refrigerator. They recorded a net cooling power of 0.50 W at 4.2 K.

Thummes et al. [166] provided extensive experimental results for the three stage refrigerator consisting of a liquid nitrogen bath with heat exchangers and two subsequent pulse tube stages. Er_3Ni shot was used for the regenerator matrix in the coldest stage. The authors achieved a no load temperature of 2.13 K at third stage cold end. Experimental results presented by Chen et al. [167] shows the minimum attainable temperature of 3.1 K at the cold end of the second stage by a two stage pulse tube refrigerator using a novel phase shifter named a double-orifice. A lowest cooling temperature of 3.0 K was reported by Chen et al. [168] using double-orifice two-stage pulse tube refrigerator and reported that the thermodynamic efficiency of the pulse tube refrigerator could be increased by using the double orifice model, a more efficient phase shifter than the single orifice model. Wang [169] developed a computer program for numerical simulation of two stage pulse tube refrigerator taking into account the properties of the magnetic regenerative material, the non-ideal gas properties of ^4He and the heat transfer in the regenerator and heat exchanger. The

numerical model results were compared with the experimental results and found to be in good agreement. Using the similar numerical simulation method, the performance and internal process of a GM cooler and two configurations of two stage 4 K PTR were analysed [170]. The presence of a DC flow through the double inlet valve in a DIPTR was numerically observed.

The lambda transition is the obstacle for ^{4}He to reach below 2 K temperature. Theoretically Xu et al. [171] found that the above problem could be avoided by using ^{3}He. Subsequently the performance of the 4 K pulse tube refrigerator could be improved significantly replacing ^{4}He by ^{3}He and a lowest temperature of 1.78 K was obtained at the cold head in a three stage pulse tube refrigerator. Atrey et al. [172] developed a computer program for a three-stage, free displacer, split type Stirling cryocooler and experimentally validated it. Ju [173] proposed a numerical model based on mixed Eulerian-Lagrangian for calculating and understanding the internal working phenomenon and the variations of dynamic parameters of a two-stage PTR. The PTR was designed for below 4 K at the cold end. The physical factors such as pressure drop, thermal properties of helium, multi-layered magnetic regenerative materials, and heat transfer in the regenerator and heat exchangers were taken into account. A two stage 4 K PTR was experimentally introduced by Wang [174] for helium liquefaction purpose. The liquefaction rate was improved by precooling the inefficiency of the second stage regenerator. They claimed a helium liquefaction rate of 4.8 l/day for a power consumption of 4.6 kW.

Qiu et al. [175] used a ceramic magnetic regenerative material $GdAlO_3$ to increase the COP and cooling power of a 4 K two-stage pulse tube cooler. They reported a cooling power of 200 mW at 2.8 K, 300 mW at 3.13 K, and 400 mW at 3.70 K at the cold head of second stage with a 4.8 kW input power. Tanaeva and Waele [176] provided extensive experimental results for a three-stage pulse-tube refrigerator. It was compact in shape and light weight, required small input power and uses a small amount of working gas and regenerator material. In addition the PTR was flexible and convenient for modifications. Using ^{3}He as the working fluid the minimum attainable refrigeration no-load temperature of 1.73 K and a cooling power of 124 mW at 4.2 K was achieved. Using SAGE-software simulation Dietrich and Thummes [96] optimised the operating conditions and cold head geometry of a two-stage Stirling-type U-shape pulse tube cryocooler and conducted experiments. They achieved a minimum attainable

no load temperature 13.7 K and refrigeration power of 12.9 W at 25 K with an input power of 4.6 kW.

A valveless linear compressor was developed to drive a two-stage pulse tube cryocooler by Yan et al. [177]. They discussed the design, manufacturing and experimental testing of linear compressor used for the two stage pulse tube refrigerator and a lowest temperature of 14.2 K was achieved using this compressor. Yan et al. [178] conducted an experimental study on a two stage stirling type pulse tube cryocooler driven by a linear compressor. The compressor was a moving magnet type and had dual-opposed-piston configuration, in which a plate spring was used. By providing a pressure ratio of 1.3 – 1.5, a temperature of 14.2 K was achieved at the cold head of second stage.

Sun et al. [179] designed and manufactured a high-power two-stage stirling-type PTC having U-shaped configuration in both the stages and experimentally achieved no-load refrigeration temperature of 29.6 K at 55 Hz and 27.1 K at 40 Hz. They suggested that the regenerator streaming problem in a large cold head could be avoided by arranging a number of smaller PTC cold heads parallelly on the same compressor. Kasthurirengan et al. [13] carried out theoretical and experimental studies of a two-stage pulse tube cryocooler (PTC) to achieve a temperature below 3 K. The working fluid used was helium. They used stainless steel meshes along with lead (Pb) granules and combination of Pb, Er_3Ni and $HoCu_2$ in layered structures as the first and second stage regenerator materials and reported a no-load temperature of 3 K.

2.9 Other type Pulse Tube Refrigerator

The structural characteristics and the mechanical performance of a co-axial PTR with a multi-bypass was experimentally investigated by Cai et al. [180] . The details of experimental analysis and the results of the multi-bypass method were well described by the authors. It was also reported that the lowest temperature at the cold end using the co-axial pulse tube refrigerator with multi-bypass was 33 K. Wang et al. [181] experimentally investigated the effects of the middle bypass valve on the performance of the multi-bypass pulse-tube refrigerator (MPTR) and also determined the minimum attainable temperature. It was also reported that the multi-bypass could reach a lower temperature than DIPTR. The authors found a lowest temperature of 23.8 K and a cooling load of 3.6 W at 77 K with the MPTR. It was shown that the middle bypass

section behaves as the second refrigerate part in the MPTR. The advantage of a four valve pulse tube refrigerator is that it does not require a heat exchanger at the hot end of the pulse tube and no necessity of the reservoir. Kaiser et al. [182] applying the first law of thermodynamic for an open systems to sub volumes of a four-valve pulse tube refrigerator investigated the ideal cold generating process. They reported that the COP increases for a decrease in the ratio of high to low pressure. For gas separation and liquefaction a new type of pulse tube refrigerator with low temperature switching valve, was proposed by Liang et al. [183]. Instead of a regenerator a recuperative heat exchanger was used and instead of an orifice a switching valve was mounted in the new type of PTR model. There was a 40 % increase in adiabatic efficiencies comparing to primarily used cryocoolers and also investigated the methods for increasing the adiabatic efficiency.

To increases the efficiency of the pulse tube refrigerator, two or more reservoirs were attached at the hot end of the pulse tube through the valves. The details of working principle and basic mechanism for the active-buffer pulse tube refrigerator (ABPTR) were numerically investigated by Zhu et al. [11]. They reported the cooling capacity at 80 K at 145 W using two- reservoirs, 160 W using four buffers. Also, they calculated that the Carnot percent at 80 K is 12% using the two reservoirs and 13% using three reservoirs and the four reservoirs.

To enhance the performance of a single stage PTR with the aid of various simplifying assumptions a detailed thermodynamic investigation of the working process of an active valve pulse tube refrigerator was proposed by Yuan and Pfotenhauer [184]. It was reported that the performance of the active valve pulse tube refrigerator was better than that of an orifice pulse tube refrigerator. The idea of two double-inlet was suggested by Luwei et al. [185] and compared the performance with multi-bypass PTR and DIPTR. From the experiment, a lowest temperature of 37 K with two double inlet valves and 50 K with one double inlet valve was reported. Pan et al. [186] conducted two sets of experiments for the single-stage valve pulse tube refrigerators. The first one was the 4-valve and the other one was the active buffer mode and compared the performance. They found a no-load temperature was achieved at 24.6 K by the 4-valve configuration, whereas 100 W at 57 K were achieved in both type models with an input power of 7 kW.

Brito and Peskett [187] introduced a prototype of miniature free warm expander pulse tube. This configuration was similar to an OPTR one, the only difference was the orifice and the reservoir replaced by a secondary piston. It was reported that the secondary piston could be driven with the appropriate amplitude and phase by the pneumatic force of the pressure cycle. The loss mechanism in refrigerator also discussed. Dai et al. [12] proposed a new type PTR called V-M type pulse tube refrigerator. A thermal compressor similar to that of a V-M cryocooler was used instead of mechanical compressor, which was the main difference from the Stirling type or G-M type pulse tube refrigerator. A cool down temperature of 5.25 K was achieved by pre-cooling the hot end of the third regenerator to 19 K by another ordinary DIPTR. A single-stage DIPTR with two antiparallel needle valves was designed and tested by Qui et al. [188] to obtain the lowest attainable cooling temperature range of 15 – 40 K. The magnetic material Er_3Ni was used as the regenerative material to improve the efficiency of the regenerator. With an input power of 6 kW, a lowest refrigeration temperature of 12.6 K was obtained, at no load condition.

2.10 Optimisation of Pulse Tube Refrigerator

Jafari et al. [189] proposed a genetic algorithm (GA) optimisation method, coupled to a one-dimensional finite volume method and implemented as a computer program for the modeling and optimization of a Stirling-type pulse tube refrigerator. The multi-objective optimization procedure was applied to provide the optimized design parameters such as charge pressure, operating frequency, and temperature of after-cooler as well as swept volume of compressor. The procedure was selected to obtain the maximum coefficient of performance (COP) and the minimum cooling temperature (T_{cold}) as two objective functions. The frequency of refrigerator is found as the most sensitive factor which affects the COP even with little changes.

In the last two decades, several researchers have focussed their attention on the optimization of the pulse tube refrigerator's performance. de Waele [190] proposed the optimization of the pulse tube refrigerator and reported that under certain conditions the optimum state found, if the variation of the pressure in the pulse tube is proportional to the variation of the compressor pressure. Razani et al. [191] optimized the orifice pulse tube refrigerator by the use of a thermodynamic model based on the exergy flow in a pulse tube refrigerator. The model consists of a regenerator, pulse tube and a phase shifter. They reported that, for no void in the regenerator, the optimum

state can be found if the mass flow rate and pressure are in phase at the cold side of the regenerator and for a void in the regenerator the optimum state can found if the phase shift at the cold side of the regenerator can be controlled by the phase shifter to get significant improvement in both the cooling capacity and efficiency. Ki and Jeong [192] optimised the pulse tube refrigerator driven by a single-piston linear compressor by using the slit type heat exchanger instead of the mesh type heat exchanger. It gives an optimum performance of 3.5 Watt at 60 K. Jafarin et al. [193] studied the optimum design of a pulse tube refrigerator based on the second law of thermodynamics. They have reported an optimum cooling power of 110 W at a minimum temperature of 80 K near the cold head. In order to achieve the maximum COP or cooling capacity, Ghahremani et al. [194] optimised the performance of a DIPTR and reported that the optimum COP and cooling capacity was 0.07 and 335 W respectively.

2.11 Review of response surface methodology on heat transfer field

Most of the optimisation studies concerned with the effects of parameters on the cryocooler analysis have been performed using a one-parameter-at-a-time method, where this method provides one parameter at a time instead of all simultaneously. This method is time consuming and expensive. To cross over such problems, response surface methodology (RSM) which is one of the statistical design tools can be used for prediction of interaction between many parameters and for process optimization also. RSM defines the effect of independent variables, alone or in combination, on the process [195]. RSM has been tested to be a powerful statistical tool for optimization of thermal and fluid flow processes in many cases [196-208]. Optimization of thermo acoustic prime mover was conducted by Hariharan et al. [206] using response surface methodology. The influence of stack position and its length, resonator length, plate thickness, and plate spacing on pressure amplitude and frequency in a thermos acoustic prime mover was investigated. They used Delta-EC software package for simulation purpose. In their next work [205] using similar solution method they optimized the parameters like frequency, stack position, stack length, and plate spacing involving in designing thermo acoustic refrigerator using the Response Surface Methodology (RSM).

Chapter 3

REVIEW OF MATHEMATICAL ANALYSIS OF PULSE TUBE REFRIGERATOR MODELS

3.1 Introduction

The simplicity of PTR makes it more advantageous than other cryocooler. It has no moving part at its low temperature end, which makes it high reliability, low vibration, long life time, small size and weight. The transport phenomenon inside the PTR is very complicated and the details of the mechanism underlying their performance are not well understood due to oscillation flow and presence of a porous region inside it. So it is important to construct a proper design of each component. Hence it is very essential to understand the thermodynamics of porous media and oscillating flow inside the PTR.

This chapter is intended to the derivation of heat and fluid flow analysis for pulse tube refrigerator using various proposed mathematical analysis. Various mathematical methods proposed by different researchers such as enthalpy flow model, phasor analysis, electrical analogy etc. In this chapter we discussed few mathematical models which are commonly used for analysing pulse tube refrigerator.

3.2 Operational Principle of Pulse tube refrigerator

It is essential to understand where the heat rejection and absorption occurs and how the cyclic process operates in a PTR. Before understanding the operating principle of PTR, it is very essential to understand the operating principle of a conventional refrigeration system. The vapour compression cycle shown in Figure 3.1 operates in a steady flow process where heat is transported from the evaporator to the condenser by a constant and steady mass flow rate. The operating principles of PTRs are rather different from conventional refrigeration systems. The methods of extracting heat from the cold region to the hot region are different. The PTR generally based on regenerative type heat exchanger where as conventional refrigeration systems based on the recureptive heat exchanger.

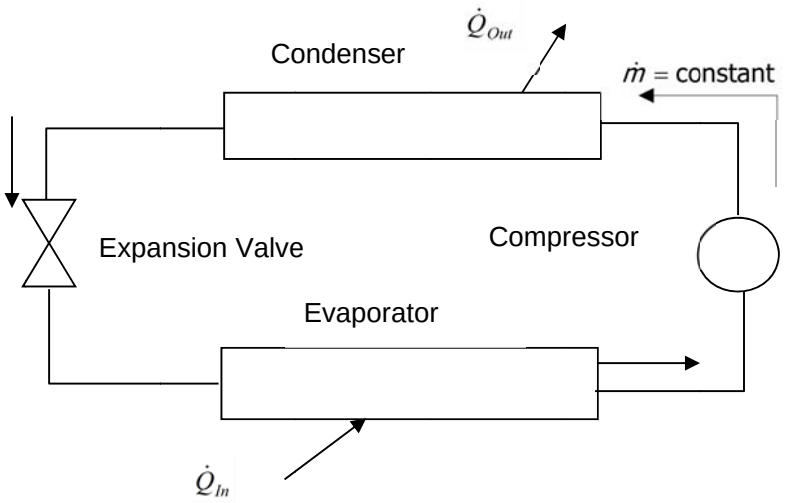

Figure 3.1 Schematic diagram of the simple vapour compression cycle

In the pulse tube refrigerator the cooling process is due to the oscillating pressure inside the system. The heat is absorbed and rejected at the heat exchangers which are located at both ends of the pulse tube during cyclic process. Because PTR operates in steady-periodic mode, the thermodynamic properties such as enthalpy flow, $\langle \dot{H} \rangle$, heat flow, $\langle \dot{Q} \rangle$, and power $\langle \dot{W} \rangle$ are calculated in the form of cyclic integrals. The suitable instant thermodynamic properties are integrated over the whole cycle and divided by the period of that cycle to obtain the cyclic averaged quantity. For illustration, the compressor power is estimated from the following integration.

$$\langle \dot{W} \rangle_{PV} = f\oint P\frac{dV}{dt}dt = \frac{1}{\tau}\oint P(t)\dot{V}(t)dt \qquad (3.1)$$

Where f is frequency, τ is the period of the cycle, P and V, are instantaneous pressure and volume respectively. The average enthalpy flow over one cycle $\langle \dot{H} \rangle$ and average heat flow rate, $\langle \dot{Q} \rangle$, are also calculated similarly.

3.3 Pulse Tube Refrigerator analysis Methods

To analyse the pulse tube refrigerator models the solution methods are categorised into three major groups [209]

1. First Order Analysis

(i) Surface Heat Pumping

(ii) Enthalpy flow Analysis

(iii) Phasor Analysis

2. Second Order Analysis

(i) Thermodynamic Non-symmetry effect

(ii) Approximate Model (Adiabatic and Isothermal Models)

3. Third Order Analysis

(i) Numerical Methods

(ii) CFD Analysis

3.3.1 Mass flow Analysis

Assuming ideal gas as the working fluid and pulse tube behaves adiabatically during simulation, the mass flow rate is not same along the pulse tube. The mass accumulation takes place due to pressure oscillation. Applying the first law of thermodynamics to the control volume drawn around the pulse tube section as shown in Figure 3.2.

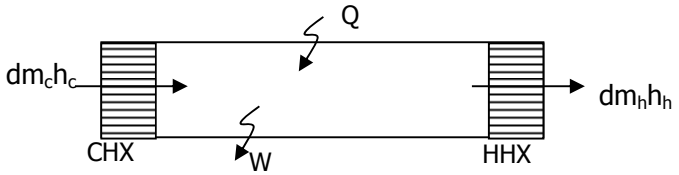

Figure 3.2 Energy balance for pulse tube section.

$$dm_c h_c + dQ = dm_h h_h + dW + (\Delta U)_\sigma \tag{3.2}$$

For adiabatic pulse tube dQ=0. On time rate Equation (3.2) becomes

$$\left.\begin{aligned}
\frac{dW}{dt} &= -\frac{(\Delta U)_\sigma}{dt} + \frac{dm_c}{dt}h_c - \frac{dm_h}{dt}h_h \\
p\frac{dV}{dt} &= -C_v\left(\frac{dm_c}{dt}T_c - \frac{dm_h}{dt}T_h\right) + C_p\left(\frac{dm_c}{dt}T_c - \frac{dm_h}{dt}T_h\right) \\
p\frac{dV}{dt} &= R\left(\frac{dm_c}{dt}T_c - \frac{dm_h}{dt}T_h\right) \\
p\frac{dV}{dt} &= R\left(T_h\frac{dm_h}{dt} - T_c\frac{dm_c}{dt}\right)
\end{aligned}\right\} \quad (3.3)$$

For an adiabatic system

$$pV_t^{\gamma} = \text{constant}$$

On differentiating the above equation with time gives

$$\gamma p\frac{dV_t}{dt} + V_t\frac{dp}{dt} = 0 \quad (3.4)$$

Substituting $\frac{dV_t}{dt}$ from Equation (3.4) in equation (3.3) yields

$$\frac{dm_c}{dt} = \frac{V_t}{RT_c\gamma}\frac{dp}{dt} + \frac{T_h}{T_c}\frac{dm_h}{dt} \quad (3.5)$$

Equation (3.5) may be written as

$$\dot{m}_c = \frac{V_t}{RT_c\gamma}\frac{dp}{dt} + \frac{T_h}{T_c}\dot{m}_h$$

$$\dot{m}_c = \frac{V_t\dot{P}}{RT_c\gamma} + \frac{T_h}{T_c}\dot{m}_h \quad (3.6)$$

The above equation can be rewritten as,

$$\dot{m}_c = \dot{m}_p + \frac{T_h}{T_c}\dot{m}_h \quad (3.7)$$

Where ṁ is the corresponding mass flow rate due to pressure oscillation.

In pulse tube, pressure and temperature variations are given as

$$P = P_0 + P_1\cos(\omega t) \quad (3.8)$$

$$T = T_0 + T_1\cos(\omega t) \quad (3.9)$$

Mass flow rate at the hot end is proportional to pressure change

$$\dot{m}_h \ \alpha \ \Delta P$$

Where $\Delta P = P_0 + P_1 \cos(\omega t) - P_0 = P_1 \cos(\omega t)$

So hot end mass flow rate can be expressed as

$$\dot{m}_h = C_1 P_1 \cos(\omega t) \tag{3.10}$$

Substituting in Equation (3.9) and it can be expressed as,

$$\dot{m}_c = \frac{\omega V_t}{R T_c \gamma} P_1 \cos(\omega t + \pi/2) + \frac{T_h}{T_c} C_1 P_1 \cos \omega t \tag{3.11}$$

3.3.2 Enthalpy Flow Analysis

The enthalpy flow model for PTR was proposed by Radebaugh [10]. It is based on the application of first law and second law of thermodynamics to an open system. In this method each individual component are considered separately as an open system. The schematic diagram of an orifice pulse tube refrigerator along with energy flow at various components is shown in Figure 3.3. It is shown that the heat absorbed at the cold heat exchanger (CHX) from the system and the heat of compressor is rejected at after cooler and system heat is rejected at hot end heat exchanger (HHX).

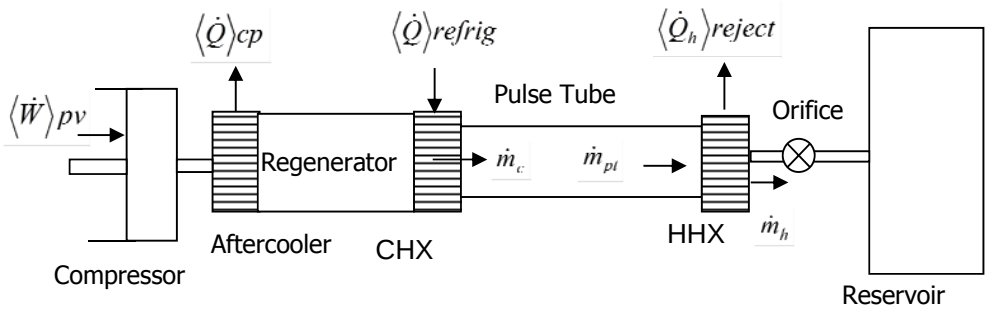

Figure 3.3 First law of thermodynamics energy balance for an OPTR.

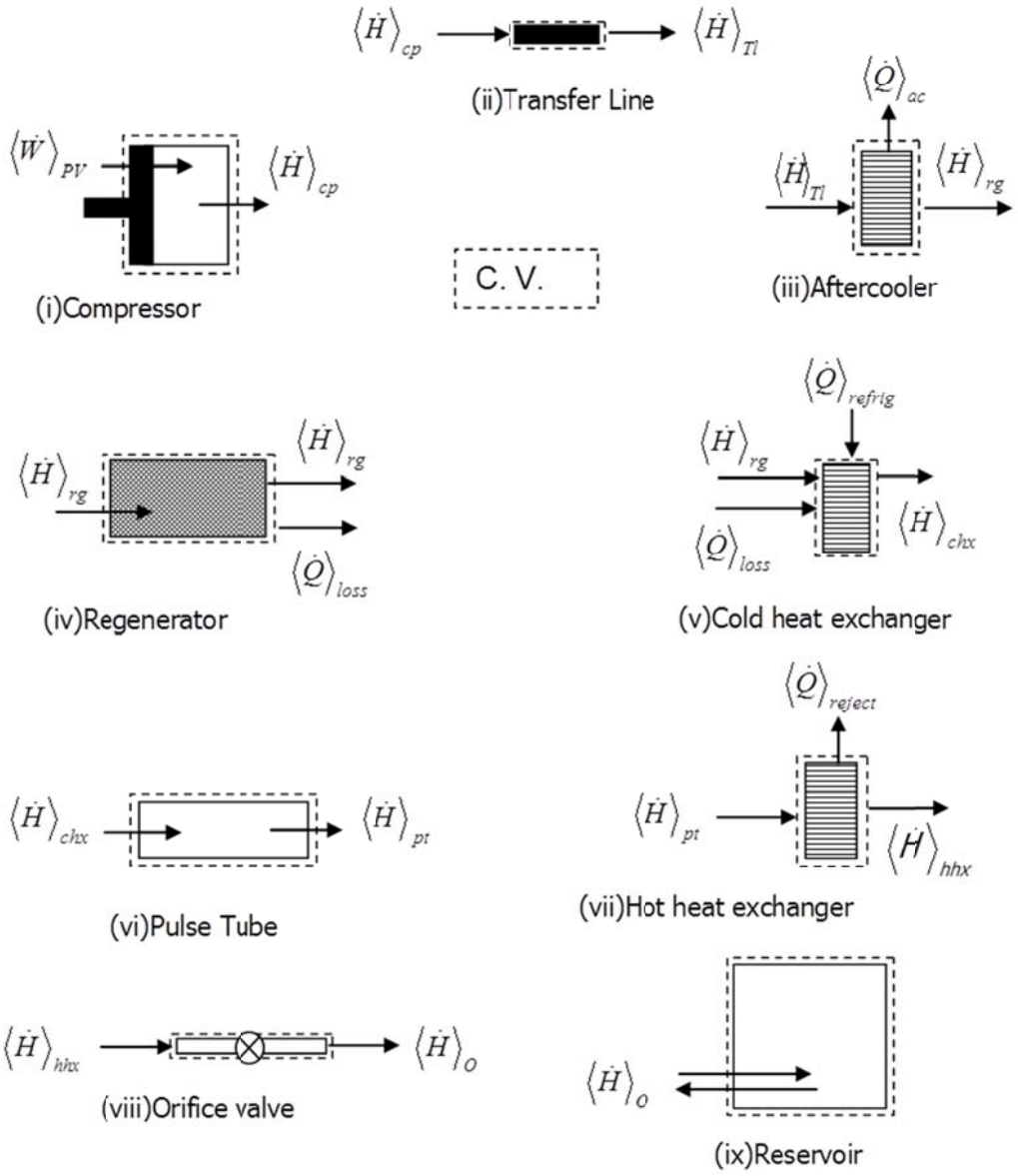

Figure 3.4 Energy balance of system components in an OPTR.

The after cooler rejects heat, which is produced during the compression process at the compressor. The rest of the energy that is not rejected through the after cooler is carried through by the enthalpy flow $\langle \dot{H} \rangle_{rg}$ in the regenerator. This can be seen in the component energy balance schematics shown in Figure 3.4. The regenerator enthalpy

flow $\langle \dot{H} \rangle_{rg}$, the additional refrigeration load $\langle \dot{Q} \rangle_{refrig}$, and the heat flow representing all the losses, $\langle \dot{Q} \rangle_{loss}$ (such as gas conduction, solid matrix conduction, and dispersion), are all absorbed at the CHX, therefore,

$$\langle \dot{H} \rangle_{chx} = \langle \dot{Q} \rangle_{refrig} + \langle \dot{H} \rangle_{rg} + \langle \dot{Q} \rangle_{loss} \tag{3.12}$$

The enthalpy flows from the cold heat end of the pulse tube to the hot end of pulse tube and at the HHX heat is rejected to the ambient. The rest enthalpy which has not been rejected from HHX transported to the reservoir through the orifice as shown in Figure 3.4.

The average enthalpy flow over a cycle by assuming ideal gas flow is given by

$$\langle \dot{H} \rangle_{chx} = \frac{C_p}{\tau} \int_0^{\tau} \vec{m} \cdot \vec{T} \; dt = \frac{C_p}{\tau} \int_0^{\tau} mT \cos\theta \; dt \tag{3.13}$$

Where τ is the period of the cycle, C_p is the heat capacity. The phasor quantities, $\vec{m}$ and $\vec{T}$ are mass flow rate and temperature respectively. The above equation, illustrates that if an oscillating mass flow rate $\dot{m}$ is in phase with the oscillating gas temperature T then a net enthalpy flow exists in the pulse tube flowing from the cold end to the hot end (i.e., $\langle \dot{H} \rangle_{chx}$ >0). Note that $\dot{m}$ >0 when flow is from left to right.

On the other hand, if an oscillating mass flow rate $\dot{m}$ is out of phase with oscillating gas temperature T, then little or no enthalpy flow will exist in the pulse tube, which results in minimum cooling. Figure 3.5 depicts two examples of phase shift between gas temperature and mass flux. The first example in Figure 3.5 (a) demonstrates a case where the mass flow rate and the temperature oscillations are about 90 degrees apart. In this condition, very small or no enthalpy flow takes place. With the temperature and the time mass flow rate being 90 degrees out of phase, one phasor quantity will always be minimum when the other one is at its peak. Thus, out of phase relationships tend to produce poor refrigeration due to minimum enthalpy flow in the pulse tube. On the other hand, if the mass flow rate and the temperature oscillations are in phase as illustrated in the second example (Figure 3.5 (b)), positive enthalpy flow can exist in the pulse tube. Thus, in-phase and out -phase are the two extreme conditions.

For perfect intercooler regeneration and without any loss,

$$\left\langle \dot{H}_{rg} \right\rangle = 0 \text{ and } \left\langle \dot{Q} \right\rangle_{loss} = 0$$

Refrigerating effect is obtained as

$$\dot{Q}_{refrig} = \left\langle \dot{H} \right\rangle_{chx} = \frac{1}{\varsigma} \int_0^{\varsigma} \dot{m}_c T dt \tag{3.14}$$

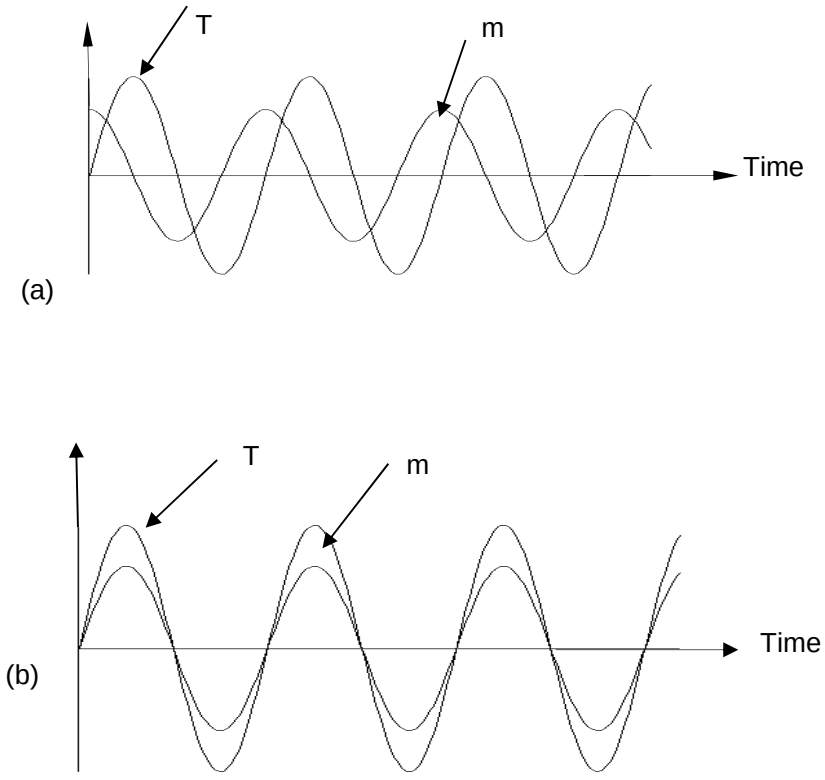

Figure 3.5 Phase shift relation for gas temperature and mass flow rate.

3.3.3 Electrical Analogy

Based on electrical analogy Roach and Kashani [8] formulated a model that characterizes the components of an ITPTR. The regenerator and the inertance tubes are represented by discrete, distributed volumes. This model can predict the phase angle between the pressure and mass flow; however, a disadvantage of this electrical analogy

approach is that it is not possible to accurately deal with the presence of temperature gradients in the actual cooler.

The following equations define the relations between electrical current, I and voltage, V, for the cases of a resistor of resistance, R. an inductor of inductance, L., and a capacitor of capacitance, C.

Resistor : V = IR

Inductor: $V = L\frac{dI}{dt}$

Capacitor: $\frac{dV}{dt} = \frac{I}{C}$

Evaluating the 1-D momentum conservation equation for the flow in a tube of radius, r, and similar relations can be found for gas flow (analogous to current) and pressure (analogous to voltage) in the elements of a pulse tube cryocooler

$$\rho\frac{\partial u}{\partial t} = -\frac{\partial P}{\partial x} - \frac{\mu . u}{K_p} \tag{3.15}$$

Where P is the pressure, ρ is the gas density, u is the average velocity in the tube. μ is the viscosity and K_p is the Darcy permeability.

Substituting the relationship between volumetric flow rate, U, and velocity $u = \frac{U}{\pi r^2}$, and arranging terms yields

$$-\frac{\partial P}{\partial x} = \frac{\rho}{\pi r^2}.\frac{\partial u}{\partial t} + \frac{\mu . U}{\pi r^2 K_p} \tag{3.16}$$

If these parameters are independent of the distance x, along the tube, then the equation can be integrated along the tube for its entire length γ, yielding:

$$-\Delta P = \frac{\rho\lambda}{\pi r^2}.\frac{\partial u}{\partial t} + \frac{\lambda\mu . U}{\pi r^2 K_p} \tag{3.17}$$

Using the above analogy between pressure-voltage and mass flow-current then comparing above equation it is found that the fluid flow analogy of resistance is:

$$R = \frac{\mu\lambda}{\pi r^2 K_p} \tag{3.18}$$

and is in series with the fluid flow analogy of inductance with value:

Inductance of the Inertance tube $L = \frac{\rho\lambda}{\pi r^2} = \frac{\rho\lambda}{A}$

The term "inductance' for the electrical circuit changes to the term "inertance" for the fluid flow case.

From the ideal gas law for volume flowing in an isothermal volume, V_t the pressure rise will be:

$$\frac{\partial P}{\partial t} = \frac{P_{av} U}{V_t} \tag{3.19}$$

The above equation is analog to capacitor equation so analogous capacitance value

$$C = \frac{V_t}{P_{av}} \tag{3.20}$$

The Figure 3.6 and Figure 3.7 shows the impedance of OPTR and ITPTR respectively.

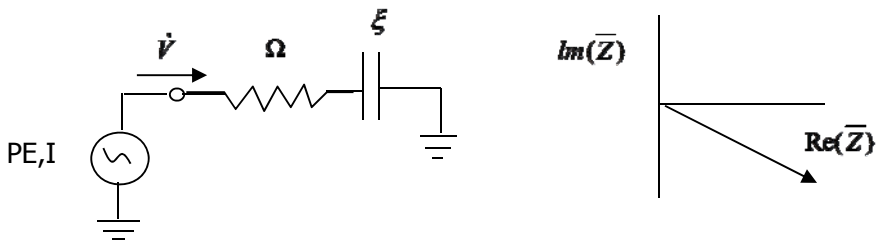

Figure 3.6 Impedance for OPTR.

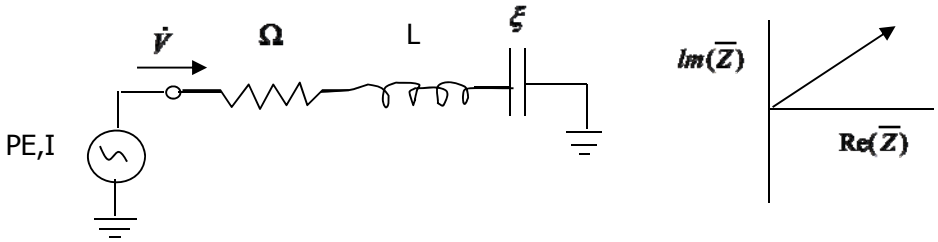

Figure 3.7 Impedance for ITPTR.

OPTR is equivalent to $\Omega - \xi$ circuit as shown in Figure 3.6. From Equation (3.21) it is clear that the impedance Z is always negative for OPTR. In OPTR the impedance phasor lies in the fourth quadrant, hence the mass flow rate (electrical current) leads pressure (electrical voltage). The waveforms of the current and voltage are shown in Figure 3.8.

$$\text{Impedance} = \mathrm{Z} = \Omega + \frac{1}{j\omega\xi} = \sqrt{\left[\Omega^2 + \left(\frac{1}{\omega\xi}\right)^2\right]} \qquad (3.21)$$

ITPTR is equivalent to $\Omega - L - \xi$ circuit as shown in Figure 3.7. From equation, it is clear that the impedance Z could be positive, or negative. In case of ITPTR the impedance may lie in first or fourth quadrant depending upon the value of L and ξ. Those values depend on the dimension of the inertance tube and the reservoir. The mass flow rate will lead pressure if the impedance phase angle is negative and mass flow rate will lag if this phase angle is positive.

$$\text{Impedance} = \mathrm{Z} = \Omega + j\left(\omega L - \frac{1}{\omega\xi}\right) = \sqrt{\left[\Omega^2 + \left(\omega L - \frac{1}{\omega\xi}\right)^2\right]} \qquad (3.22)$$

Figure 3.8 shows the phase lag representation of OPTR. This depicts that Voltage V_m lags current I_m by phase angle θ.

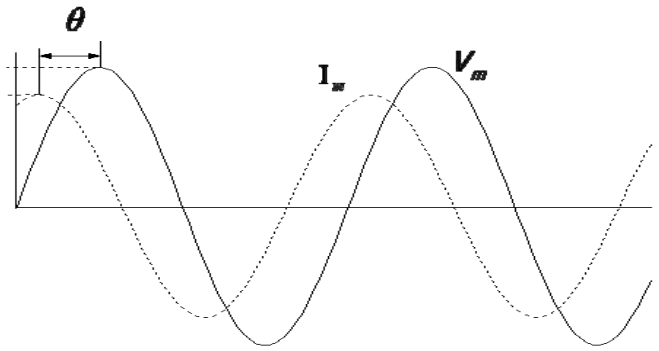

Figure 3.8 Phase lag representation of OPTR

The acoustic power or PV power generated in the compressor is transmitted to the cold end of pulse tube through the regenerator. The majority of the losses in a pulse tube refrigerator system are associated with the regenerator; these losses are due to axial thermal conduction, pressurization of the void volume, power dissipation associated with frictional pressure drop, and thermal ineffectiveness. Among them acoustic power loss and thermal ineffectiveness are the two major loss in the regenerator which are directly related with the amplitude of the mass flow rate in the regenerator. From this concept it can be decided that the most efficient pulse-tube will

offer the largest amount of acoustic power to the cold end for the smallest amount of mass flow rate.

The time averaged $P\dot{V}$ power or acoustic power transfer through the regenerator is given as [210]:

$$\dot{W} = \underset{(1^{st})}{P_1\dot{v}} = \underset{(2^{nd})}{\frac{1}{2}P_1\dot{v}\cos\theta} = \underset{(3^{rd})}{\frac{1}{2}P_1\frac{|\dot{m}|}{\rho}\cos\theta} = \underset{(4^{th})}{\frac{1}{2}RT_{ra}\frac{P_1}{P_{avg}}|\dot{m}|\cos\theta} \qquad (3.23)$$

Where P_1 is the oscillating component of pressure, $\dot{V}$ is the volumetric flow rate, θ the phase between pressure and mass flow, $\dot{m}$ is the mass flow rate, ρ is the average density, R is the specific gas constant of the operating gas, T is the average temperature, P_{avg} is the average pressure, and the modulus denote the absolute value. The term after the first equal sign in the above equation represents the general expression for acoustic power, the cyclic integral of the instantaneous product of pressure and volumetric flow rate at the cold end of the regenerator. The second term is related to the harmonic approximation of this integral; the pressure and volumetric flow rate are taken to be pure sinusoidal and θ is the phase difference between them. On substituting the ratio of mass flow rate to nominal or average density for volume flow rate we get the third term. Finally, the fourth expression is obtained by using the ideal gas to substitute for the average density.

From Equation (3.23) it is understandable that the PV power is proportional to the mass flow rate that is in phase with the pressure variation. In the context of phasor, the acoustic power is given by the product of the projection of the mass flow vector onto the pressure wave vector and the magnitude of the pressure variation. Throughout the refrigerator acoustic power flow is constant, but the regenerator losses are proportional to the magnitude of the mass flow in the regenerator. Hence, in order to minimize the ratio of the regenerator losses to the transmitted acoustic power, the phase (θ) should be minimized within the regenerator (not at the inlet to the expansion space). The mass flow rate entering the hot end of the regenerator will tend to lead the mass flow rate leaving the cold end of the regenerator due to the compliance associated with the void volume in the regenerator. The optimum condition can be achieved when the phase between pressure and mass flow rate become zero near the midpoint of regenerator. The phase between the mass flow rate and pressure $-\theta^{o}$ (mass flow rate leads the pressure) at the hot end of the regenerator and θ^{o} (mass flow rate lags the pressure) at the cold end of the regenerator. Phase shift is a function of void volume

and flow resistance associated with regenerator. The optimum phase-relations for a pulse tube refrigerator with inertance tube and reservoir is shown in Figure 3.10. Note that the use of the inertance tube allows a negative phase (the pressure leads the mass flow rate) at the hot end of the pulse tube. The mass flow rates in the components of the simplified pulse tube refrigerator (pulse tube, regenerator, and compressor) are presented in phasor diagram. The phasor notation shows magnitudes and phase angle of the mass flow rates at various locations in the system relative to the pressure variation (note that the pressure is assumed to be spatially uniform in the system).

3.3.4 Phasor Analysis

A phasor diagram for a pulse tube refrigerator (PTR) is a vectorial representation of mass flow rate, pressure, and temperature at different locations as a function of time. By using a phasor diagram, the operation of different types of pulse tube refrigerators can be well understood. The phasor analysis helps to understand the importance of phase difference between mass flow rate at the cold end and the pressure pulse in the pulse tube refrigerator. The refrigerating effect for different types of PTR strongly depends on the phase shift arrangement and also on the phase difference.

3.3.5 Phasor diagram of BPTR

A vector representation of Equation. (3.7) is known as phasor diagram. The phasor diagram for basic pulse tube refrigerator is shown in Figure 3.9. The figure shows both the mass flow and the pressure phasors. For a BPTR there is no orifice valve and reservoir. The hot end of the pulse tube is closed, so hot end mass flow rate is zero $(\dot{m}_h = 0)$. The cold end mass flow rate $\dot{m}_c$ is at right angle to pressure vector. Since the pressure in the pulse tube is 90° from the mass flow there is no refrigeration (Ideally refrigerating effect for BPTR is zero). In practice, heat transfer between the gas and the pulse tube wall due to surface heat pumping causes a small phase shift. This is due to pressure drop for the associated gas flow, which result small refrigeration. Under such condition, the compressor work is compensated by the regenerator loss.

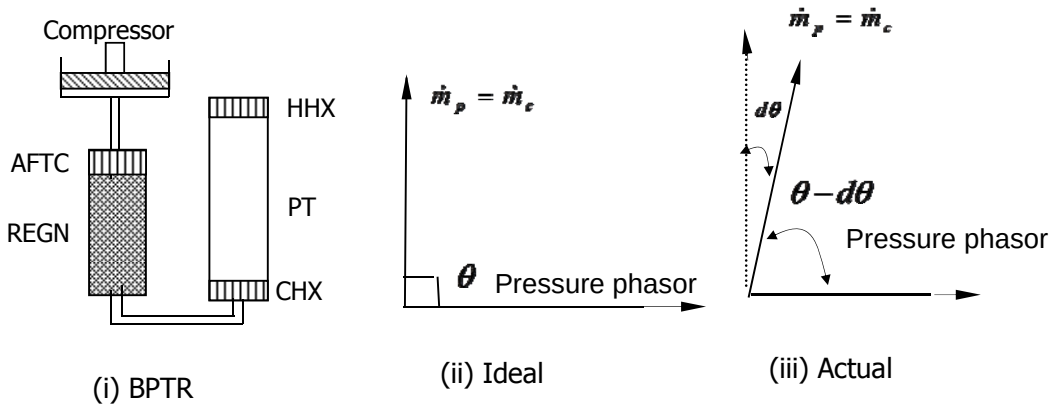

Figure 3.9. Phasor representation of cold end mass flow rate and pressure for BPTR.

3.3.6 Phasor diagram of ITPTR

The phase-relations between the mass flow rates and pressure in Figure 3.10 can be understood by examining equations (3.6) and (3.7). Recall that the pressure phasor lies on the real axis. Because the pressure and its time derivative are sinusoidal and the pressure everywhere in the pulse tube is the same, the rate at which mass is accumulated in the volumes represented by the pulse tube, regenerator and the compressor must lag the pressure by 90^o and therefore be in the direction of the imaginary axis. Through proper selection of the geometry of the inertance tube and reservoir, the phase at the warm end of the pulse tube can be set to essentially any value, positive or negative. Thus the desired 0^o phase is created at the midpoint of the regenerator and the magnitude of the average mass flow rate processed by the regenerator (the average of $\dot{m}_h$ and $\dot{m}_c$) is minimized for a given acoustic power. Minimizing the magnitude of the average mass flow rate in the regenerator results in smaller regenerator losses and allows a larger fraction of the acoustic power to be converted to refrigeration power.

3.3.7 Phasor diagram of OPTR

The phasor diagram for an orifice pulse tube refrigerator is shown in Figure 3.11. The orifice coupled to a reservoir allows for only resistive and capacitive impedance (there is no possibility of inductive impedance). Therefore, the mass flow rate at the warm end of the pulse tube can never lead the pressure, as it did in for an

ITPTR as shown in Figure 3.10. Rather, the best possibility occurs when the reservoir volume is made infinitely large which forces the mass flow rate at the end of the pulse tube to be in phase with the pressure; this is seen in Figure 3.11 by the fact that the mass flow rate lies on the real axis. It can be clearly seen from Figure 3.11 that the average mass flow rate in the regenerator for the same acoustic power is much higher than in Figure 3.10. This discussion motivates the need for inertance tubes in high efficiency pulse tube systems in order to minimize regenerator losses by providing the optimum phase shift.

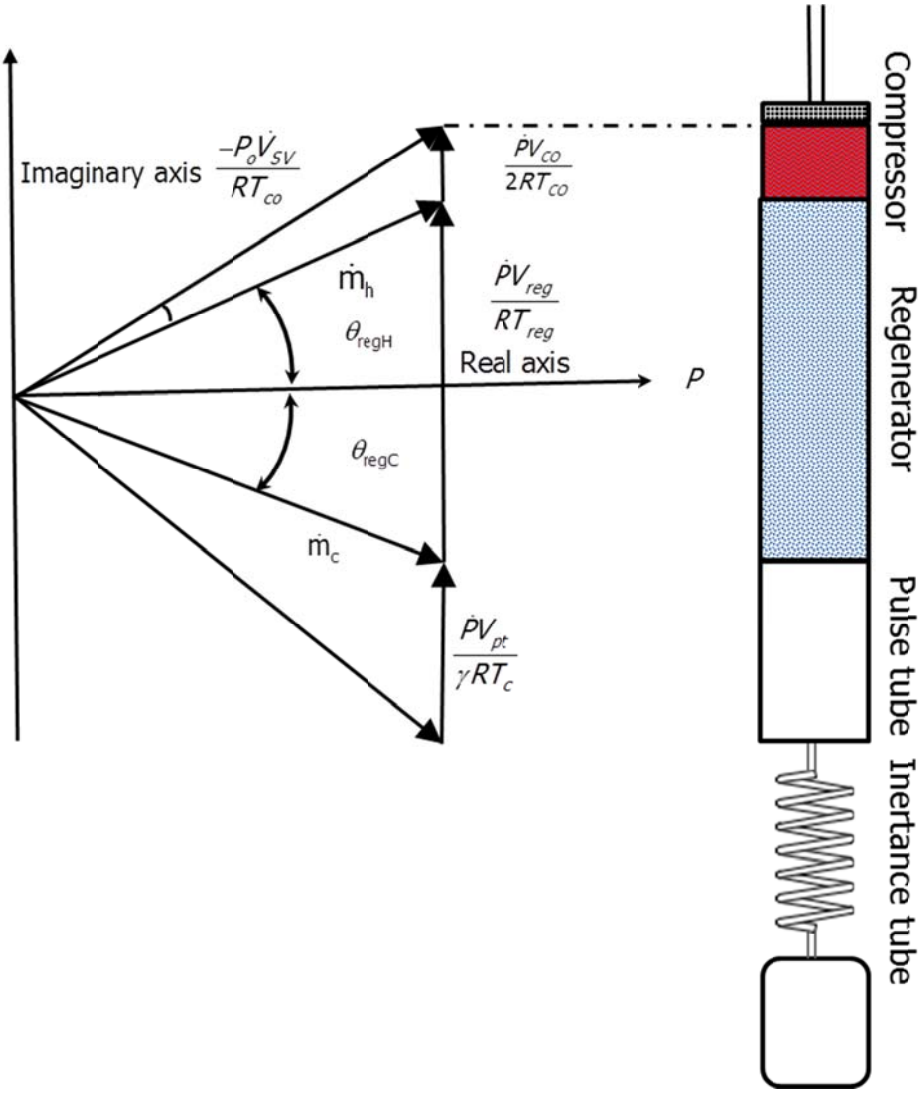

Figure 3.10 Phaser Diagram for the optimal phase shift in a ITPTR [210]

.

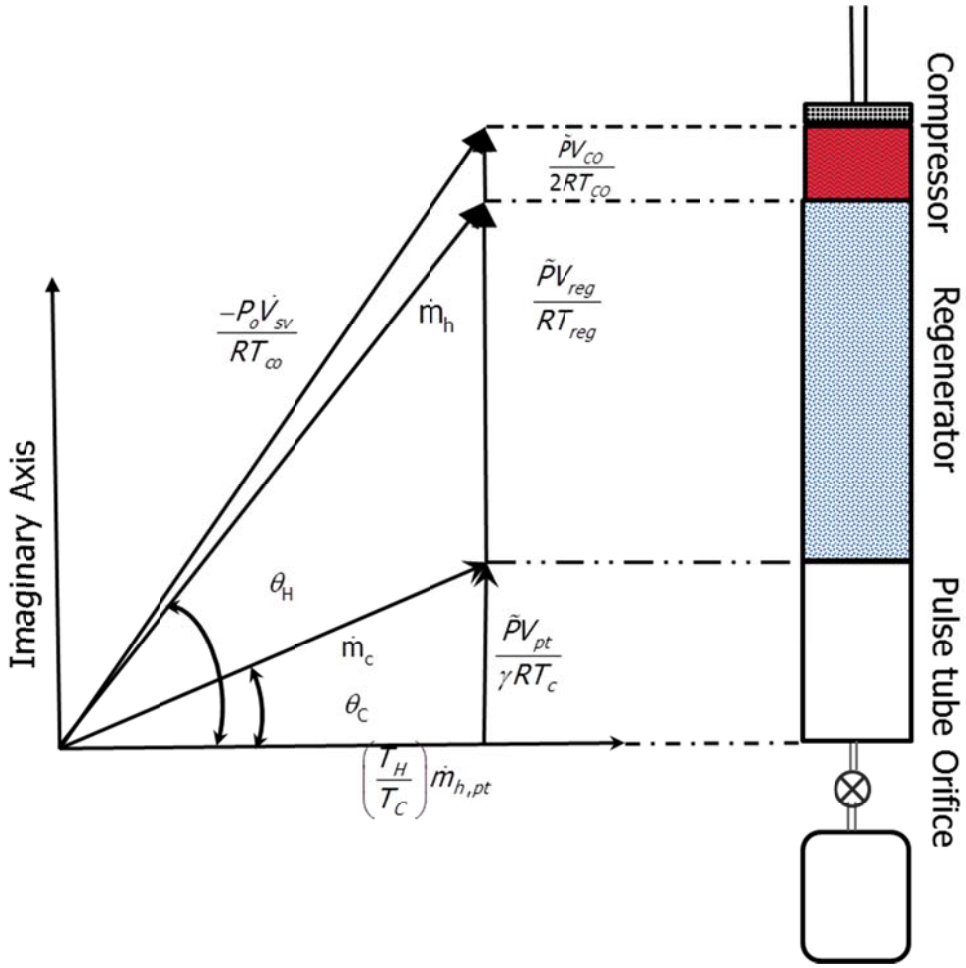

Figure 3.11 Phasor diagram for phase shift that can be achieved with OPTR.

3.4 Analysis of Regenerator

Regenerator is a very important component of the pulse tube refrigerator. The performance of PTR is very much depend upon proper design of regenerator and selection of proper regenerator material for the given temperature range. Modelling the regenerator as a porous media requires some input parameters like porosity, inertial resistance and viscous resistance factors. Hence it is very essential to understand the thermodynamics of fluid flow of porous media inside the regenerator.

During analysis of regenerator some basic parameters like porosity, viscous resistance factor and inertial resistance factor are taken under consideration. This section deals with the estimation of these basic parameters for regenerator porous matrix. The coefficients of porous media can be extracted from the experimental data in the form of pressure drop against velocity through the component. The oven wire mesh

screen (Figure 3.12) is the most commonly used regenerator material. Its advantages are that it provides a high heat transfer area with minimum pressure drop and it is readily available in mesh sizes from 50 mesh (50x50 opening per inch) to over 250 mesh. It is also available in many different materials. Woven bronze screen regenerators are widely used in the first stage of all commercial regenerative cryogenic refrigerators to provide cooling down to 30K. Below 30K, the loss in specific heat of the commercially available materials, such as bronze and stainless steel, limits the effectiveness of screen packing.

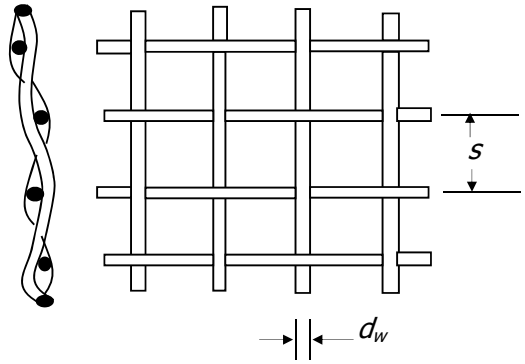

Figure 3.12 Woven wire mesh screens.

Some important parameters related to regenerator analysis are described here. The parameters used in the description of screen regenerators are the porosity and area density.

The term porosity is defined as:

$$\text{Porosity } (\phi) = \frac{\text{total volume of void space}}{\text{total volume of the matrix}} \tag{3.24}$$

The area density can be defined as:

$$\text{Area density } (\sigma) = \frac{\text{total surface area of connected voids}}{\text{total volume of the matrix}} \tag{3.25}$$

From the porosity and area density, the important relationship for the hydraulic radius for a screen packing is given by

$$r_h = \frac{\varphi}{\sigma} = \frac{\text{Fluid volume}}{\text{Heat transfer area}} = \frac{\text{Area}}{\text{Wetted perimeter}} \tag{3.26}$$

Experimentally, the porosity and area density can be found from the dimensions and weight of the screens. The porosity is found by weighing the packed regenerator and subtracting their tare weight of the regenerator canister.

$$\varphi = 1 - \frac{W_p}{\rho_m V_r} \tag{3.27}$$

Where W_p is the weight of the packed matrix material, ρ_m is the density of the packing (matrix), and V_r is the regenerator volume. The area density for one screen as shown in Figure 3.13 is computed by calculating the circumferential heat transfer area of the wires and the total volume encompassed in one segment of screen mesh:

$$\begin{aligned}\sigma = \frac{A_s}{V_r} &= \frac{1/2(\text{wire wetted perimeter})(\text{length of the opening})(4\text{sides})}{(\text{volume encompassing the wires})} \\ &= \frac{\frac{1}{2}(\pi\ d_w)(1/m)(4)}{(1/m)^2 t_s} = \frac{2\pi m\ d_w}{t_s}\end{aligned} \tag{3.28}$$

Where d_w is the wire diameter, t_s is the screen thickness, and m is the mesh size.

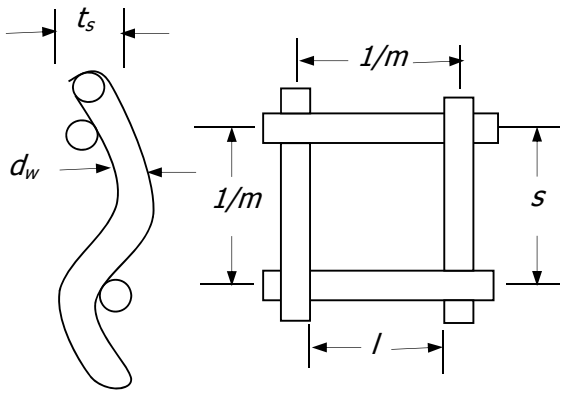

Figure 3.13 Geometry of woven screen

From the area density, the total regenerator heat transfer area is given by

$$A = \sigma \text{ xTotal volume of regenerator} = \left(\frac{2\pi\ md_w}{t_s}\right)\left(\frac{\pi}{4}d_0^2\right)(t_s n) = d_w\left(\frac{\pi}{4}d_0^2\right)(nm) \tag{3.29}$$

Where d_o is the outer diameter of the screens and n is the total number of screens used to pack the regenerator.

Analytically the porosity and area density are calculated by considering a small segment of the screen with a transverse pitch, x_t (designating the transverse spacing/ factor between wires) and a lateral pitch, x_l (designating the longitudinal spacing/ factor between wires). Referring to Figure 3.13 the pitches are related to the mesh size and screen thickness by [211];

$\frac{1}{m} = s = x_t d_w$ and $t_s = 2x_l d_w$

The Figure 3.13 is based on a perfect stacking of square mesh screens in which the weaving causes no inclination of the wires and the screen layers are not separated. These idealization leads to a matrix packing where the screen thickness, t_s, is equal to $2d_w$, and the porosity is given by

$$\varphi = 1 - \frac{V_m}{V_r} = 1 - \frac{2\left[(\pi/4)d^2{}_w\right](x_t d_w)}{(x_t d_w)^2 (2d_w)} = 1 - \frac{\pi}{4x_t} \tag{3.30}$$

Where V_m is volume occupied by the screen material, $x_t = \frac{1}{d_w m}$ where m is mesh per inch; d_w is the wire diameter of screen.

For a woven screen regenerator, it is necessary to specify an additional analytical parameter, to define the ratio of the minimum free flow area to the frontal area. From the description of the screen geometry, shown in Figure 3.13.

$$\beta = \frac{\text{open area}}{\text{total area}} = \frac{(x_t d_w - d_w)^2}{(x_t d_w)^2} = \frac{(x_t - 1)^2}{(x_t)^2} = \left(\frac{l}{s}\right)^2 \tag{3.31}$$

The area density is given by

$$\sigma = \frac{\pi}{x_t d_w} \tag{3.32}$$

From the porosity expression, equation (3.30) and area density equation (3.32), the hydraulic radius expression given by equation (3.32) can be expressed as

$$r_h = \frac{\varphi\ d_w}{4.0(1-\varphi)} \tag{3.33}$$

3.5 Step by step design of a Stirling-type PTR

Various authors provide well developed numerical models for designing a pulse tube refrigerator that simultaneously solves the equations of mass, momentum and energy conservation. While such models are recommended for an accurate design, they are impractical as a means to introduce a physical spontaneous justification for pulse tube design. So it is very useful to present a step by step procedure for an approximate design of the pulse tube refrigerator, [212]. The study covers designing required operation parameter, calculating necessary PV power at the hot end and cold end of the regenerator, estimating the dimensions of regenerator and pulse tube and determining the length of the inertance tube. The important parameter of a cryocooler is net cooling capacity, desire operating temperature, operating average pressure, dynamic pressure and the operating frequency.

The pressure is assumed to uniform at any instant of time during the cycle and can be written as:

$$P(t) = p_0 + p_d \sin(\omega t) \tag{3.34}$$

Where $\omega = 2\pi f$, f , the cycle frequency, P_0, the average pressure and P_d the dynamic pressure

The oscillating flow gives an acoustic power to the pulse tube refrigerator system is related to the pressure and mass flow oscillation given by:

$$\dot{W}_{ac} = \frac{1}{2} P_d \dot{m} \frac{RT}{P_0} \cos\theta \tag{3.35}$$

Where $\dot{m}$, the mass flow rate, T, the time averaged temperature, R, the specific gas constant for ideal gas, and θ is the phase angle between the pressure wave and mass flow oscillation. From the above Equation (3.35), it can be pointed that the acoustic power in the regenerator varies approximately linear with the temperature so that the acoustic power at the cold end ($W_{ac,c}$) relate to the acoustic power at the hot end ($W_{ac,,h}$) by:

$$\dot{W}_{ac,c} = \frac{T_c}{T_h} \dot{W}_{ac,h} \tag{3.36}$$

Where T_c is the regenerator cold end temperature and T_h is the regenerator hot end temperature. The performance of the PTR can be defined as the ratio of the net cooling power to the acoustic power generated in the compressor:

$$COP = \frac{Q_c}{\dot{W}_{ac,h}} \tag{3.37}$$

It can be seen from the equation (3.37) that the COP can be maximized by minimizing the compressor power.

Phase angle at the regenerator cold end

The major losses of a PTR are associated with the regenerator and are proportional to the average magnitude of the mass flow. The phasor diagram, in the form of the mass flow, pressure and mass storage in a regenerator is shown in Figure 3.14.

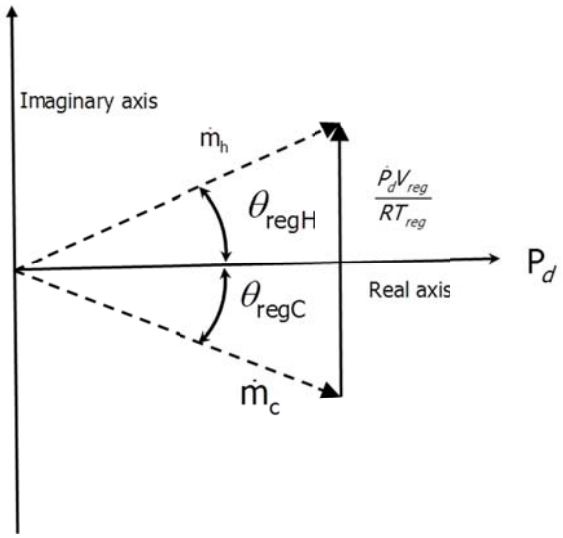

Figure 3.14 Phasor diagram displaying magnitude and phase of mass flow in the regenerator.

The mass conservation in the regenerator is found from the vectorial addition as:

$$\dot{m}_h = \dot{m}_c + \frac{\dot{P}V_{reg}}{RT_{reg}} \tag{3.38}$$

Where $\dot{m}_h$, the mass flow rate at the hot end of the regenerator, $\dot{m}_c$ the mass flow rate at the cold end of the regenerator, the second term on the right hand side of Equation (3.38), signifies the mass storage in the dead volume of the regenerator, V_{reg}, at a temperature T_{reg} and $\dot{P}$ is the time derivative of P(t).

From the Equation (3.35), the term $\dot{m}\cos\theta$, represents the projection of the mass flow vector on the pressure axis, which is constant throughout the regenerator.

Hence regulating the angle $\theta_{r,H}$ and $\theta_{r,C}$ away from the condition, given by equations results in a larger average mass flow rate in the regenerator.

$$\left|\theta_{r,H}\right| = \left|\theta_{r,C}\right| \tag{3.39}$$

Although this condition is an ideal case, it is important for minimizing the regenerator losses and there for maximizing the COP of the pulse tube refrigerator. From Figure 3.14 it can be written while satisfying equation (3.39) as,

$$\dot{m}_c \sin\theta_{r,c} = \frac{1}{2}\frac{\omega P_d V_{reg}}{RT_{reg}} \tag{3.40}$$

Again by combining equation (3.35) and (3.36) we get,

$$\dot{m}_c \cos\theta_{r,c} = \frac{2\dot{W}_{ac,c}P_o}{P_d RT_c} \tag{3.41}$$

Combing equation (3.40) and (3.41), and removes the mass flow term

$$\theta_{r,c} = \arctan\left(\frac{\omega P_d^2 V_{reg} T_c}{4\dot{W}_{ac,c} P_o T_{reg}}\right) \tag{3.42}$$

Using the equations (3.36) and (3.37) the $W_{ac,c}$ can be presented in terms of COP

$$\dot{W}_{ac,c} = \frac{T_c}{T_h}\frac{\dot{Q}_c}{COP} \tag{3.43}$$

For an optimized constant mass flux, the cooling capacity of the regenerator can be mounted directly with the regenerator area. This can be verified by analyzing the linear relation between the amplitude of mass flow at the cold end of the regenerator and the cooling capacity. Combining the Equation(3.36), (3.37),and (3.41) , it can be written as

$$\dot{m}_c = \frac{2}{T_w}\frac{\dot{Q}_c}{COP}\frac{P_0}{P_d}\frac{1}{R\cos\theta_c} \tag{3.44}$$

Combining equation (3.44) with optimum inverse mass flux, the expression for the gas flow area given by:

$$A_g = \left(\frac{A_g}{\dot{m}_c}\right)_{opt}\frac{2}{T_w}\frac{\dot{Q}_c}{COP}\frac{P_0}{P_d}\frac{1}{R\cos\theta_c} = \frac{V_{reg}}{L_{reg}} \tag{3.45}$$

An iterative solution to equations of (3.42) and (3.45) yields the value of A_g and $\theta_{r,c}$

With the optimum geometry for the regenerator, the next step is design the pulse tube.

Pulse tube Dimension and volume

The maximum value of cold end swept volume, $V_{c,pt}$ is given by

$$V_{c,pt} = \frac{2\dot{V}_c}{\omega} = \frac{2\dot{m}_c RT}{\omega P_0} \tag{3.46}$$

Radebaugh [213] provided the concept of 'empirical rule of thumb' for the total volume of pulse tube, which should be three to five times larger than $V_{c,pt,}$ for low temperature (4K - 20 K), the value of five times $V_{c,pt}$ is suitable, while for operation around 100 K, three times $V_{c,pt}$ is more suitable.

There is a major limitation associated with pulse tube aspect ratio. The suitable aspect ratio can avoid the turbulence in the oscillating boundary layer at the pulse tube walls. The critical Reynolds number for oscillating flow was defined by Akhavan [214]:

$$\mathrm{Re}_{crit} = \frac{\rho u_{crit}\delta}{\mu} = 280; \delta = \sqrt{\frac{2\nu}{\omega}} \tag{3.47}$$

Where ρ, the density, u, the amplitude of the cross sectional mean velocity and μ, the dynamic viscosity, while δ is the boundary layer thickness depend on ν, the kinematic viscosity and ω, the angular frequency. The equation (3.47) shows that a minimum limit to the cross sectional area of the pulse tube for a given mass flow rate. From equation (3.46) it can correlate a maximum velocity and the associated minimum area as:

$$u_{crit} A_{\min} = \dot{V} = \frac{\dot{m}RT}{P_0} \tag{3.48}$$

From equation (3.47) and (3.48) , the limit on the cross sectional area is:

$$A_{\min} = \frac{\dot{m}\delta}{\mathrm{Re}_{crit}\,\mu} \tag{3.49}$$

The larger minimum area will define the minimum cross sectional area for the pulse tube. The limit of cross sectional area must be considered at both hot and cold ends.

The Figure 3.15 presents the vectorial diagram results from the equation for conservation energy in the pulse tube.

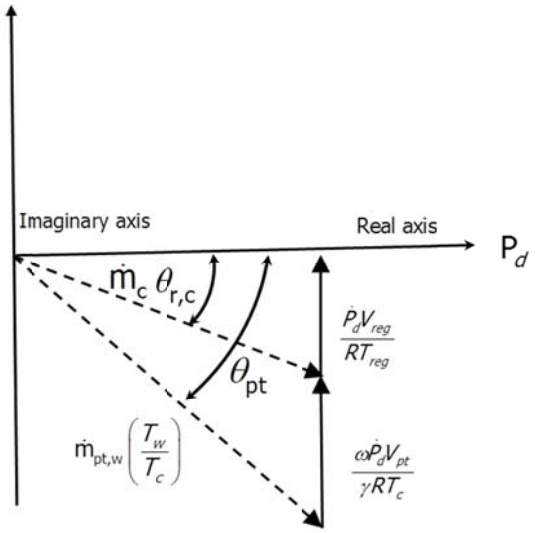

Figure 3.15 Phase diagram showing the relationship between the mass flow vectors in the pulse tube

An expression for the magnitude of the mass flow at the hot end of pulse tube and θ_{pt} are obtained geometrically from as:

$$\dot{m}_{pt,w} = \frac{T_c}{T_h}\sqrt{\left\{\left(\frac{2\dot{W}_{ac,c}P_0}{p_d R T_c}\right)^2 + \left[\left(\frac{\omega P_d V_{reg}}{2RT_{reg}}\right) + \left(\frac{\omega P_d V_{pt}}{\gamma R T_c}\right)\right]^2\right\}} \tag{3.50}$$

From the Figure 3.15, the geometrical relations associated with θ_{pt} can be expressed as:

$$\begin{aligned} \dot{m}_{pt,w}\left(\frac{T_w}{T_c}\right)\cos\theta_{pt} &= \dot{m}_c \cos\theta_{r,C} = \frac{2\dot{W}_{ac,c}P_0}{p_d R T_c} \\ \dot{m}_{pt,h}\left(\frac{T_h}{T_c}\right)\sin\theta_{pt} &= \frac{\omega P_d V_{reg}}{2RT_{reg}} + \frac{\omega P_d V_{pt}}{\gamma R T_c} \end{aligned} \tag{3.51}$$

Finally the expression for θ_{pt} is obtained as:

$$\theta_{pt} = \arctan\left[\frac{\omega P_d^2\left(V_{reg}\gamma T_c + 2V_{pt}T_{reg}\right)}{4\gamma T_{reg}\dot{W}_{ac,c}P_0}\right] \tag{3.52}$$

Inertance tube Dimension

The diameter and length of the inertance tube are estimated by the required phase angle, θ_{pt}, where it interfaces with the warm end of pulse tube, and the acoustic power flows at the same location.

Chapter 4

CFD ANALYSIS OF PULSE TUBE REFRIGERATOR

4.1 Introduction

This chapter describes the various computational fluid dynamics (CFD) models which have been used in this investigation to study the pulse tube refrigerators. CFD has been extensively used for the analysis of systems involving fluid flow, heat transfer and associated phenomenon such as chemical reactions by means of numerical simulations. This method is very efficient and powerful, having a wide range of industrial application. It generates high accuracy results, at the expanse of large computational time. There are numbers of commercially CFD tools available such as STAR-CD, FLUENT, CFX, PHONICS, FLOW3D etc. Fluent is one of the most highly efficient and accurate one. Fluent [215] is a state-of-the-art CFD code for analyze the fluid flow and heat transfer problems in industrial application. It has the capability to customize the boundary condition and can significantly enhance its capabilities using user-defined functions (UDFs). It also has capability for generating deforming meshes using the dynamic meshing method for moving boundary problem. The porous media model can be modelled using Fluent. Due to such versatility of Fluent, it is chosen for solving of the Stirling type PTR.

The characteristic illustration of the pulse tube refrigerator profile and boundary conditions for numerical investigation of Stirling type ITPTR has been accomplished, by using commercial software, FLUENT. The basic requirement of any model for CFD simulation is their proper dimensions and suitable boundary conditions. Thus, in this present investigation the geometrical model and mesh of each component of pulse tube refrigerator are generated in Gambit software. In the first part of the study Stirling type ITPTR investigation is carried out. The performance is investigated in terms of temperature and pressure contours for both cases.

4.2 Numerical Modelling of ITPTR

Parametric studies of inertance tube pulse tube refrigerator are performed with different length of the pulse tube using the FLUENT package. The present study covers

both thermal equilibrium model and non-equilibrium models of the porous zone. In thermal equilibrium at any time at a spatial position the temperatures of the working fluid and solid matrix are equal. So this thermal equilibrium model solves a single energy equation for both solid matrix and working fluid, which does not interpret the thermal interaction between the working fluid and solid matrix. But in a non-equilibrium model it considers the thermal interaction between the working fluid and solid matrix. Hence it solves two separate energy equations, one for working fluid and other for solid matrix. In the present model thermal inertia plays an important character in porous zones like regenerator, hence thermal non equilibrium model seems to be more realistic than thermal equilibrium model. This model calculates the thermal losses in the porous zones.

4.2.1 The ITPTR Geometry

A schematic view of inertance pulse tube model is shown in Figure 4.1. The geometrical details of individual constituent of the numerical model and their functions are identified below:

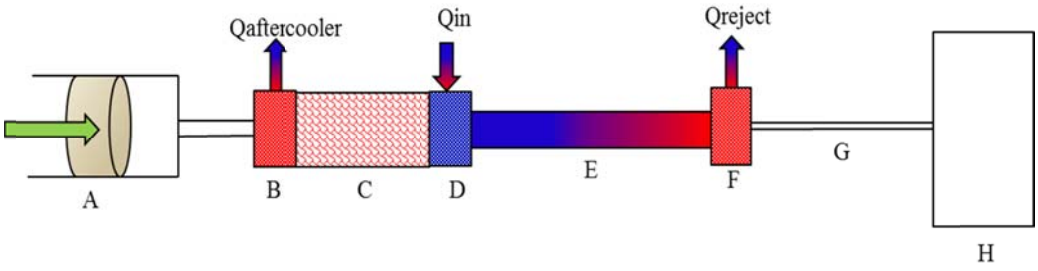

Figure 4.1 Schematic model of ITPTR, A- compressor, B- after cooler, C- regenerator, D-cold heat exchanger, E-pulse tube, F-hot heat exchanger, G-inertance tube, H-reservoir

1. **Compressor**. To generate a periodic pressure wave inside the pulse tube refrigerator a compressor is used, which convert the electric power into mechanical energy. It performs gas pressurization and depressurization inside the closed system. Generally valve less type reciprocating compressor is used for Stirling model.

2. **Transfer Line**. It is a minute tube connecting between compressor and after cooler. It transfers the compressed gas from compressor to after cooler and sends back the decompressed gas from after cooler to compressor.
3. **After cooler**. The function of the after cooler is to extract the heat from the working fluid generated by the compressor during compression process. This minimizes the working fluid temperature so that the regenerator can work more efficiently. It is basically cooled by water.

Figure 4.2 Typical pictures of the after cooler

4. **Regenerator.** The regenerator is the heart of the pulse tube refrigerator. It behaves as a thermal flywheel and it is the most important component in pulse tube refrigerator. Its function is to absorb heat from the incoming compressed gas during the compression stroke, and give up that heat back to the gas during the expansion stroke. To store the heat, a solid matrix is used. Generally stainless steel wire screens usually consider as the regenerator storage material, as they have higher heat transfer areas, low pressure drop, high heat capacity and low thermal conductivity. A typical regenerator housing is shown in Figure 4.3.

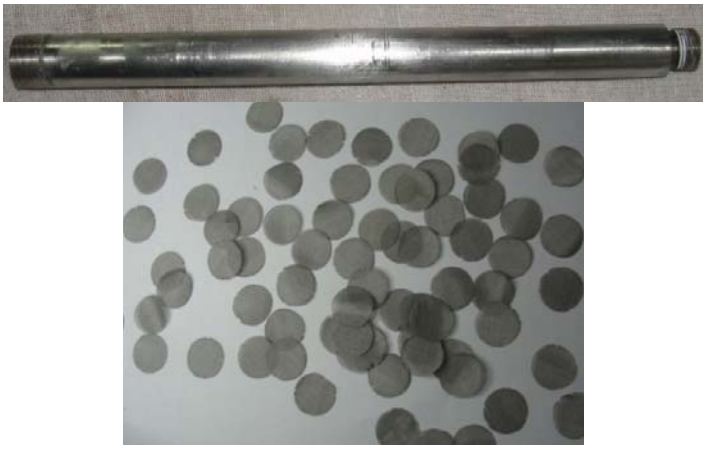

Figure 4.3 Typical pictures of regenerator and matrix

5. **Cold Head Heat Exchanger.** It is an intermediate heat exchanger between regenerator and pulse tube. This is the component where cooling load is absorbed by the system. It is also called the cold finger. Copper wire mesh screens are used to exchange heat with the housing wall, and thereby receive the applied heat load.

Figure 4.4 Typical pictures of Cold heat exchanger

6. **Pulse Tube.** The pulse tube is the main component of the pulse tube refrigerator. It is a hollow tube situated in between the cold end and the warm end heat exchangers. Pulse tube carries away heat from the CHX to the WHX by an enthalpy flow. Generally stainless steel is used as pulse tube material due to its lower thermal conductivity.
7. **Hot Heat Exchanger**. The system heat is rejected at the hot end heat exchanger. It is based upon the first law analysis that the heat rejected to the atmosphere in the hot heat exchanger is equal to the heat load in the cold heat exchanger and viscous losses. Usually, the hot heat exchanger is cooled by use of water cooling system.
8. **Inertance Tube.** Inertance tube is otherwise known as the phase shifter. It adjusts the phase between mass flow rate and pressure. It is a long and narrow tube connecting the hot end heat exchanger and the reservoir.
9. **Reservoir.** The reservoir acts as storage device in which the change in pressure is very small during compression and expansion process. It is connected to the hot end heat exchanger through inertance tube. A combination of a phase shifter and reservoir provides proper phase angle in the system.

4.2.2 Governing Equations

The, continuum based conservation of mass, momentum, energy equations along with the equation of state of the working fluid are used for all components, of the pulse tube refrigerator system. Helium is used as the working fluid and its density is related to pressure and temperature through equation of state. The general governing equations used by the Fluent code [215] are as follows. The velocity components appearing in the equations are the superficial velocity components in the case of porous zones. The z axis is deployed along the axis of the pulse tube with the origin located at the mid stroke of the piston.

Conservation of mass or continuity equation:

$$\frac{\partial \rho}{\partial t} + \nabla.(\rho \vec{v}) = S_m \tag{4.1}$$

Where

∇ = Gradient operator

ρ = Density of the gas

$\vec{v}$ = superficial Velocity in vector form

S_m = Source term

t = Time

Conservation of momentum equation:

$$\frac{\partial}{\partial t}(\rho \vec{v}) + \nabla.(\rho \vec{v}\vec{v}) = -\nabla p + \nabla.\left(\bar{\bar{\tau}}\right) + \rho \vec{g} + \vec{F} \tag{4.2}$$

Where:

p = Static pressure

$\bar{\bar{\tau}}$ = Stress Tensors

$\vec{g}$ = Gravity acceleration

$\vec{F}$ = External body forces

Stress Tensors can be defined as:

$$\bar{\bar{\tau}} = \mu\left[(\nabla \vec{v} + \nabla \vec{v}^T) - \frac{2}{3}\nabla.\vec{v}I\right] \tag{4.3}$$

Where:

μ = Fluid molecular viscosity

I = Unit (Identity) tensor

T = Transpose

Conservation of energy:

$$\frac{\partial}{\partial t}(\rho E) + \nabla.(\vec{v}(\rho E + p)) = \nabla.(k_{eff}\nabla T - \sum_j h_j \vec{J}_j + (\bar{\bar{\tau}}_{eff}.\vec{v})) + S_h \qquad (4.4)$$

Where

$$E = h - \frac{p}{\rho} + \frac{v^2}{2}$$

$$h = \int_{T_{ref}}^{T} C_P dT$$

$$k_{eff} = k + k_t$$

Where

k = Gas thermal conductivity

k_{eff}= effective conductivity

k_t = Turbulence thermal conductivity

C_P = Specific heat of gas

h = Local enthalpy

T = Temperature of the gas

v = Local velocity

J_j = Diffusion flux of species J

S_h = Source term

The above equations can be simplified for 2 D axi-symmetry geometries as:

Continuity Equation

$$\frac{\partial \rho}{\partial t} + \frac{\partial}{\partial x}(\rho v_x) + \frac{1}{r}\frac{\partial}{\partial r}(r \rho v_r) = S_m \qquad (4.5)$$

r = Radial coordinate

x = Axial coordinate

v_r = superficial velocity in radial direction

v_x = superficial Velocity in axial direction

Momentum equation in axial direction:

$$\frac{\partial}{\partial t}(\rho v_x)+\frac{1}{r}\frac{\partial}{\partial x}(r\rho v_x v_x)+\frac{1}{r}\frac{\partial}{\partial r}(r\rho v_r v_x)=-\frac{\partial p}{\partial x} +\frac{1}{r}\frac{\partial}{\partial x}\left[r\mu\left(2\frac{\partial v_x}{\partial x}-\frac{2}{3}(\nabla.\vec{v})\right)\right]+\frac{1}{r}\frac{\partial}{\partial r}\left[r\mu\left(\frac{\partial v_x}{\partial r}+\frac{\partial v_r}{\partial x}\right)\right]+S_x \tag{4.6}$$

Momentum equation in radial direction

$$\frac{\partial}{\partial t}(\rho v_r)+\frac{1}{r}\frac{\partial}{\partial x}(r\rho v_x v_r)+\frac{1}{r}\frac{\partial}{\partial r}(r\rho v_r v_r)=-\frac{\partial p}{\partial r} +\frac{1}{r}\frac{\partial}{\partial r}\left[r\mu\left(2\frac{\partial v_r}{\partial r}-\frac{2}{3}(\nabla.\vec{v})\right)\right]+\frac{1}{r}\frac{\partial}{\partial x}\left[r\mu\left(\frac{\partial v_r}{\partial x}+\frac{\partial v_x}{\partial r}\right)\right] -2\mu\frac{v_r}{r^2}+\frac{2}{3}\frac{\mu}{r}(\nabla.\vec{v})+\rho\frac{v_z^2}{r}+S_r \tag{4.7}$$

Where,

$$\nabla.\vec{v}=\frac{\partial v_x}{\partial x}+\frac{\partial v_r}{\partial r}+\frac{v_r}{r} \tag{4.8}$$

Where S_x and S_r are the two source terms in the axial and radial direction which values is zero for nonporous zone. For the porous zone the momentum equation can be defined by adding two new terms to the volume averaged momentum equation: the Darcy term and the Forchheimer term which are responsible for flow resistance through the porous media. The Darcy term causes the pressure drop, directly proportional to velocity whereas the Forchheimer term, causes the pressure drop, proportional to the square of the velocity. Assuming the solid matrix homogeneous and isotropic, the following momentum source terms are included in the x and r volume averaged momentum equations:

$$S_x=-\left(\frac{\mu}{\beta}v_x+\frac{1}{2}C\rho|\vec{v}|v_x\right) \tag{4.9}$$

$$S_r=-\left(\frac{\mu}{\beta}v_r+\frac{1}{2}C\rho|\vec{v}|v_r\right) \tag{4.10}$$

Where μ = Fluid molecular viscosity

β = Permeability

C = Inertial resistance factor

v = superficial velocity

In the above equation the first term is called Darcy term and the second term is called the Forchheimer term which are responsible for the pressure drop inside the porous zone. For thermal equilibrium assumption the porous matrix energy equation solves one single energy equation for both fluid and solid matrix but for thermodynamic non-equilibrium assumption it solve two separate energy equation for the fluid and the porous structure is accounted. The aforementioned thermodynamic non equilibrium is usually small. However and often a single energy equation representing both the solid and gas phase is used. Accordingly, in this study, local thermal equilibrium assumption is applied. The single energy equation is used as,

Energy Equation:

$$\frac{\partial}{\partial t}(\varphi\rho_f E_f + (1-\varphi)\rho_s E_s) + \nabla.(\vec{v}(\rho_f E_f + P)) = \nabla.(k_{eff}\nabla T + \tau.\vec{v}) \qquad (4.11)$$

Where, $k = \phi k_f + (1-\phi)k_s$

$E_f = h - p/\rho_f + v^2/2$

ϕ = porosity of medium

k_s = Solid medium thermal conductivity

k_f =Fluid thermal conductivity

E_f = Total fluid energy

E_s = Total solid energy

The energy equation for thermal non-equilibrium model, are written as follows:

Energy equation for matrix

$$\underbrace{\frac{\partial}{\partial t}(\rho_s C_s T_s)}_{energy\ storage} = \underbrace{\vec{\nabla}.(k_s\vec{\nabla}T_s)}_{heat\ \text{conduction loss}} + \underbrace{\frac{hA_s(T_f - T_s)}{1-\phi}}_{\text{heat } transfer} \qquad (4.12)$$

$$\text{i.e. } \frac{\partial}{\partial t}(\rho_s C_s T_s) = \frac{1}{y}\frac{\partial}{\partial y}\left[k_s y\frac{\partial T_s}{\partial y}\right] + \frac{\partial}{\partial x}\left[k_s\frac{\partial T_s}{\partial x}\right] + \frac{hA_s(T_t - T_s}{1-\phi} \qquad (4.13)$$

Where S_s is equal to $hA_s(T_f - T_s)/(1-\phi)$

Energy equation for gas

$$\underbrace{\frac{\partial}{\partial t}\left(\rho_f E_f\right)+\vec{\nabla}.\left[\vec{v}\left(\rho_f E_f\right)\right]}_{\text{energy storage}}+\underbrace{\vec{\nabla}.\left[\vec{v}\left(p\right)\right]}_{\substack{\text{pressure gradient}\\(\text{friction loss})}}=\vec{\nabla}.\left[\underbrace{k\vec{\nabla}T_f}_{\text{heat conduction loss}}+\underbrace{\left(\tau.\vec{v}\right)}_{\text{viscous dissipation loss}}\right]+\underbrace{\frac{hA_v\left(T_s-T_f\right)}{\phi}}_{\text{heat transfer}} \tag{4.14}$$

For non-porous zones, the energy source term S_G is zero. For porous zones, it is stated as, $hA_v\left(T_s-T_f\right)/\phi$

4.2.3 Calculation of other parameters

Heat transfer coefficient between regenerator solid matrix and working fluid

The heat transfer coefficient for oscillating flow in the regenerator proposed by Tanaka *et al.* [134] is,

$$h=0.33\frac{k_f}{D_e}\left(\frac{\rho D_e 2V_s\rho}{\mu A_s\phi}\right)^{0.67} \tag{4.15}$$

Where k_f is the thermal conductivity of working fluid, D_e is the equivalent hydraulic diameter, ϕ is the porosity, V_s is the piston swept volume and A_s is the total surface area.

Thermal conductivity of porous matrix

Neglecting the working fluid contribution, the thermal conductivity of solid matrix Proposed by Koh and Fortini [216]:

$$k_s=\frac{1-\zeta}{1+11\zeta}k \tag{4.16}$$

Where k is defined as the thermal conductivity of solid matrix used in porous zone and k_s is defined as effective thermal conductivity of the solid matrix while considering the porosity ζ.

The compressor input power

$$W_{comp}=\frac{1}{\tau}\oint P_{Vavg}\frac{dV}{dt}dt \tag{4.17}$$

where P_{Vavg} is the volume averaged pressure inside the swept volume of the compressor.

Interpretation of the fields variables are well defined in Fluent for computing several attributes over the domain. Some important variables are discussed here [215].

- The **Area** of a surface is computed by summing the areas of the faces that define the surface. Faces on a surface are either triangular or quadrilateral in shape.

$$A = \int dA \sum_{i=1}^{n} |A_i| \tag{4.18}$$

In the above expression the index 'i' denotes a face and the summation extends over all the '*n*' faces.

- The Integral on a surface is computed by summing the product of the facet area and the selected field variable. If the face is on a boundary surface, an interpolated face value is used for the integration instead of the cell value. This is done to improve the accuracy of the calculation and to ensure that the result matches the boundary conditions specified on the boundary and the fluxes prescribed on the boundary.

$$\varsigma_{i1} = \int \varsigma dA = \sum_{i=1}^{n} \varsigma_i |A_i| \tag{4.19}$$

- The **Area-Weighted Average** of a quantity is computed by dividing the summation of the product of the selected field variable and face area by the total area of the surface:

$$\varsigma_{aw} = \frac{1}{A} \int \varsigma dA = \frac{1}{A} \sum_{i=1}^{n} \varsigma_i |A_i| \tag{4.20}$$

- The **Flow Rate** of a quantity through a surface is computed by summing the product of density and the selected field variable with the dot product of the face area vector and the face velocity vector.

$$\varsigma_{fr} = \int \varsigma \rho \vec{v} d\vec{A} = \sum_{i=1}^{n} \varsigma_i \rho_i \vec{v}_i \left| d\vec{A}_i \right| \tag{4.21}$$

- The **Mass Flow Rate** through a surface is computed by summing the product of density with the dot product of the face area vector and the face velocity vector.

$$\varsigma_{mf} = \int \rho \vec{v} d\vec{A} = \sum_{i=1}^{n} \rho_i \vec{v}_i . \left| d\vec{A}_i \right| \tag{4.22}$$

- The **Mass-Weighted Average** of a quantity is computed by dividing the summation of the product of the selected field variable and the absolute value of

the dot product of the facet area and momentum vectors by the summation of the absolute value of the dot product of the facet area and momentum vectors.

$$\varsigma_{mw} = \frac{\int \varsigma\rho \left|\vec{v}d\vec{A}\right|}{\int \rho \left|\vec{v}d\vec{A}\right|} = \frac{\sum_{i=1}^{n} \varsigma_i \rho_i \left|\vec{V}_i.d\vec{A}_i\right|}{\sum_{i=1}^{n} \rho_i \left|\vec{V}_i.d\vec{A}_i\right|} \tag{4.23}$$

The Sum of a specified field variable on a surface is computed by summing the value of the selected variable at each facet

$$\varsigma_{sm} = \sum_{i=1}^{n} \varsigma_i \tag{4.24}$$

- The **Facet Average** of a specified field variable on a surface is computed by dividing the summation of the facet values of the selected variable by the total number of faces.

$$\varsigma_{fa} = \frac{\sum_{i=1}^{n} \varsigma_i}{n} \tag{4.25}$$

- The **Volume Flow Rate** through a surface is computed by summing the dot product of the face area vector and the face velocity vector

$$\varsigma_{vf} = \vec{v}.d\vec{A} = \sum_{i=1}^{n} \vec{V}_i.d\vec{A}_i \tag{4.26}$$

- The **Facet Minimum** of a specified field variable on a surface is the minimum facet value of the selected variable on the surface.
- The **Facet Maximum** of a specified field variable on a surface is the maximum facet value of the selected variable on the surface.

4.2.4 Details of Problem Geometry and CFD Modelling

The wall thickness of the computational model is assumed negligible in the present investigation. The aftercooler and hot heat exchanger is assumed as perfect cooling. The cold heat exchanger wall is maintained at adiabatic condition (i.e., no load) and also the other walls of the system maintained at same boundary condition. The swept volume of the compressor is 1.16 cm^3. As it is stirling type dual piston (valve less) compressor, it has negligible clearance volume. The geometrical details of various models tested are given in Table 4.1. The wall material and the boundary conditions are common for all cases as specified in Table 4.1. The models differ from one another only in the change in pulse tube length keeping all other components are fixed.

Table 4.1 Geometry details and boundary conditions

constituent part	*Diameter (m)*		*Length (m)*		*Boundary condition*
	Cha et al. [100]	*Present model*	*Cha et al. [100]*	*Present model*	
Compressor (A)	0.02	0.02	0.0075	0.008	Adiabatic
Transfer line (B)	0.0031	0.0035	0.101	0.1	Adiabatic
After cooler (C)	0.008	0.008	0.02	0.02	300 K
Regenerator (D)	0.008	0.008	0.058	0.06	Adiabatic
Cold heat exchanger (E)	0.008	0.008	0.0057	0.006	Adiabatic
Pulse tube (F)	0.005	0.005	0.06	**	Adiabatic
Hot heat exchanger(G)	0.008	0.008	0.012	0.012	300 K
Inertance tube (H)	0.00085	0.0009	0.684	0.7	Adiabatic
Reservoir (I)	0.026	0.025	0.13	0.12	Adiabatic

** Value taken from Table 4.2.

Geometry and Mesh generation

Before simulation, it is necessary to model the geometry of the pulse tube refrigerator using any pre-processor modelling software package. Figure 4.5 shows the two dimensional schematic geometry of the ITPTR. Here, GAMBIT [217] is used as the pre-processor for modelling the geometry and mesh generation of various parts of the pulse tube refrigerator. In the present case the computational domain is axisymmetric so half of the domain is taken for analysis as shown in Figure 4.6. Zero wall thickness considered for modelling. The pulse tube and the regenerator walls are chosen to be made of stainless steel. The regenerator fluid is defined as porous media. The porosity value is taken as 0.6, permeability as 1.06 x 10^{-10} m^2 and the inertial resistance of 76,090m^{-1}. The thermal conductivity, viscosity and specific heat of the working gas are taken to be temperature dependent. The temperature dependent thermo-physical properties are collected from the NIST database. The details of the geometry are listed in Table 4.1. The wall material and the boundary conditions are fixed for all the parametric cases.

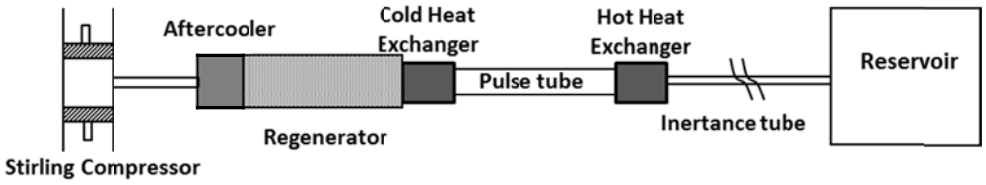

Figure 4.5 Two-dimensional representation of ITPTR

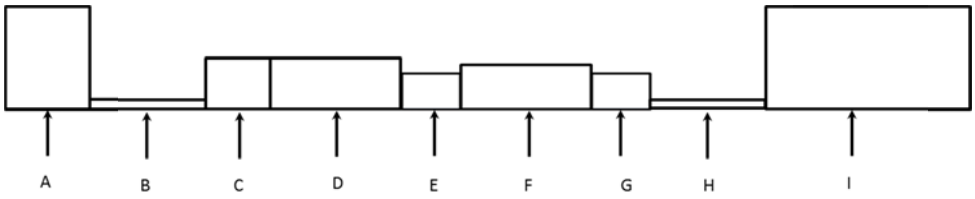

Figure 4.6 Axi-symmetric view for ITPTR

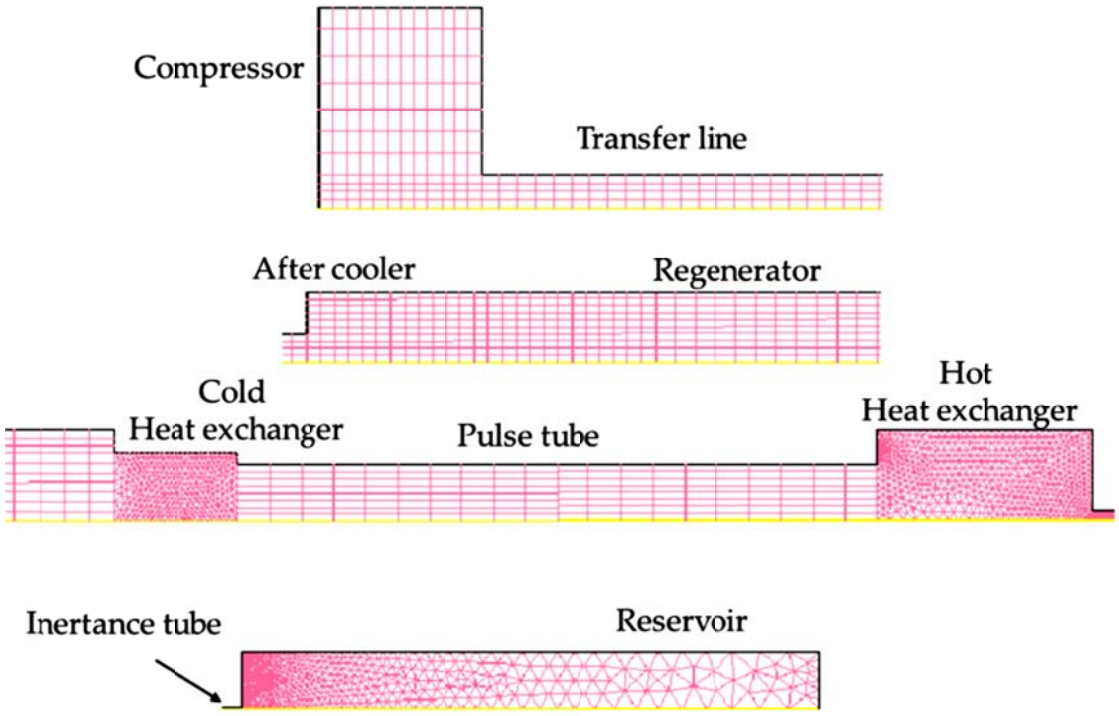

Figure 4.7 Mesh generated in GAMBIT for two-dimensional axis-symmetric geometry of ITPTR

After modelling the geometry of pulse tube refrigerator it is essential to generate mesh. The understanding for generating mesh is that a partial differential equation produces an infinite dimensional problem and the solution must in general be sought in a finite dimensional space. By defining the problem to a finite set of points in which a finite dimensional representation of the solution is chosen, the problem becomes accomplishable for simulations. During mesh generation at first node points are created then the actual meshes along the faces are generated. Different options for mesh generation are available in Gambit to list a few are triangular elements, hexahedral elements and tetrahedral elements. The junction regions of the components are represented with finer meshes for better numerical resolution as shown in Table 4.8.

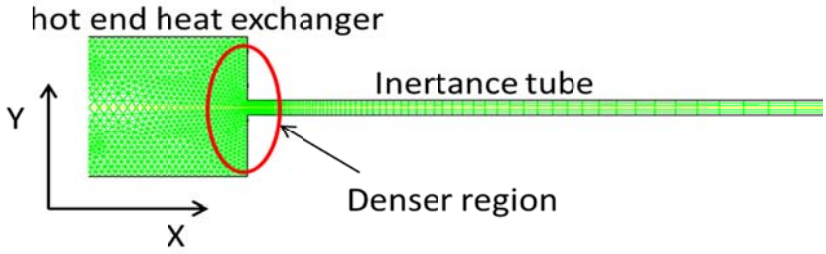

Figure 4.8 Typical meshes of the computational domain

Initial and Boundary Conditions

It is necessary to define proper specification of the initial and boundary conditions to accurately calculate the governing equation and capture the physics of physical model. A summary of the boundary conditions for the present case is shown in Table 1. The initial mean charging pressure is 30 bar. The wall of the cold heat exchanger, reservoir wall, inertance tube wall and compressor walls are maintained at adiabatic conditions. The after-cooler walls and the hot heat exchanger walls are maintained at an ambient temperature of 300 K. The operating condition, wall material and the boundary conditions remain constant in all the cases. The models differ from one another only in their length of the pulse tube. For top wall which is defined as a piston input specification include velocity UDF for piston head motion for Stirling type PTR model. Once all the initial condition, operating conditions and boundary conditions are specified, the Fluent code can be executed.

Defining the Porous Zone

The regenerator, of a pulse tube refrigerator is to be modeled using porous-media methods. A porous zone is modeled as a special type of fluid zone. To indicate that the fluid zone is a porous region, porous zone option in the fluid panel is enabled in Fluent. The panel expands to show the porous media inputs. The user inputs for the porous media model are:set the viscous resistance coefficients and inertial resistance coefficients, and define the direction vectors for which they apply. The flow losses are determined by choosing appropriate values for inertial resistance, permeability and porosity. The porous zones are modelled by considering extra momentum source terms in the momentum equations and the energy source terms in the fluid and matrix energy equations.

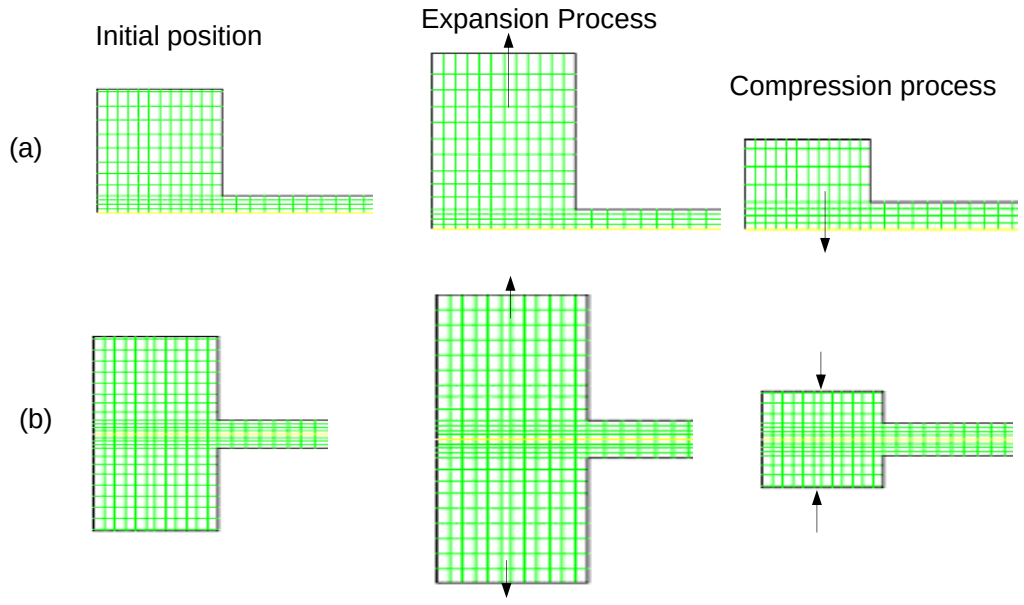

Figure 4.9 Mesh motion preview of dynamic meshing model

Dynamic mesh modelling

In order to model the compressor dynamic meshing is used, as the compressor volume changes with respect to time. To track the piston head velocity of compressor a suitable DEFINE_CG_MOTION User Defined Function (UDF) is written and attached properly. The updating of the mesh is automatically done by FLUENT at each time step, depending upon the new position of the piston. Various dynamic meshing methods like "dynamic-layering", "remeshing" and "spring-based smoothening" are used as against simulating a moving piston and for updating the meshing in the deforming volume. The operating frequency f is chosen as 34 Hz and the angular velocity is $\omega = 2\pi f$. The two piston heads oscillate about its center with the relation

$a = a_0 \sin(\omega t)$. Where 'a' is the piston displacement and $a_0 = 0.0045$ m is the amplitude with a time increment of 0.0005 s is assumed during simulation. Table 4.9 shows the mesh motion preview of the dynamic meshing model.

4.3 Method of Solution

Algorithm

The most important factor in the simulation is the suitable numerical scheme. Axisymmetric, unsteady, cell based second order implicit time; physical velocity with segregated solver is considered for the present analysis. For solving the discretized governing equations unsteady pressure based segregated solver with implicit formulation is used. Due to dynamic meshing first order method is used. The governing equations given by equations (4.5-4.14) assuming two-dimensional axis-symmetric turbulent flow in cylindrical coordinates along with the boundary conditions represent a set of non-linear, coupled differential equations, which are solved iteratively using the finite volume method. PISO algorithm with a PRESTO (pressure staggered option) scheme for the pressure velocity coupling is used for the pressure correction equation. The PRESTO scheme uses the discrete continuity balance for a "staggered" control volume about the face to compute the "staggered" (i.e., face) pressure. This procedure is similar in spirit to the staggered meshes, comparable accuracy is obtained using a similar algorithm. The PRESTO scheme for pressure interpolation is available for all meshes in Fluent. PISO (Pressure Implicit with Splitting of Operators) algorithm is used for better convergence. For unsteady problems it is an efficient method to solve the Navier-Stokes equations. Suitable under relaxation factors for momentum, pressure and energy have been used for the better convergence. Quardilateral as well as triangular cells is used for the computational domain. For all equations convergence of the discretized equations are said to have been achieved when the whole field residual is kept at 10^{-6}. A line-by line solver based on the TDMA (Tri-diagonal matrix algorithm) is used to iteratively solve the algebraic equations obtained after discretization. Details of the numerical method and solution procedures may be found in the work of Versteeg and Malalasekera [218] and Patankar [219]. Proper under relaxation factors are used for the solution of the pressure correction equation, the two momentum equations and the energy equation respectively.

Grid Independency test

In order to ensure the accuracy of the computation grid, a detailed verification of the grid independence test for the cold end temperature of the model has been conducted. The grids chosen for the computational domain have 2421, 3147, 3986, 8734 and 14742 nodes. Figure 4.10 shows the cold end temperature values for different sizes of the grid number for the grid independence test. It shows that the grid number 3986 is good enough for simulation purposes. So, in the present work, 3986 numbers of grids are adopted.

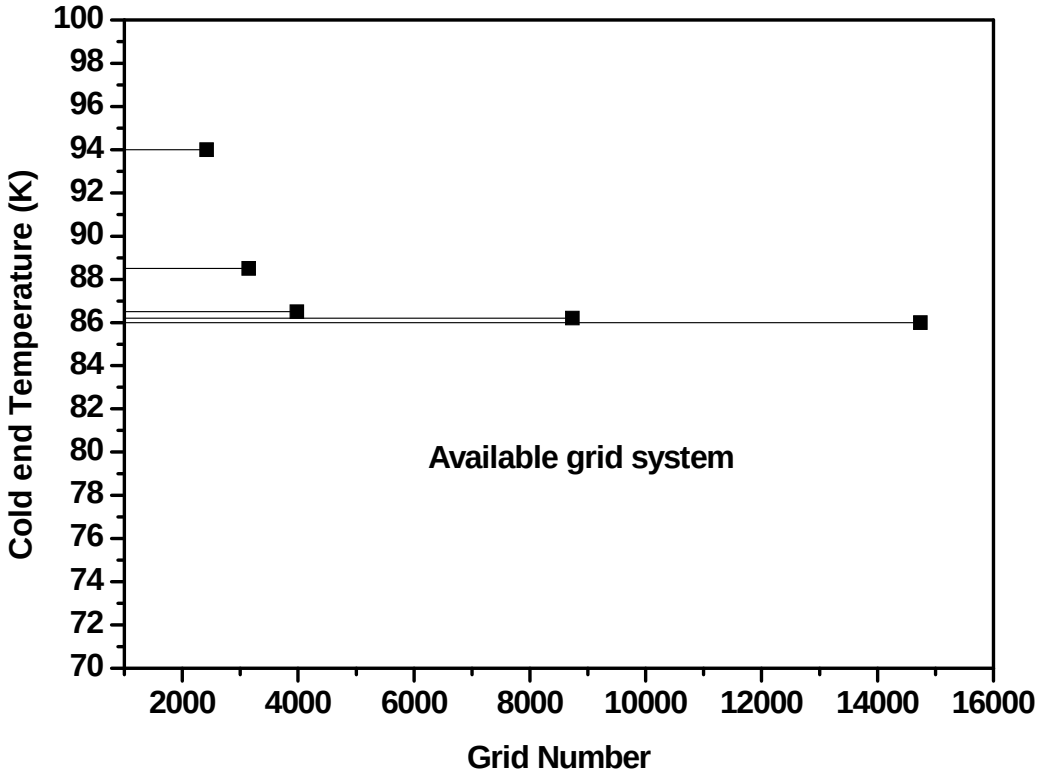

Figure 4.10 Test for grid independency

Validation with previously published works

In order to verify the accuracy of the algorithm and the method of solution, present numerical model is verified, by comparing it with the previously published work of Cha et al. [100]. The validated model is a thermal equilibrium model of regenerator and without wall thickness of each part. Figure 4.11 shows that the cool down curve of the present numerical results match well with those of the Cha et al. model. And also, the no load steady state temperature of 86 K at cold end is achieved with the present model, using 3986 cell number, whereas 87 K is reported by Cha et al. using 4200 cell number.

Solution Initialization

After completing geometry, mesh modelling, defining initial and boundary conditions, it is required to initialize the Fluent code before starting the iteration process. The meaning of initializing is to provide an initial guess for the first step iteration of the solution. In the initialization process, the user must specify which zone is being provided with initial condition. Different model properties viz. continuity, x-velocity, y-velocity, energy, k and ε are monitored by Fluent's solver and checked for convergence. This criterion requires that the scaled residuals decrease to 10^{-3} for all equations except the energy equation, where the criterion is 10^{-6}. At the end of each solver iteration, the

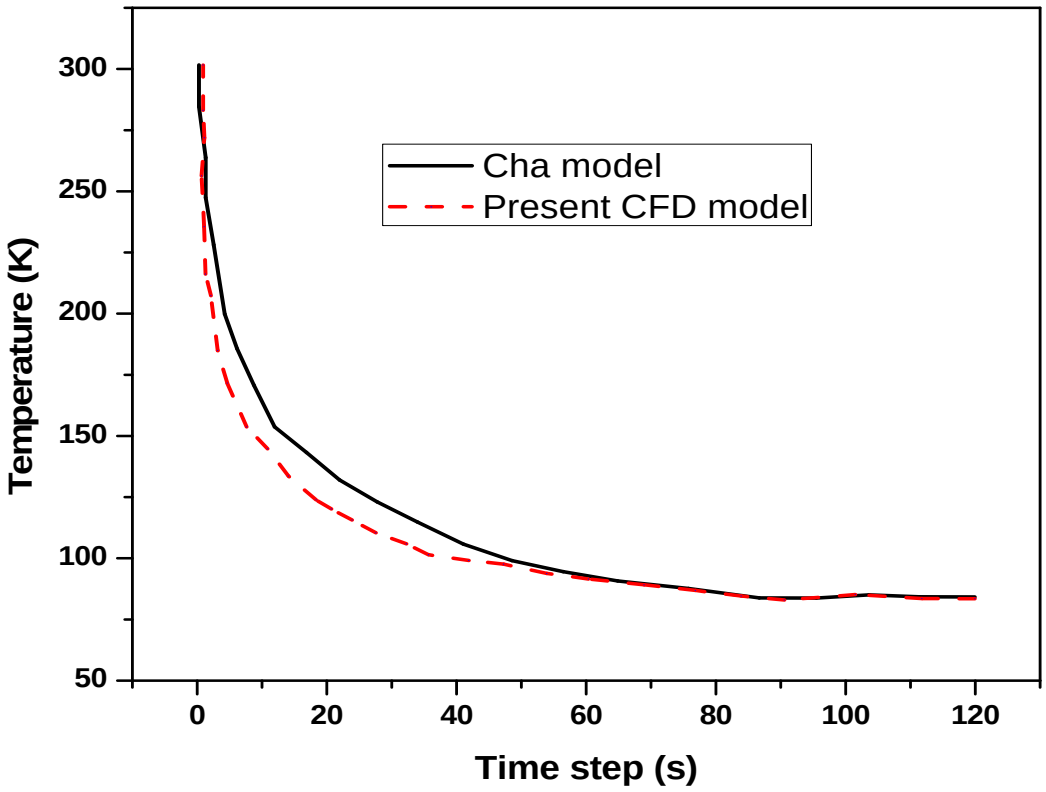

Figure 4.11 Comparison of cool down behaviour.

residual sum for each of the conserved variables is computed and stored. Thus, it records the convergence history. Once all the above mentioned steps are over, iteration can be initiated with the time step of 0.0005 second with total number of iterations more than 700000 and the number of iterations per time step to be 50. To run a single

case and to reach a steady state temperature at the cold end, it takes more than 20 days by a computer with 3 GHz processor and 8.0 GB of RAM for 2-D simulations.

Temperature dependent properties

The thermal conductivity, viscosity and specific heat of the working fluid and the solid matrixes are considered as temperature dependent. The temperature dependent thermo-physical properties are obtained from the NIST database. User Defined Functions (UDFs) for the calculation of variable thermo-physical properties of the working medium and the porous matrixes are written and appropriately hooked to the FLUENT panel. This user defined function calls particular cell temperature from FLUENT panel and updates the property values after each time step. FLUENT offers the flexibility for updating the properties after various numbers of time steps. Since the temperature variation in pulse tube is sharp, the properties are updated after each time step.

4.4 Results and Discussion

The Computational fluid dynamic approach has been adopted to solve the single stage Stirling type inertance tube pulse tube refrigerator (ITPTR) numerically by using FLUENT. The results obtained from the numerical simulations are used for performance analysis.

Porosity effect on cool down performance

The most important part of the pulse tube refrigerator is the regenerator. Regenerator consists of matrix as shown in Figure 4.3. The porosity of matrix affects the performance of the regenerator. So an investigation conducted for the present ITPTR model for varying porosity value. Figure 4.12 shows the result in terms of cold end temperature of ITPTR. From the result of simulation, it is reported that at the porosity value of 0.6 the optimum result is found relative to other values.

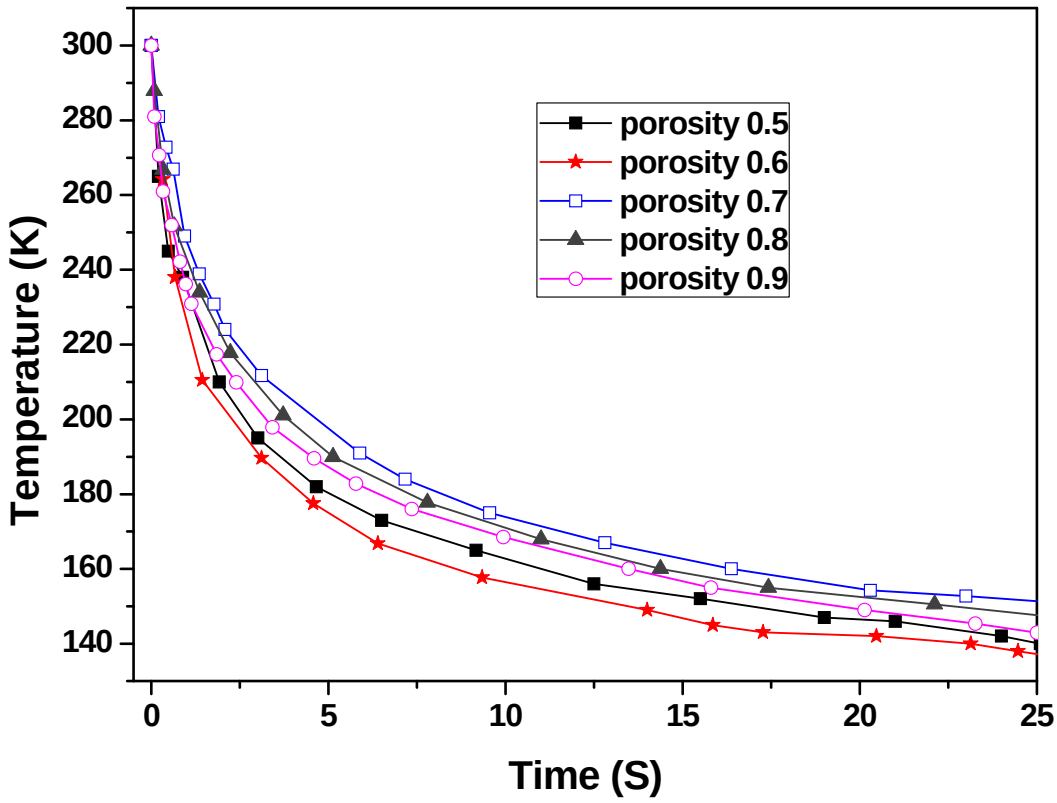

Figure 4.12 Cool down temperature vs. time for different porosity inside regenerator.

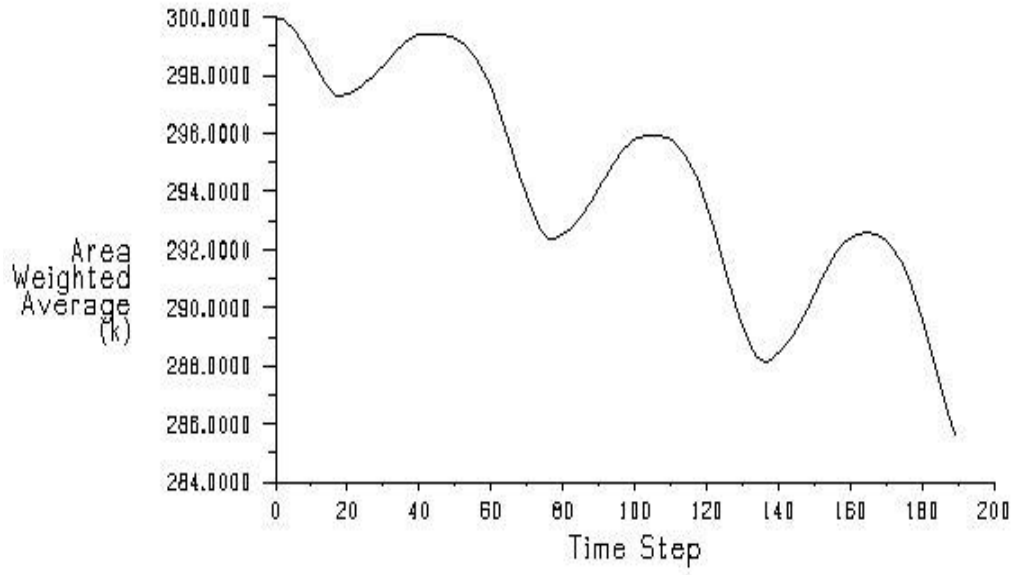

Figure 4.13 Mean Average temperature at the inlet of pulse tube during starting of simulation.

Temperature distributions

Figure 4.13 shows the mean average temperature variation inlet of the pulse tube or at the exit of the cold heat exchanger for the first 140 time steps for the thermal equilibrium model. The downward trend of the temperature plot shows a rapid cooling at the cold heat exchanger during starting of simulation. Figure 4.14 shows the Cyclic Average Mean Static Temperature of the cold end heat exchanger plotted against the cool down time for the different pulse tube length. These results are obtained with an assumption of zero wall thickness and thermal equilibrium of porous matrix and working fluid. The performance of various pulse tube models is presented based on the effect of pulse tube length in terms of cool down temperature at the cold heat exchanger at no load condition. It is found that with increase in length of the pulse tube, the lowest cold end temperature can attain. The increase in length causes higher viscous losses in the system so high compressor power is required.

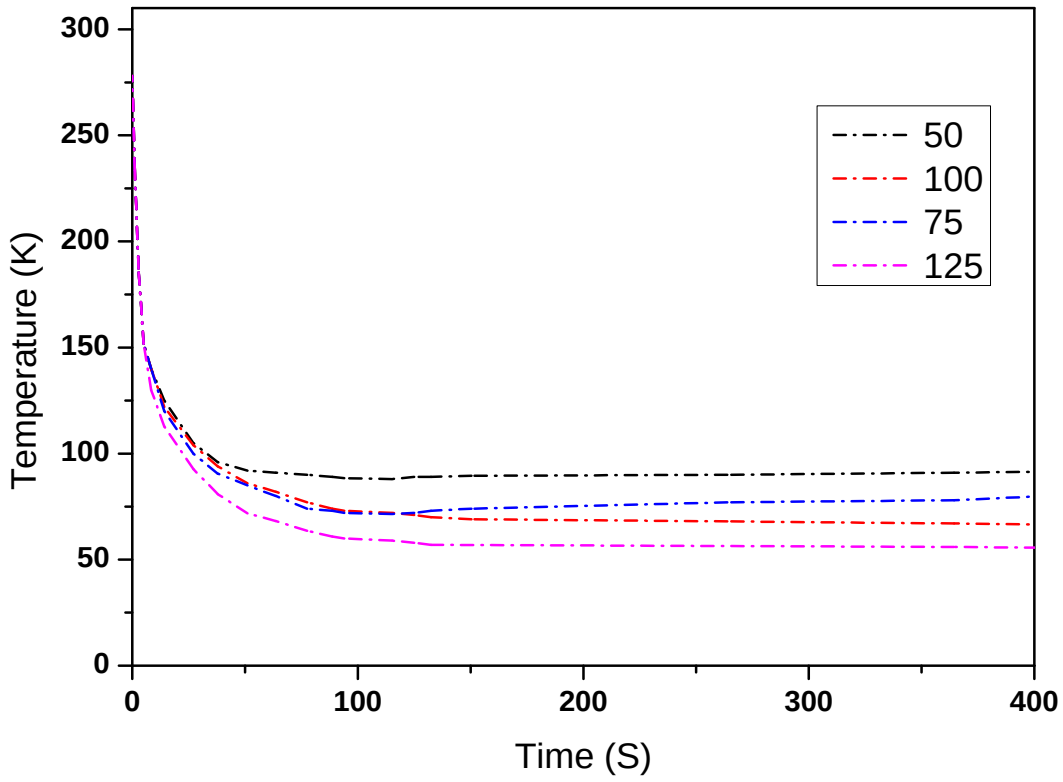

Figure 4.14 Mean average cool down temperature for different model with thermal equilibrium temperature

Table 4. 2 Different pulse tube model of varying pulse tube length

Model	Pulse Tube Demeter (mm)	Pulse Tube Length (mm)
Model 1	5	50
Model 2	5	75
Model 3	5	100
Model 4	5	125

To study the two dimensional effect, the result obtained by Fluent is shown by taking the snapshot view of the temperature contour along the axial direction at the no load condition for the pulse tube model 4 (Table 2) in Figure 4.15. From this figure, it is observed that there is a good agreement of temperature gradient at regenerator, cold heat exchanger, pulse tube and the hot heat exchanger. The modelling is done with the thermal equilibrium model of the porous zone of the system. It is also observed that due to the surface heat pumping through the pulse tube, an axial increase in temperature from cold end heat exchanger to the hot end heat exchanger is presented. So at any time the temperature remains nearly constant with small fluctuation at any position. Near the cold heat exchanger wall temperature found at 58 K whereas after the hot heat exchanger wall are above 300 K. Figure 4.16 shows the density contour of the model 4.

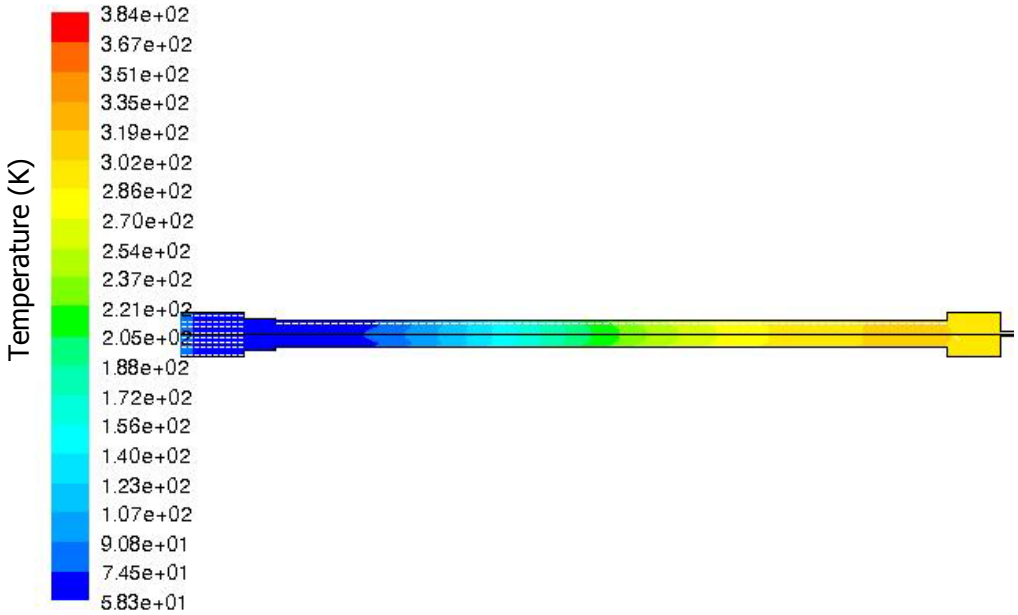

Figure 4.15 Temperature variation contour inside cold heat exchanger , pulse tube and hot heat exchanger of model 4

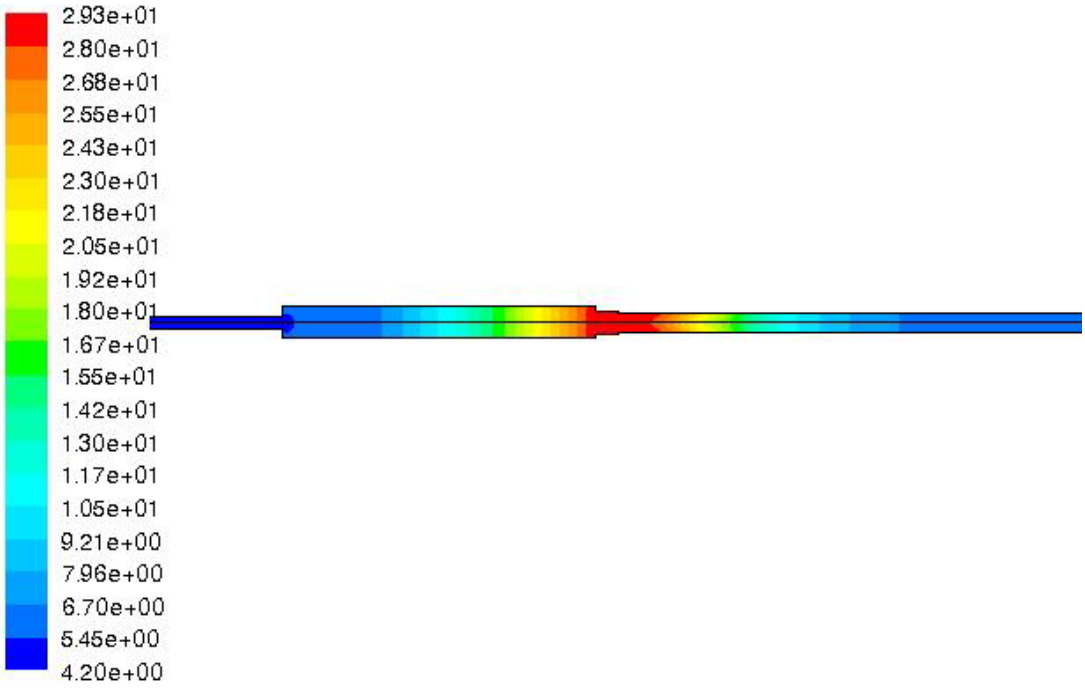

Figure 4.16 Density contours for model 4.

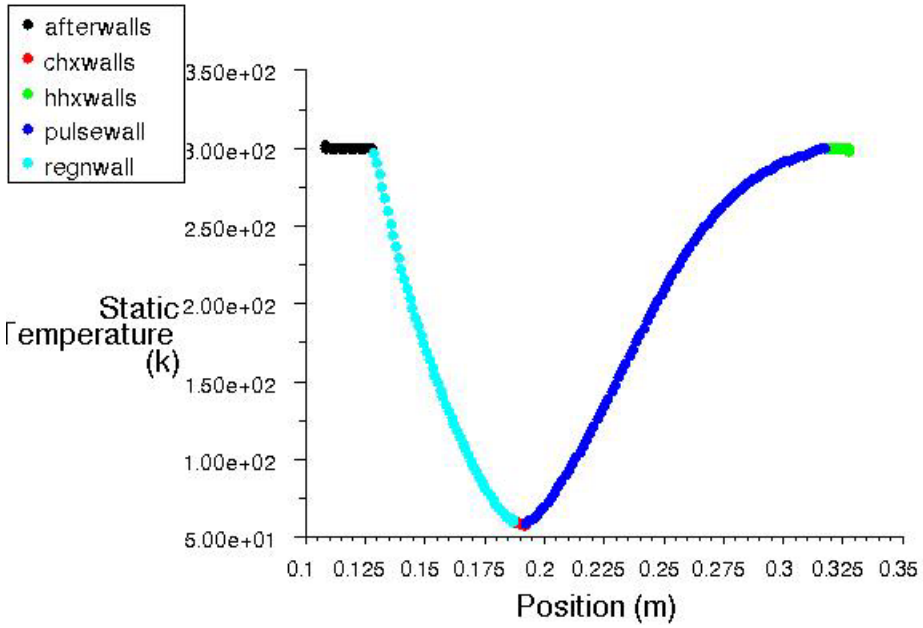

Figure 4.17 Axial temperature plot variation from after cooler to hot heat exchanger after steady state of model 4

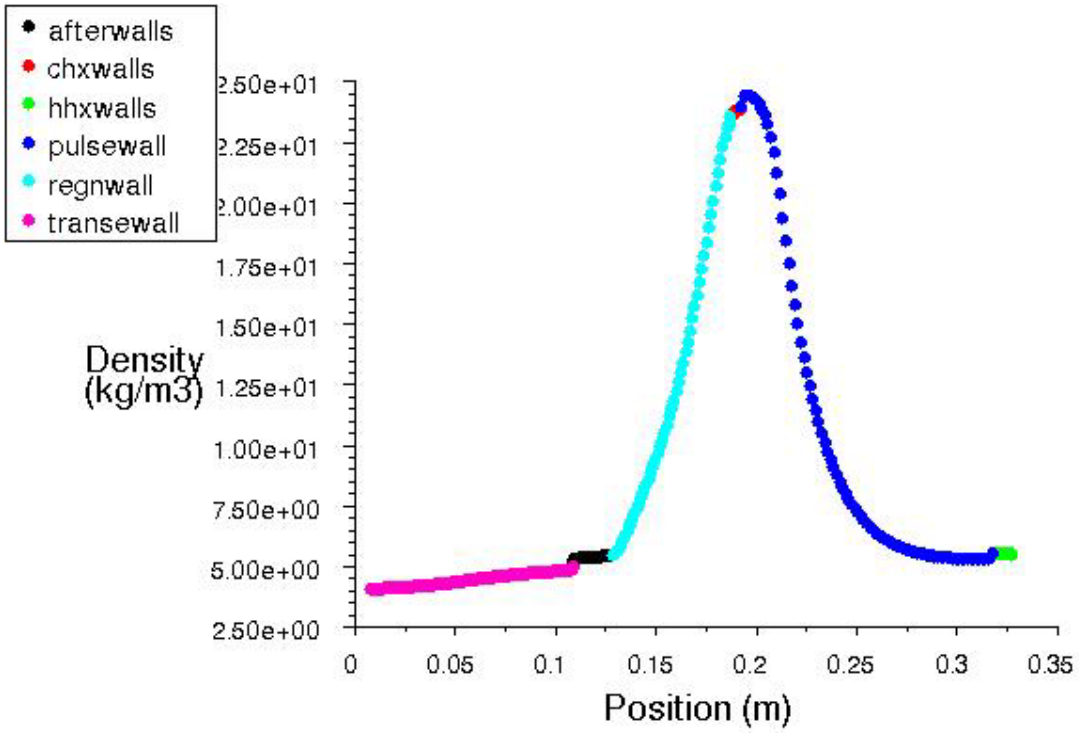

Figure 4.18 Density variation along axial direction for model 4

Figure 4.17 shows the axial temperature variation of the computational domain of the pulse tube refrigerator. It may be recalled that perfect cooling is assumed in the compressor after cooler. It can be seen that a good temperature gradient is established axially between the regenerator, pulse tube and the hot heat exchanger, respectively. The modelling is done with a thermal equilibrium model of the regenerator. The figure also shows that the axial temperature gradient is maintained in the pulse tube. It also presents the drop in temperature from the after cooler to hot end exchangers.

Pressure distributions during the simulation

Figure 4.19 shows the oscillatory pressure profile for the pulse tube model at starting of simulation. It can be clearly visible from the figure that the pressure oscillates between 21 bar and 39 bar over one cycle during first 140 time steps. Figure 4.20 presents the periodic pressure variation for the same model after 623580 iterations. The pressure inside the computational domain attains a mean value of 25 bar from the charging pressure of 31 bar, after reaching the steady periodic condition which is in between 19 bar and 30 bar over one cycle. From Figure 4.20 it can be seen that the variation of pressure over one complete cycle is not accurately sinusoidal.

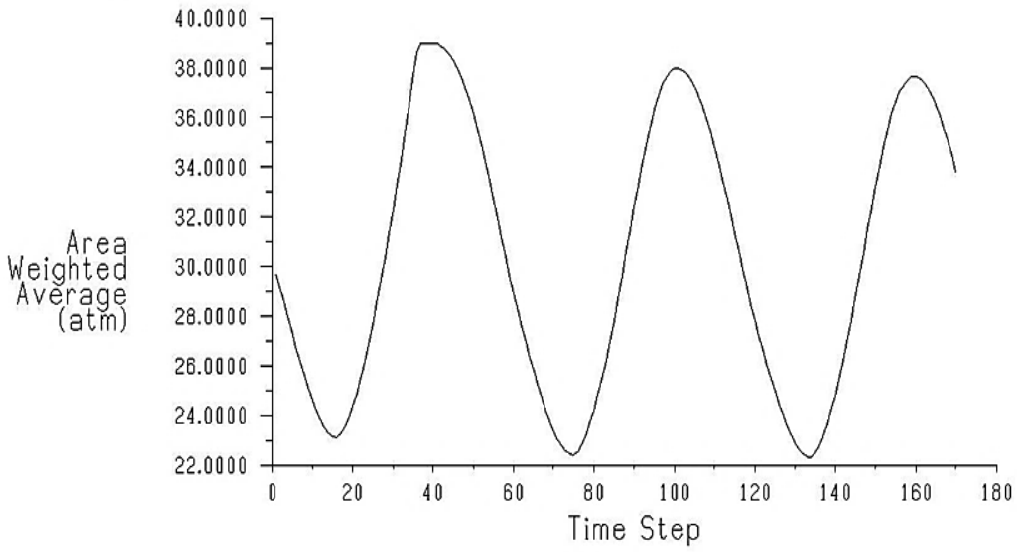

Figure 4.19 Area weighted Average pressure at the inlet of pulse tube during starting of simulation

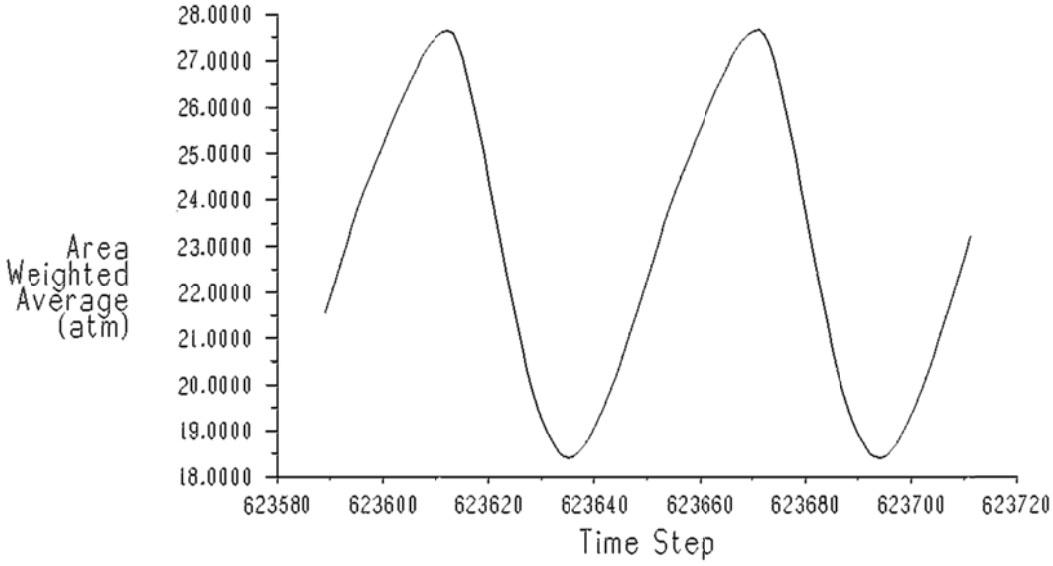

Figure 4.20 Area Weighted Average Pressure inlet of pulse tube after 623580 iterations

This is due to the complex interaction of the solid matrix and the gas inside the system. This type of misleading pressure profiles is due to the thermal damping effects of porous zones and temperature dependent properties of the solid and the fluid. A similar conclusion may be drawn with respect to the misleading occurring in the temperature

profiles. Due to the coupling, pressure profile is affected by the misleading in the temperature profile. The pressure drop through porous zones is affected by Darcy and Forchheimer terms, which are depend upon the physical property variation due to change in temperature.

Figures 4.21–4.24 illustrate the pressure variation during the simulation inside the computational domain of the pulse tube refrigeration model at any instant position of the piston. The pressure variation inside the pulse tube from 23.1 bar up to 37.5 bar is observed from the figure. Figures 4.21 shows the axial pressure variation inside the computational domain starting from compressor up to reservoir while the piston reaches to the far end dead position at both ends. At that position the compressor pressure is 20.6 bar and the pulse tube pressure is 22.9 bar, where reservoir pressure is maintained at 30.4 bar. It can be noted from the figure that during this instant of time the reservoir attains the maximum pressure while minimum pressure is attained inside the compressor. Figure 4.22 shows the axial pressure inside the domain from compressor to reservoir when the piston is reaches at middle position during compression. At that position the compressor pressure is 37.25 bar and the pulse tube average pressure is 32.1 bar, where the reservoir pressure is 30.2 bar. When the piston reaches its near end dead position at both sides during compression process, the axial pressure variation of the system is shown in Figure 4.23. At this position the compressor has maximum pressure of 37.86 bar and minimum pressure is 30.1 bar inside the reservoir and the pressure inside the pulse tube is 37.5 bar. During the expansion process when piston is reached at middle position a pressure variation plot is shown in Figure 4.24. At this position the compressor has pressure of 28.1 bar, pressure inside pulse tube is 31 bar and the reservoir pressure is 30.4 bar. From the pressure fluctuation analysis during one complete cycle it can be concluded that when there is maximum pressure at one end the other end of the system has the minimum pressure. This is the main purpose of the study that to analyze the pressure variation through the whole system during a complete cycle.

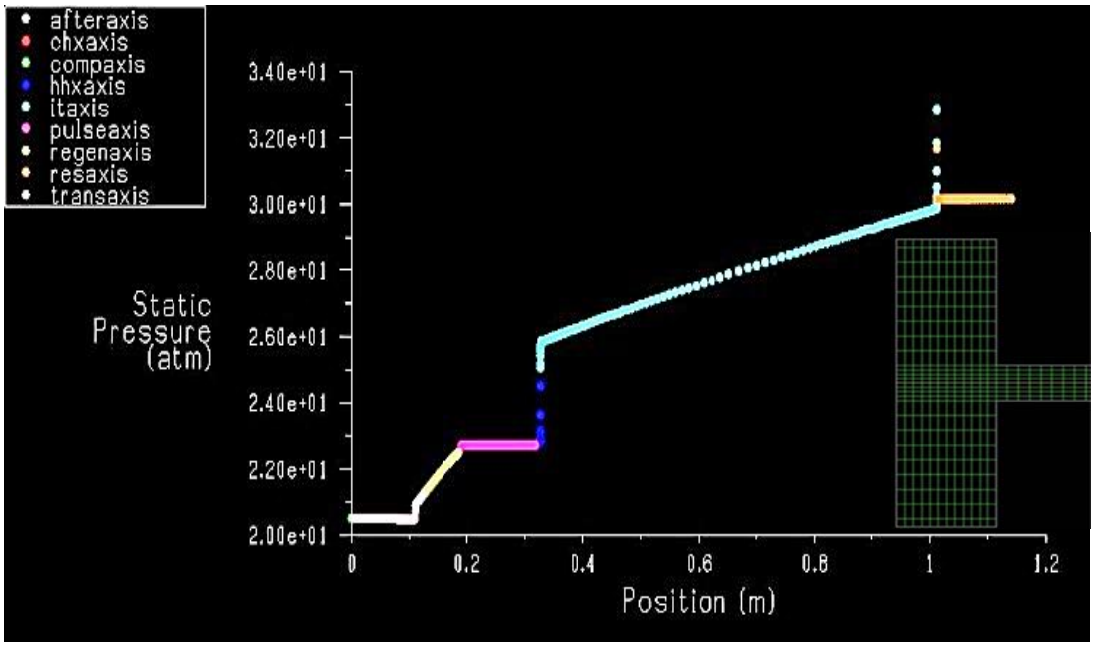

Figure 4.21 Axial Pressure inside the ITPTR, when piston reaches to the far end dead position at both ends.

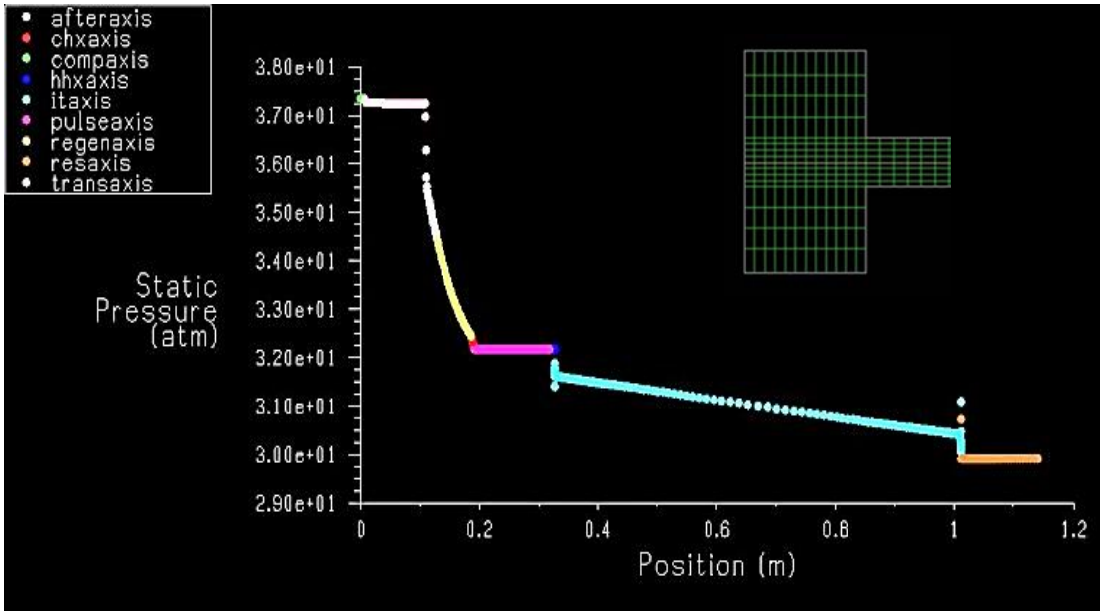

Figure 4.22 Axial Pressure inside the ITPTR, when the piston is in middle position during compression

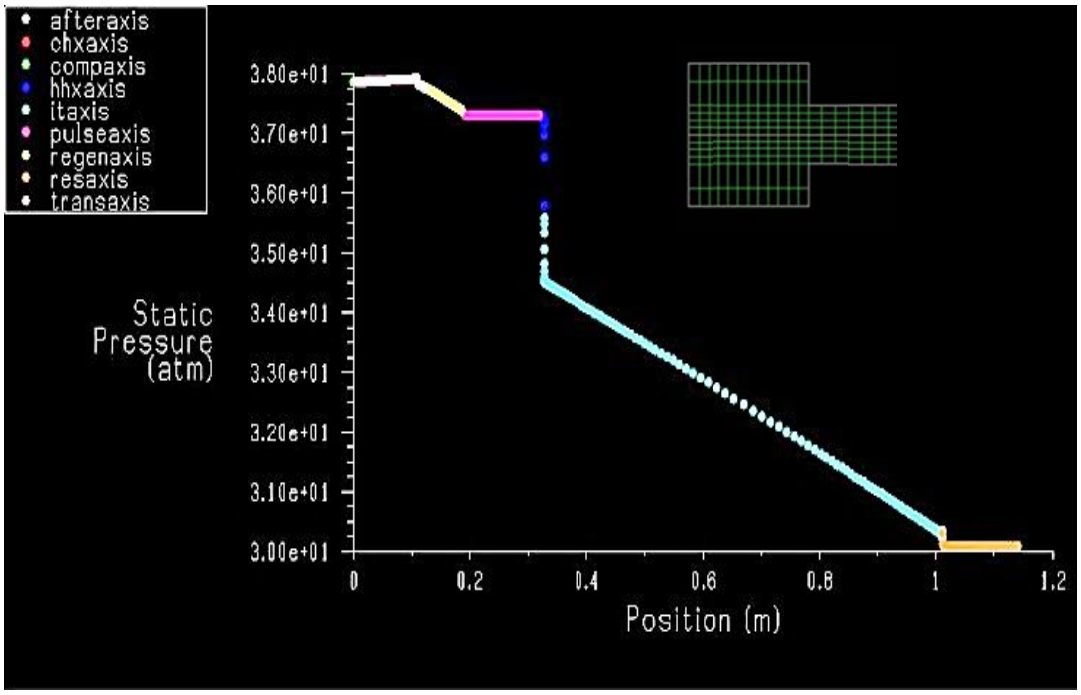

Figure 4.23 Axial Pressure inside the ITPTR, when piston reaches its near end dead position at both sides

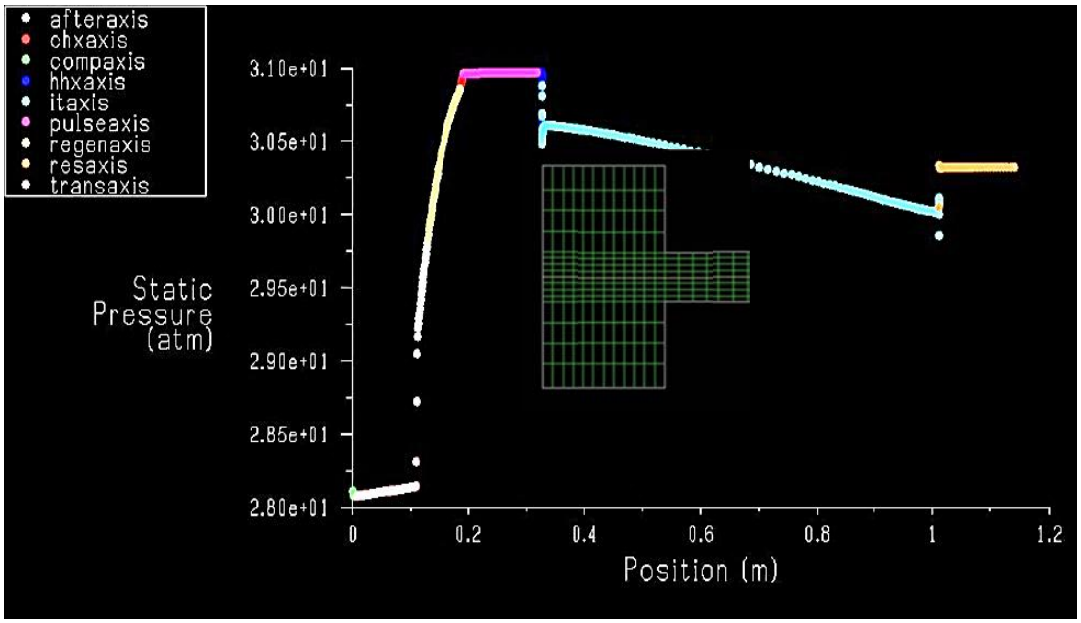

Figure 4.24 Axial Pressure inside the ITPTR, when the piston is in middle position during expansion

Analysis of thermal-non equilibrium of porous Zone

As discussed earlier in this chapter the thermal equilibrium model solves a single energy equation for both solid matrix and working fluid in porous zone, hence it cannot differentiate between the porous matrix and working fluid temperatures, but in thermal non-equilibrium model it accumulates the heat transfer interaction between solid porous matrix and working fluid. Hence, in the thermal non-equilibrium model the heat transfer coefficient in regenerator plays a vital role while in thermal equilibrium model it is infinite. Figure 4.25 gives a comparison of the results between thermal equilibrium model and non-equilibrium model in terms of average mean temperature against the time step at the cold end. The analysis presented here is without wall thickness for Model 4. A case with thermal non-equilibrium of porous zones represents a realistic model. Both thermal equilibrium model and non-equilibrium models exhibit rapid cooling followed by levelling off of the temperatures. However the final cold heat exchanger temperature reaches by thermal non equilibrium model is higher than that of the thermal equilibrium model. The thermal non-equilibrium model takes longer time (above 200 seconds) for reaching the steady state while the thermal equilibrium model attains a steady state much earlier, i.e., in about below 200 seconds. The final temperature reached with the thermal equilibrium model is lower than that of the thermal non-equilibrium model. The reason behind the lower temp at the cold end of the thermal equilibrium model than thermal non equilibrium (TNE) model is that the thermal non-equilibrium model dissipates the thermal losses in the regenerator. The decrease in performance of the thermal non equilibrium model is due to presence of thermal losses in the porous zones.

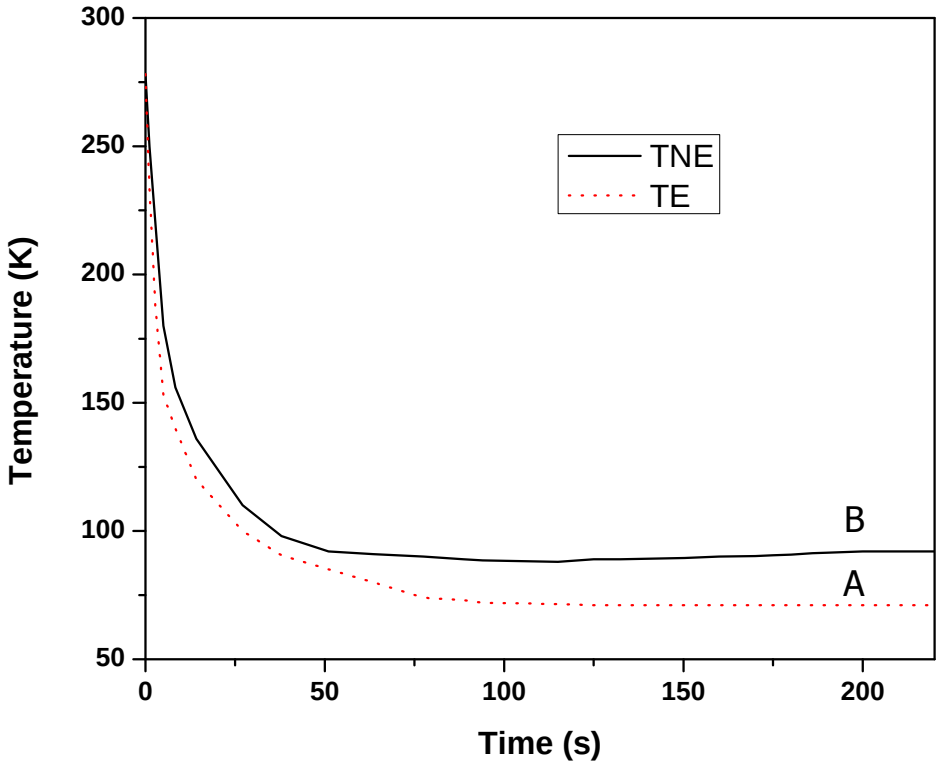

Figure 4.25 Comparison of the results between thermal equilibrium model and non-equilibrium model in terms of average mean temperature

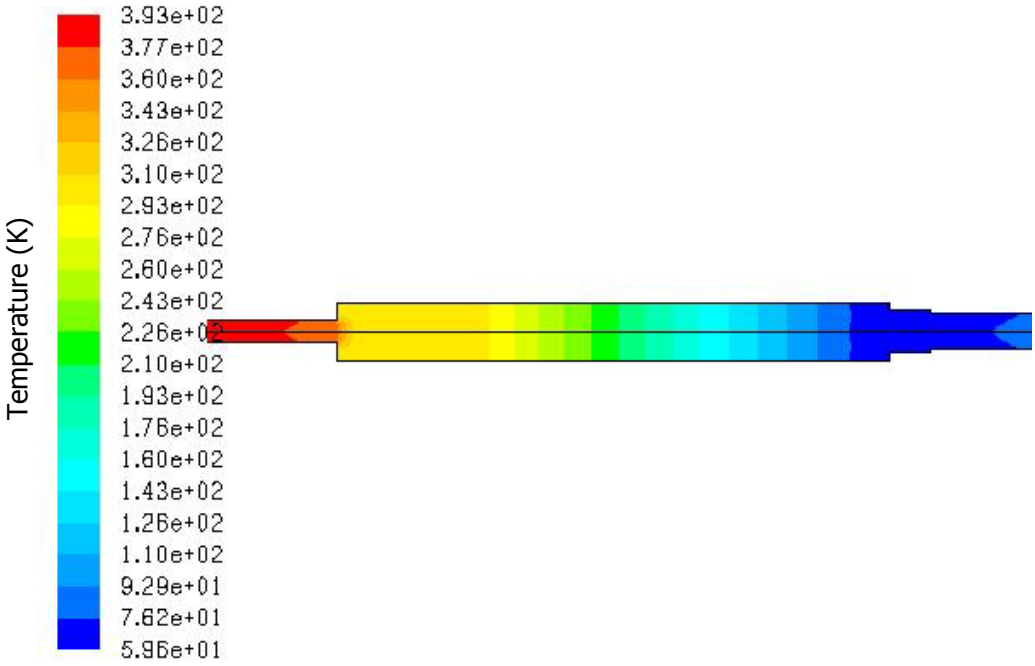

Figure 4.26 Temperature variation contour inside regenerator after steady state temperature achieved for thermal equilibrium model

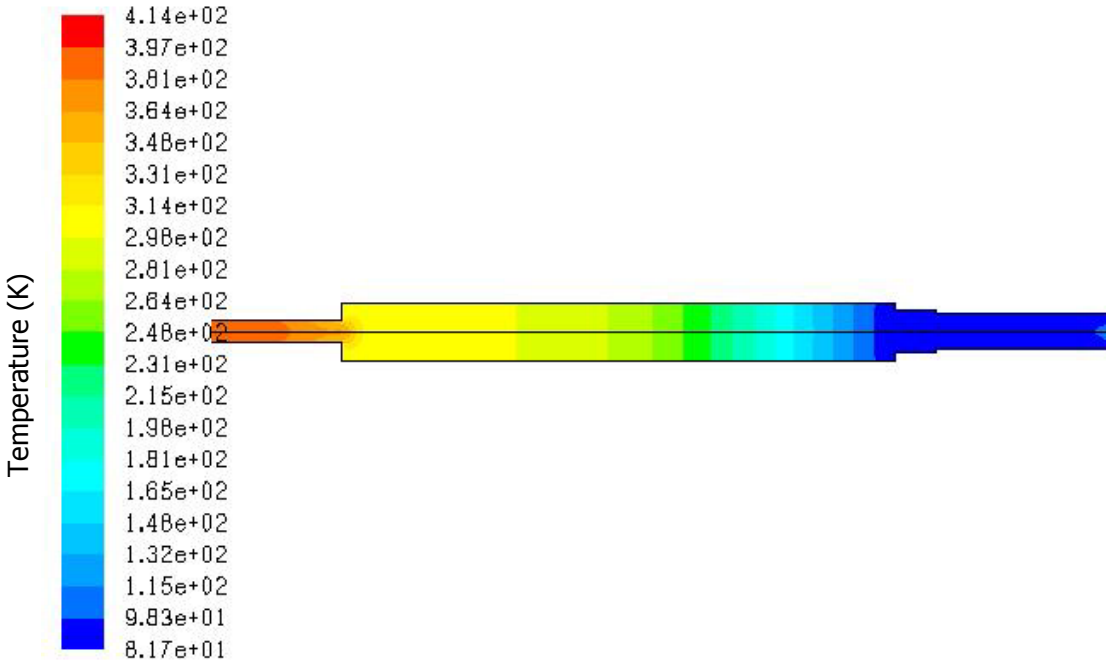

Figure 4.27 Temperature variation contour inside regenerator after steady state temperature achieved for thermal non-equilibrium model

Figure 4.26 and Figure 4.27 shows the instantaneous temperature variation inside a regenerator after reaching steady periodic condition. Comparing the above two figures, it is observed that the temperature variation differs slightly in magnitude. However the difference in the time instants of the above figure should also be taken into account. The slight change in temperature profile is due to the heat transfer correlation for solid fluid interaction.

Phase relationships

The variation of the averaged pressure and mass flow rate at the outlet of cold heat exchanger end and the variation of the area weighted average temperature vs mass flow rate at the exit of pulse tube are shown in Figure 4.28 and 4.29. It is described in the previous published literature, Radebaugh [10] that the phase angle between mass flow rate and temperature plays a vital role in the evaluation of performance of pulse tube refrigerator design. The Figures 4.28 shows that at the end of the cold heat exchanger, the mass flow rate is lagging the pressure by a small phase angle which is similar to Radebaugh [10]. The Figures 4.29 illustrates the variation of the area weighted average temperature and mass flow rate at the exit of the pulse tube. It can be noted from this figure that the temperature and the mass flow rate are

almost out of phase. This condition of phase shift is due to small enthalpy flow through the pulse tube and the analysis is performed for no load condition.

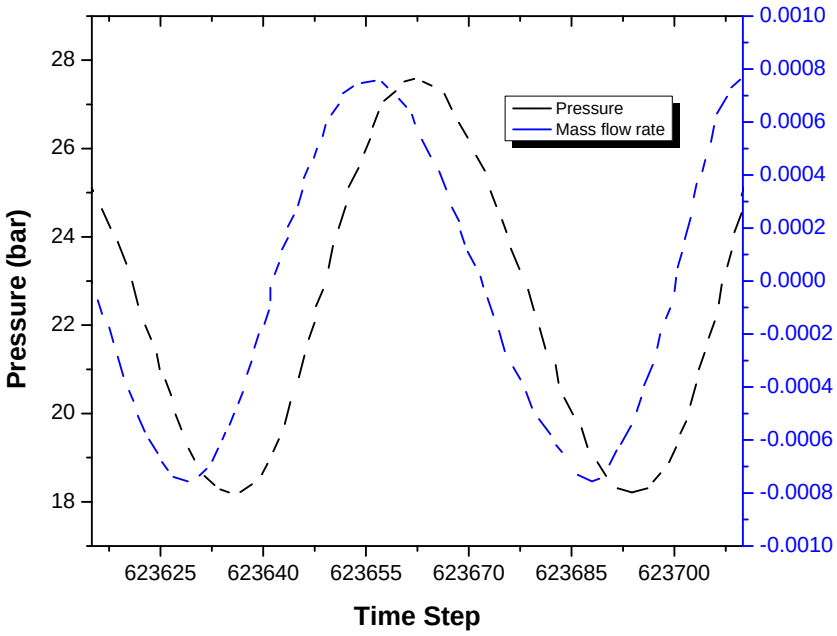

Figure 4.28 Phase relation between mass flow rate and pressure at cold heat exchanger for ITPTR after steady state achieved.

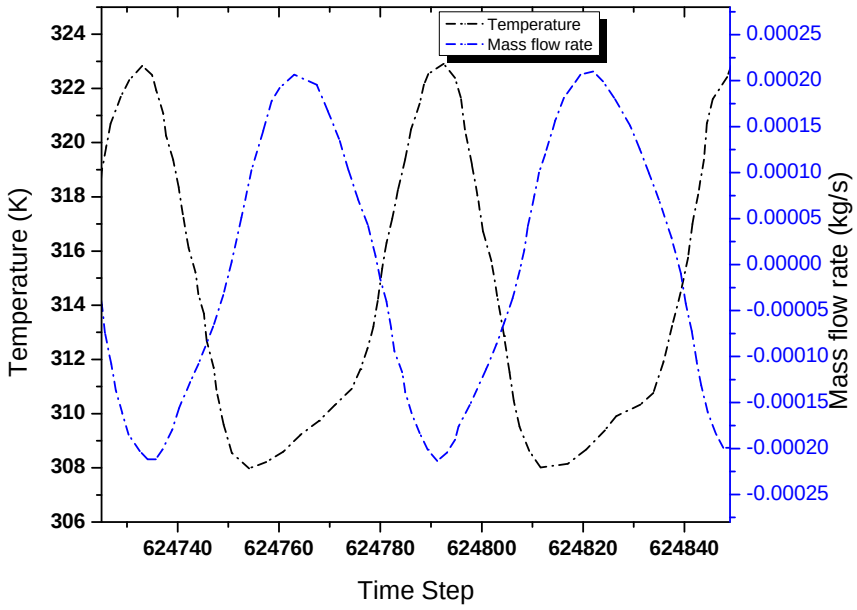

Figure 4.29 Phase relation between mass flow rate and temperature at hot heat exchanger for ITPTR after steady state achieved.

4.5 Summary

The numerical simulation, using the commercial computational fluid dynamic (CFD) simulation software package, FLUENT is used to modelling and analysing the ITPTR model includes compressor, after cooler, regenerator, pulse tube, cold and warm heat exchangers, inertance tube and reservoir. The simulation is conducted taking into account the axis-symmetric flow conservation equations and negligible wall thickness. For modelling the inertance tube pulse tube refrigerator both thermal equilibrium and thermal non-equilibrium models are considered. Unlike the previous basic method, phasor analysis and linear network as reported in literature, the present CFD model performs more accurate result comparing to them. It is found from the analysis that the decrease in cold end temperature with increase in pulse tube length is mainly due to the reduction of turbulence and also due to the considerable reduction of heat transfer coefficient between pulse tube wall and working fluid. The oscillatory flow solid-fluid interactions are modelled with the more realistic thermal non-equilibrium model for porous zones. It can be reported that increase of cold end temperature in thermal non-equilibrium in the porous zones is due to temperature interaction between solid matrix and working fluid and also influence of Forchheimer term is reasonably substantial in the investigation of flow through porous medium. It can be noted that the compressor work increases with increase in length of pulse tube due to more viscous flow. The minimum temperature is achieved at the cold end of the 5 mm diameter pulse tube, 125 mm among out of four models considered for analysis with the frequency of 34 Hz.

Chapter 5

MODELING AND OPTIMIZATION OF INERTANCE TUBE PULSE TUBE REFRIGERATOR

5.1 Introduction

The previous chapter highlights the heat transfer and transport phenomenon of the inertance tube pulse tube refrigerator, using FLUENT package. The performance of a pulse tube refrigerator depends on many parameters such as the operating frequency, charging pressure, geometrical dimensions (pulse tube, regenerator, inertance tube), working fluid, etc. From the review of the literature, it is reported that the traditional one-factor-at-a-time approach has been widely used for the design or optimization of these parameters. This method is time-consuming and expensive and fails to consider any possible interaction between factors, which is a major disadvantage. To overcome such problems, response surface methodology (RSM) is one of the statistical design tools, widely used by researchers. The RSM is an optimization method, which performs a series of numerical analyses for a given set of design points and generates a response surface of the given input parameter over the design space. It can be used for the prediction of the interaction between many parameters and for process optimization also. The RSM defines the effect of the independent variables, alone or in combination, on the process [220]. The RSM has been tested to be a powerful statistical tool for the optimization of thermal and fluid flow processes in many cases. In order to get the optimum configuration (length and diameter) of the ITPTR, the RSM has been used in the present work as the optimization method where the rest of the parameters are kept constant.

The main objective of this chapter is to minimize the cold head temperature and input compressor power, following the Multi-objective algorithm. The RSM based Box-Behnken design is adopted to evaluate the effect of the geometrical parameter on T_{cold} and W_{comp} using the numerical method. Box-Behnken design offers a three-level incomplete factorial designs following a second- order design. This design is an experimental design for response surface methodology, formulated by George E. P. Box and Donald Behnken in 1960. This design has been preferred for the analysis because it performs non sequential experiments; having few design points. It is helpful in the

safe operating zone for the process as these designs do not have axial points. On the other hand, central composite designs have an axial point outside the cube which may not be in the region of interest or may be impossible to run as they are beyond the safe operating zone.

SAGE being one dimensional nature, it takes less time to generate the results. So it is used to generate the results for present investigation. After the generation of output results, the next step is to use the data for the analysis of variance (ANOVA) to produce a second order regression equation. Finally, the layout of the ITPTR is optimized based on the generated RSM and NSGA-II algorithm. The detail of the methodology used in this work is illustrated in Figure 5.12.

5.2 Sage Modelling

This section describes the detail modelling and simulation of ITPTR to indetify the performance characteristics by using Sage simulation software. It can solve the 1-D equations for the pulse tube refrigerator model using the pulse tube version of the Stirling simulation software. It is a graphical interface that performs simulation and optimization of a fundamental class of cryocooler models. Model classes include mass spring damper resonant systems, Stirling-cycle machines, and others. The sage model is formed in a hierarchical tree structure of components in the form of icons where each icon classically contains numerous layers of additional sub-components. The root or (highest level) of the present Sage model of the ITPTR is shown in Figure 5.1. Sage is user friendly software which holds a drag-and-drop interface of typical components found in both Stirling and pulse tube cryocoolers. For example an element, such as a heat exchanger encloses a number of tubes, wall thickness and diameter of tube, each component can be independently identified in terms of geometry, and numerical data can be entered. The Sage software empowers the user to map, solve or optimize the model, and generates output files which can be transferred to packages like Microsoft Excel for further investigation. The compressor with 60 ml of swept volume is coupled in Sage to model the present ITPTR. The initial geometric parameters are based on general relationships, such as the cross-sectional area of the pulse tube is proportional to the cooling power requirement; the pulse tube volume is approximately 38% of the compressor swept volume and the reservoir is approximately 52 times the pulse tube volume. The individual components used in the sage modelling of this ITPTR are discussed in this section.

At the root level (highest level) the ITPTR can be distributed into two main sub-assemblies: the compressor zone and the cold space zone. They are connected by a transfer line as shown in Figure 5.1. The details of modelling of the individual components are illustrated as below.

- **Compressor**

  Filling pressure (pressure source)

  Piston and Cylinder

- **Cold space**

  After cooler

  Regenerator

  Cold heat exchanger

  Pulse tube

  Hot heat exchanger

  Inertance tube

  Reservoir

Various connecting tubes and flow diffusion sections are also incorporated to modelling accurately. All of these subassemblies and components are individually covered here. In order to gain some physical resemblance between the sage model and the actual hardware, in general the model is set up to address the components from the left-to-right direction as shown in Figure 5.11. Additionally, when a 'positive' or 'negative' attachment is encountered, negative refers to the left side of the component and positive refers to the right side of the component as shown in Figure 5.1.

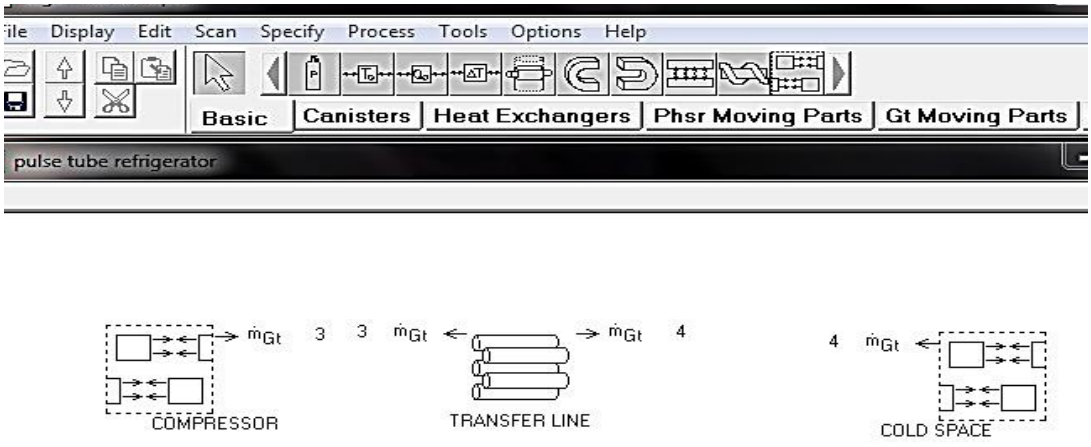

Figure 5.1 Root level components of ITPTR

5.2.1 Modelling of Compressor

The compressor comprises of a single constrained piston driving a compression space. Generally the linear motor efficiency is estimated and then applied to the pressure-volume (PV) power determined by Sage to predict the electrical input to the compressor. The compressor can be designed in Sage using the available components. These components are, one pressure source and the generic cylinder from the "Basic" tab, and a constrained piston and cylinder composite component which already includes the necessary child components from the "Composite" tab. These parent level model components are shown in Figure 5.2.

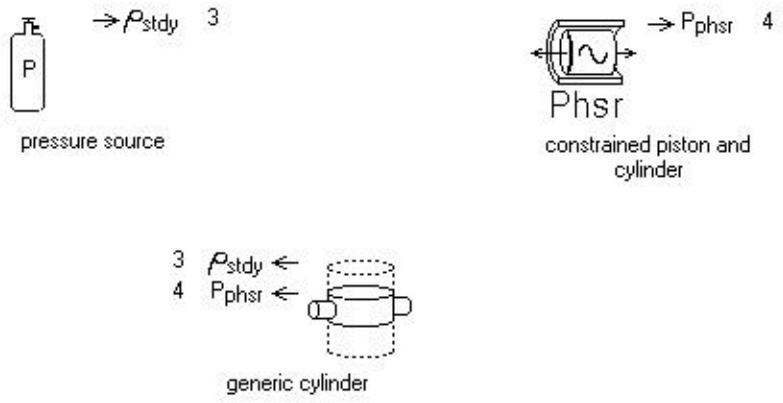

Figure 5.2 Parent (root) level model components of a compressor

The pressure source component establishes the charge pressure for the ITPTR with the built-in density attachment ρ_{std}. This pressure source is precisely connected to the gas domain, compression space (generic cylinder). The pressure source behaves as an infinite isobaric gas reservoir. There is only one input variable of the pressure source that is P_{charge} (charge pressure). When the pressure source connected to the gas domain the density in the gas domain adjusts itself so that time average pressure is continuous across the connection, and hence the time-average pressure at the negative end of the gas domain becomes P_{charge}. As mentioned before the pressure source is connected to a generic cylinder as shown in Figure 5.2, which is the model for the compression space of the compressor. Figure 5.3 illustrates the child level components of the generic cylinder containing the supplementary components, cylinder-space gas from the 'Gas Domain' tab and isothermal surface from the 'cylinder walls' tab. Both of these

components originate with built-in heat flow associates, which retains this child level and model the thermal interaction between the gas and solid boundary. In Figure 5.3, cylinder space gas is labelled with a 'C', which stands for cylinder-space gas domain. In the child level of generic cylinder the isothermal surface has not added to any child components, but the cylinder-space gas is added with child level components as shown in Figure 5.3. The cylinder-space gas contains one charge gas inlet, one positive gas

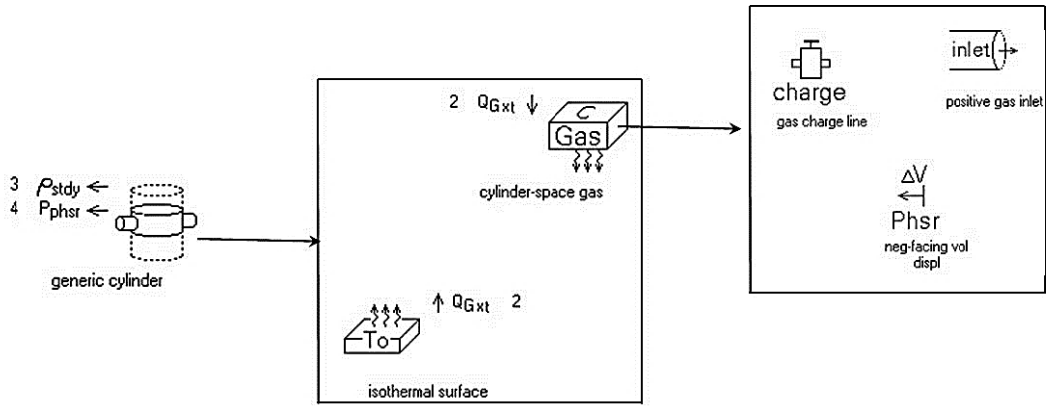

Figure 5.3 Child level components of cylinder-space gas model.

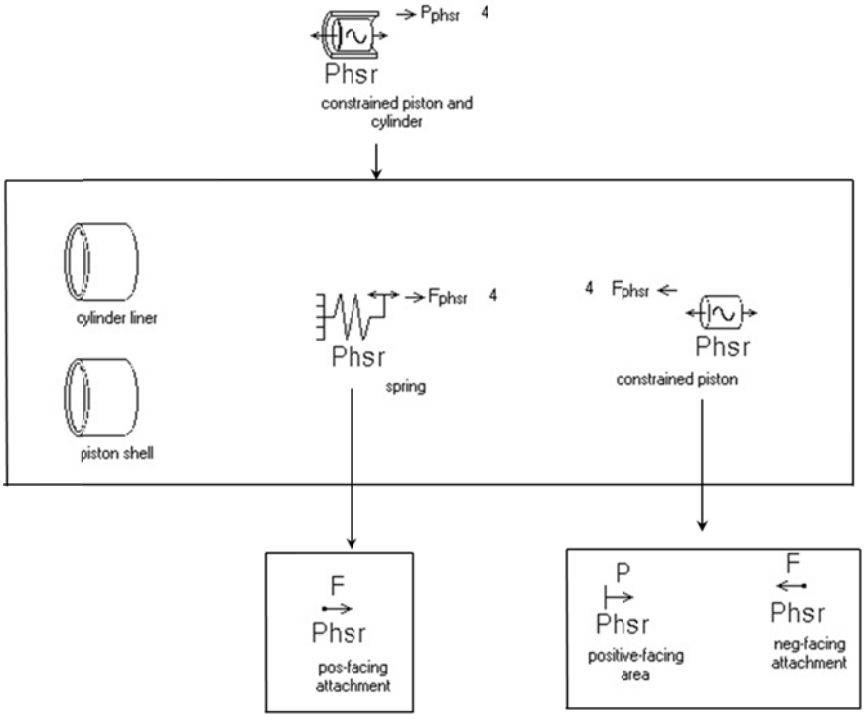

Figure 5.4 Child level components of constrained piston and cylinder composite model.

inlet and one negative facing volume component. The gas charge line component is attached from the 'Charge/Inlets' tab. This component contains the density element ρ_{stdy}, which is responsible for attachment to the pressure source at root level. This attachment regulates the system working mean pressure. The negative volume displacement component added from the 'Volume Displacements' tab contains the P_{phsr} and attached to the root level for connection to the constrained piston to represent the volume displacement at the boundary between the face of the piston and the gas. While it seems that something is incomplete by attaching a volume displacement to an area, one input of the constrained piston is its amplitude and this combination of piston area and amplitude complete the volume displacement connector. Lastly, the positive gas inlet attachment also added from the "Charge/inlets" tab which is exported to the root level for attachment. This represents the fact that the variable volume gas space is connected to some other external system rather than simply compressing and expanding in a dead volume.

5.2.2 Modelling of Piston and Cylinder

The cylinder composite component is available in 'composite' tab as shown in Figure 5.2. It consists of a liner cylinder, one piston shell, a spring and a constrained piston as the child component as shown in Figure 5.4.

The 'constrained piston and cylinder' refers that the motion of the piston, i.e. the amplitude and phase are defined by input values only and not depend on other forces acting upon it. Its motion is driven by the forces acting upon the piston. The spring component is added at this level from the 'springs and Dampers' tab to model the attachment between the piston and the planar spring. There are no further child components associated with either the piston shell or cylinder liner.

Within the constrained piston child component of it and cylinder parent level component, two attachments are added from the "mechanical attachment" tab. The first attachment is a positive-facing area, which physically represents the face of the compressor piston. This attachment is exported out from this child level up to the top or root level for later attachment. The other is the negative-facing attachment. F_{phsr}, which physically represents the attachment of the piston to the spring. This attachment is exported out from this child level up to the constrained piston and cylinder level (Figure 5.4) for later attachment. The only child component added to the spring component is the positive-facing attachment which connects to the negative-facing attachment of the

constrained piston at the constrained piston and cylinder level (Figure 5.4). The compressor and the cold space are connected by a connecting tube. It is added from the child component tab 'tube bundle' available in heat exchanger components as shown in Figure 5.1. The modelling of connecting tube is similar to the compression space model as shown in Figure 5.5.

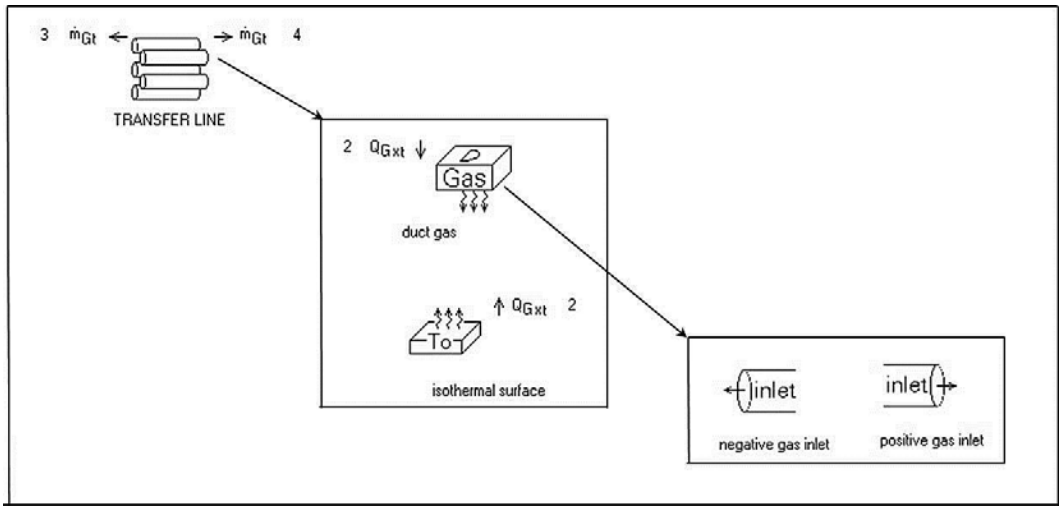

Figure 5.5 Child level components of connecting tube.

However, the duct gas labelled with a 'D' is shown in Figure 5.5. As discussed before 'C' stands for a cylinder-space gas domain whereas the 'D' sands for a duct gas domain. It can be seen that there is a connection between the gas domain and an isothermal surface. In the duct gas domain both a positive and negative gas inlet are included and attached to the root level with connection to the compression space and the rest of the system. Again, it is more appropriate to include the connecting tube along with the compressor rather than the cold head model. Some of the components shown in the edit view are not listed as part of the model tree. This is because these components have no input or output data associated with them. Therefore, they are used purely in the edit view window to indicate a connection between two other components.

5.2.3 Modelling of Cold Space

Figure 5.6 describe the most significant components of the cold space portion of the Sage model. These include after cooler, regenerator, cold heat exchanger, pulse tube, hot heat exchanger, inertance tube and reservoir. Additionally, some components

are attached to increase accuracy. A heat sink and a heat source are also attached to model the parasitic heat flow between them.

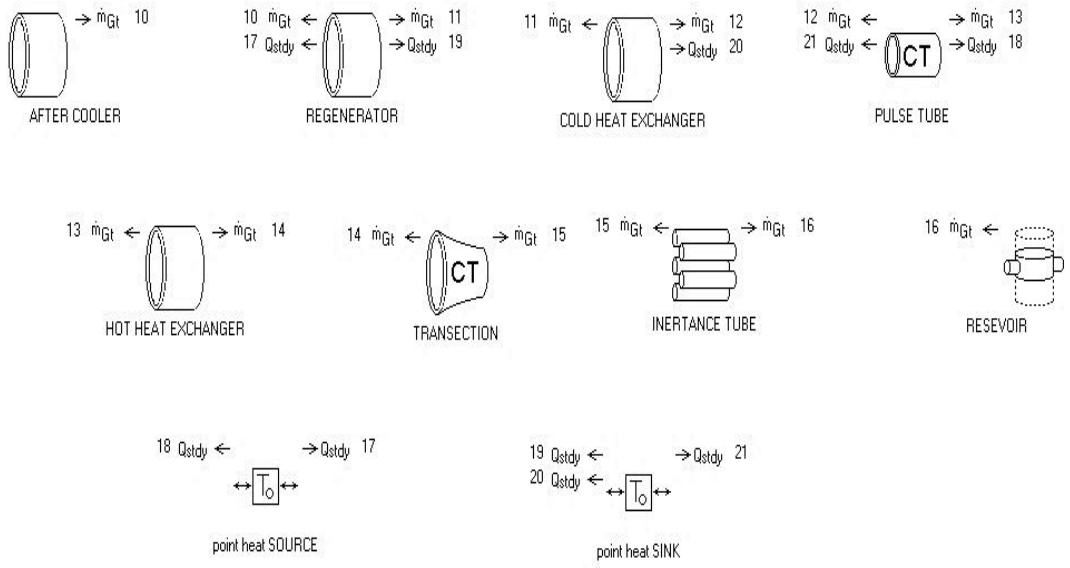

Figure 5.6 Root level components of cold head model.

After cooler, cold heat exchanger and hot heat exchanger are heat exchangers which transfer heat to or from, an external heat source or sink. They are all designed by initially selecting a tubular canister from the 'canisters' tab. The child components within all heat exchangers are the same type as they are isothermal. The child component of heat exchangers is shown in Figure 5.7. The first level of the child component is simply the matrix of the heat exchanger. In this case a woven screen matrix is selected from the 'Matrices' tab. The child levels consist of a gas domain and an isothermal surface as shown in Figure 5.7. Notice the 'M' represents a matrix gas domain, rather than the two gas domains discussed earlier. A matrix gas domain is used within a porous matrix or within uniform channels of tiny hydraulic diameter. Below the gas component are positive and negative gas inlets, whose connections are exported up to the root level as can be seen in Figure 5.7.

5.2.4 Parasitic Warm Source and Cold Sink

Both the parasitic warm source and the parasitic cold sink, shown in Figure 5.6 is basically a point heat source and are inserted from the 'Basic' tab. Even though these are considered thermal solids, the only property accompanying with them is the temperature. There are no physical properties or area properties associated with them.

They are used only to combine steady heat flow connections, Q_{std}, which are child components attached to the root level. To calculate parasitic losses such as solid conduction, the temperatures are associated with an infinite source or sink.

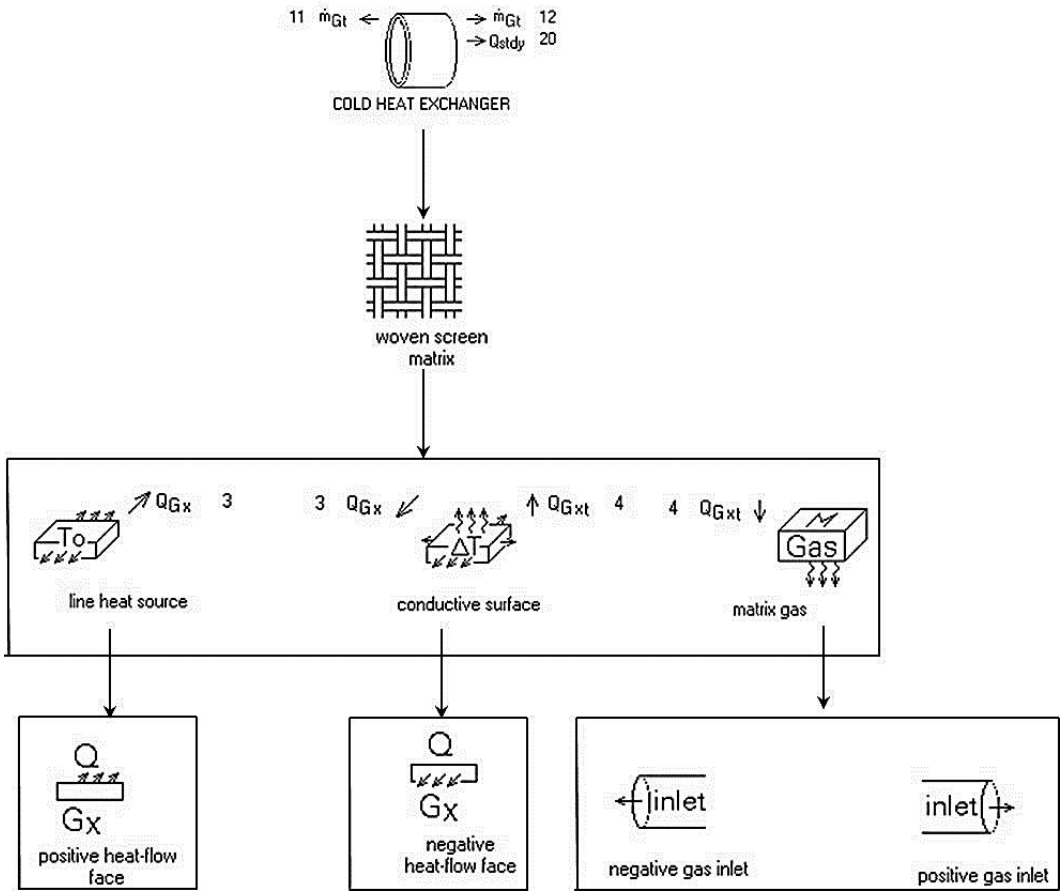

Figure 5.7 Child level components of heat exchanger models.

5.2.5 Modelling of Regenerator

The regenerator model is assembled by preliminary with a tubular canister from the 'Canisters' tab. The regenerator is one special type of heat exchanger different from the other type of heat exchangers as discussed above. The other type of heat exchangers contains a solid matrix, are considered as isothermal. These heat exchangers either transfer heat from some external heat source to the gas or transfer heat from the gas to some external heat sink. In the first level child component the regenerator contains a random fiber of solid matrix instead of woven screens unlike the other type heat exchangers as shown in Figure 5.8. This level is also a heat conductor,

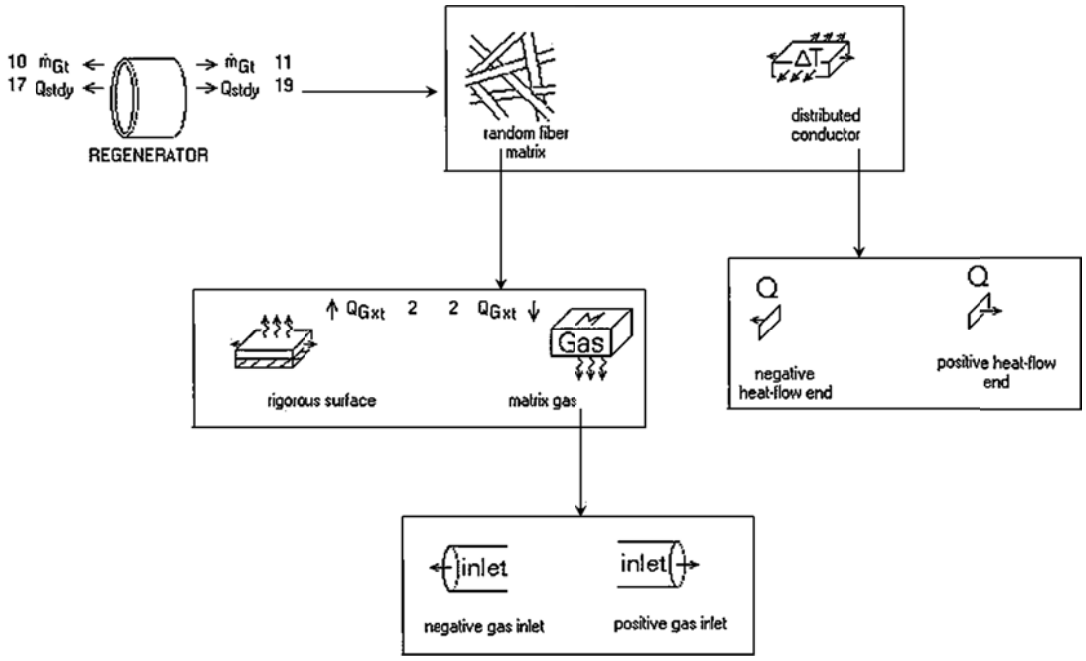

Figure 5.8 Child level component of regenerator

or basically termed as a bar conductor. This is available in the 'Heat Flows' tab. This component models a solid conduction path and has built-in heat flow connectors which are exported to the root level for connection to the heat source and heat sink to model the parasitic conduction losses in the regenerator wall. The random fiber matrix with its child components are shown in same Figure 5.8. However, this figure shows that the surface is modelled as a rigorous surface rather than an isothermal surface. A rigorous surface is a type of quasi-adiabatic surface. This means that at the interface between the solid and the gas there is a time varying sinusoidal heat flux with zero or near zero mean value. The heat flow connection between the matrix gas and rigorous surface models this interaction. There are no child components of the rigorous surface and the matrix gas contains the usual positive and negative gas inlets.

5.2.6 Modelling of Pulse tube

The pulse tube is named as the compliance tube within Sage. The compliance tube is a component specific to the pulse tube model class and is chosen from the 'Heat Exchangers' tab.

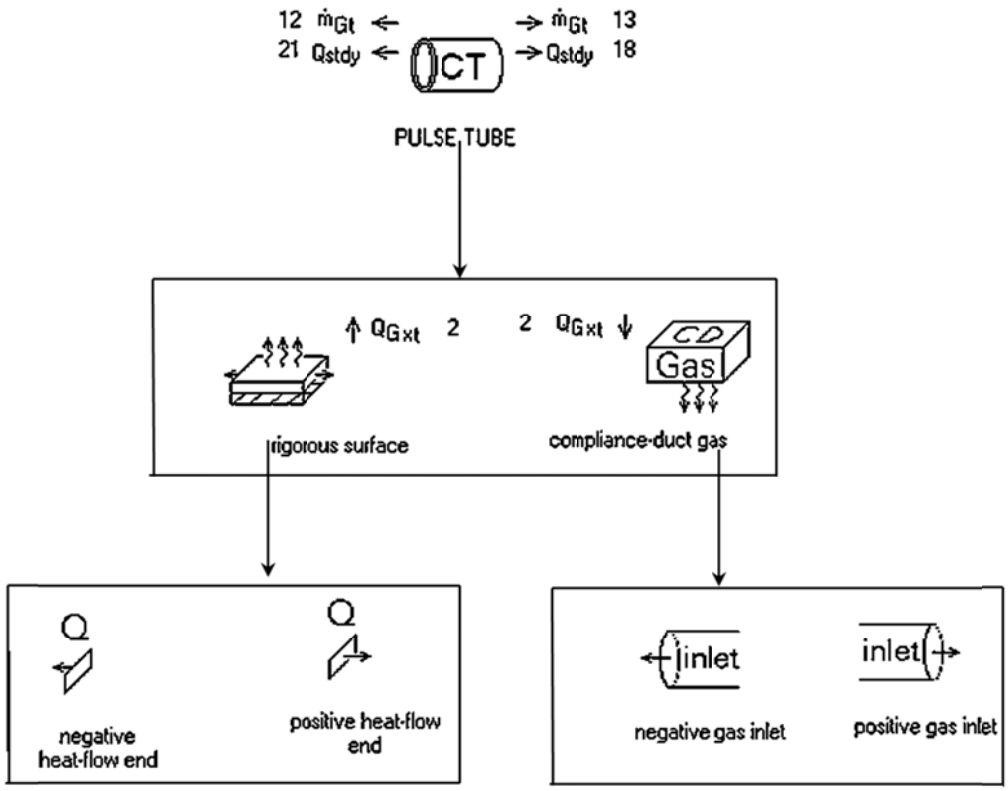

Figure 5.9 Child level component of pulse tube

The compliance tube is a child component of the Stirling-class tube-bundle heat exchanger. The main difference is that it substitutes a compliance duct gas domain in its toolbox and adds a radiation-transport model component, in case one wants to model radiation transport along the tube. Wall conduction is available in the thick-wall toolbox component already presented. The child components of the compliance tube are shown in Figure 5.9. The compliance-duct gas domain is shown by the 'CD' label in this figure. However, the compliance-duct gas domain addresses the convective losses in the wall boundary layer caused by the presence of an axial temperature gradient. In all the compliance duct gas domain accounts for molecular conduction, turbulent conduction, free convection, boundary convection and streaming convection. The rigorous surface gas domain contains the positive and negative gas inlets.

5.2.7 Modelling of Inertance tube

The root level components that comprise the inertance assembly are shown in Figure 5.10. The inertance tube is connected to a large volume reservoir with their child components of the duct gas domain and isothermal surfaces are shown in Figure 5.10.

Again, positive and negative gas inlets are child components within the duct gas domain. The reservoir is modelled same as the cylinder space from Figure 5.3 with a cylinder space as domain and an isothermal surface. At this point the system ends and thus there is only a negative gas inlet within the cylinder space gas domain as shown in Figure 5.6.

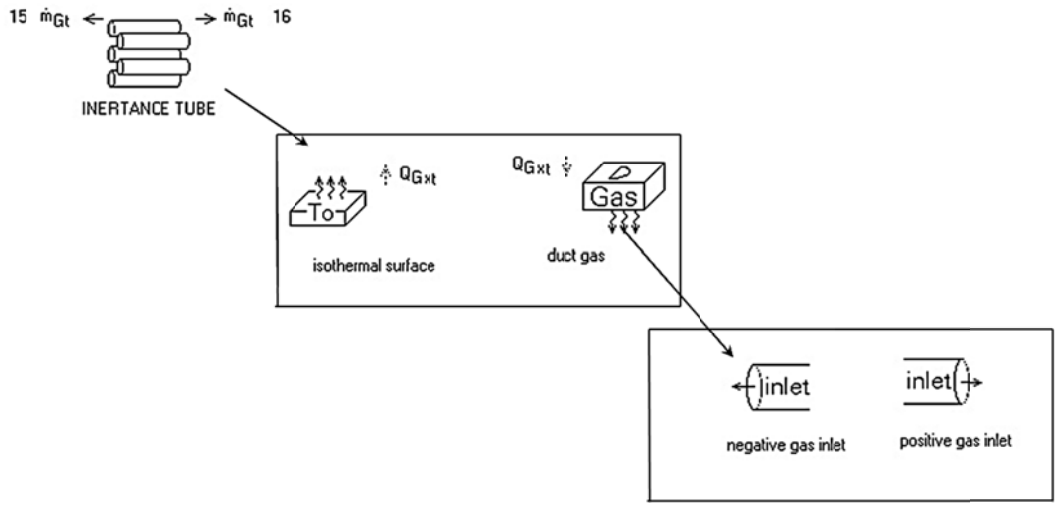

Figure 5.10 Child level component of pulse tube

5.3 ITPTR Assembly

The components and subassemblies, or building blocks, shown in Figure 5.1 to Figure 5.10 are assembled together to create the model of the entire ITPTR. There are additionally diffuser components at the hot heat exchanger in the ITPTR model that have not been discussed. These are modelled as very small compliance tubes with a compliance duct gas. But instead of a rigorous surface as in the pulse tube, or compliance tube component, these contain isothermal surfaces.

Figure 5.11 relates the Sage model numbering system as discussed above section to the components shown in the schematic of Figure 4.1. The numbers correspond to the appropriate boundary connections with Sage. Note that not all components in the Sage models are shown in the schematic diagram.

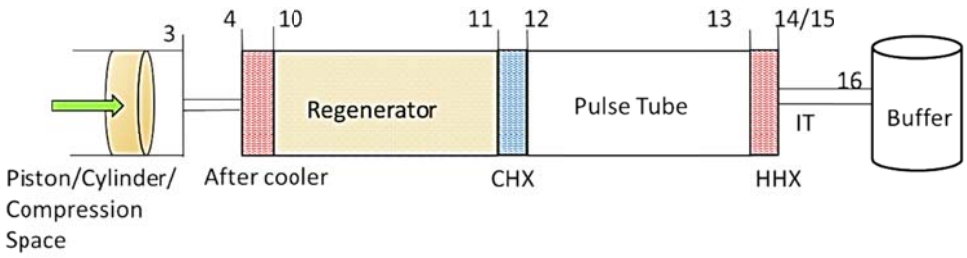

Figure 5.11 ITPTR schematic labelled with corresponding numbers from Sage model.

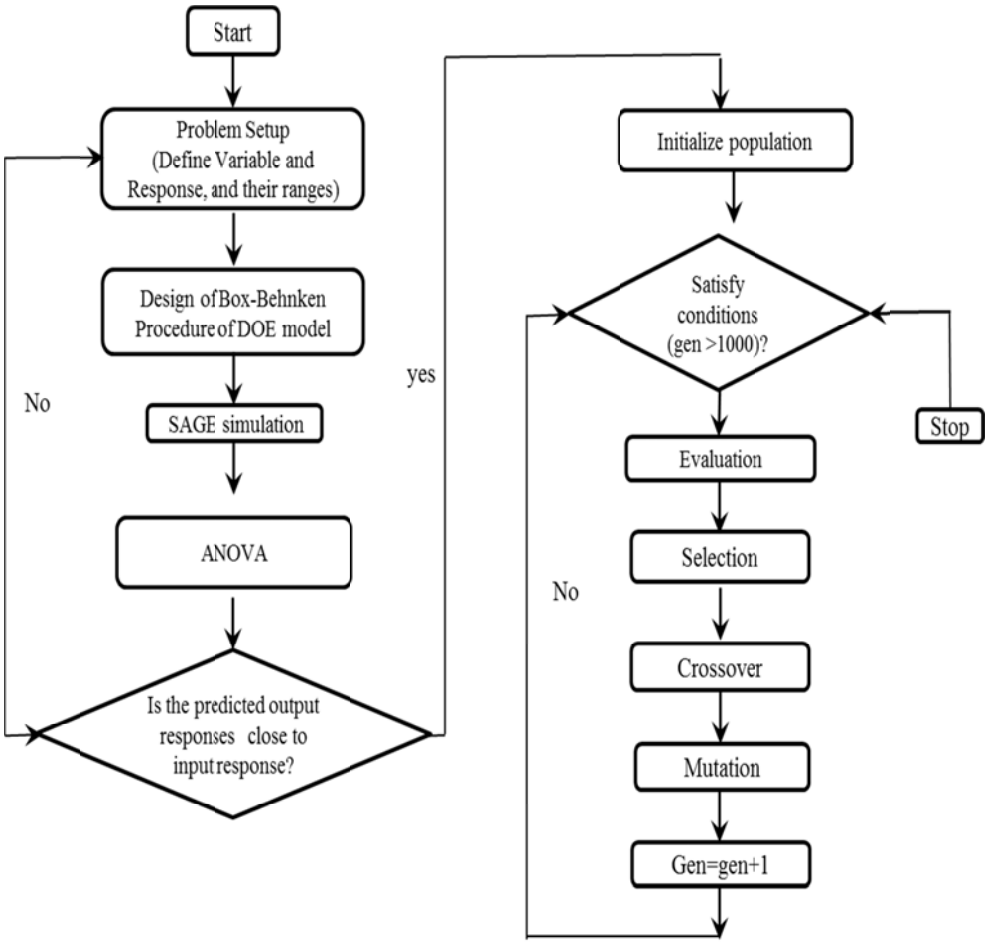

Figure 5.12 Flowchart of the analysis and optimization process

5.4 Response surface methodology (RSM)

The results of the numerical analysis for ITPTR are obtained through the design of experiment (DOE) approach, such as response surface methodology (RSM). DOE is basically a scientific approach to effectively plan and perform experiments using statistics and is commonly used to improve the quality of a product or process with the

least number of simulation runs. Such approaches enable the user to define and study the effect of every single condition possible in a simulation, where several factors are involved [221, 222]. Response surface methodology is an assembly of statistical and mathematical methods beneficial for the developing, refining and optimizing processes. It deals with the circumstances where several input variables potentially affect the performance measure or quality of a product or process. The performance measure or quality is known as the response. The objective is to establish a suitable approximation of the true functional relationship between the independent variables and the process responses through response surface methodology. Generally, a second-order model as given in Equation (5.1) is employed in response surface methodology.

$$y = \beta_0 + \sum_{i=1}^{k} \beta_i X_i + \sum_{i=1}^{k} \beta_{ii} X_i^2 + \sum_{kj} \sum \beta_{ij} X_i X_j + \varepsilon \qquad (5.1)$$

Where *y* is the corresponding response for the input variables X_i, where X_i^2 and X_i X_j are the square and interaction terms of the parameters respectively. β_0, β_i, β_{ii} and β_{ij} are the unknown regression coefficients, and ε is the error. The Box-Behnken design is preferred over central composites as it is able to run the simulation with the least number of runs. It accomplishes the task with the non-sequential analysis and fewer design points. A three factorial and three levels (-1, 0, +1) is used for the construction of a second-order response surface model. The variables (factors) used in the study are the pulse tube diameter (A), pulse tube length (B), regenerator diameter (C) and regenerator length (D). The variable values generated from the RSM are used for numerical solutions to obtain the cold head temperature (T_{cold}) and input compressor power (W_{comp}) values. They are reported in the "response" column of Table 5.2. The real values of the process variables (factors), their variation limits and number are selected, based on the preliminary simulation. The coded values along with the real values of the factors are shown in Table 5.1. A regression model is proposed and the results are studied using the Design Expert 7.0.0.

Table 5.1 Real and coded levels of the independent variables

Parameters	Real values (mm) of coded levels		
	-1	0	1
Pulse tube diameter, A	8	12	16
Pulse tube length, B	75	100	125
Regenerator diameter, C	15	20	25
Regenerator Length, D	50	100	150

Table 5.2 Box-Behnken design of experiment along with observed and predicted response.

Run	Coded levels of variables				Actual levels of variables				Response (% degradation)		Response (%degradation)		Phase difference across regenerator	
	A	B	C	D	A	B	C	D	T_{cold} Observed	T_{cold} Predicted	W_{comp} Observed	W_{comp} Predicted	At hot end	At cold end
1	-1	-1	0	0	8	75	20	100	60.5	59.77	107.6	106.63	22.86	-42.83
2	1	-1	0	0	16	75	20	100	50.9	51.78	77.73	79.31	34.37	1.79
3	-1	1	0	0	8	125	20	100	45.9	43.92	102.4	94.33	22.72	-38.76
4	1	1	0	0	16	125	20	100	96.5	95.28	68.01	67.01	39.55	53.222
5	0	0	-1	-1	12	100	15	50	61.1	64.89	149.1	156.17	8.21	-14.96
6	0	0	1	-1	12	100	25	50	55.9	51.91	69.15	60.25	26.79	-13.82
7	0	0	-1	1	12	100	15	150	40.8	42.13	139.2	137.97	30.72	-28.00
8	0	0	1	1	12	100	25	150	96	93.33	43.43	42.05	48.36	-22.88
9	-1	0	0	-1	8	100	20	50	67.3	66.2	118.3	121.27	1.72	38.09
10	1	0	0	-1	16	100	20	50	70.15	66.08	68.8	70.57	35.02	26.96
11	-1	0	0	1	8	100	20	150	52.3	52.88	87.5	79.69	37.1	-47.82
12	1	0	0	1	16	100	20	150	97.3	98.24	77.37	75.75	8.37	41.91
13	0	-1	-1	0	12	75	15	100	47.9	44.59	161.7	155.13	16.25	-33.8
14	0	1	-1	0	12	125	15	100	46.1	45.35	143.8	139.01	22.16	-8.36
15	0	-1	1	0	12	75	25	100	47.2	49.61	54.97	55.39	40.92	-34.296
16	0	1	1	0	12	125	25	100	73.2	78.37	43.3	46.91	48.5	-1.484
17	-1	0	-1	0	8	100	15	100	65.1	64.15	169.5	163.13	15.67	-49.92
18	1	0	-1	0	16	100	15	100	63.8	60.63	130.3	128.5	26.84	28.46
19	-1	0	1	0	8	100	25	100	55	57.03	61	59.55	40.93	-41.91
20	1	0	1	0	16	100	25	100	108	105.79	38.8	39.89	50.88	39.83
21	0	-1	0	-1	12	75	20	50	54.4	43.84	105.8	107.62	6.36	-24.84
22	0	1	0	-1	12	125	20	50	56.1	53.6	88.38	87.08	20.91	-2.68
23	0	-1	0	1	12	75	20	150	38.41	48.26	85.07	81.18	36.42	-40.05
24	0	1	0	1	12	125	20	150	51	68.02	78.63	77.12	37.57	-5.472
25	0	0	0	0	12	100	20	100	39.5	40	88.69	88.25	28.76	-22.54
26	0	0	0	0	12	100	20	100	41	40	91	88.25	28.76	-22.54
27	0	0	0	0	12	100	20	100	40	40	87	88.25	28.76	-22.54
28	-1	0	0	1	8	100	20	150	52.3	52.88	87.5	79.69	37.1	-47.82
29	1	0	0	1	16	100	20	150	97.3	98.24	77.37	75.75	8.37	41.91

5.5 Results and discussion

5.5.1 Regression model and analysis of variance (ANOVA)

The analysis of variance (ANOVA) is performed, based on the proposed model to find out the interaction between the process variables and the responses. The quality of fit for the polynomial model is expressed with the coefficient of determination (R^2) and the statistical significance is checked by the F-value (Fischer variation ratio) and p-value (significant probability value). The model terms are selected or rejected based on the probability value within 95% confidence interval (or 5% significance level). Finally, three-dimensional response surface plots are drawn in order to visualize the individual interaction effects of the independent variables on the cold end temperature and compressor input power. A total of 29 sets of runs obtained from the Box-Behnken (Appendix 2) and the corresponding output responses are shown in Table 5.2 for T_{cold} and W_{comp}. It is observed that the cold head temperature varies due to a variation in the dimension of the pulse tube and regenerator in between 38 K and 108 K, and W_{comp} varies from 38.8 W to 169.5 W.The results obtained from the design of experiment are analysed using the ANOVA (analysis of variance) method.

5.5.2 Analysis of factors influencing T_{cold}

The ANOVA results of the proposed quadratic model for T_{cold} are presented in Table 5.3. The value of "Prob.>F" for this model is less than 0.05 (i.e. 95 % confidence), which indicates that the model is considered to be statistically significant, which is desirable as it demonstrates that the terms in the model have a significant effect on the response. The proposed model's significance and accuracy are evaluated using the mean square value, Adjusted R-Squared Value, F-value and P-value are presented in this table. The important coefficient R^2 in the resulting ANOVA table is defined as the ratio of the explained variation to the total variation and is a measure of the degree of fit. When R^2 approaches to unity, the better response model fits the actual data. The value of R^2 calculated in Table 5.3 is 0.9713. The "Pred R-Squared" of 0.9260 is in reasonable agreement with the "Adjusted R-Squared" of 0.9426. The "Lack of Fit F-value" of 1.54 implies that the Lack of Fit is not significant relative to the pure error. A non-significant lack of fit is good, which is required for a model to fit. As all the model statistics and diagnostic plots are significant, it can be proposed to handle the design space. In order to ensure that the present model adequately represents the real

system, the predicted RSM generated models versus actual value plots are shown in Figure 5.13. It is observed from the comparison that the data are almost normally distributed with some deviation in an acceptable range of error. And also, the normal probability plot and residual plot for T_{cold} are shown in Figure 5.14 and Figure 5.15, respectively, and these figures display an identical trend of behaviour observed in the actual value of T_{cold}. The regression equation developed from the ANOVA in terms of the coded factors for T_{cold}, is given in Equation (5.2).

Table 5.3 ANOVA results of the response surface quadratic model for T_{cold}.

Source	Squares	df	Mean Square	F Value	Prob > F	
Model	10156.756	14	725.4826	33.8271	< 0.0001	significant
A-PDia	1534.540	1	1534.541	71.55109	< 0.0001	
B-Plength	652.6875	1	652.6875	30.43288	< 0.0001	
C-RDia	1084.900	1	1084.901	50.58571	< 0.0001	
D-Rlength	266.0208	1	266.0208	12.40376	0.0034	
AB	826.5625	1	826.5625	38.54016	< 0.0001	
AC	683.8225	1	683.8225	31.88461	< 0.0001	
AD	517.5625	1	517.5625	24.1324	0.0002	
BC	196	1	196	9.138899	0.0091	
BD	25	1	25	1.165676	0.2985	
CD	1024	1	1024	47.74608	< 0.0001	
A^2	2549.387	1	2549.388	118.8704	< 0.0001	
B^2	37.36216	1	37.36216	1.742087	0.2081	
C^2	945.7662	1	945.7662	44.09827	< 0.0001	
D^2	788.4364	1	788.4365	36.76245	< 0.0001	
Residual	300.255	14	21.44679			
Lack of Fit	238.255	10	23.8255	1.537129	0.3606	not significant
Pure Error	62	4	15.5			
Cor Total	10457.011	28				

$$Tcold = 40.00 + 1.31*A + 7.38*B + 9.51*C + 4.71*D + 14.37*A*B + 13.07*A*C + 11.37*A*D + 7.00*B*C + 2.50*B*D + 16.00*C*D + 19.82*A^2 + 2.40*B^2 + 12.08*C^2 + 11.03*D^2 \quad (5.2)$$

where A, B, C and D are the coded values of the pulse tube diameter, pulse tube length, regenerator diameter and regenerator length, respectively. Figure 5.16 (a) demonstrates the response surface 3-D plot of the effect of the interactive relationship between T_{cold}, pulse tube diameter and regenerator diameter while keeping the other factors constant. It shows that the minimum temperature can be achieved by increasing the pulse tube diameter from 8 mm to 11 mm at which the minimum no load temperature of 37.6 K is obtained at the cold head. A further increase in the pulse tube diameter may increase the cold head temperature. Similarly, by increasing the regenerator diameter from 15 mm to 17.8 mm, the minimum cold head temperature can be achieved and further increase in the regenerator diameter may cause an increase in the cold head temperature. The amalgamated effect of the pulse tube length and regenerator length on the cold head temperature is shown in Figure 5.16 (b) in terms of the response surface 3-D plot while keeping the other factors constant. The figure demonstrates that the increase in the pulse tube length causes an increase in the cold head temperature. So in the present case, the minimum 75mm tube length is treated as the optimized length. This figure also demonstrates that by increasing the regenerator length from 50 mm to 85 mm, the minimum cold head temperature can be achieved and further increase in the regenerator length may cause an increase in the cold head temperature.

5.5.3 Analysis of factors influencing W_{comp}

The results of the proposed quadratic model for the input compressor work W_{comp} in the form of ANOVA are presented in Table 5.4. The proposed model's significance and accuracy are evaluated using the mean square value, Adjusted R-Squared Value, F-value and P-value are presented in this table. The model is significant as p-value < 0.0001 and corresponding F-value is 265.84. There is only a 0.01% chance that a "Model F-Value" could be large due to noise. In the proposed model the R^2 value is 0.9933 and the "Pred R-Squared" value is 0.9809.The "Pred R-Squared" of 0.9809 is in reasonable agreement with the "Adjusted R-Squared" of 0.9895. The "Lack of Fit F-value" of 2.09 implies that the Lack of Fit is not significant relative to the pure error. The non-significant lack of fit is good which is required for a model to fit. As all the model statistics and diagnostic plots are significant, it can be proposed to handle the design space. In order to ensure that the present model adequately represents the real

system, the predicted RSM-generated models versus actual value plots are shown in Figure 5.17. It is observed from the comparison of model that the data are almost normally distributed with some deviation in an acceptable range of error. And also the normal probability plot and residual plot for W_{comp} are shown in Figure 5.18 and Figure 5.19 and respectively, and these figures display an identical trend of behaviour observed in the actual value of W_{comp}. The regression equation developed from the ANOVA in terms of the coded factors for W_{comp} is given in Equation (5.3):

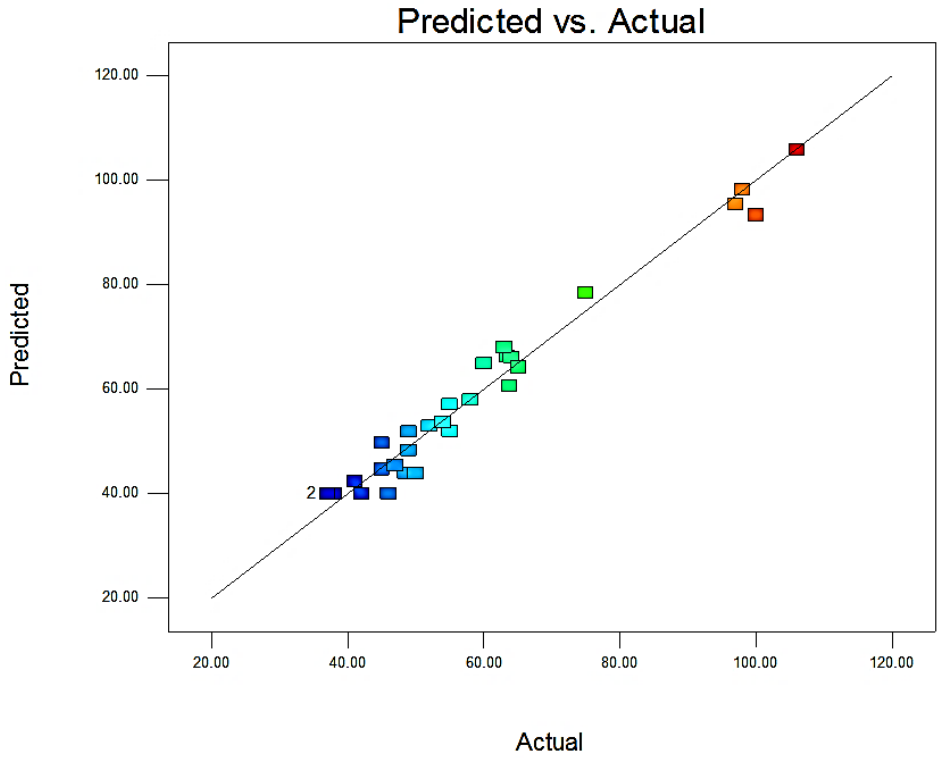

Figure 5.13 Actual versus predicted values for T_{cold}

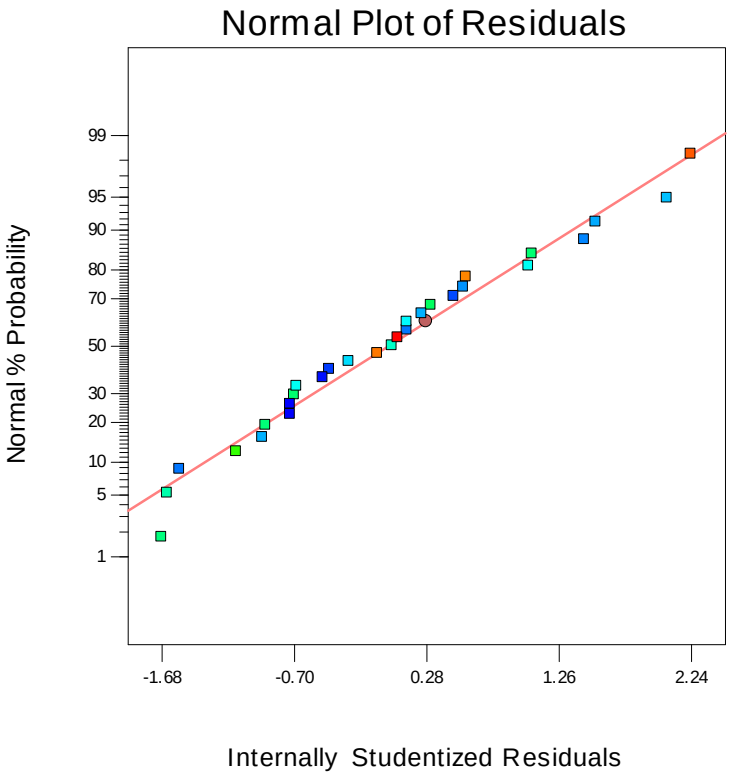

Figure 5.14 Normal probability plot for T_{cold}

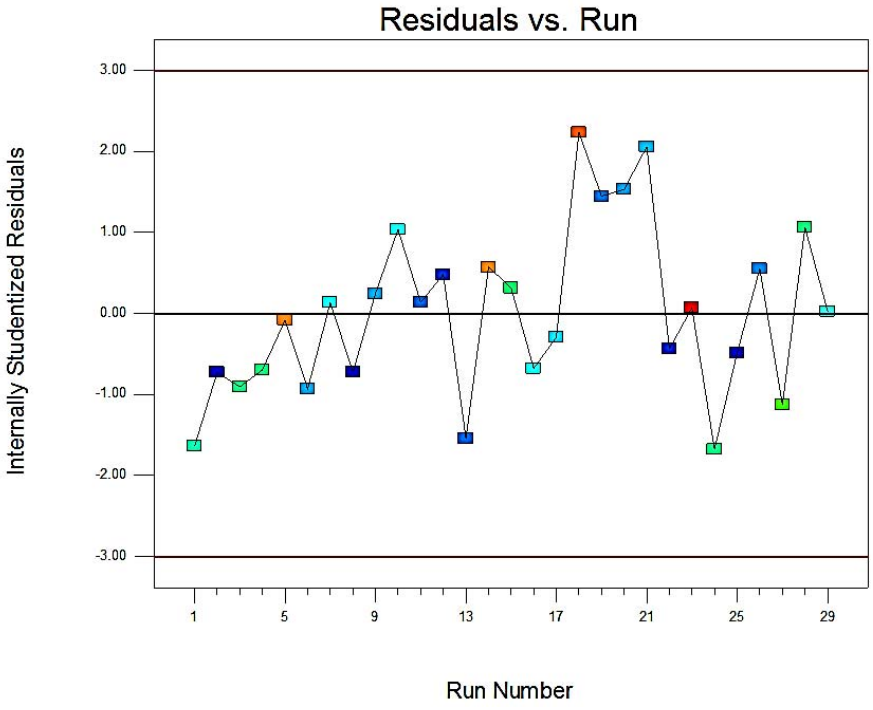

Figure 5.15 Residual plot for T_{cold}

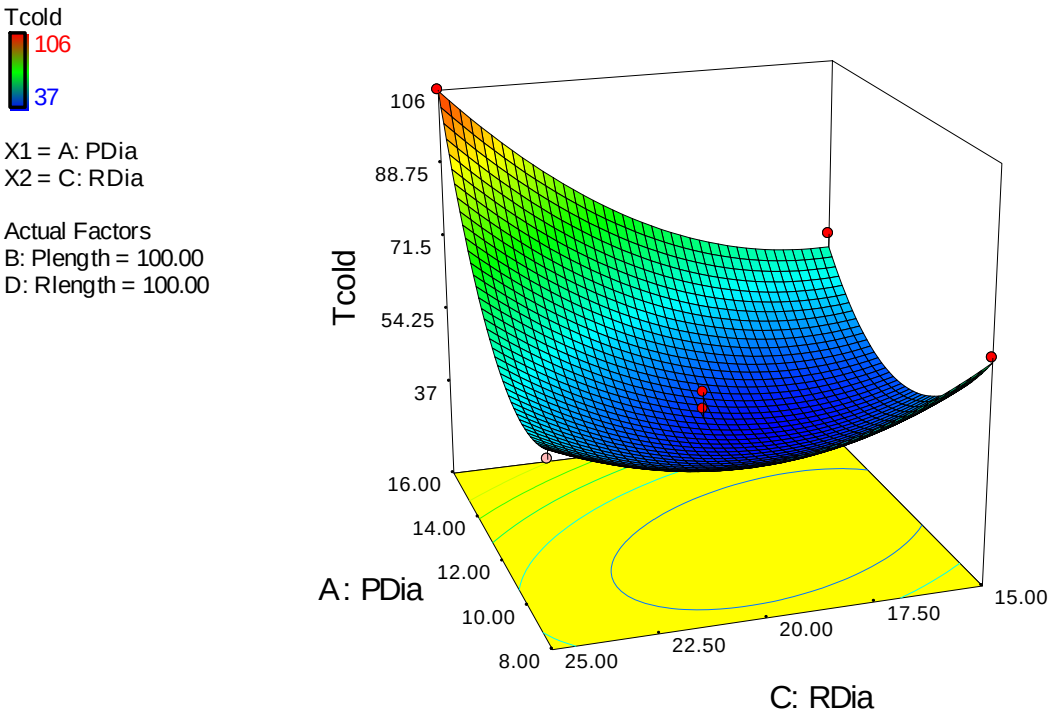

(a) Effect of pulse tube diameter (A) and regenerator diameter (C) (unit: K, mm)

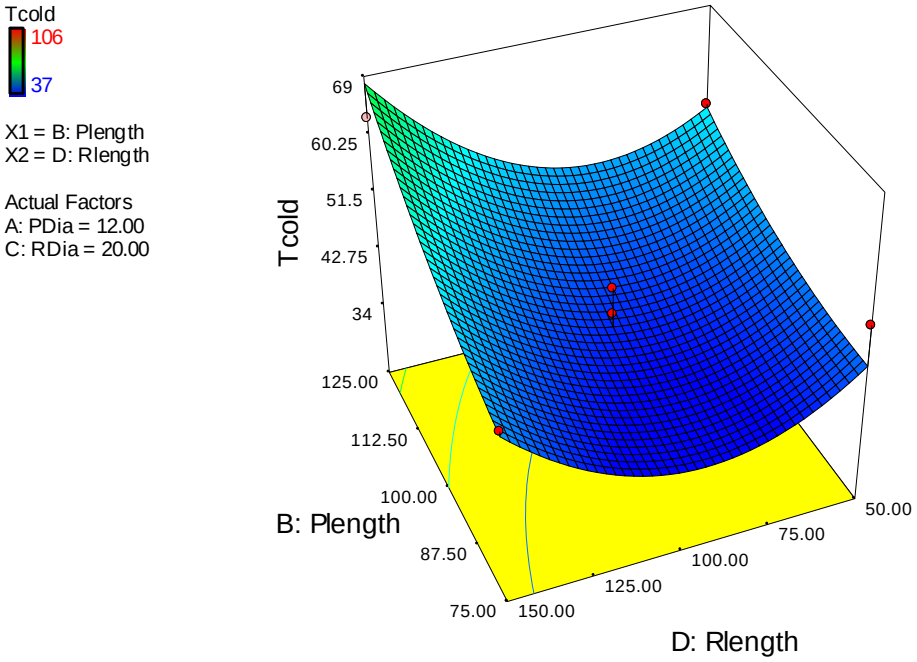

(b) Effect of pulse tube length (B) and regenerator length (D) (unit: K, mm).

Figure 5.16 The response surface 3D plot of cold head temperature (T_{cold}),

$$Wcomp = 88.25 - 13.66*A - 6.15*B - 47.96*C - 9.10*D + 3.83*A*C + 11.69*A*D + 1.91*B*C + 4.12*B*D - 1.43*A^2 + 10.86*C^2 \quad (5.3)$$

where A, B, C and D are the coded values of the pulse tube diameter, pulse tube length, regenerator diameter and regenerator length, respectively.

Table 5.4 ANOVA results of the response surface quadratic model for W_{comp}

Source	Squares	Degrees of freedom	Mean Square	F-Value	Prob > F	
Model	32851.42015	10	3285.142	265.8433	< 0.0001	significant
A-PDia	2237.5083	1	2237.508	181.0657	< 0.0001	
B-Plength	453.2552083	1	453.2552	36.67874	< 0.0001	
C-RDia	27605.77613	1	27605.78	2233.94	< 0.0001	
D-Rlength	992.8102083	1	992.8102	80.34111	< 0.0001	
AC	58.6756	1	58.6756	4.748201	0.0429	
AD	546.1569	1	546.1569	44.19662	< 0.0001	
BC	14.630625	1	14.63063	1.183953	0.2909	
BD	67.8976	1	67.8976	5.494473	0.0308	
A^2	14.19581286	1	14.19581	1.148767	0.2980	
C^2	814.5171129	1	814.5171	65.91311	< 0.0001	
Residual	222.433867	18	12.35744			
Lack of Fit	195.633867	14	13.97385	2.085649	0.2496	not significant
Pure Error	26.8	4	6.7			
Cor Total	33073.85402	28				

Figure 5.20 (a) illustrates the response surface 3-D plot of the effect of the interactive relationship between the W_{comp}, pulse tube diameter and regenerator diameter while keeping the other factors constant. It indicates that for a large size of diameter of both the pulse tube and regenerator, less amount of compressor input power is required. The amalgamated effect of the pulse tube length and regenerator length on the W_{comp} is shown in Figure 5.20 (b) in terms of the response surface 3-D plot while keeping the other factors constant. It demonstrates that the increase in the pulse tube length and regenerator length causes a small change in the input power of the compressor. The detail of phase shift at the inlet and outlet of regenerator are presented in Table 5.2.

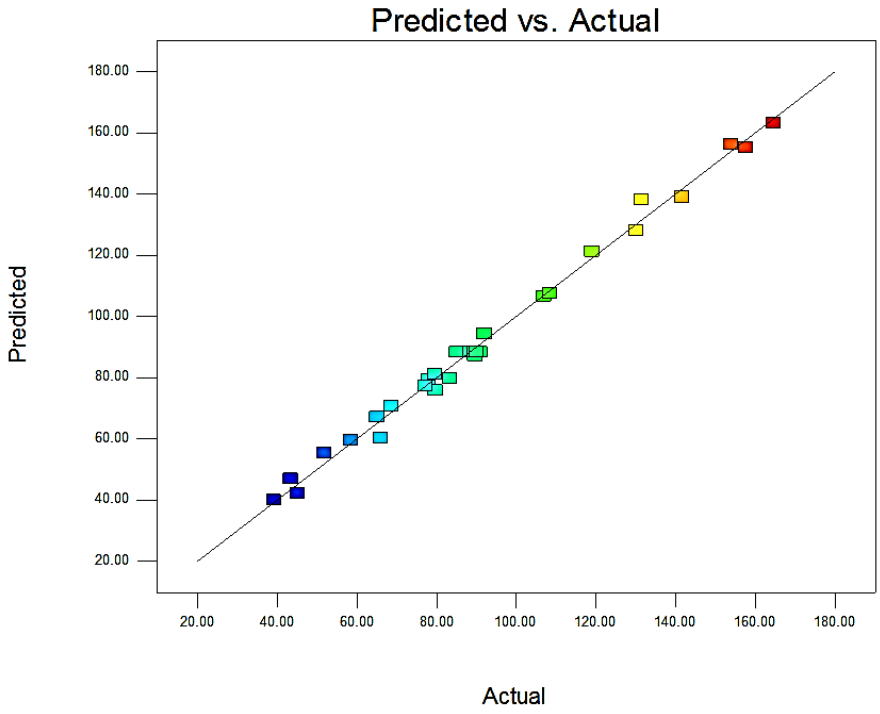

Figure 5.17 Actual versus predicted values for W_{comp}

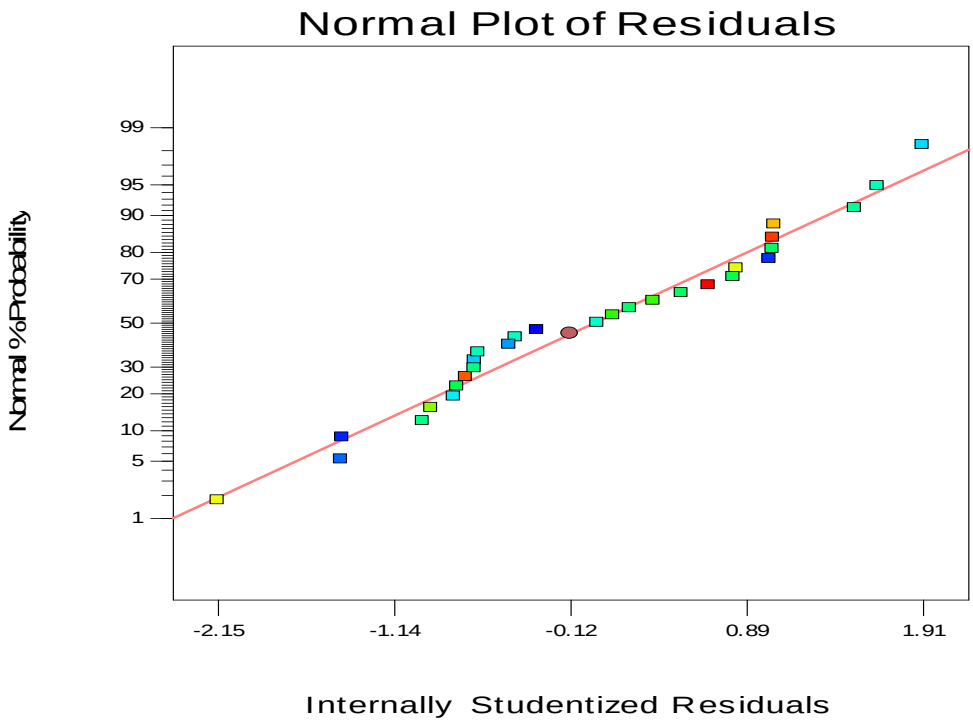

Figure 5.18 Normal probability plot for W_{comp}

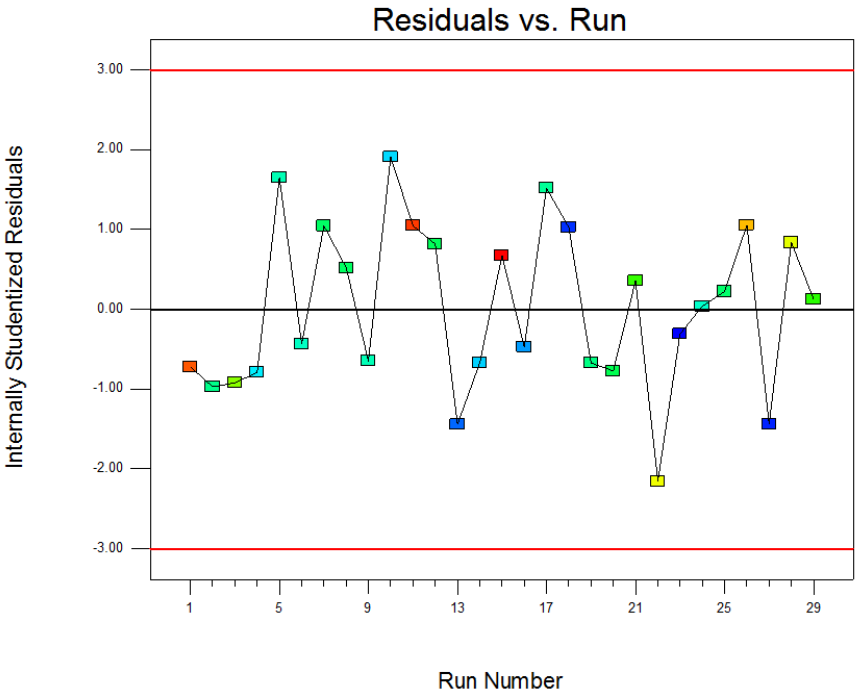

Figure 5.19 Residual plot for W_{comp}

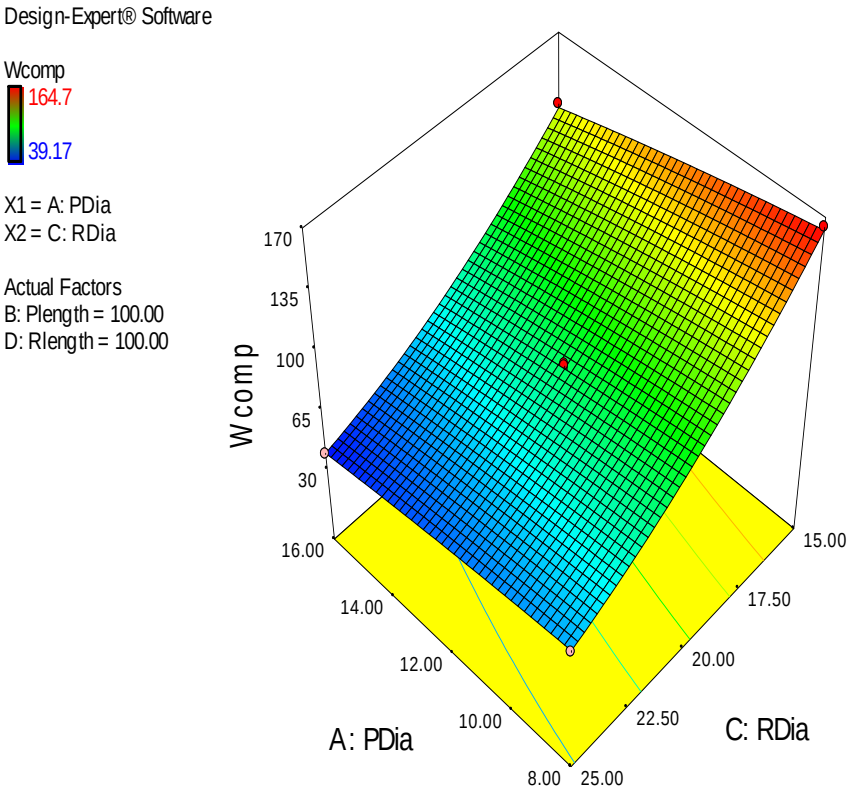

(a) Effect of pulse tube diameter (A) and regenerator length (C) (unit: W, mm)

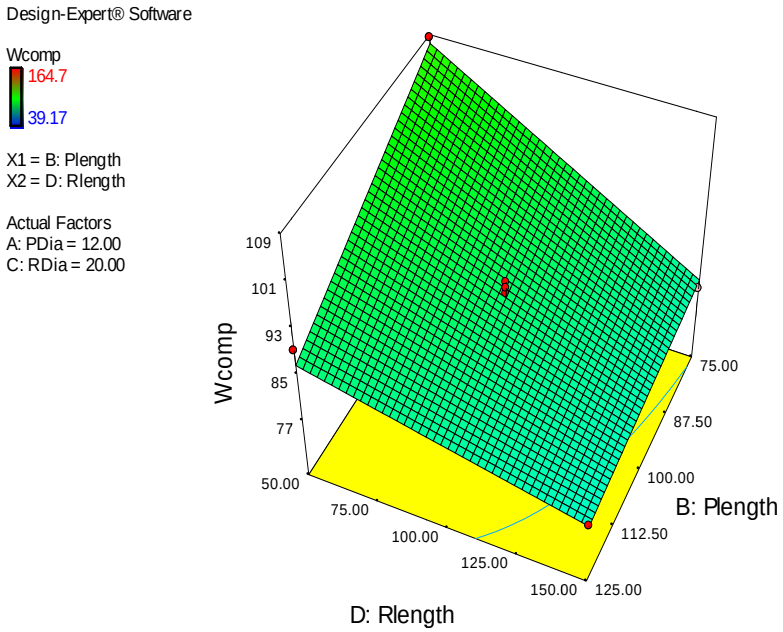

(b) Effect of pulse tube length (B) and regenerator length (D) (unit: W, mm)

Figure 5.20 The response surface 3D plot of compressor input power (W_{comp})

5.6 Multi-objective Evolutionary Algorithms

An evolutionary approach, such as the non-dominated shorting genetic algorithm is proposed to optimize the multi-objective responses. Unlike the single objective optimization, a set of optimal solutions termed as Pareto-optimal solutions is obtained in the case of multi-objective optimization. The Genetic algorithm (GA) is a category of population based stochastic search technique which is closely modelled on the natural process of evolution with the importance on breeding and the existence of the fittest. The algorithm starts with a set of primary solutions instead of starting with a single point. GA operators create probabilistic results leading to stochasticity. These operators are accountable for providing the search direction to a GA. The selection operator opts for the best solutions and the crossover operator unites good genetic material from two good solutions to form the best solution. Improved strings are produced by altering the string locality in the mutation operator. The reproduction operator eliminates bad things and if good strings are created, they are highlighted. In multi objective optimization, a set of mutually dominant solutions is generated which is exclusive and distinctive with respect to all objectives. Multi-objective optimization aims at convergence to the Pareto-optimal set and maintains diversity and distribution in solutions. A number of literature

[189, 223-226] based on multi-objective algorithms have been reported in engineering application out of them the NSGA-II [227], is chosen for this investigation. The multi-objective evolutionary algorithm based on non-dominated sorting is known as the Non-dominated Sorting Genetic Algorithm II (NSGA II). It utilizes elitist a non-dominated sorting along with the crowding distance sorting to get the non-dominated set. The algorithm is skilled enough to handle constrained multi-objective optimization problems with binary coding and real parameters. GA requires the fitness value or objective function for the optimization problem. Hence, it is essential that a decision variable should relate to the objective.

In the present work, the objectives are the minimizations of both T_{cold} and W_{comp}, which are functions of the decision variables, viz., pulse tube diameter and length, and regenerator diameter and length. Accordingly, the empirical relation between the input parameters and process responses obtained in equations (5.2) and (5.3) are used as the functional relations (Appendix 2). The objective functions are given below.

Objective 1 = W_{comp}

Objective 2 = T_{cold}

Table 5.5 Selected solutions from pareto optimal solution set and corresponding variable

SL No	A	B	C	D	W_{comp}	T_{cold}
1	14.62578	88.45384	24.6439224	56.04009	51.43606	58.70423
2	15.89712	114.9118	24.9039371	52.96548	35.17943	99.71579
3	12.95483	75.67757	21.511543	78.31189	80.61532	36.85883
4	12.89086	75.12838	19.989692	88.59774	92.6734	35.83691
5	13.16342	84.3197	24.1646747	84.12444	58.08971	49.30446
6	16	124.9975	24.9988225	50.19165	30.64074	113.4261
7	13.15658	76.92123	23.4482054	81.05095	64.72501	42.0237
8	14.94841	110.234	24.905052	58.31847	41.78619	82.89589
9	15.84462	109.1368	24.9038098	52.92973	37.33482	92.44319
10	13.08051	83.88019	21.3198499	87.38444	77.66808	39.41027
11	14.85274	116.8091	24.9872984	51.68942	39.63846	87.44903
12	13.71213	75.1024	23.734579	88.02741	60.14809	46.26508
13	14.90305	89.89685	24.6574533	58.00704	49.40933	62.60915
14	14.88046	108.5202	24.8577186	56.96376	42.82395	79.80368

15	13.97919	92.48448	24.2834052	70.52878	53.90447	57.16309
16	15.96571	116.9724	24.9449969	51.12519	33.80095	103.0091
17	13.10556	75.77559	20.7740162	82.2182	85.51777	37.7478
18	13.06947	80.51699	22.7976334	78.31095	68.95155	40.83412
19	14.4907	82.14634	24.3699082	60.43415	55.08384	52.4978
20	15.91189	122.4761	24.8400386	52.34957	32.79875	108.2469
21	15.63315	89.33256	24.6573652	56.00053	45.96201	69.0902
22	13.0267	75.51437	20.7502207	80.46632	86.50358	39.56583
23	14.86062	108.0805	24.5888181	55.58221	44.19673	77.27509
24	13.26093	79.66957	22.2882937	69.78429	73.53463	39.41882
25	12.57665	75.00299	19.3591323	95.80832	98.74976	37.55319

There are two responses which might not be applicable simultaneously for all industrial applications. The NSGA II code's simulation is generated by using the MATLAB toolbox. The choice of responses depends purely on the requirements of the users. The constrained values are selected from the numerical observations. These results of the constrained Pareto-optimal solutions are for two combinations of W_{comp} and T_{cold}. An initial population size of 80 is set with the simple crossover and bitwise mutation with a crossover probability, Pc = 0.8, migration fraction 0.2, migration interval 20 and Pareto fraction 0.35. The sample set of optimal solutions with the process parameters for W_{comp} and T_{cold} are given in Table 5.5. Figure 5.21 shows the Pareto-optimal front solutions for responses of the W_{comp} and T_{cold} combination.

Table 5.6 Conformation results for W_{comp} and T_{cold}

Optimized combination							
Pulse tube diameter (mm)	Pulse tube length (mm)	Regenerator Diameter(mm)	Regenerator Length (mm)	W_{comp} (W)	T_{cold} (K)	Phase difference across regenerator	
						At hot end	At cold end
12.8908	75.128	19.989	88.597	93.2	36.2	21.79	-27.64

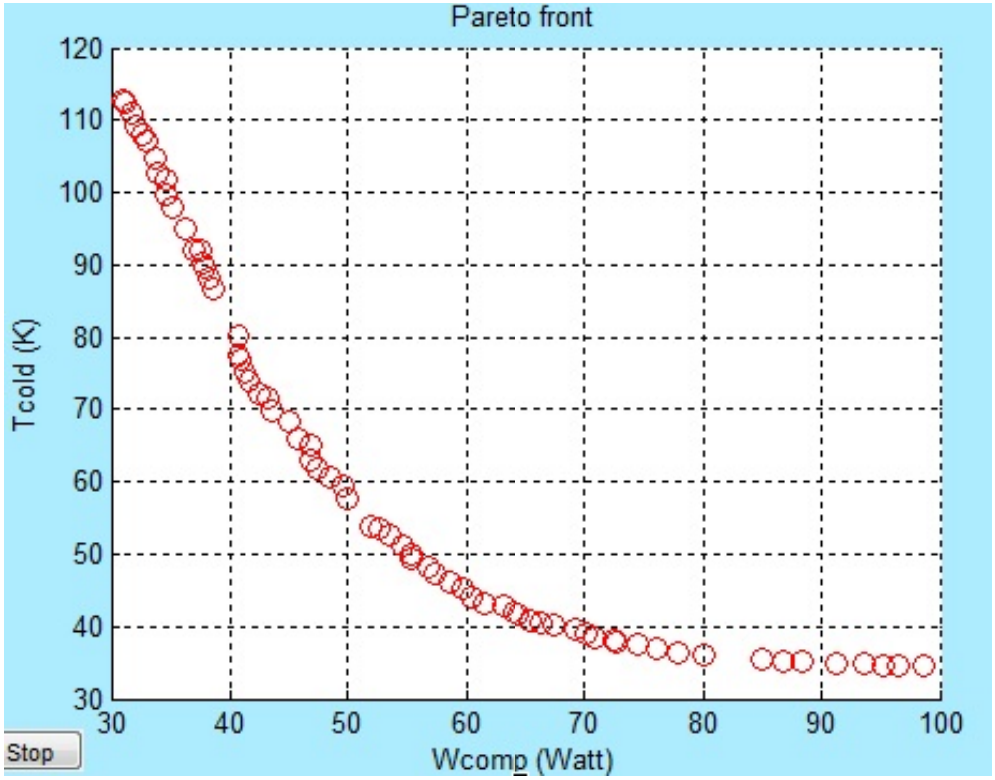

Figure 5.21 Multi-objective NSGA-II Pareto font result plot for ITPTR

5.7 Confirmation test

Once the optimal level of the pulse tube and regenerator dimensions are identified as acquired from the analysis, a confirmation test has been performed for the T_{cold} and W_{comp} to validate the responses. The results of the confirmation test for the responses are listed in Table 5.6. The percentage error is found to be in the acceptable range. The range of percentage error between the numerical and the predicted values of W_{comp} and T_{cold} lies within 5%, and the confirmation runs are within the 95% prediction interval. The phase shift analysis reveals that at the optimum condition the input power factor to the regenerator is almost equal to the output power factor at the outlet of the regenerator. The regenerator is a critical part in a cryocooler and losses inside the regenerator should be minimised by optimising the phase relationship. The optimum phase relationship means that the mass flow and pressure waves at midpoint of regenerator are nearly in the same phase. Under such optimum parameters, the phase shift between pressure and mass flow rate across the regenerator is given in Table 5.6. The phasor diagram for the optimized case is shown in Figure 5.22.

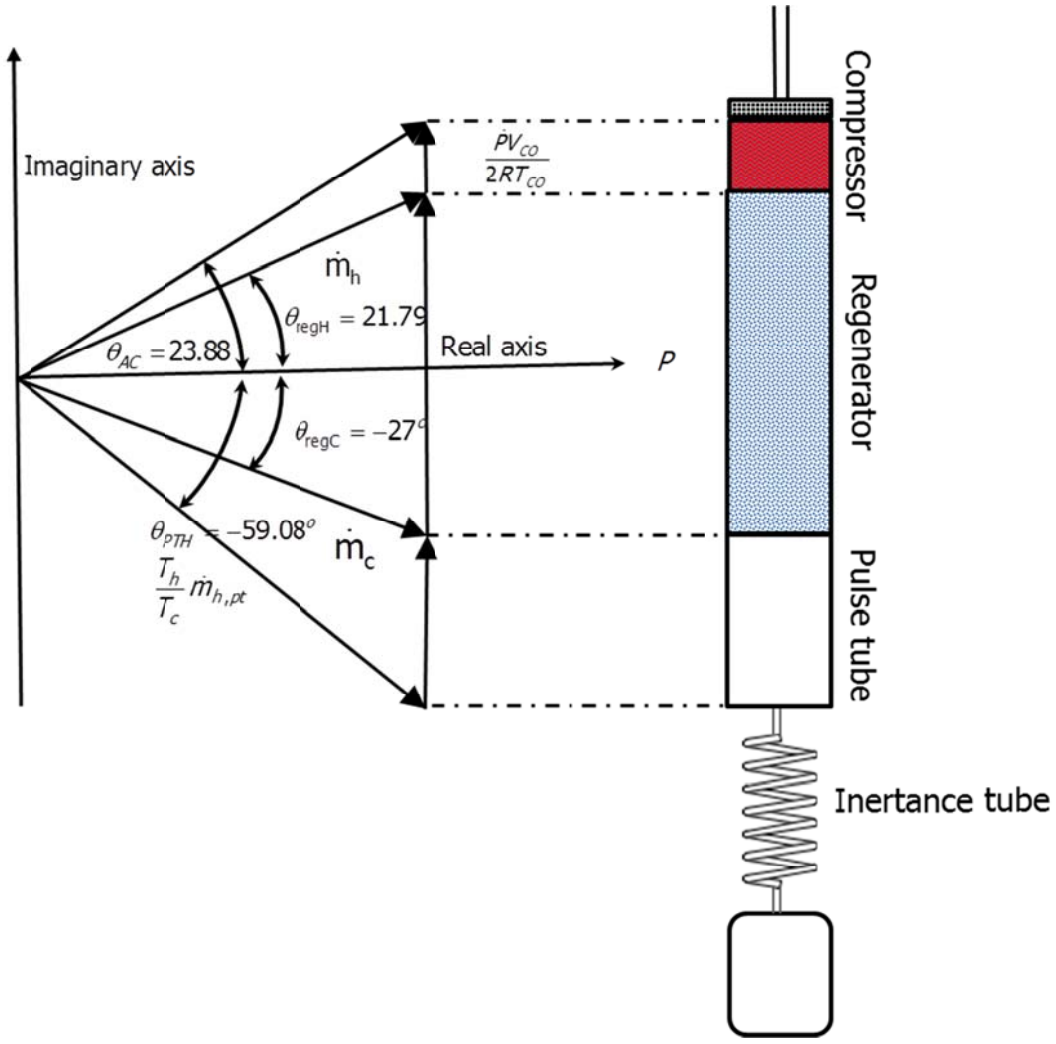

Figure 5.22 Phasor diagram of ITPTR for optimized case

5.8 Summary

A powerful, efficient and highly accurate optimization methodology, coupling RSM and NSGA II are introduced to optimize the dimensions of the ITPTR, using the numerical approach. The main purpose is to understand the effect of the pulse tube and regenerator geometrical parameters on the ITPTR performance. The RSM and NSGA II are successfully applied to obtain the Pareto-optimal front and statistically analysed the results. The Non-dominated sorting genetic algorithm (NSGA II) is used for the multi objective optimization of responses and the pareto fronts are obtained for both the T_{cold} and W_{comp}. Any solution in the Pareto front is an optimal solution. The main conclusions can be drawn as follows:

- The proposed response surface methodology is used to analyse the relationship of the process parameters such as the Pulse tube diameter, Pulse tube length, and regenerator diameter and regenerator length, to responses such as the T_{cold} and $W_{comp,}$ which are tested using the ANOVA analysis.
- The proposed generated heat transfer model is significant as the values of the F test and Prob > F is confirmed from the ANOVA analysis.
- The results generated from the response surface methodology revealed that up to a certain limit, an increase in the diameter of the pulse tube and regenerator led to the decrease of the cold head temperature, after which further increase the diameter causes an increase in the temperature. It is also concluded that the bigger is the diameter of the pulse tube and regenerator, the lesser is the amount of input compressor power required.
- The numerical experiments with the optimum layout of the proposed ITPTR are analysed for the accuracy of the optimization results. This confirms that the presented response surface methodology in this study is effective to optimize the model, reducing the experimental expense in optimization or improvement.
- Finally, the conclusion of the present investigation indicates that modelling and optimization of the pulse tube refrigerator system can be implemented using the RSM and NSGA-II to save time, cost and effort.

Chapter 6

MODELING AND OPTIMIZATION OF ORIFICE PULSE TUBE REFRIGERATOR

6.1 Introduction

The modelling and optimisation of inertance tube pulse tube refrigerator using SAGE software is presented in the previous chapter. In this chapter numerical modelling and optimisation of Gifford–McMahon (GM) type orifice pulse tube refrigerator is summarised. The numerical code SAGE, with graphical user interface, has been used to investigate the influence of geometrical and operating parameters on performance.

The difference between Stirling type pulse tube refrigerator model and GM type pulse tube refrigerator (PTR) is the operating frequency. The Stirling type pulse tube refrigerator can operate under high frequency, whereas GM type pulse tube refrigerator limits its working frequency. Hence the compressors used for both the case is different type. Generally a rotary valve is used as the pressure distribution system in GM type PTR. Therefore, a GM type pulse tube refrigerator usually works at low frequencies with large oscillating amplitudes to yield lower temperature compared to Stirling model.

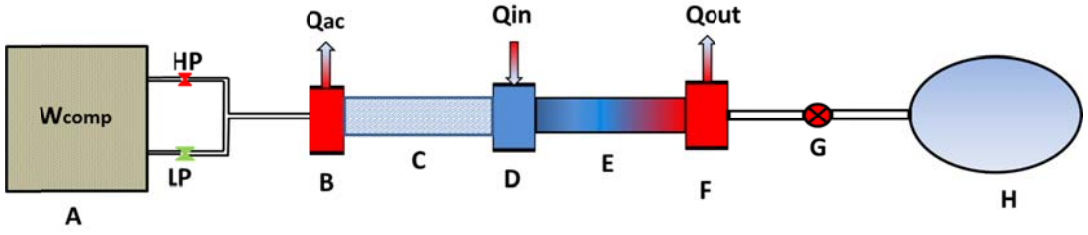

Figure 6.1 Schematic model of orifice pulse tube refrigerator. A- compressor, B- after cooler, C- regenerator, D-cold heat exchanger, E-pulse tube, F-hot heat exchanger, G-orifice valve, H-buffer

6.2 Geometry of orifice pulse tube refrigerator

The schematic diagram with details of an orifice pulse tube refrigerator is presented in Figure 6.1. The extra part of an orifice pulse tube refrigerator than an inertance tube pulse tube refrigerator is the orifice instead of the inertance tube. The orifice valve locates between the hot end of pulse tube and the reservoir. The opening

of the orifice controls the phase angle between pressure wave and mass flow rate near the hot end of pulse tube.

6.3 Modeling of OPTR

The description of sage modelling for the OPTR is very similar to that of ITPTR model as described in section 5.2. The additional boundary conditions are listed in the respective sections. Details of modelling of the regenerator, heat exchanger, transfer line, reservoir, other parameters and temperature dependent properties are similar as those described in earlier model in section 5.2.

At the root level (highest level) the OPTR can be distributed into two main subassemblies: the compressor zone and the cold space zone. They are connected by a transfer line as shown in Figure 6.2. The details of GM type compressor modelling are described in the following sections.

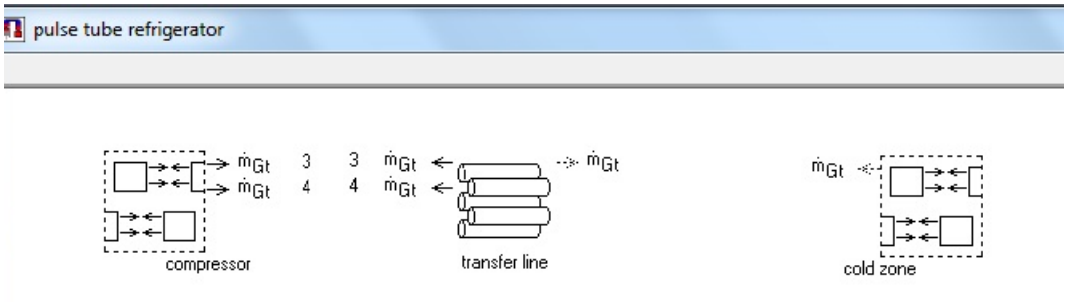

Figure 6.2 Root level components of OPTR

6.3.1 Modelling of Compressor

The compressor comprises of a mass flow pump, one pressure source, two pressure buffers (one high and another is low pressure), two rotary valves (discharge rotary valve and suction rotary valve). The compressor can be designed in sage using the available components are, from the "Basic" tab, and necessary child components from the "Composite" tab. These parent level model components are shown in Figure 6.3.

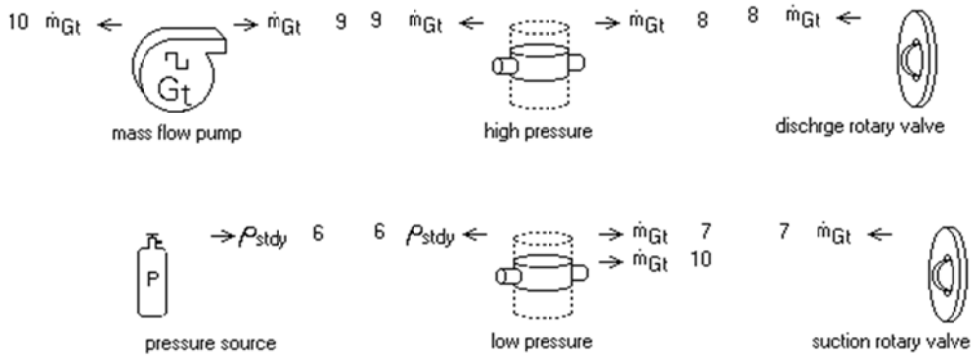

Figure 6.3 Parent (root) level model components of the compressor

6.3.2 OPTR Assembly

The components and subassemblies, or building blocks, shown in Figure 6.2 and Figure 6.3 are assembled together to create the model of the entire OPTR. Figure 6.4 relates the Sage model numbering system as discussed on the above section to the components shown in the schematic of Figure 6.1. The numbers correspond to the appropriate boundary connections with Sage. Note that not all components shown in the Sage models are shown in the schematic.

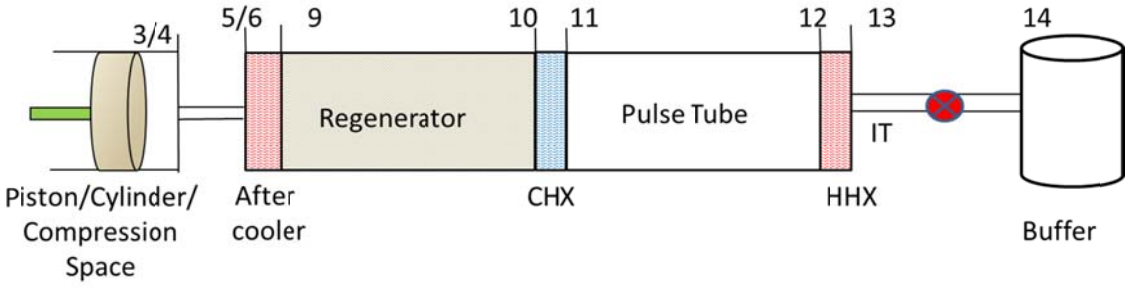

Figure 6.4 OPTR schematic labelled with corresponding numbers from Sage models

6.4 Response surface methodology (RSM)

The results of the numerical analysis of OPTR are obtained through the design of experiment (DOE) approach, such as response surface methodology (RSM). The numerical investigation has been conducted to investigate the effect of pulse tube diameter (A), pulse tube length (B), regenerator diameter (C), regenerator length (D), frequency (E), charging pressure (F), and orifice diameter (G) on performance measured in terms of cold head temperature (T_{cold}) and input compressor power (W_{comp})

values. In the present study, the Box-Behnken design has been selected to obtain the interaction between the output response functions and independent input variables. There are 62 numerical runs performed in a Box-Behnken RSM design with three levels of seven factors and six centre points. For the smooth numerical run, the parametric levels are decoded using the Equation.(6.1).

$$\text{Coded Value } (Z) = \frac{X - \frac{X_{max} + X_{min}}{2}}{\frac{X_{max} - X_{min}}{2}} \qquad (6.1)$$

where, Z is coded value (-1, 0, 1), X_{max} and X_{min} is maximum and minimum value of actual parameters and X is the actual value of the corresponding parameter. Table 6.1 shows the coding of the process parameters. Tble 6.2 presents the RSM Box-Bhenkhen design and results for seven variables in coded form and real input variables. The details of the methodology used in this work are illustrated in Figure 5.12.

Table 6.1 Real and coded levels of the independent variables

Process Parameters	Symbols	Code		
		-1	0	1
Pulse tube diameter, A (mm)	A	10	15	20
Pulse tube length, B (mm)	B	80	100	120
Regenerator diameter, C (mm)	C	15	20	25
Regenerator Length, D (mm)	D	60	80	100
Frequency, E (Hz)	E	6	12	18
Charging pressure, F (bar)	F	5	10	15
Orifice diameter, G (m)	G	0.0006	0.00075	0.0009

Table 6.2 Box-Behnken design of experiment along with observed and predicted response.

Run order	Factor (coded units)							Actual levels of variables								
	A	B	C	D	E	F	G	A	B	C	D	E	F	G	T_{cold}	W_{comp}
1	0	0	0	1	1	1	0	15	100	20	60	6	5	0.00075	59	1259
2	0	0	0	1	1	1	0	15	100	20	100	6	5	0.00075	48	1288
3	0	0	0	1	1	1	0	15	100	20	60	18	5	0.00075	87.5	972.8
4	0	0	0	1	1	1	0	15	100	20	100	18	5	0.00075	79	994.2
5	0	0	0	1	1	1	0	15	100	20	60	6	15	0.00075	68	435.7
6	0	0	0	1	1	1	0	15	100	20	100	6	15	0.00075	55	411.9
7	0	0	0	1	1	1	0	15	100	20	60	18	15	0.00075	100	265.7

8	0	0	0	1	1	1	0	15	100	20	100	18	15	0.00075	88	271.3
9	1	0	0	0	0	1	1	10	100	20	80	12	5	0.0006	85.5	1069
10	1	0	0	0	0	1	1	20	100	20	80	12	5	0.0006	88	1067
11	1	0	0	0	0	1	1	10	100	20	80	12	15	0.0006	83	341.2
12	1	0	0	0	0	1	1	20	100	20	80	12	15	0.0006	90	304.1
13	1	0	0	0	0	1	1	10	100	20	80	12	5	0.0009	128.7	1103
14	1	0	0	0	0	1	1	20	100	20	80	12	5	0.0009	69	1099
15	1	0	0	0	0	1	1	10	100	20	80	12	15	0.0009	150	369.4
16	1	0	0	0	0	1	1	20	100	20	80	12	15	0.0009	71	311.7
17	0	1	0	0	1	0	1	15	80	20	80	6	10	0.0006	44	650.9
18	0	1	0	0	1	0	1	15	120	20	80	6	10	0.0006	49.5	632.5
19	0	1	0	0	1	0	1	15	80	20	80	18	10	0.0006	97.5	438.6
20	0	1	0	0	1	0	1	15	120	20	80	18	10	0.0006	110	438.7
21	0	1	0	0	1	0	1	15	80	20	80	6	10	0.0009	130	825
22	0	1	0	0	1	0	1	15	120	20	80	6	10	0.0009	74.6	656.2
23	0	1	0	0	1	0	1	15	80	20	80	18	10	0.0009	78.5	462.5
24	0	1	0	0	1	0	1	15	120	20	80	18	10	0.0009	85	460.9
25	1	1	0	1	0	0	0	10	80	20	60	12	10	0.00075	121	560
26	1	1	0	1	0	0	0	20	80	20	60	12	10	0.00075	76	501
27	1	1	0	1	0	0	0	10	120	20	60	12	10	0.00075	86.5	530.7
28	1	1	0	1	0	0	0	20	120	20	60	12	10	0.00075	94	494.3
29	1	1	0	1	0	0	0	10	80	20	100	12	10	0.00075	112.5	538.4
30	1	1	0	1	0	0	0	20	80	20	100	12	10	0.00075	69	514
31	1	1	0	1	0	0	0	10	120	20	100	12	10	0.00075	84.5	526.4
32	1	1	0	1	0	0	0	20	120	20	100	12	10	0.00075	82.5	511
33	0	0	1	1	0	0	1	15	100	15	60	12	10	0.0006	77.5	535.3
34	0	0	1	1	0	0	1	15	100	25	60	12	10	0.0006	93	482.6
35	0	0	1	1	0	0	1	15	100	15	100	12	10	0.0006	68.5	559.3
36	0	0	1	1	0	0	1	15	100	25	100	12	10	0.0006	85	480.3
37	0	0	1	1	0	0	1	15	100	15	60	12	10	0.0009	69.2	556.7
38	0	0	1	1	0	0	1	15	100	25	60	12	10	0.0009	74.5	497.8
39	0	0	1	1	0	0	1	15	100	15	100	12	10	0.0009	67	582.4
40	0	0	1	1	0	0	1	15	100	25	100	12	10	0.0009	71	498.1
41	1	0	1	0	1	0	0	10	100	15	80	6	10	0.00075	160	1053
42	1	0	1	0	1	0	0	20	100	15	80	6	10	0.00075	51.5	679
43	1	0	1	0	1	0	0	10	100	25	80	6	10	0.00075	140	895.6
44	1	0	1	0	1	0	0	20	100	25	80	6	10	0.00075	52	577.7
45	1	0	1	0	1	0	0	10	100	15	80	18	10	0.00075	82.6	479.2
46	1	0	1	0	1	0	0	20	100	15	80	18	10	0.00075	107	478.8
47	1	0	1	0	1	0	0	10	100	25	80	18	10	0.00075	102	433.8
48	1	0	1	0	1	0	0	20	100	25	80	18	10	0.00075	116	435.7
49	0	1	1	0	0	1	0	15	80	15	80	12	5	0.00075	59	1151
50	0	1	1	0	0	1	0	15	120	15	80	12	5	0.00075	66.5	1147
51	0	1	1	0	0	1	0	15	80	25	80	12	5	0.00075	58.5	1151
52	0	1	1	0	0	1	0	15	120	25	80	12	5	0.00075	67	1147
53	0	1	1	0	0	1	0	15	80	15	80	12	15	0.00075	62.3	351.9
54	0	1	1	0	0	1	0	15	120	15	80	12	15	0.00075	72	344.9
55	0	1	1	0	0	1	0	15	80	25	80	12	15	0.00075	75	299.2
56	0	1	1	0	0	1	0	15	120	25	80	12	15	0.00075	83.3	292.7
57	0	0	0	0	0	0	0	15	100	20	80	12	10	0.00075	44.1	489
58	0	0	0	0	0	0	0	15	100	20	80	12	10	0.00075	44.9	483
59	0	0	0	0	0	0	0	15	100	20	80	12	10	0.00075	45.2	480
60	0	0	0	0	0	0	0	15	100	20	80	12	10	0.00075	44.3	486
61	0	0	0	0	0	0	0	15	100	20	80	12	10	0.00075	45.2	480
62	0	0	0	0	0	0	0	15	100	20	80	12	10	0.00075	44.4	485

6.5 Results and discussion

6.5.1 Regression model and analysis of variance (ANOVA)

The analysis of variance (ANOVA) is performed, based on the proposed model to find out the interaction between the process variables and the response. The quality of the fit of the polynomial model is expressed with the coefficient of determination (R^2), and the statistical significance is checked by the F-value and P-value. Finally, three-dimensional response surface plots are drawn, in order to visualize the individual and the interaction effects of the independent variables, on the cold end temperature and compressor input power. A total of 62 sets of runs obtained from the Box-Behnken, and the corresponding output responses are shown in Table 6.2, for T_{cold} and W_{comp}. It is observed that, the cold head temperature varies due to a variation in the dimension of the pulse tube and regenerator, and operating conditions in between 44 K and 160 K, and W_{comp} varies from 265 W to 1288 W. The results are analysed, using the ANOVA (analysis of variance), obtained from the design of experiment.

Table 6.3 ANOVA table for cold end temperature (T_{cold})

Source	Squares	df	Square	Value	Prob > F	
Model	35934.55	22	1562.37	15.05	< 0.0001	significant
A-PD	5713.42	1	5713.42	55.04	< 0.0001	
B-PL	32.43	1	32.43	0.31	0.5794	
C-RD	229.4	1	229.4	2.21	0.1454	
D-RL	385.6	1	385.6	3.71	0.0614	
E-Freq	1691.76	1	1691.76	16.3	0.0003	
F-Pcharg	432.65	1	432.65	4.17	0.0482	
G-Orifice	392.04	1	392.04	3.78	0.0594	
AB	1104.5	1	1104.5	10.64	0.0023	
AE	6897.25	1	6897.25	66.45	< 0.0001	
AG	2745.4	1	2745.4	26.45	< 0.0001	
BE	593.4	1	593.4	5.72	0.0219	
BG	559.45	1	559.45	5.39	0.0257	
CE	286.8	1	286.8	2.76	0.1047	
CF	72	1	72	0.69	0.4101	
CG	64.41	1	64.41	0.62	0.4357	
EG	3007	1	3007	28.97	< 0.0001	
FG	70.81	1	70.81	0.68	0.414	
A^2	10047.4	1	10047.4	96.8	< 0.0001	
B^2	246.53	1	246.53	2.38	0.1316	
C^2	430.42	1	430.42	4.15	0.0487	
D^2	109.63	1	109.63	1.06	0.3106	
E^2	2024.62	1	2024.62	19.51	< 0.0001	

G^2	1540.81	1	1540.81	14.84	0.0004	
Residual	3944.29	38	103.8			
Lack of Fit	3484.29	33	105.58	1.15	0.4892	Not significant
Pure Error	460	5	92			
Cor Total	39878.83	61				

6.5.2 Analysis of factors influencing T_{cold}

The ANOVA results of the proposed quadratic model for T_{cold} are presented in Table 6.3. The suggested model's significance and accuracy are calculated, using the Adj R-squared value, mean square value, P-value and F-value, and presented. The model is significant as the corresponding F-value of 15.05. In the proposed model the R^2 value is 0.9011 and the "Pred R-Squared" value is 0.6733. The "Pred R-Squared" of 0.6733 is in sensible agreement with the "Adj R-Squared" of 0.8412. The "Lack of Fit F-value" of 1.54 implies that the Lack of Fit is not significant relative to the pure error. As all the model statistics and diagnostic plots are significant, it can be proposed to handle the design space. In order to ensure that the present model adequately represents the real system, the predicted RSM-generated models versus actual value plots are shown in Figure 6.5. It is observed from the comparison of models, that the data are almost normally distributed in an acceptable range of error, with some deviations. And also, the normal probability plot and the residual plot for T_{cold} are shown in Figure 6.6 and 6.7 respectively, and these figures show an identical trend of behaviour observed in the actual value of T_{cold}. The regression equation developed from the ANOVA in terms of the coded factors for T_{cold}, is given in equation (6.2):

$$\begin{aligned} Tcold = {} & 57.23 - 15.43*A - 1.16*B + 3.09*C - 4.01*D\ 4.01*D + 8.40*E + 4.25*F + 4.04*G + 11.75*A*B + \\ & 29.36*A*E - 18.53*A*G + 8.61*B*E - 8.36*B*G + 5.99*C*E + 3.00*C*F - 2.84*C*G - \\ & 19.39*E*G + 2.98*F*G + 26.95*A^2 + 4.22*B^2 + 5.58*C^2 + 2.81*D^2 + 12.10*E^2 + 10.55*G^2 \end{aligned} \quad (6.2)$$

where A, B, C, D, E, F and G are the coded values of the pulse tube diameter, pulse tube length, regenerator diameter, regenerator length, operating frequency, charging pressure, and orifice diameter, respectively. The interaction effect of input design parameters for cold end temperature and input compressor power are visualized through 3-D response surface plots. In order to investigate the performance of the OPTR, the operating condition such as charging pressure and operating frequency, and the geometrical parameters are varied, and in each case the cold end temperature and

input compressor power are noted. It is observed that the minimum temperature is achieved at the cold end of the pulse tube refrigerator of 44 K with a compressor power 651 W which is produced by the combination of the pulse tube diameter 15 mm, the regenerator diameter 20 mm, and the orifice diameter 0.0006 m. The combined interaction effects of pulse tube diameter and length of cold head temperature are shown in Figure 6.8 (a) in 3-D surface plot, while keeping the other factors constant. It shows that the minimum temperature can be achieved, by increasing the pulse tube diameter from 10 mm to 17.5 mm, at which the minimum no load temperature of 44 K is observed at the cold head. Furthermore, an increase in the pulse tube diameter may increase the cold head temperature.

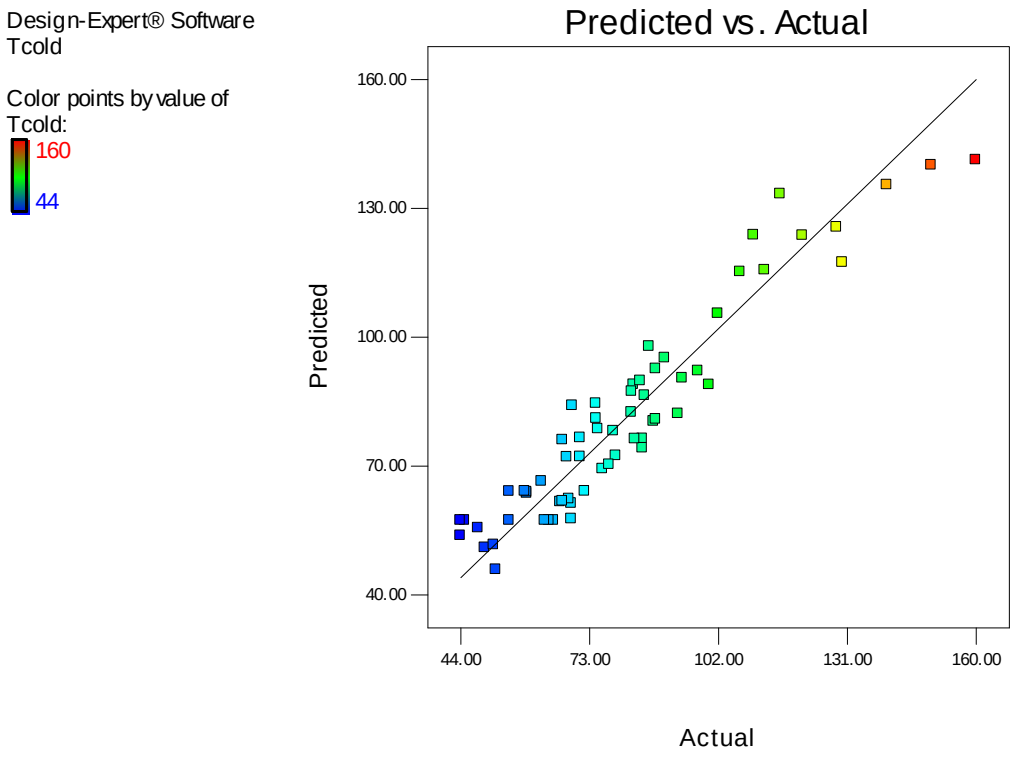

Figure 6.5 Actual versus predicted values for Tcold

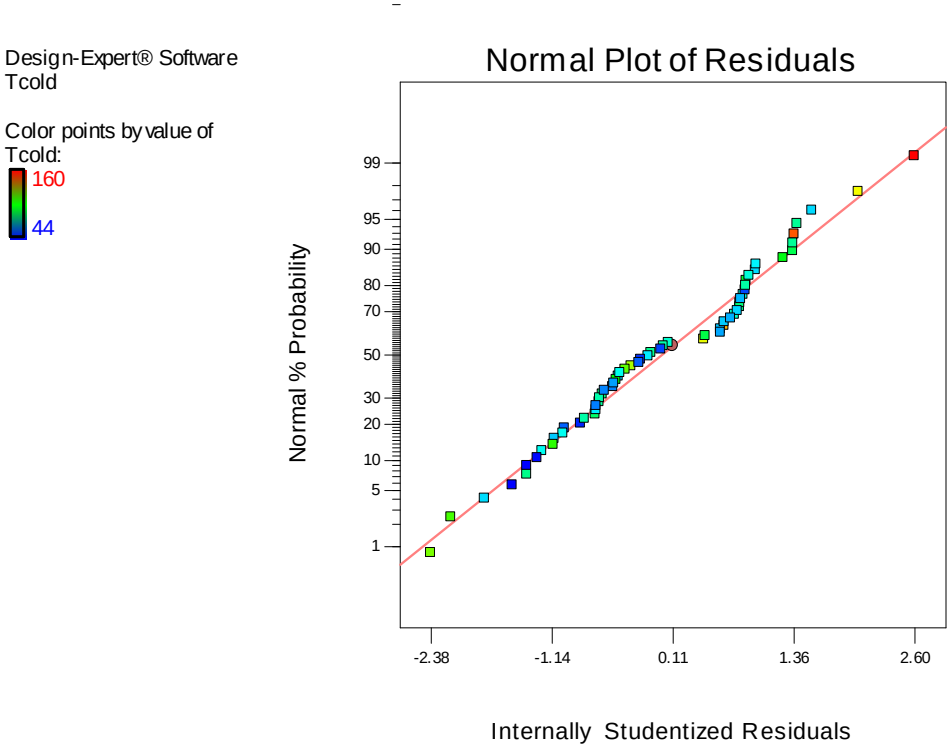

Figure 6.6 Normal probability plot for T_{cold}

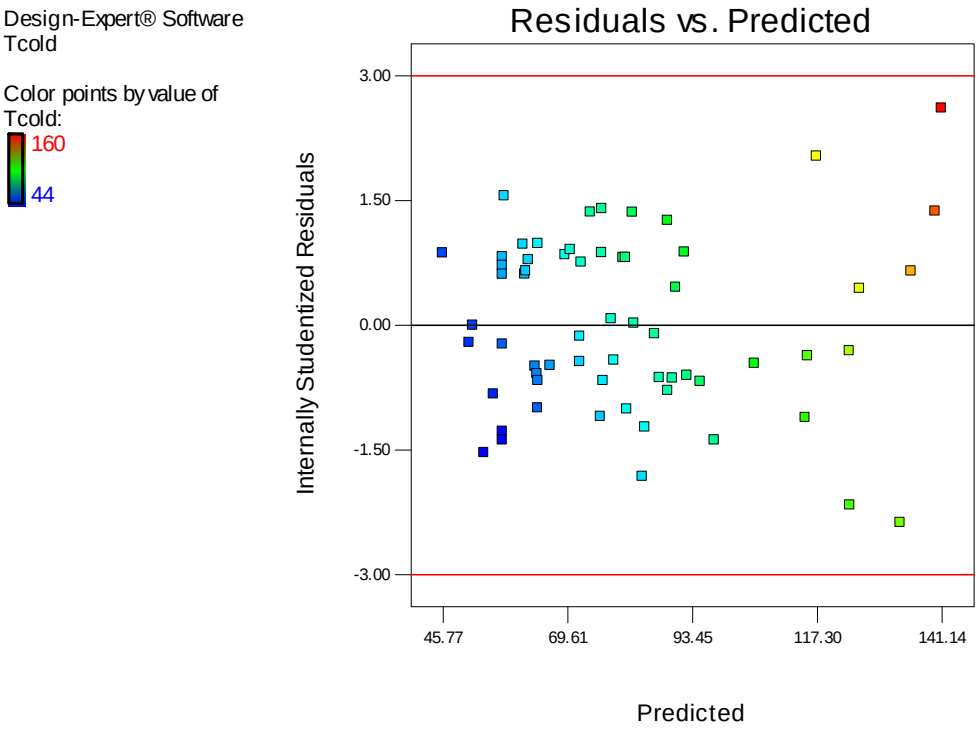

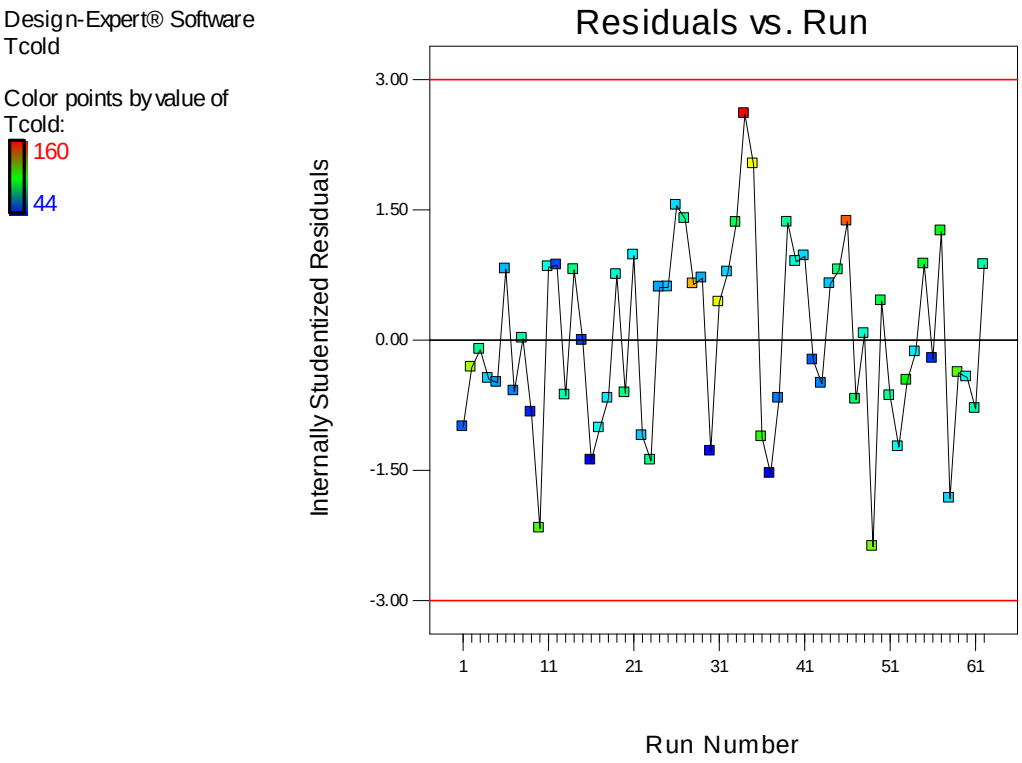

Figure 6.7 Residual plots for T_{cold}

This figure also demonstrates, that the increase in the pulse tube length causes an increase in the cold head temperature, hence, for the present case, the minimum 80 mm tube length is treated as the optimized length. The amalgamated effect of the regenerator diameter and frequency on the cold head temperature is shown in Figure 6.8 (b) in terms of the response surface 3-D plot, while keeping the other factors constant. It shows that cold head temperature increases monotonically with an increase of pulse tube diameter. Cold end temperature decreases with increases in frequency from 9 Hz up to 13 Hz and then it increases with further increases in frequency. The amalgamated effect of the charging pressure and the orifice opening on the cold head temperature is shown in Figure 6.8 (c) in terms of the response surface 3-D plot, while keeping the other factors constant. It shows that cold head temperature increases monotonically with increase of charging pressure. Cold end temperature decreases with increases in frequency from 0.0007 up to 0.0008 and then it increases with further increases in frequency.

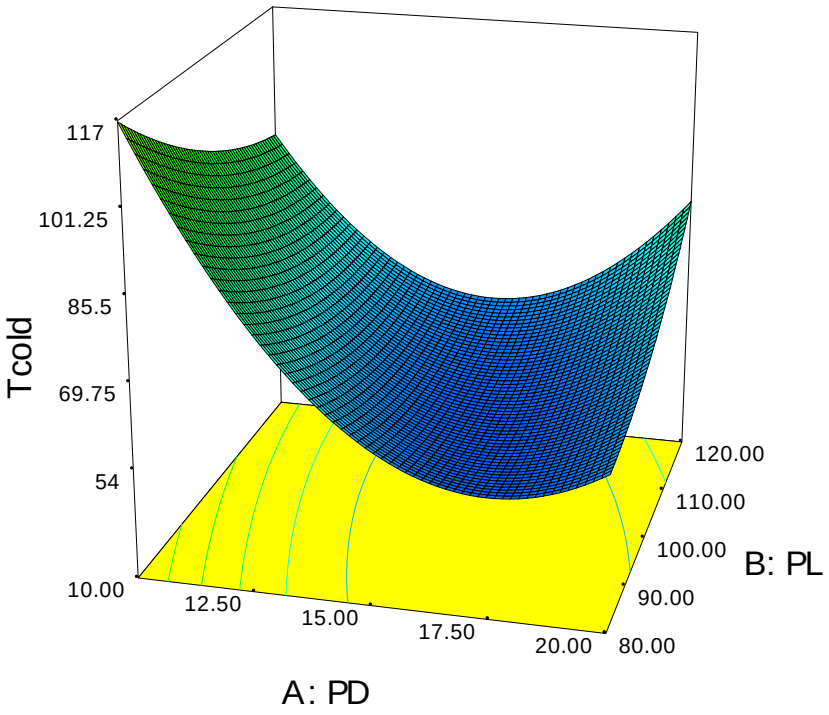

(a) effect of pulse tube diameter (A) and pulse tube length (B)

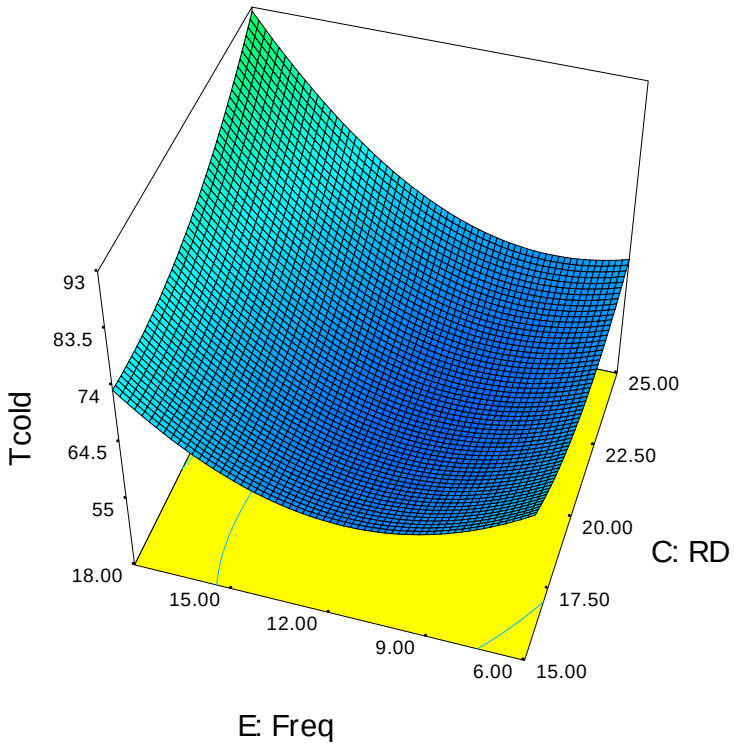

(b) Effect of regenerator diameter (C) and frequency (E),

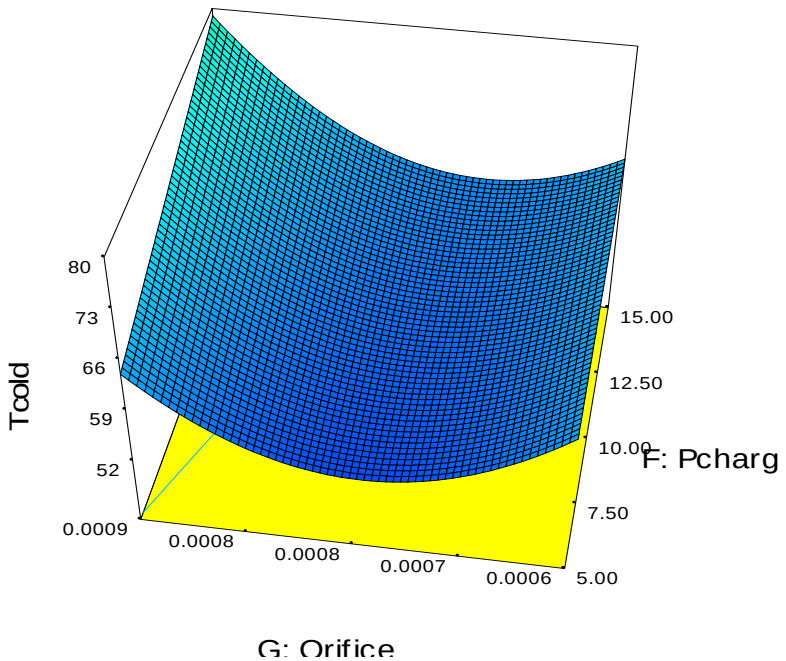

(c) Effect of orifice opening (G) and Charging pressure (F).

Figure 6.8 The response surface 3D plot of cold head temperature (T_{cold}) of OPTR.

6.5.3 Identification of factors influencing W_{comp}

The analysis of variance (ANOVA) for W_{comp} is presented in Table 6.4. For significance check, F value given in Table 6.4 is used. The F-value of 105.15 in the ANOVA table implies that the model is significant. Some *Prob* > F (p-value) values for this proposed quadratic model are less than 0.05 (i.e., α = 0.05, or 95% confidence). This directs that the factors having a low p-value in the quadratic model are considered to be statistically significant, which is desirable, as it demonstrates that the terms in the model have a significant effect on the response. An insignificant lack of fit is desirable because it indicates any term left out of model is not significant and developed model fits well. The lack of fit (p-value = 3.04) indicates that model is adequate. For a model to fit the experimental data, the coefficient of determination R^2 value should be close to 1. The R^2 value of 0.9867, which indicates the high correlation between observed and predicted values and only 1.33% of the total variations cannot be explained by the model. As a further check, the normality test of residuals is carried out. Adding variable to a model always increases R^2, regardless of whether the additional variables are statistically significant or not. Thus it is possible for models that have large values of R^2 to yield poor results. As R^2 always increases on adding terms to the model, use of

adjusted R^2 (adjusted determination coefficient) is preferred. In general, the adjusted R^2 does not always increases as variables are added to the model. In fact, if unnecessary terms are added, the value of adjusted R^2 often decreases. A large difference in R^2 and adjusted R^2 indicates the inclusion of insignificant terms to the model. In the present model, adjusted R^2 value of 0.9689 and R^2 value of 0.9867 are close enough to suggest an excellent correlation between the response and independent variables. In overall, the results of the ANOVA indicate that the proposed model is statistically significant, and can be used to navigate the design space. It is evident from Figure 6.9 that residuals are distributed as per normal distribution.

The regression equation developed from the ANOVA in terms of the coded factors for W_{comp} is given in Equation (6.3).

$$Wcomp = 511.67 - 38.60 * A - 10.88 * B - 30.29 * C + 3.49 * D - 134.68 * E - 393.68 * F + 17.63 * G + 86.68 * A * E - 11.10 * A * F + 23.21 * B * E - 0.69 * B * F - 19.01 * B * G - 6.46 * C * D + 21.28 * C * E - 13.11 * C * F - 8.57 * D * F + 33.68 * E * F - 18.96 * E * G + 21.21 * A^2 + 5.76 * B^2 + 36.03 * C^2 - 16.67 * D^2 + 60.19 * E^2 + 182.13 * F^2 - 6.96 * G^2 \quad (6.3)$$

Table 6.4 ANOVA table for W_{comp}

Source	Squares	df	Square	Value	Prob > F	
Model	4.83E+06	25	1.93E+05	105.18	< 0.0001	significant
A-PD	35759.04	1	35759.04	19.47	< 0.0001	
B-PL	2842.73	1	2842.73	1.55	0.2215	
C-RD	22022.04	1	22022.04	11.99	0.0014	
D-RL	291.9	1	291.9	0.16	0.6925	
E-Freq	4.35E+05	1	4.35E+05	237.02	< 0.0001	
F-Pcharg	3.72E+06	1	3.72E+06	2025.25	< 0.0001	
G-Orifice	7462.43	1	7462.43	4.06	0.0513	
AE	60100.45	1	60100.45	32.72	< 0.0001	
AF	985.68	1	985.68	0.54	0.4686	
BE	4310.56	1	4310.56	2.35	0.1343	
BF	3.78	1	3.78	2.06E-03	0.9641	
BG	2891.8	1	2891.8	1.57	0.2176	
CD	334.11	1	334.11	0.18	0.6723	
CE	3621	1	3621	1.97	0.1689	
CF	1375.5	1	1375.5	0.75	0.3925	
DF	588.25	1	588.25	0.32	0.5749	
EF	9072.05	1	9072.05	4.94	0.0326	
EG	2876.61	1	2876.61	1.57	0.2188	
A^2	6074.99	1	6074.99	3.31	0.0773	
B^2	448.39	1	448.39	0.24	0.6242	
C^2	17520.98	1	17520.98	9.54	0.0039	

D^2	3750.63	1	3750.63	2.04	0.1616	
E^2	48915.51	1	48915.51	26.63	< 0.0001	
F^2	4.48E+05	1	4.48E+05	243.83	< 0.0001	
G^2	654.3	1	654.3	0.36	0.5543	
Residual	66118.12	36	1836.61			
Lack of Fit	62784.79	31	2025.32	3.04	0.1085	Not significant
Pure Error	3333.33	5	666.67			
Cor Total	4.90E+06	61				

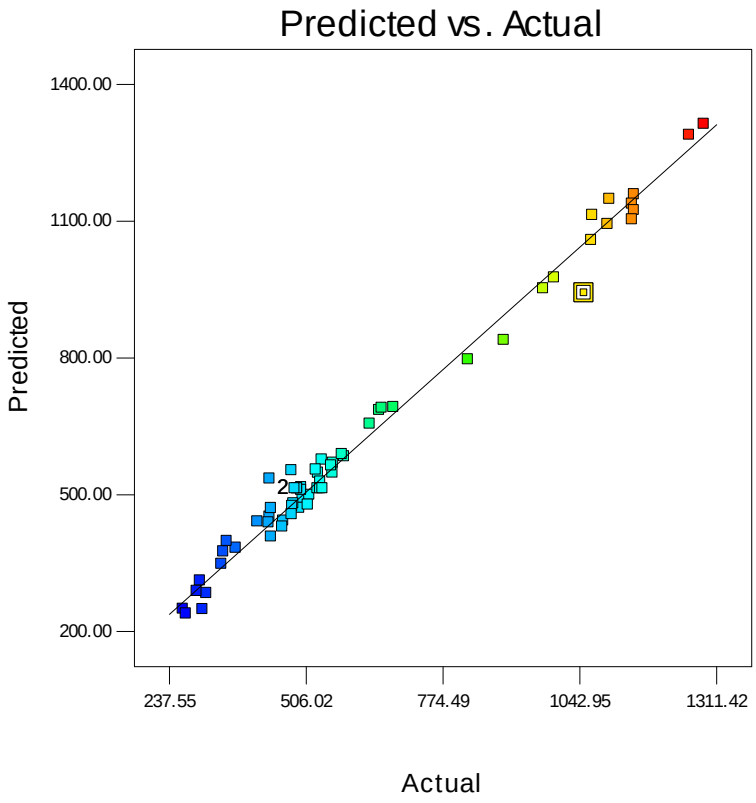

Figure 6.9 Actual versus predicted values for W_{comp}

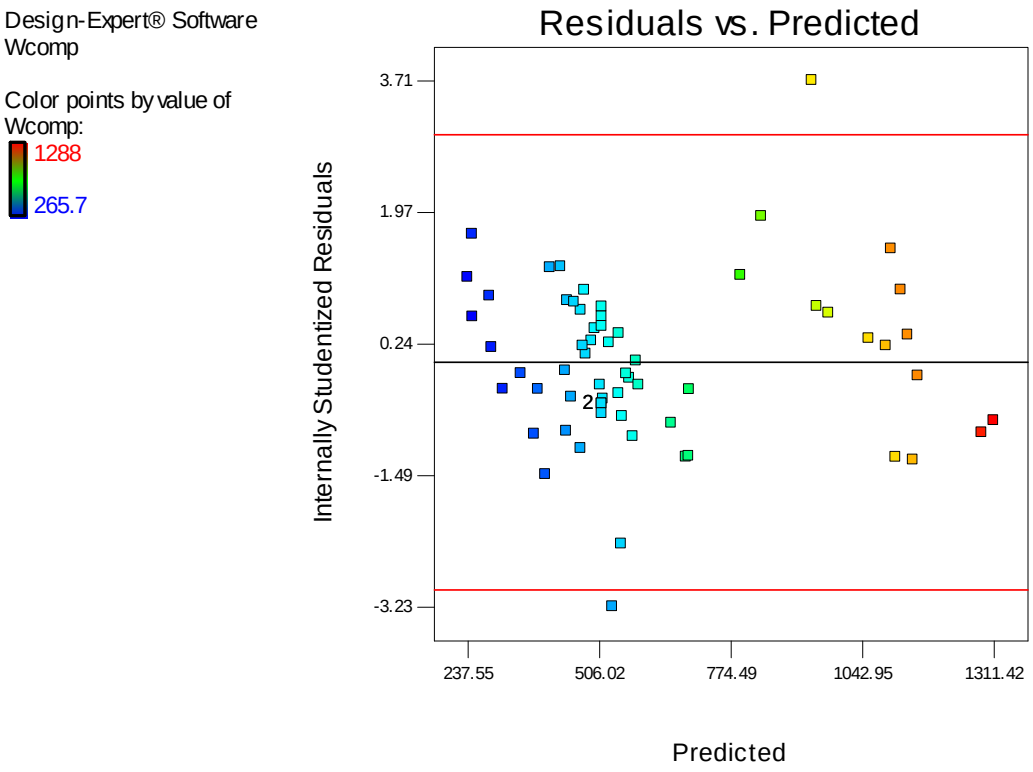

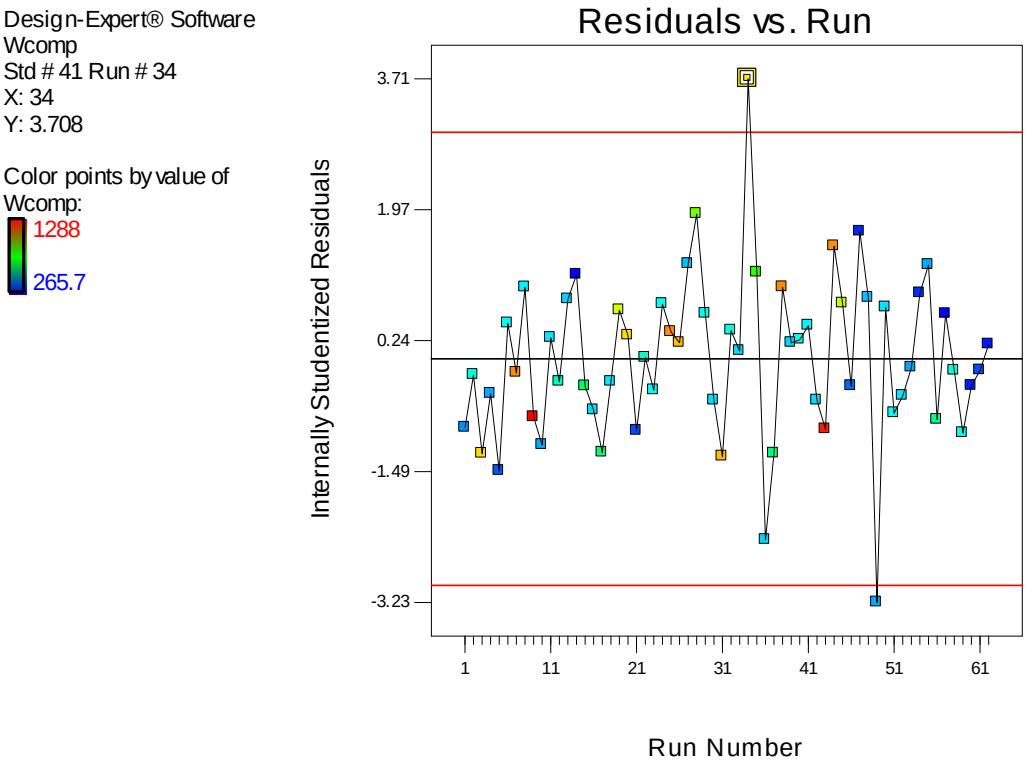

Figure 6.10 Residual plot for W_{comp}

where A, B, C, D, E, F and G are the coded values of the pulse tube diameter , pulse tube length, regenerator diameter, regenerator length, frequency, charging pressure , and orifice diameter, respectively. Compressor input power is another important response in the pulse tube refrigerator as it directly affects the cost of the machine. Figure 6.11 (a) shows the interrelationship between W_{comp}, pulse tube diameter and charging pressure. The surface plot presents that pulse tube diameter and charging pressure affects compressor input power considerably. More compressor power is required for system operation if the charging pressure is low. It shows that more than 1100 W power required when the charging pressure is 5 bar and below 300 W power required while the charging pressure is 15 bar as in the present operating condition. It also indicates that for a large size of diameter of the pulse tube less amount of compressor input power is required. The amalgamated effect of the pulse tube length and operating frequency on the W_{comp} is shown in Figure 6.11 (b), in terms of the response surface 3-D plot, while keeping the other factors constant. It indicates that more compressor power needed for low operating frequency and less compressor power required for high operating frequency. It is reported that more than 700 W power required when the charging pressure is 6 Hz and below 450 W power required while the operating frequency is 18 Hz. The small opening of orifice causes high compressor power while increases in opening causes low compressor power as shown in Figure 6.11 (c). It demonstrates that the increase in the pulse tube length and regenerator length causes a small change in the input power of the compressor. The combined interaction effects of the regenerator diameter and length on input power of the compressor is shown in Figure 6.11 (d) in terms of 3-D surface plot, while keeping the other factors constant. It shows that increase in regenerator diameter from 15 mm up to 21 mm requires decreases in compressor input power and it requires a lowest compressor power at 22.5 mm and further increase in diameter causes increase in input compressor power.

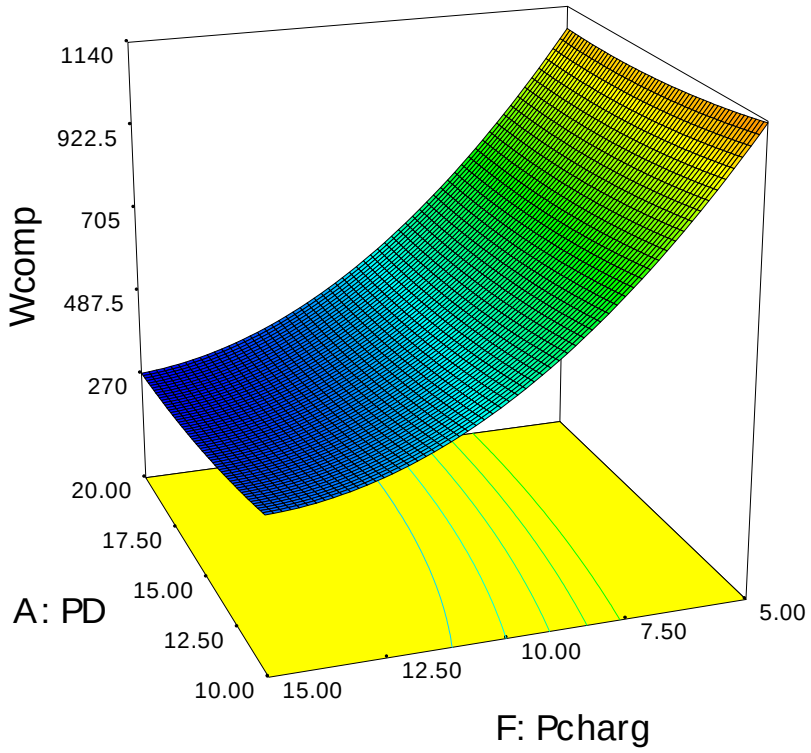

(a) effect of pulse tube diameter (A) and charging pressure (F)

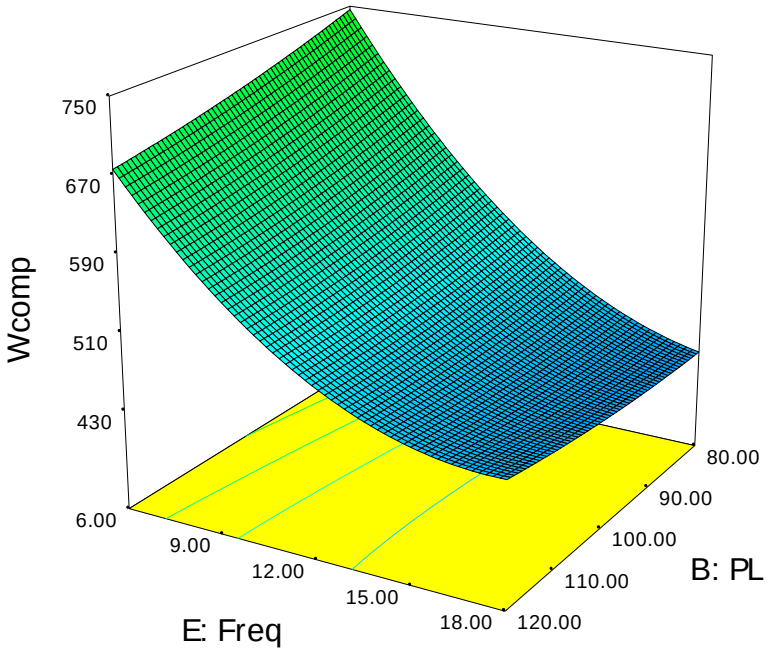

(b) effect of pulse tube length (B) and operating frequency (E)

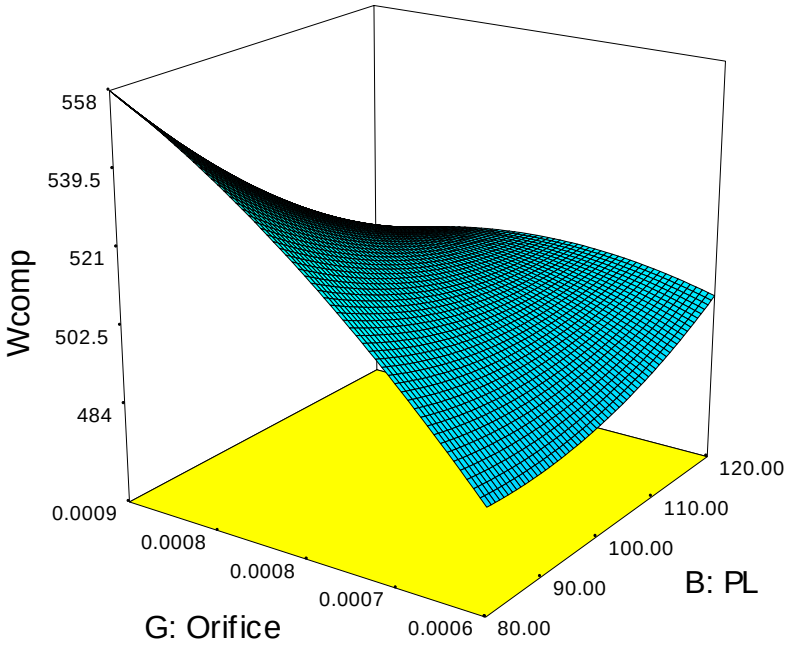

(c) effect of pulse tube length (B) and orifice opening (G)

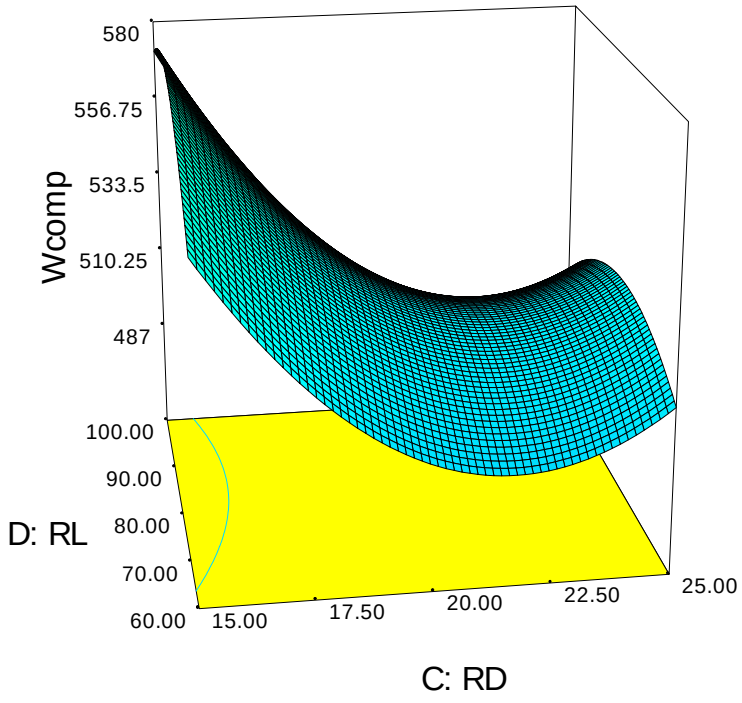

(d) effect of regenerator length (D) and regenerator diameter (C)

Figure 6.11 The response surface 3-D plot of input power of the compressor (W_{comp}).

6.6 *Multi-objective optimization of OPTR*

In the present work, the objectives are the minimizations of both T_{cold} and W_{comp}, which are functions of the decision variables, viz., pulse tube diameter and length, and regenerator diameter and length. Accordingly, the empirical relation between the input parameters and process responses obtained in equations (6.2) and (6.3), are used as the functional relations. The objective functions are given below.

Objective 1 = W_{comp}

Objective 2 = T_{cold}

There are two responses, which might not be applicable simultaneously for all industrial applications. The NSGA II simulation is generated by using the MATLAB toolbox as described in Section 5.6. The choice of responses depends purely on the requirements of the process engineer and industries. The constrained values are selected from the numerical observations. These results of the constrained Pareto-optimal solutions are for two combinations of W_{comp} and T_{cold}. An initial population size of 50 is set with the simple crossover and bitwise mutation, with a crossover probability, Pc = 0.8, migration fraction 0.2, migration interval 20, and Pareto fraction 0.35. The sample set of optimal solutions with the process parameters for W_{comp} and T_{cold} have been presented in Table 6.5. Figure 6.12 shows the Pareto-optimal front solutions for responses of the W_{comp} and T_{cold} combination.

Ranking of solution

It is very difficult to judge the best solution from the large number of non-dominated values by NSGA II. So to avoid such problems multi-attribute decision making (MADM) methods are implemented to find scores for the solutions and the solution showing maximum score is chosen as the best one. The decision of ranking of alternate solution is considerably affected, since the weights assigned in multi-attribute decision making process for transforming multiple objectives into a single equivalent objective score are sensibly subjective in nature. In order to keep off the associated uncertainty due to the subjective assigning of weights from the outputs and to take out the exact information from the available mathematical data, maximum deviation theory (MDT) proposed by [228] is implemented in this present work. The non-dominated solutions obtained NSGA II solutions are used as the decision matrix. Each element of the decision matrix indicates the value of b_{th} attribute of a_{th} substitute, where a=1, 2

...n, and b=1, 2...m. Normalization of each attribute is carried out to transform different scales and units among various attributes into a common measurable scale. In the present case the rating matrix is normalized lower the better scale, by the following equation. $x_{ab}^{*} = \frac{\max_{a}\{x_{ab}\} - x_{ab}}{\max_{a}\{x_{ab}\} + \min_{a}\{x_{ab}\}}$ for lower the better attributes

(6.4)

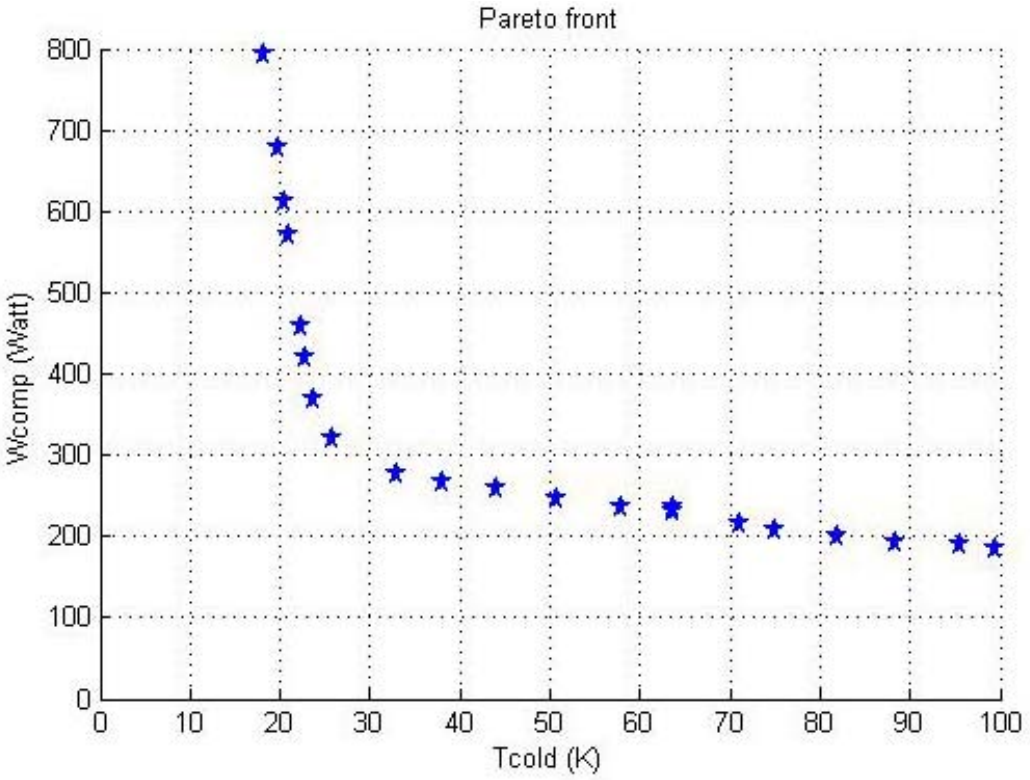

Figure 6.12 Pareto front of NSGA-II solution for OPTR

Table 6.5 Pareto optimal solution for W_{comp} and T_{cold} with corresponding parameters setting

SN	A	B	C	D	E	F	G	T_{cold}	W_{comp}
1	10.4	109.7	23.886	99.9735	17.9365	14.9545	0.00061	111.055	202.293
2	18.6	98.64	21.556	93.776	6.06045	5.07801	0.00085	34.8946	1218.32
3	18.6	98.64	21.556	88.776	6.06045	5.07801	0.00085	35.1050	1220.54
4	18.6	97.16	21.972	94.3955	6.29263	6.05144	0.00085	36.1576	1060.86
5	18.6	98.64	21.556	91.2987	6.06045	5.07801	0.00085	34.955	1219.68
6	12.9	110.9	23.886	99.9735	17.9365	14.8568	0.00068	93.6586	206.533
7	18.6	98.52	21.374	93.9796	6.35645	5.86883	0.00085	36.2568	1084.37
8	10.4	104.7	23.886	98.7235	17.5615	14.9545	0.00061	113.561	210.421

9	18.6	97.50	22.218	89.5674	6.07891	7.36479	0.00085	38.7202	904.619
10	18.4	103.5	21.510	94.8582	6.52718	8.80396	0.00085	40.5543	692.307
11	18.6	98.64	21.556	90.1124	6.06045	5.07801	0.00085	35.0144	1220.15
12	18.6	98.64	21.556	88.776	6.06045	5.07801	0.00085	35.1050	1220.54
13	10.8	111.0	23.499	99.7993	17.8853	14.9387	0.00062	104.788	203.272
14	10.9	104.9	23.886	99.4616	17.6830	14.9357	0.00062	107.829	207.040
15	18.6	97.59	21.473	93.7908	6.09343	6.84540	0.00085	36.4524	956.782
16	10.4	109.7	23.886	99.9735	17.9365	14.9545	0.00061	111.055	202.293
17	18.6	98.64	21.556	96.2987	6.06045	5.07801	0.00085	37.8693	1235.25
18	19.0	101.3	22.385	97.2940	9.19355	14.6208	0.00087	56.1153	269.300
19	17.7	104.3	23.637	98.7439	11.2134	13.9404	0.00083	63.1934	275.687
20	18.6	98.64	21.556	93.776	6.06045	5.07801	0.00085	34.8946	1218.32
21	10.9	87.17	23.888	99.5568	17.7214	14.8778	0.00062	117.699	214.232
22	18.5	98.32	21.104	74.1743	6.25061	14.6997	0.00085	45.8676	355.779
23	18.6	98.39	21.490	93.3576	6.06946	5.76301	0.00085	35.4966	1110.77
24	17.6	104.4	23.446	96.3810	8.71952	12.1254	0.00082	51.6829	394.712
25	11.1	106.4	23.835	96.4943	16.9021	14.4220	0.00063	104.036	225.581
26	18.8	98.05	21.208	95.5043	6.23989	9.85724	0.00086	39.2037	604.121
27	18.9	99.11	22.114	96.3978	7.60250	10.9912	0.00086	45.7927	465.544
28	18.7	98.20	21.620	94.3287	6.10210	8.86143	0.00086	38.2283	710.914
29	17.1	98.64	22.258	96.3327	8.03988	8.41676	0.00081	54.2220	750.601
30	18.6	98.64	19.056	95.1124	6.06045	6.32801	0.00085	41.7989	1057.11
31	18.6	108.3	21.393	93.0718	6.10861	8.06239	0.00086	43.0693	773.966
32	18.6	98.62	21.507	81.8690	6.10239	8.23927	0.00085	38.7382	785.698
33	18.8	95.97	21.507	96.2743	7.08363	11.5715	0.00086	43.0024	449.031
34	14.8	108.4	24.014	93.0085	16.4512	14.7814	0.00074	84.9132	233.094
35	13.6	101.5	22.655	99.9420	11.7287	14.8828	0.00071	74.6031	287.780
36	18.6	105.8	21.416	93.0786	6.09856	7.71187	0.00085	39.2043	826.376
37	18.6	98.53	21.549	86.8308	6.08779	7.9518	0.00085	37.7581	818.912
38	18.6	98.48	21.069	86.1369	6.32731	6.88184	0.00085	37.5413	946.858
39	18.1	105.2	21.812	99.3171	6.37616	11.8731	0.00084	47.5557	463.508
40	18.8	97.76	22.105	95.5302	7.08352	9.17704	0.00086	41.4820	643.576
41	18.5	98.62	21.369	88.1056	6.20781	9.07980	0.00085	38.8069	690.323
42	17.8	104.7	22.488	99.3704	8.04828	6.8608	0.00083	42.4433	892.362
43	15.8	104.1	23.530	99.2766	13.0535	14.7208	0.00077	69.2464	243.429
44	17.6	99.03	21.039	94.8693	8.61506	8.80346	0.00082	44.1637	660.426
45	18.6	97.34	21.604	94.3840	6.27175	10.9564	0.00085	40.9620	523.825
46	10.7	102.6	22.053	94.0305	17.5595	9.77325	0.00062	88.1822	422.065
47	15.8	101.5	21.368	98.7976	9.46593	14.7506	0.00077	56.3780	312.416
48	10.9	112.1	23.888	95.8068	17.7214	14.8778	0.00062	102.803	215.060
49	19.9	99.13	22.907	94.5571	6.48126	6.1902	0.00089	38.4759	1024.89
50	10.8	111.0	24.749	99.7993	17.8853	14.9387	0.00062	109.403	205.725

The deviation in performance values of each alternative is calculated using MDT. For the attribute ($A_b|$ b=1, 2…m), the deviation value of the alternative ($S_a|$ a = 1, 2 ….n) from all the other alternatives can be calculated by the following equation

$$D_{ab}\left(w_b\right)=\sum d\left(\tilde{r}_{ab},\tilde{r}_{ab}\right)w_b \tag{6.5}$$

Where w_b is the weight of the attributes to be calculated and $D_{ab}(w_b)$ is the deviation value of the alternatives.

The entire deviation rates of all choices with respect to other choice for the attribute (A_b| b =1, 2… m) can be calculated by the following equation.

$$D_b\left(w_b\right)=\sum_{a=1}^{N}D_{ab}\left(w_b\right)=\sum_{a=1}^{N}\sum_{c=1}^{N}d\left(\tilde{r}_{ab},\tilde{r}_{ab}\right)w_b \tag{6.6}$$

Where $D_b(w_b)$ is the total deviation value of all the alternatives.

The deviation of all the attributes along all the choices is computed by the following equation

$$D\left(w_b\right)=\sum_{b=1}^{M}D_b\left(w_a\right)=\sum_{b=1}^{M}\sum_{a=1}^{N}\sum_{c=1}^{N}d\left(\tilde{r}_{ab},\tilde{r}_{lbc}\right)w_b \tag{6.7}$$

Where $D(w_b)$ is the deviation of all the attributes along all the alternatives.

In order to find the weight vector *w* to maximize all deviation values for all the attributes, a linear programming model is designed, and the expression is given by

$$\begin{cases} D\left(w_b\right)=\sum_{b=1}^{M}\sum_{a=1}^{N}\sum_{c=1}^{N}d\left(\tilde{r}_{ab},\tilde{r}_{cb}\right)w_b \\ s.t\sum_{b=1}^{M}w_b^2=1, w_{,}\geq 0, b=1,2,.....M \end{cases} \tag{6.8}$$

The above equation can be solved by the help of a Lagrange function

$$L\left(w_j,\alpha\right)=\sum_{j=1}^{M}\sum_{i=1}^{N}\sum_{l=1}^{N}d\left(\tilde{r}_{ij},\tilde{r}_{lj}\right)w_j+\lambda\left(\sum w_j^2-1\right) \tag{6.9}$$

where,α is the Lagrange multiplier. The partial derivative of $L(w_b,\alpha)$ with respect to w_b and α are

$$\begin{cases} \frac{dL}{dw_b}=\sum_{a=1}^{N}\sum_{a=1}^{N}d\left(\tilde{r}_{ab},\tilde{r}_{bc}\right)+2\lambda w_b=0 \\ \frac{dL}{d\lambda}=\sum_{b}^{M}w_b^2-1=0 \end{cases} \tag{6.10}$$

w_b and α values can be computed from equation (6.9) and (6.10)

$$\begin{cases} 2\alpha = -\sqrt{\sum_{b=1}^{M}\left(\sum_{a=1}^{N}\sum_{c=1}^{N} d\left(\tilde{r}_{ab},\tilde{r}_{bc}\right)\right)^2} \\ w_b = \dfrac{\sum_{a=1}^{N}\sum_{c=1}^{N} d\left(\tilde{r}_{abb},\tilde{r}_{bc}\right)}{\sqrt{\sum_{b=1}^{M}\left(\sum_{a=1}^{N}\sum_{c=1}^{N} d\left(\tilde{r}_{ab},\tilde{r}_{bc}\right)\right)^2}} \end{cases} \quad (6.11)$$

The final normalized attribute weights can be calculated by the following equation

$$w_b = \frac{\sum_{a=1}^{N}\sum_{c=1}^{N} d\left(\tilde{r}_{ab},\tilde{r}_{bc}\right)}{\sum_{b=1}^{M}\sum_{a=1}^{N}\sum_{c=1}^{N} d\left(\tilde{r}_{ab},\tilde{r}_{bc}\right)} \quad (6.12)$$

The results obtained through NSGA II algorithm in terms of the non-dominated solutions are ranked by assessing the composite score of each solution by addition of the weighted performance of all attributes. Considering the ranking of the solutions, one can choose suitable operating condition and dimensions from the top ranking solutions. The Solution ranking of the optimal solution set for T_{cold} and W_{comp} has been given in Table 6.6.

Table 6.6 Solution ranking of the optimal solution set for T_{cold} and W_{comp} obtained using maximum deviation theory

SN	Objective function values		Normalized objective function values		Weighted objective function values		Composite score	Solution ranking
	T_{cold}	W_{comp}	N T_{cold}	NW_{comp}	WN T_{cold}	WN W_{comp}		
1	111.059	202.2938	0.0802	1.0000	0.03675	0.54197133	0.5787	35
2	34.89468	1218.324	1.0000	0.0164	0.458029	0.00888417	0.4669	44
3	35.10504	1220.544	0.9975	0.0142	0.456865	0.00771915	0.4645	48
4	36.15769	1060.861	0.9847	0.1688	0.451042	0.09150112	0.5425	39
5	34.955	1219.684	0.9993	0.0151	0.457695	0.00817032	0.4658	46
6	93.65864	206.5335	0.2903	0.9959	0.132981	0.53974685	0.6727	19
7	36.25687	1084.374	0.9835	0.1461	0.450494	0.07916464	0.5296	41
8	113.5619	210.4215	0.0500	0.9921	0.022889	0.53770688	0.5605	37
9	38.72029	904.619	0.9538	0.3201	0.436868	0.17347767	0.6103	26
10	40.55431	692.3079	0.9317	0.5256	0.426723	0.28487236	0.7115	16
11	35.01442	1220.155	0.9986	0.0146	0.457366	0.00792349	0.4652	47
12	35.10504	1220.544	0.9975	0.0142	0.456865	0.00771915	0.4645	48
13	104.7889	203.2728	0.1559	0.9991	0.071415	0.54145766	0.6128	25
14	107.8297	207.0406	0.1192	0.9954	0.054596	0.53948077	0.5940	32
15	36.45244	956.7824	0.9812	0.2696	0.449412	0.14610877	0.5955	30
16	111.0559	202.2938	0.0802	1.0000	0.03675	0.54197133	0.5787	35
17	37.8693	1235.256	0.9641	0.0000	0.441575	0.00000000	0.4415	50
18	56.11533	269.3006	0.7437	0.9351	0.340649	0.50681438	0.8474	2
19	63.19347	275.6873	0.6582	0.9289	0.301497	0.50346343	0.8049	6
20	34.89468	1218.324	1.0000	0.0164	0.458029	0.00888417	0.4669	44
21	117.6998	214.2326	0.0000	0.9884	0.00000	0.53570729	0.5357	40
22	45.86761	355.7799	0.8675	0.8514	0.397333	0.46144074	0.8587	1
23	35.49666	1110.771	0.9927	0.1205	0.454699	0.06531464	0.5200	42
24	51.68297	394.7123	0.7973	0.8137	0.365166	0.44101383	0.8061	5
25	104.0361	225.5814	0.1650	0.9775	0.075579	0.52975287	0.6053	28
26	39.20372	604.1218	0.9480	0.6110	0.434194	0.33114156	0.7653	11
27	45.79273	465.5443	0.8684	0.7451	0.397747	0.40384992	0.8015	7
28	38.22833	710.9145	0.9597	0.5076	0.439589	0.27510988	0.7146	15
29	54.22206	750.6014	0.7666	0.4692	0.351121	0.25428711	0.6054	27
30	41.79895	1057.111	0.9166	0.1725	0.419838	0.09346873	0.5133	43
31	43.06939	773.9668	0.9013	0.4466	0.412811	0.24202783	0.6548	22

32	38.73829	785.6988	0.9536	0.4352	0.436768	0.23587235	0.6726	20
33	43.00242	449.0319	0.9021	0.7611	0.413181	0.41251359	0.8256	3
34	84.91327	233.0945	0.3959	0.9702	0.181356	0.52581088	0.7071	18
35	74.60318	287.7809	0.5205	0.9172	0.238385	0.49711824	0.7355	12
36	39.20434	826.3766	0.9480	0.3958	0.43419	0.21452961	0.6487	23
37	37.75818	818.9125	0.9654	0.4031	0.44219	0.21844585	0.6606	21
38	37.54138	946.858	0.9680	0.2792	0.443389	0.15131587	0.5947	31
39	47.55576	463.5081	0.8471	0.7471	0.387995	0.40491826	0.7929	9
40	41.48204	643.5763	0.9204	0.5728	0.421591	0.31044066	0.7320	13
41	38.80691	690.3234	0.9528	0.5275	0.436389	0.28591357	0.7223	14
42	42.44337	892.3622	0.9088	0.3320	0.416274	0.17990851	0.5961	29
43	69.24648	243.4292	0.5851	0.9602	0.268015	0.52038852	0.7884	10
44	44.16375	660.4266	0.8881	0.5565	0.406758	0.30159973	0.7083	17
45	40.96208	523.825	0.9267	0.6887	0.424467	0.37327142	0.7975	8
46	88.18225	422.0652	0.3565	0.7872	0.163274	0.42666239	0.5899	33
47	56.37808	312.4162	0.7406	0.8934	0.339195	0.48419265	0.8233	4
48	102.803	215.0603	0.1799	0.9876	0.0824	0.53527305	0.6176	24
49	38.47592	1024.893	0.9568	0.2037	0.438219	0.11037271	0.5485	38
50	109.4033	205.7257	0.1002	0.9967	0.045891	0.54017066	0.5860	34

Table 6.7 Conformation results of W_{comp} and T_{cold} for optimized case of OPTR

	Optimized combination								
A	B	C	D	E	F	G	Tcold (K)	Wcomp (W)	Phase difference at cold end of regenerator
18.59	98.32	21.10	74.17	6.2	14.69	0.0008	46.64	357.215	32.214^0

6.7 Confirmation test

Once the optimal level of the pulse tube and regenerator dimensions are identified as acquired from the analysis, a confirmation test has been performed for the T_{cold} and W_{comp} to validate the responses. The results of the confirmation test for the responses are listed in Table 6.7. The percentage error is found to be in the acceptable range. The range of percentage error between the numerical and the predicted values of W_{comp} and T_{cold} lies within 5 %, and the confirmation runs are within the 95% prediction interval. The phase shift analysis for an OPTR [229] reveals that for setting the phase, the flow will be in phase at the orifice, but not at the regenerator midpoint. Hence at the cold

end of regenerator the phase angle is approximately 30° or more at the cold end, and as much as 70° at the warm end of regenerator. A phase angle of 32.214^0 is observed at cold end of regenerator for the optimised case of OPTR as given in Table 6.7.

6.8 Summary

This numerical investigation proposes a hybrid, integrated approach of response surface methodology (RSM) coupled with multi objective optimization (NSGA-II) for the optimization of the geometrical dimensions and operating condition of the orifice pulse tube refrigerator. The RSM and NSGA II are successfully implemented to obtain the Pareto-optimal front and statistically examine the results. Any solution in the pareto front is an optimal result. Maximum deviation theory (MDT) of objective weights determination is used to estimate the weights for the attributes. The composite score for all the non-dominated solutions is obtained through summing the weighted objective values. The best solution is selected from all the non-dominated solution considering the highest composite score to avoid subjectiveness and impreciseness in the decision making. The main conclusions can be drawn as follows:

- The proposed response surface methodology is used to study the the interactive and complex effects of various important process variables such as pulse tube diameter, pulse tube length, regenerator diameter, regenerator length, frequency, charging pressure, and orifice diameter on performance measured in terms of cold head temperature (T_{cold}) and input compressor power (W_{comp}),
- The proposed generated OPTR model is significant as the values of the F test and Prob > F is confirmed from the ANOVA analysis.
- The ANOVA method revealed that up to a certain limit of increase in the diameter of the pulse tube and regenerator, charging pressure and orifice opening, led to the decrease of the cold head temperature, after which further increase causes an increase in the temperature.
- Pulse tube diameter is found to be an important parameter, which significantly affect both the responses whereas charging pressure affects significantly compressor power than the cold end temperature.

- The numerical investigation with the optimum layout of the proposed OPTR is analyzed for the accuracy of the optimization results. This confirms that the presented response surface methodology in this study is effective to optimize the model, reducing the experimental expense in design of pulse tube refrigerator.
- Finally, the proposed model can be used for selecting ideal process states for achieving improved pulse tube model.

Chapter 7

CONCLUSIONS

The present work covers a theoretical investigation of ITPTR and OPTR using available PTR simulation packages. In the first part of the study, the commercial CFD package, FLUENT is used for investigation the ITPTR. It includes a compressor, three heat exchangers, one regenerator, one pulse tube, one inertance tube and one reservoir. The analysis conducted with the assumptions of no gravity and ideal gas for both thermal equilibrium and non-equilibrium models. The system pressure for different positions of the piston during operation is presented. The phase shift between pressure and mass flow rate during the start of the simulation and after the steady state condition is discussed. Different (L/D) ratio of pulse tube is considered by changing length, while the physical dimensions of other components and operating conditions are kept same. The unsteady CFD model successfully calculates the PTR performance through solving Navier–Stokes equations for fluid momentum and heat transfer along with an energy equation.

Complex inter relationships among parameters make it difficult to ascertain the parametric setting by simple analysis of parameter variation effect. In this direction Desisgn of Experiment (DOE) related methodology is adopted in the second part of the study. It is preferred for asserting the effect of each possible condition in an investigation under the influence of numerous parameter considered with better precision in less experimental or simulation runs. For better accuracy result and less simulation run time, SAGE software is used. The analysis is conducted for both ITPTR and OPTR. In ITPTR case four parameters like pulse tube diameter (A), pulse tube length (B), regenerator diameter (C) and regenerator length (D) are considered as the input parameter, whereas cold head zero load temperature and compressor input power are chosen as output responses. Finally a multi-objective evolutionary algorithm used to optimize the parameters. The optimized dimensions with output results are presented in Table 5.6. The phase relation between the mass flow rate and pressure for the optimized case is presented in Figure. 5.22.

In the case of OPTR seven parameters like, pulse tube diameter (A), pulse tube length (B), regenerator diameter (C), regenerator length (D), frequency (E), charging

pressure (F), and orifice diameter (G) are considered to evaluate the performance in terms of cold head temperature (T_{cold}) and input compressor power (W_{comp}). The optimization of these parameters is also conducted and reported in Table 6.7.

Scope of Future Work

The present work leaves a wide scope for future investigators to explore many aspects of PTR. Some important suggestions for future research include:

(i) Based on the results generated in this work, laboratory experimental work need to be explored for ITPTR and OPTR in order to ascertain their correctness.

(ii) The miniature pulse tube refrigerators which investigated in this study are all single stage. The multistage miniature PTRs are not analysed, hence the CFD study as well as statistical analysis of multistage configurations need attention for investigation.

(iii) At present, the analysis is conducted for the PTRs under no load condition, hence the work can be extended to the model for a load condition at the cold head which will explore the cooling power at a specified refrigerating temperature.

References

1. **Matsubara, Y.** In *Future trend of pulse tube cryocooler research*, Proceedings of the twentieth international cryogenic engineering conference, Beijing, China, (Year), 189-196.

2. **Radebaugh, R.,** Development of the Pulse Tube Refrigerator as an Efficient and Reliable Cryocooler. *Proceedings of Institute of Refrigeration, London* (2000).

3. **Gifford, W. E.; Longsworth, R. C.,** Pulse Tube Refrigeration. *ASME paper No. 63-WA-290, presented at Winter Annual Meeting of the ASME, Philadelphia, Pennsylvania* (1963), 69.

4. **Gifford, W. E.; Longsworth, R. C.,** Surface Heat Pumping. In *Advances in Cryogenic Engineering*, Timmerhaus, K. D., Ed. Springer US (1966); Vol. 11, pp 171-179.

5. **Mikulin E; Tarasov A; M, S.,** Low-temperature expansion pulse tubes. *Adv Cryo Eng* (1984), *29*, 629-637.

6. **Zhu, S.; Wu, P.; Chen, Z.,** A single stage double inlet pulse tube refrigerator capable of reaching 42 K. *ICEC 13 Proc Cryo* (1990), *30* (256-261).

7. **Kanao, K.-i.; Watanabe, N.; Kanazawa, Y.,** A miniature pulse tube refrigerator for temperatures below 100K. *Cryogenics* (1994), *34, Supplement 1* (0), 167-170.

8. **Roach, P.; Kashani, A.,** Pulse Tube Coolers with an Inertance Tube: Theory, Modeling, and Practice. In *Advances in Cryogenic Engineering*, Kittel, P., Ed. Springer US (1998); Vol. 43, pp 1895-1902.

9. **Iwase, T.; Biwa, T.; Yazaki, T.,** Acoustic impedance measurements of pulse tube refrigerators. *Journal of Applied Physics* (2010), *107* (3), 034903.

10. **Radebaugh, R.; Zimmerman, J.; Smith, D.; Louie, B.,** A Comparison of Three Types of Pulse Tube Refrigerators: New Methods for Reaching 60K. In

Advances in Cryogenic Engineering, Fast, R. W., Ed. Springer US (1986); Vol. 31, pp 779-789.

11. **Zhu, S.; Kakimi, Y.; Matsubara, Y.,** Investigation of active-buffer pulse tube refrigerator. *Cryogenics* (1997), *37* (8), 461-471.

12. **Dai, W.; Matsubara, Y.; Kobayashi, H.,** Experimental results on V-M type pulse tube refrigerator. *Cryogenics* (2002), *42* (6–7), 433-437.

13. **Kasthurirengan, S.; Srinivasa, G.; Karthik, G. S.; Nadig, D. S.; Behera, U.; Shafi, K. A.,** Experimental and theoretical studies of a two-stage pulse tube cryocooler operating down to 3 K. *International Journal of Heat and Mass Transfer* (2009), *52* (3–4), 986-995.

14. **Qiu, L. M.; Cao, Q.; Zhi, X. Q.; Gan, Z. H.; Yu, Y. B.; Liu, Y.,** A three-stage Stirling pulse tube cryocooler operating below the critical point of helium-4. *Cryogenics* (2011), *51* (10), 609-612.

15. **Wang, K.; Zheng, Q. R.; Zhang, C.; Lin, W. S.; Lu, X. S.; Gu, A. Z.,** The experimental investigation of a pulse tube refrigerator with a 'L' type pulse tube and two orifice valves. *Cryogenics* (2006), *46* (9), 643-647.

16. **Shiraishi, M.; Murakami, M.,** Visualization of oscillating flow in a double-inlet pulse tube refrigerator with a diaphragm inserted in a bypass-tube. *Cryogenics* (2012), *52* (7–9), 410-415.

17. **Hofler, T. J.,** Thermoacoustic refrigerator design and performance. (1986).

18. **Yang, L.; Zhou, Y.; Liang, J.,** DC flow analysis and second orifice version pulse tube refrigerator. *Cryogenics* (1999), *39* (3), 187-192.

19. **Ju, Y. L.; Wang, C.; Zhou, Y.,** Dynamic experimental investigation of a multi-bypass pulse tube refrigerator. *Cryogenics* (1997), *37* (7), 357-361.

20. **Gerster, J.; Thürk, M.; Reißig, L.; Seidel, P.,** Hot end loss at pulse tube refrigerators. *Cryogenics* (1998), *38* (6), 679-682.

21. **Zhu, S.; Kawano, S.; Nogawa, M.; Inoue, T.,** Work loss in double-inlet pulse tube refrigerators. *Cryogenics* (1998), *38* (8), 803-807.

22. **Yang, X.; Chung, J. N.,** Size effects on miniature Stirling cycle cryocoolers. *Cryogenics* (2005), *45* (8), 537-545.

23. **Zhu, S.; Peiyi, W.; Zhongqi, C.,** Double inlet pulse tube refrigerators: an important improvement. *Cryogenics* (1990), *30* (6), 514-520.

24. **de Waele, A. T. A. M.,** Pulse-tube refrigerators: principle, recent developments, and prospects. *Physica B: Condensed Matter* (2000), *280* (1–4), 479-482.

25. **Popescu, G.; Radcenco, V.; Gargalian, E.; Ramany Bala, P.,** A critical review of pulse tube cryogenerator research. *International Journal of Refrigeration* (2001), *24* (3), 230-237.

26. **Richardson, R. N.; Evans, B. E.,** A review of pulse tube refrigeration. *International Journal of Refrigeration* (1997), *20* (5), 367-373.

27. **Chakravarthy, V. S.; Shah, R. K.; Venkatarathnam, G.,** A review of refrigeration methods in the temperature range 4–300 K. *Journal of Thermal Science and Engineering Applications* (2011), *3* (2), 020801.

28. **Gifford, W. E.; Longsworth, R. C.,** Pulse-tube refrigeration Trans. . *ASME* (1964), 264-268.

29. **Gifford, W. E.; Kyanka, G. H.,** Reversible pulse tube refrigerator. *Advances in cryogenic engineering* (1967), *12*, 619-630.

30. **de Boer, P. C. T.,** Thermodynamic analysis of the basic pulse-tube refrigerator. *Cryogenics* (1994), *34* (9), 699-711.

31. **de Boer, P. C. T.,** Analysis of basic pulse-tube refrigerator with regenerator. *Cryogenics* (1995), *35* (9), 547-553.

32. **Bauwens, L.** In *Basic pulse-tube refrigerator in the narrow limit*, Energy Conversion Engineering Conference, 1996. IECEC 96., Proceedings of the 31st Intersociety, IEEE: (Year), 1195-1200.

33. **Lee, J. M.; Kittel, P.; Timmerhaus, K. D.; Radebaugh, R.,** Flow patterns intrinsic to the pulse tube refrigerator. In *Proc 7th Int Cryocooler Conf* (1993); pp 125-139.

34. **Jeong, E. S.,** Secondary flow in basic pulse tube refrigerators. *Cryogenics* (1996), *36* (5), 317-323.

35. **Koshimizu, T.; Kubota, H.; Takata, Y.; Ito, T.,** Numerical simulation of heat and fluid flow in basic pulse tube refrigerator. *International Journal of Numerical Methods for Heat & Fluid Flow* (2005), *15* (7), 617-630.

36. **Huang, B. J.; Tzeng, T. M.,** Performance characteristics of pulse tube refrigerators. *Cryogenics* (1993), *33* (12), 1132-1136.

37. **Hofmann, A.; Pan, H.,** Phase shifting in pulse tube refrigerators. *Cryogenics* (1999), *39* (6), 529-537.

38. **Richardson, R. N.,** Pulse tube refrigerator — an alternative cryocooler? *Cryogenics* (1986), *26* (6), 331-340.

39. **Ju, Y. L.,** Thermodynamic analysis of GM-type pulse tube coolers. *Cryogenics* (2001), *41* (7), 513-520.

40. **Kasuya, M.; Nakatsu, M.; Geng, Q.; Yuyama, J.; Goto, E.,** Work and heat flows in a pulse-tube refrigerator. *Cryogenics* (1991), *31* (9), 786-790.

41. **Maréchal, J.-C.; Pety, J.; Simon, Y.; David, M.,** Analytical comparison of different types of pulse tubes refrigerators. *Cryogenics* (1994), *34, Supplement 1* (0), 163-166.

42. **Smith, W. R.,** One-dimensional models for heat and mass transfer in pulse-tube refrigerators. *Cryogenics* (2001), *41* (8), 573-582.

43. **Liang, J.; Ravex, A.; Rolland, P.,** Study on pulse tube refrigeration Part 1: Thermodynamic nonsymmetry effect. *Cryogenics* (1996), *36* (2), 87-93.

44. **Liang, J.; Ravex, A.; Rolland, P.,** Study on pulse tube refrigeration Part 2: Theoretical modelling. *Cryogenics* (1996), *36* (2), 95-99.

45. **Liang, J.; Ravex, A.; Rolland, P.,** Study on pulse tube refrigeration Part 3: Experimental verification. *Cryogenics* (1996), *36* (2), 101-106.

46. **Kittel, P.; Kashani, A.; Lee, J. M.; Roach, P. R.,** General pulse tube theory. *Cryogenics* (1996), *36* (10), 849-857.

47. **de Waele, A. T. A. M.; Steijaert, P. P.; Gijzen, J.,** Thermodynamical aspects of pulse tubes. *Cryogenics* (1997), *37* (6), 313-324.

48. **de Waele, A. T. A. M.; Steijaert, P. P.; Koning, J. J.,** Thermodynamical aspects of pulse tubes II. *Cryogenics* (1998), *38* (3), 329-335.

49. **Olson, J. R.; Swift, G. W.,** Acoustic streaming in pulse tube refrigerators: tapered pulse tubes. *Cryogenics* (1997), *37* (12), 769-776.

50. **Zhu, S.; Chen, Z.,** Enthalpy flow rate of a pulse tube in pulse tube refrigerator. *Cryogenics* (1998), *38* (12), 1213-1216.

51. **Yang, L.; Yuan, Z.; Jingtao, L.; Wenxiu, Z.,** Analytical study of the performance of pulse tube refrigerator with symmetry-nozzle. *Cryogenics* (1999), *39* (9), 723-727.

52. **Baek, S. H.; Jeong, E. S.; Jeong, S.,** Two-dimensional model for tapered pulse tubes. Part 1: theoretical modeling and net enthalpy flow. *Cryogenics* (2000), *40* (6), 379-385.

53. **Baek, S. H.; Jeong, E. S.; Jeong, S.,** Two-dimensional model for tapered pulse tubes. Part 2: mass streaming and streaming-driven enthalpy flow loss. *Cryogenics* (2000), *40* (6), 387-392.

54. **Chan Park, H.; Soo Jeong, E.; Jeong, S.,** Two-dimensional model for tapered pulse tubes: Part 3: unsteady components of second-order mass flux and temperature. *Cryogenics* (2002), *42* (8), 485-493.

55. **Qiu, L. M.; Thummes, G.,** Valve timing effect on the cooling performance of a 4 K pulse tube cooler. *Cryogenics* (2002), *42* (5), 327-333.

56. **Will, M. E.; Tanaeva, I. A.; Li, R.; de Waele, A. T. A. M.,** New rotary valves for pulse-tube refrigerators. *Cryogenics* (2004), *44* (11), 793-800.

57. **Lu, G. Q.; Cheng, P.,** On cycle-averaged pressure in a G–M type pulse tube refrigerator. *Cryogenics* (2002), *42* (5), 287-293.

58. **de Boer, P. C. T.,** Maximum attainable performance of pulse tube refrigerators. *Cryogenics* (2002), *42* (2), 123-125.

59. **Yang, L. W.,** Experimental research of high frequency tapered pulse tube cooler. *Cryogenics* (2009), *49* (12), 738-741.

60. **Wu, P.; Zhu, S.** In *Mechanism and numerical analysis of orifice pulse tube refrigerator with a valve less compressor Cryogenica and Refrigeration*, Proc. Int. Conf., Cryogenica and Refrigeration (Year), 85-90.

61. **Lee, J. M.; Dill, H. R.,** The influences of gas velocity on surface heat pumping for the orifice pulse tube refrigerator. *Advances in cryogenic engineering* (1990), *35*, 1223-1229.

62. **de Boer, P. C. T.,** Pressure Heat Pumping in the Orifice Pulse-Tube Refrigerator. In *Advances in Cryogenic Engineering*, Kittel, P., Ed. Springer US (1996); Vol. 41, pp 1373-1382.

63. **de Boer, P. C. T.,** Heat removal in the orifice pulse-tube. *Cryogenics* (1998), *38* (3), 343-357.

64. **Richardson, R. N.,** Valved pulse tube refrigerator development. *Cryogenics* (1989), *29* (8), 850-853.

65. **Storch, P.; Radebaugh, R.,** Development and Experimental Test of an Analytical Model of the Orifice Pulse Tube Refrigerator. In *Advances in Cryogenic Engineering*, Fast, R. W., Ed. Springer US (1988); Vol. 33, pp 851-859.

66. **Razani, A.; Dodson, C.; Abhyankar, N. S.; Flake, B.,** A Model for Energy and Exergy Flow in an Orifice Pulse Tube Refrigerator. In *Cryocoolers 13*, Ross, R., Jr., Ed. Springer US (2005); pp 353-362.

67. **Godshalk, K. M.; Jin, C.; Kwong, Y. K.; Hershberg, E. L.; Swift, G. W.; Radebaugh, R.,** Characterization of 350 Hz Thermoacoustic Driven Orifice Pulse Tube Refrigerator with Measurements of the Phase of the Mass Flow and Pressure. In *Advances in Cryogenic Engineering*, Kittel, P., Ed. Springer US (1996); Vol. 41, pp 1411-1418.

68. **Zhang, X. B.; Qiu, L. M.; Gan, Z. H.; He, Y. L.,** Effects of reservoir volume on performance of pulse tube cooler. *International Journal of Refrigeration* (2007), *30* (1), 11-18.

69. **Wu, P. Y.; Zhang, L.; Qian, L. L.; Zhang, L.,** Numerical Modeling of Orifice Pulse Tube Refrigerator by Using the Method of Characteristics. In *Advances in Cryogenic Engineering*, Kittel, P., Ed. Springer US (1994); Vol. 39, pp 1417-1423.

70. **Rawlins, W.; Radebaugh, R.; Bradley, P. E.; Timmerhaus, K. D.,** Energy Flows in an Orifice Pulse Tube Refrigerator. In *Advances in Cryogenic Engineering*, Kittel, P., Ed. Springer US (1994); Vol. 39, pp 1449-1456.

71. **Wang, C.; Wu, P.; Chen, Z.,** Numerical modelling of an orifice pulse tube refrigerator. *Cryogenics* (1992), *32* (9), 785-790.

72. **Nika, P.,** Étude paramétrique comparée des performances des réfrigérateurs à tube à gaz pulsé classique et hybride. *International Journal of Thermal Sciences* (1999), *38* (2), 175-183.

73. **Wang, C.; Wu, P.; Chen, Z.,** Modified orifice pulse tube refrigerator without a reservoir. *Cryogenics* (1994), *34* (1), 31-36.

74. **Bauwens, L.,** Interface Loss in the Small Amplitude Orifice Pulse Tube Model. In *Advances in Cryogenic Engineering*, Kittel, P., Ed. Springer US (1998); Vol. 43, pp 1933-1940.

75. **Kittel, P.,** Ideal orifice pulse tube refrigerator performance. *Cryogenics* (1992), *32* (9), 843-844.

76. **David, M.; Maréchal, J. C.; Simon, Y.; Guilpin, C.,** Theory of ideal orifice pulse tube refrigerator. *Cryogenics* (1993), *33* (2), 154-161.

77. **Zhu, S. W.; Chen, Z. Q.,** Isothermal model of pulse tube refrigerator. *Cryogenics* (1994), *34* (7), 591-595.

78. **Roach, P.; Kashani, A.,** A Simple Modeling Program for Orifice Pulse Tube Coolers. In *Cryocoolers 9*, Ross, R. G., Jr., Ed. Springer US (1997); pp 327-334.

79. **Huang, B. J.; Chuang, M. D.,** System design of orifice pulse-tube refrigerator using linear flow network analysis. *Cryogenics* (1996), *36* (11), 889-902.

80. **Xu, M. Y.; He, Y. L.; Chen, Z. Q.,** Analysis of an orifice pulse tube refrigerator using the method of characteristics. *Cryogenics* (1999), *39* (9), 751-757.

81. **Kuriyama, F.; Radebaugh, R.,** Analysis of mass and energy flow rates in an orifice pulse-tube refrigerator. *Cryogenics* (1999), *39* (1), 85-92.

82. **de Boer, P. C. T.,** Optimization of the orifice pulse tube. *Cryogenics* (2000), *40* (11), 701-711.

83. **Zhang, X. B.; Qiu, L. M.; Gan, Z. H.; He, Y. L.,** CFD study of a simple orifice pulse tube cooler. *Cryogenics* (2007), *47* (5–6), 315-321.

84. **Antao, D. S.; Farouk, B.,** Computational fluid dynamics simulations of an orifice type pulse tube refrigerator: Effects of operating frequency. *Cryogenics* (2011), *51* (4), 192-201.

85. **Antao, D. S.; Farouk, B.,** Numerical simulations of transport processes in a pulse tube cryocooler: Effects of taper angle. *International Journal of Heat and Mass Transfer* (2011), *54* (21–22), 4611-4620.

86. **Neveu, P.; Babo, C.,** A simplified model for pulse tube refrigeration. *Cryogenics* (2000), *40* (3), 191-201.

87. **He, Y. L.; Tao, Y. B.; Gao, F.,** A new computational model for entire pulse tube refrigerators: Model description and numerical validation. *Cryogenics* (2009), *49* (2), 84-93.

88. **Jahanbakhshi, R.; Saidi, M. H.; Ghahremani, A. R.,** Numerical modeling of pulse tube refrigerator and sensitivity analysis of simulation. *HVAC&R Research* (2013), *19* (3), 242-256.

89. **Antao, D. S.; Farouk, B.,** Experimental and numerical investigations of an orifice type cryogenic pulse tube refrigerator. *Applied Thermal Engineering* (2013), *50* (1), 112-123.

90. **Farouk, B.; Antao, D. S.,** Numerical analysis of an OPTR: Optimization for space applications. *Cryogenics* (2012), *52* (4–6), 196-204.

91. **Gu, C.; Zhou, Y.; Wang, J.; Ji, W.; Zhou, Q.,** CFD analysis of nonlinear processes in pulse tube refrigerators: Streaming induced by vortices. *International Journal of Heat and Mass Transfer* (2012), *55* (25–26), 7410-7418.

92. **Arablu, M.; Jafarian, A.; Deylami, P.,** Numerical simulation of a two-stage pulse tube cryocooler considering influence of abrupt expansion/contraction joints. *Cryogenics* (2013), *57* (0), 150-157.

93. **Huang, T.; Caughley, A.,** Comparison of sage and CFD models of a diaphragm pressure wave generator. *AIP Conference Proceedings* (2012), *1434* (1), 1217-1225.

94. **Boroujerdi, A. A.; Ashrafizadeh, A.; Mousavi Naeenian, S. M.,** Numerical analysis of stirling type pulse tube cryocoolers. *Cryogenics* (2011), *51* (9), 521-529.

95. **Ashwin, T. R.; Narasimham, G. S. V. L.; Jacob, S.,** CFD analysis of high frequency miniature pulse tube refrigerators for space applications with thermal non-equilibrium model. *Applied Thermal Engineering* (2010), *30* (2–3), 152-166.

96. **Dietrich, M.; Thummes, G.,** Two-stage high frequency pulse tube cooler for refrigeration at 25 K. *Cryogenics* (2010), *50* (4), 281-286.

97. **Banjare, Y. P.; Sahoo, R. K.; Sarangi, S. K.,** CFD simulation and experimental validation of a GM type double inlet pulse tube refrigerator. *Cryogenics* (2010), *50* (4), 271-280.

98. **Zhang, X.-b.; Gan, Z.-h.; Qiu, L.-m.; Liu, H.-x.,** Computational fluid dynamic simulation of an inter-phasing pulse tube cooler. *J. Zhejiang Univ. Sci. A* (2008), *9* (1), 93-98.

99. **Paek, I.; Braun, J. E.; Mongeau, L.,** Evaluation of standing-wave thermoacoustic cycles for cooling applications. *International Journal of Refrigeration* (2007), *30* (6), 1059-1071.

100. **Cha, J. S.; Ghiaasiaan, S. M.; Desai, P. V.; Harvey, J. P.; Kirkconnell, C. S.,** Multi-dimensional flow effects in pulse tube refrigerators. *Cryogenics* (2006), *46* (9), 658-665.

101. **Dodson, C.; Razani, A.; Roberts, T.,** Numerical Simulation of Oscillating Fluid Flow in Inertance Tubes. *Cryocooler 15* (2009), 261-269.

102. **Cao, Q.; Gan, Z.; Liu, G.; Li, Z.; Wu, Y.; Qiu, L.** In *Theoretical and experiment study on a pulse tube cryocooler driven with a linear compressor*, Cryocooler, (Year), 149-156.

103. **Sobol, S.; Katz, Y. a.; Grossman G. ,** A Study of a Miniature In-Line Pulse Tube Cryocooler. *Cryocoolers 16* (2011), 87-95.

104. **Hofmann, A.,** Numeric Code for the Design of Pulse Tube Coolers. In *Cryocoolers 13*, Ross, R., Jr., Ed. Springer US (2005); pp 323-332.

105. **Mitchell, M. P.; Bauwens, L.,** Modeling Pulse Tube Coolers with the MS* 2 Stirling Cycle Code. In *Cryocoolers 10*, Springer (2002); pp 379-385.

106. **Roach, P. R.; Kashani, A.,** A Simple modeling program for orifice pulse tube coolers. In *Cryocoolers 9*, Springer (1997); pp 327-334.

107. **Liang, J.; Zhou, Y.; Zhu, W.,** Development of a single-stage pulse tube refrigerator capable of reaching 49 K. *Cryogenics* (1990), *30* (1), 49-51.

108. **Baks, M. J. A.; Hirschberg, A.; van der Ceelen, B. J.; Gijsman, H. M.,** Experimental verification of an analytical model for orifice pulse tube refrigeration. *Cryogenics* (1990), *30* (11), 947-951.

109. **Huang, B. J.; Yu, G. J.,** Experimental study on the design of orifice pulse tube refrigerator. *International Journal of Refrigeration* (2001), *24* (5), 400-408.

110. **Ishimura, M.; Bodegom, E.,** Experimental Results of a Single Stage Linear Orifice Pulse Tube Refrigerator. In *Advances in Cryogenic Engineering*, Kittel, P., Ed. Springer US (1998); Vol. 43, pp 1965-1972.

111. **Kral, S.; Hill, D.; Restivo, J.; Johnson, J.; Curwen, P.; Waldron, W.; Jones, H.,** Test Results of an Orifice Pulse Tube Refrigerator. In *Advances in*

Cryogenic Engineering, Fast, R. W., Ed. Springer US (1991); Vol. 37, pp 931-937.

112. **Zhu, S.; Kakimi, Y.; Matsubara, Y.,** Waiting time effect of a GM type orifice pulse tube refrigerator. *Cryogenics* (1998), *38* (6), 619-624.

113. **Watanabe, A.; Swift, G. W.; Brisson, J. G.,** Superfluid Orifice Pulse Tube Refrigerator below 1 Kelvin. In *Advances in Cryogenic Engineering*, Kittel, P., Ed. Springer US (1996); Vol. 41, pp 1519-1526.

114. **Huang, B. J.; Sun, B. W.,** A pulse-tube refrigerator using variable-resistance orifice. *Cryogenics* (2003), *43* (1), 59-65.

115. **Kasuya, M.; Yuyama, J.; Geng, Q.; Goto, E.,** Optimum phase angle between pressure and gas displacement oscillations in a pulse-tube refrigerator. *Cryogenics* (1992), *32* (3), 303-308.

116. **Ying-wen, L.; Ya-ling, H.,** A new tapered regenerator used for pulse tube refrigerator and its optimization. *Cryogenics* (2008), *48* (11–12), 483-491.

117. **Ju, Y. L.; Wang, C.; Zhou, Y.,** Numerical simulation and experimental verification of the oscillating flow in pulse tube refrigerator. *Cryogenics* (1998), *38* (2), 169-176.

118. **Wang, C.; Wu, P. Y.; Chen, Z. Q.,** Numerical analysis of double-inlet pulse tube refrigerator. *Cryogenics* (1993), *33* (5), 526-530.

119. **Mirels, H.,** Double Inlet Pulse Tube Cryocooler with Stepped Piston Compressor. In *Advances in Cryogenic Engineering*, Kittel, P., Ed. Springer US (1994); Vol. 39, pp 1425-1431.

120. **Iskandar, M.; Tiow, D.,** Pulse tube refrigerator.

121. **Nika, P.; Bailly, Y.,** Comparison of two models of a double inlet miniature pulse tube refrigerator: Part A thermodynamics. *Cryogenics* (2002), *42* (10), 593-603.

122. **Bailly, Y.; Nika, P.,** Comparison of two models of a double inlet miniature pulse tube refrigerator: Part B electrical analogy. *Cryogenics* (2002), *42* (10), 605-615.

123. **Xiao, J. H.; Yang, J. H.; Tao, Z. D.,** Miniature Double-Inlet Pulse Tube Cryocooler: Design by Thermoacoustic Theory Compared with Preliminary Experimental Results. In *Advances in Cryogenic Engineering*, Kittel, P., Ed. Springer US (1996); Vol. 41, pp 1435-1441.

124. **He, Y.-L.; Huang, J.; Zhao, C.-F.; Liu, Y.-W.,** First and second law analysis of pulse tube refrigerator. *Applied Thermal Engineering* (2006), *26* (17–18), 2301-2307.

125. **de Boer, P. C. T.,** Characteristics of the double inlet pulse tube. *Cryogenics* (2003), *43* (7), 379-391.

126. **Chokhawala, M.; Desai, K.; Naik, H.; Naryankhedkar, K.,** Phasor analysis for double inlet pulse tube cryocooler. *Advances in cryogenic engineering* (2000), *45* (A), 159-166.

127. **Banjare, Y. P.; Sahoo, R. K.; Sarangi, S. K.,** CFD simulation of a Gifford–McMahon type pulse tube refrigerator. *International Journal of Thermal Sciences* (2009), *48* (12), 2280-2287.

128. **Ju, Y. L.; Wang, L.; Zhou, Y.,** DYNAMIC SIMULATION OF THE OSCILLATING FLOW WITH POROUS MEDIA IN A PULSE TUBE CRYOCOOLER. *Numerical Heat Transfer, Part A: Applications* (1998), *33* (7), 763-777.

129. **Dash, G. K. A.; Nandi, T. K.; Das, P. K.,** Exergy destruction in the double inlet pulse tube cryocooler (DIPTC): A parametric study. *International Journal of Energy Research* (2009), *33* (14), 1290-1308.

130. **Wang, C.; Wu, P. Y.; Chen, Z. Q.,** Theoretical and experimental studies of a double-inlet reversible pulse tube refrigerator. *Cryogenics* (1993), *33* (6), 648-652.

131. **Cai, J. H.; Zhou, Y.; Wang, J. J.; Zhu, W. X.,** Experimental analysis of double-inlet principle in pulse tube refrigerators. *Cryogenics* (1993), *33* (5), 522-525.

132. **Gan, Z. H.; Chen, G. B.; Thummes, G.; Heiden, C.,** Experimental study on pulse tube refrigeration with helium and nitrogen mixtures. *Cryogenics* (2000), *40* (4–5), 333-339.

133. **Zhou, B.; Wu, P.; Hu, S.; Chen, G.,** Experimental results of the internal process of a double inlet pulse tube refrigerator. *Cryogenics* (1992), *32, Supplement 1* (0), 24-27.

134. **Tanaka, M.; Kawamatsu, S.; Kodama, T.; Nishitani, T.; Kawaguchi, E.; Yanai, M.,** Behavior of the gas temperature and pressure in the pulse tube refrigerator. *Cryogenics* (1992), *32, Supplement 1* (0), 32-35.

135. **Ravex, A.; Rolland, P.; Liang, J.,** Experimental study and modelisation of a pulse tube refrigerator. *Cryogenics* (1992), *32, Supplement 1* (0), 9-12.

136. **Charles, I.; Duband, L.; Ravex, A.,** Permanent flow in low and high frequency pulse tube coolers – experimental results. *Cryogenics* (1999), *39* (9), 777-782.

137. **Gardner, D. L.; Swift, G. W.,** Use of inertance in orifice pulse tube refrigerators. *Cryogenics* (1997), *37* (2), 117-121.

138. **de Boer, P. C. T.,** Performance of the inertance pulse tube. *Cryogenics* (2002), *42* (3–4), 209-221.

139. **Chen, L.; Zhang, Y.; Luo, E.; Li, T.; Wei, X.,** CFD analysis of thermodynamic cycles in a pulse tube refrigerator. *Cryogenics* (2010), *50* (11–12), 743-749.

140. **Zhu, S.; Matsubara, Y.,** Numerical method of inertance tube pulse tube refrigerator. *Cryogenics* (2004), *44* (9), 649-660.

141. **Kirkconnell, C. S.; Colwell, G. T.,** Parametric Studies on a Numerical, Nonlinear Pulse Tube Flow. *Journal of Fluids Engineering* (1997), *119* (4), 831-837.

142. **Chen, N.; Yang, C. G.; Xu, L.; Xu, R. P.,** Analysis of inertance tube in the pulse tube refrigerator. *Proceedings of the Twentieth International Cryogenic Engineering Conference, Beijing, China* (2002).

143. **Dai, W.; Hu, J.; Luo, E.,** Comparison of two different ways of using inertance tube in a pulse tube cooler. *Cryogenics* (2006), *46* (4), 273-277.

144. **Cha, J. S.** CFD Simulation of Multi-Dimensional Effects in Inertance Tube Pulse Tube Cryocoolers. Georgia Institute of Technology, Atlanta, Ga, (2004).

145. **Luo, E.; Radebaugh, R.; Dai, W.; Lewis, M.; Wu, Z.; Zhang, Y.,** Thermoacoustic turbulent-flow model for inertance tubes used for pulse tube refrigerators. *Proceedings of ICEC* (2005), *20*, 383-386.

146. **Ko, J.; Jeong, S.; Ki, T.,** Effect of pulse tube volume on dynamics of linear compressor and cooling performance in Stirling-type pulse tube refrigerator. *Cryogenics* (2010), *50* (1), 1-7.

147. **Ju, Y. L.; He, G. Q.; Hou, Y. K.; Liang, J. T.; Zhou, Y.,** Experimental measurements of the flow resistance and inductance of inertance tubes at high acoustic amplitudes. *Cryogenics* (2003), *43* (1), 1-7.

148. **Park, S. J.; Koh, D. Y.; Hong, Y. J.; Kim, H. B.; Kim, S. Y.; Jung, W. S.,** A study on the in-line type inertance tube pulse tube cryocooler. *Proceedings of the Twentieth International Cryogenic Engineering Conference, Beijing, China* (2004).

149. **Ashwin, T. R.** CFD Studies of Pulse Tube Refrigerators. Indian Institute of Science Bangalore - 560 012, (2010).

150. **Xu, M.; He, Y.; Wu, P.; Chen, Z.,** Experimental research of a miniature coaxial pulse tube refrigerator using nylon tube. *Cryogenics* (1996), *36* (2), 131-133.

151. **Dang, H.,** High-capacity 60 K single-stage coaxial pulse tube cryocoolers. *Cryogenics* (2012), *52* (4–6), 205-211.

152. **Haruyama, T.; Kasami, K.; Inoue, H.; Mihara, S.; Matsubara, Y.,** Development of a High-Power Coaxial Pulse Tube Refrigerator for a Liquid Xenon Calorimeter. *AIP Conference Proceedings* (2004), *710* (1), 1459-1466.

153. **Richardson, R. N.,** Development of a practical pulse tube refrigerator: co-axial designs and the influence of viscosity. *Cryogenics* (1988), *28* (8), 516-520.

154. **Wang, J.; Zhou, Y.; Zhu, W.; Cai, J.,** Development of a liquid nitrogen precooled co-axial pulse tube refrigerator. *Cryogenics* (1993), *33* (4), 463-465.

155. **Liang, J.; Zhou, Y.; Zhu, W.; Sun, W.; Yang, J.; Li, S.,** Study on miniature pulse tube cryocooler for space application. *Cryogenics* (2000), *40* (3), 229-233.

156. **Ding, W.; Huang, P.; He, Y.; Liu, Y.; Tao, W.,** Factors influencing the lowest refrigerating temperature of the miniature co-axial pulse tube refrigerator. *Heat Transfer—Asian Research* (2005), *34* (4), 219-225.

157. **Tanaka, M.; Kodama, T.; Nishitani, T.; Araki, T.; Kawaguchi, E.; Yanai, M.,** Two stage pulse tube refrigerator with double rotary valves. *Cryogenics* (1994), *34, Supplement 1* (0), 159-162.

158. **Matsubara, Y.; Gao, J.,** Multi-staged pulse tube refrigerator for superconducting magnet applications. *Cryogenics* (1994), *34, Supplement 1* (0), 155-158.

159. **Gao, J. L.; Matsubara, Y.,** Experimental investigation of 4 K pulse tube refrigerator. *Cryogenics* (1994), *34* (1), 25-30.

160. **Matsubara, Y.; Gao, J. L.,** Novel configuration of three-stage pulse tube refrigerator for temperatures below 4 K. *Cryogenics* (1994), *34* (4), 259-262.

161. **Tanida, K.; Gao, J. L.; Yoshimura, N.; Matsubara, Y.,** Three-Staged Pulse Tube Refrigerator Controlled by Four-Valve Method. In *Advances in Cryogenic Engineering*, Kittel, P., Ed. Springer US (1996); Vol. 41, pp 1503-1509.

162. **Narayankhedkar, K. G.; Gawali, B. S.,** Design and Development of an Orifice/Inertance Pulse Tube Cryocooler Using a Linear Compressor. *AIP Conference Proceedings* (2004), *710* (1), 1380-1387.

163. **Wang, C.; Ju, Y. L.; Zhou, Y.,** The experimental investigation of a two-stage pulse tube refrigerator. *Cryogenics* (1996), *36* (8), 605-609.

164. **Wang, C.; Thummes, G.; Heiden, C.,** A two-stage pulse tube cooler operating below 4 K. *Cryogenics* (1997), *37* (3), 159-164.

165. **Wang, C.; Thummes, G.; Heiden, C.,** Experimental study of staging method for two-stage pulse tube refrigerators for liquid 4He temperatures. *Cryogenics* (1997), *37* (12), 857-863.

166. **Thummes, G.; Bender, S.; Heiden, C.,** Approaching the 4He lambda line with a liquid nitrogen precooled two-stage pulse tube refrigerator. *Cryogenics* (1996), *36* (9), 709-711.

167. **Chen, G.; Qiu, L.; Zheng, J.; Yan, P.; Gan, Z.; Bai, X.; Huang, Z.,** Experimental study on a double-orifice two-stage pulse tube refrigerator. *Cryogenics* (1997), *37* (5), 271-273.

168. **Chen, G.; Zheng, J.; Qiu, L.; Bai, X.; Gan, Z.; Yan, P.; Yu, J.; Jin, T.; Huang, Z.,** Modification test of staged pulse tube refrigerator for temperatures below 4 K. *Cryogenics* (1997), *37* (9), 529-532.

169. **Wang, C.,** Numerical analysis of 4 K pulse tube coolers: Part I. Numerical simulation. *Cryogenics* (1997), *37* (4), 207-213.

170. **Wang, C.,** Numerical analysis of 4 K pulse tube coolers: Part II. Performances and internal processes. *Cryogenics* (1997), *37* (4), 215-220.

171. **Xu, M. Y.; De Waele, A. T. A. M.; Ju, Y. L.,** A pulse tube refrigerator below 2 K. *Cryogenics* (1999), *39* (10), 865-869.

172. **Atrey, M. D.; Bapat, S. L.; Heiden, C.,** Development of a computer model for three-stage, split type, free displacer Stirling cryocooler. *Cryogenics* (1994), *34* (9), 727-732.

173. **Ju, Y. L.,** Computational study of a 4 K two-stage pulse tube cooler with mixed Eulerian–Lagrangian method. *Cryogenics* (2001), *41* (1), 49-57.

174. **Wang, C.,** Helium liquefaction with a 4 K pulse tube cryocooler. *Cryogenics* (2001), *41* (7), 491-496.

175. **Qiu, L. M.; Numazawa, T.; Thummes, G.,** Performance improvement of a pulse tube cooler below 4 K by use of GdAlO3 regenerator material. *Cryogenics* (2001), *41* (9), 693-696.

176. **Tanaeva, I. A.; de Waele, A. T. A. M.,** A small helium-3 pulse-tube refrigerator. *Cryogenics* (2005), *45* (8), 578-584.

177. **Yan, P.-d.; Gao, W.-l.; Chen, G.-b.,** Development of a linear compressor for two-stage pulse tube cryocoolers. *J. Zhejiang Univ. Sci. A* (2009), *10* (11), 1595-1600.

178. **Yan, P.; Chen, G.; Dong, J.; Gao, W.,** 15 K two-stage Stirling-type pulse-tube cryocooler. *Cryogenics* (2009), *49* (2), 103-106.

179. **Sun, D. M.; Dietrich, M.; Thummes, G.,** High-power Stirling-type pulse tube cooler working below 30 K. *Cryogenics* (2009), *49* (9), 457-462.

180. **Cai, J. H.; Wang, J. J.; Zhu, W. X.; Zhou, Y.,** Experimental analysis of the multi-bypass principle in pulse tube refrigerators. *Cryogenics* (1994), *34* (9), 713-715.

181. **Wang, C.; Wang, S. Q.; Cai, J. H.; Yuan, Z.,** Experimental study of multi-bypass pulse-tube refrigerator. *Cryogenics* (1995), *35* (9), 555-558.

182. **Kaiser, G.; Brehm, H.; Thürk, M.; Seidel, P.,** Thermodynamic analysis of an ideal four-valve pulse tube refrigerator. *Cryogenics* (1996), *36* (7), 527-533.

183. **Liang, J.; Zhang, C.; Cai, J.; Luo, E.; Zhou, Y.; Xu, L.,** Pulse tube refrigerator with low temperature switching valve: concept and experiments. *Cryogenics* (1997), *37* (9), 497-503.

184. **Yuan, J.; Pfotenhauer, J. M.,** Thermodynamic analysis of active valve pulse tube refrigerators. *Cryogenics* (1999), *39* (4), 283-292.

185. **Luwei, Y.; Yuan, Z.; Jingtao, L.,** Research of pulse tube refrigerator with high and low temperature double-inlet. *Cryogenics* (1999), *39* (5), 417-423.

186. **Pan, H.; Hofmann, A.; Oellrich, L.,** Single-stage 4-valve and active buffer pulse tube refrigerators. *Cryogenics* (2001), *41* (4), 281-284.

187. **Brito, M. C.; Peskett, G. D.,** Experimental analysis of free warm expander pulse tube. *Cryogenics* (2001), *41* (10), 757-762.

188. **Qiu, L. M.; He, Y. L.; Gan, Z. H.; Chen, G. B.,** A single-stage pulse tube cooler reached 12.6 K. *Cryogenics* (2005), *45* (9), 641-643.

189. **Jafari, S.; Mohammadi, B.; Boroujerdi, A. A.,** Multi-objective optimization of a stirling-type pulse tube refrigerator. *Cryogenics* (2013), *55–56* (0), 53-62.

190. **de Waele, A. T. A. M.,** Optimization of pulse tubes. *Cryogenics* (1999), *39* (1), 13-15.

191. **Razani, A.; Roberts, T.; Flake, B.,** A thermodynamic model based on exergy flow for analysis and optimization of pulse tube refrigerators. *Cryogenics* (2007), *47* (3), 166-173.

192. **Ki, T.; Jeong, S.,** Design and analysis of compact work-recovery phase shifter for pulse tube refrigerator. *Cryogenics* (2012), *52* (2–3), 105-110.

193. **Jafarian, A.; Saidi, M. H.; Hannani, S. K.,** Second law based modeling to optimum design of high capacity pulse tube refrigerators. *International Journal of Refrigeration* (2009), *32* (1), 58-69.

194. **Ghahremani, A. R.; Saidi, M. H.; Jahanbakhshi, R.; Roshanghalb, F.,** Performance analysis and optimization of high capacity pulse tube refrigerator. *Cryogenics* (2011), *51* (4), 173-179.

195. **Myers, R.; Montgomery, D.,** Response surface methodology.USA:. *John Wiley & Sons* (1995).

196. **Fermoso, J.; Gil, M. V.; Arias, B.; Plaza, M. G.; Pevida, C.; Pis, J. J.; Rubiera, F.,** Application of response surface methodology to assess the combined effect of operating variables on high-pressure coal gasification for H2-rich gas production. *International Journal of Hydrogen Energy* (2010), *35* (3), 1191-1204.

197. **Chiang, K.-T.; Chou, C.-C.; Liu, N.-M.,** Application of response surface methodology in describing the thermal performances of a pin-fin heat sink. *International Journal of Thermal Sciences* (2009), *48* (6), 1196-1205.

198. **Chiang, K.-T.; Chang, F.-P.,** Application of response surface methodology in the parametric optimization of a pin-fin type heat sink. *International Communications in Heat and Mass Transfer* (2006), *33* (7), 836-845.

199. **Chiang, K.-T.,** Modeling and optimization of designing parameters for a parallel-plain fin heat sink with confined impinging jet using the response surface methodology. *Applied Thermal Engineering* (2007), *27* (14–15), 2473-2482.

200. **Sun, L.; Zhang, C.-L.,** Evaluation of elliptical finned-tube heat exchanger performance using CFD and response surface methodology. *International Journal of Thermal Sciences* (2014), *75* (0), 45-53.

201. **Kim, B. S.; Kwak, B. S.; Shin, S.; Lee, S.; Kim, K. M.; Jung, H.-I.; Cho, H. H.,** Optimization of microscale vortex generators in a microchannel using advanced response surface method. *International Journal of Heat and Mass Transfer* (2011), *54* (1–3), 118-125.

202. **Wang, G.; Zhao, G.; Li, H.; Guan, Y.,** Multi-objective optimization design of the heating/cooling channels of the steam-heating rapid thermal response mold using particle swarm optimization. *International Journal of Thermal Sciences* (2011), *50* (5), 790-802.

203. **Wang, G.; Zhao, G.; Li, H.; Guan, Y.,** Research on optimization design of the heating/cooling channels for rapid heat cycle molding based on response surface methodology and constrained particle swarm optimization. *Expert Systems with Applications* (2011), *38* (6), 6705-6719.

204. **Khalajzadeh, V.; Heidarinejad, G.; Srebric, J.,** Parameters optimization of a vertical ground heat exchanger based on response surface methodology. *Energy and Buildings* (2011), *43* (6), 1288-1294.

205. **Hariharan, N. M.; Sivashanmugam, P.; Kasthurirengan, S.,** Optimization of thermoacoustic refrigerator using response surface methodology. *Journal of Hydrodynamics, Ser. B* (2013), *25* (1), 72-82.

206. **Hariharan, N. M.; Sivashanmugam, P.; Kasthurirengan, S.,** Optimization of thermoacoustic primemover using response surface methodology. *HVAC&R Research* (2012), *18* (5), 890-903.

207. **Li, Z.; Grandhi, R. V.; Shivpuri, R.,** Optimum design of the heat-transfer coefficient during gas quenching using the response surface method. *International Journal of Machine Tools and Manufacture* (2002), *42* (5), 549-558.

208. **Kumar, J.; Bansal, A.,** Photocatalytic degradation in annular reactor: Modelization and optimization using computational fluid dynamics (CFD) and response surface methodology (RSM). *Journal of Environmental Chemical Engineering* (0).

209. *CEP Short term course"Cryocoolers –Theory, Design and Practice"* Dept. of Mech. Engg. IIT, Bombay, (19-22 February 2008).

210. **Schunk, L. O.; Nellis, G.; Pfotenhauer, J.,** Experimental investigation and modeling of inertance tubes. *Journal of fluids engineering* (2005), *127* (5), 1029-1037.

211. **Banjare, Y. P.** Theoretical and experimental studies on pulse tube refrigerator. (2009).

212. **Pfotenhauer, J. M.; Gan, Z. H.; Radebaugh, R.,** Approximate design method for single stage pulse tube refrigerators. *AIP Conference Proceedings* (2008), *985* (1), 1437-1444.

213. **Radebaugh, R.** *Foundations of Cryocoolers Short Course Notes, Cryogenic Society of America, Oak Park, IL,*; (June 13, 2006).

214. **Akhavan, R.; Kamm, R.; Shapiro, A.,** An investigation of transition to turbulence in bounded oscillatory Stokes flows Part 1. Experiments. *Journal of Fluid Mechanics* (1991), *225*, 395-422.

215. ANSYS Fluent User Guide, ANSYS Inc., USA, 2010.

216. **Koh, J. C. Y.; Fortini, A.,** Prediction of thermal conductivity and electrical resistivity of porous metallic materials. *International Journal of Heat and Mass Transfer* (1973), *16* (11), 2013-2022.

217. **Inc, F.,** GAMBIT 6.2 User's guide. Fluent, Inc: (2005).

218. **Versteeg, H.; Malalasekera, W.,** An Introduction to computational fluid dynamics. 1995. *Harlow: Pearson Education Limited* (1995).

219. **Patankar, S.,** *Numerical heat transfer and fluid flow*. CRC Press (1980),

220. **Mayers, R.; Montgomery, D.,** Response surface methodology, USA *USA:. John Wiley & Sons,* (1995).

221. **Jeff, W.; C.F., H.,** Optimum design of the heat-transfer coefficient during gas quenching using the response surface method. *John Wiley and Sons, New York* (2002).

222. **Montgomery, D. C.,** D.C. Design and Analysis of Experiments. . *John Wiley and Sons, Singapore* (2003).

223. **Mehrabi, M.; Sharifpur, M.; Meyer, J. P.,** Modelling and multi-objective optimisation of the convective heat transfer characteristics and pressure drop of low concentration TiO2–water nanofluids in the turbulent flow regime. *International Journal of Heat and Mass Transfer* (2013), *67* (0), 646-653.

224. **Shafaghat, R.; Hosseinalipour, S. M.; Nouri, N. M.; Lashgari, I.,** Shape optimization of two-dimensional cavitators in supercavitating flows, using NSGA II algorithm. *Applied Ocean Research* (2008), *30* (4), 305-310.

225. **Agarwal, A.; Gupta, S. K.,** Jumping gene adaptations of NSGA-II and their use in the multi-objective optimal design of shell and tube heat exchangers. *Chemical Engineering Research and Design* (2008), *86* (2), 123-139.

226. **Wang, J.; Wang, M.; Li, M.; Xia, J.; Dai, Y.,** Multi-objective optimization design of condenser in an organic Rankine cycle for low grade waste heat recovery using evolutionary algorithm. *International Communications in Heat and Mass Transfer* (2013), *45* (0), 47-54.

227. **Deb, K.; Pratap, A.; Agarwal, S.; Meyarivan, T.,** A fast and elitist multiobjective genetic algorithm: NSGA-II. *Evolutionary Computation, IEEE Transactions on* (2002), *6* (2), 182-197.

228. **Wang, Y. M.,** Using the method of maximizing deviations to make decision for multi-indices. *System Engineering Electronic* (1998), *20* (7), 24-26.

229. **Radebaugh, R.; Lewis, M.; Luo, E.; Pfotenhauer, J. M.; Nellis, G. F.; Schunk, L. A.,** Inertance Tube Optimization for Pulse Tube Refrigerators. *AIP Conference Proceedings* (2006), *823* (1), 59-67.

230. **Montgomery, D. C.,** Design and Analysis of Experiments. Wiley, New York (2003).

Curriculum Vitae

NAME : SACHINDRA KUMAR ROUT

E-mail : sachindra106@gmail.com

Permenant Address : Nuarampas
Hatadihi
Keonjhar-758083
Odisha,India

Education:

2015	Ph.D. Dissertation submitted, NIT Rourkela
2011	M.Tech., SOA Bhubaneswar
2009	B.Tech., Degree Engg. College B.I.E.T, Bhadrak

Personal Information:

Date of Birth	07-10-1988
Nationality	Indian

Publications

1. **Rout, S.K.**, Choudhury B.K., Sahoo, R.K. and Sarangi , S.K., "Numerical Study and Analysis of Inertance-Type Pulse Tube Refrigerator".**Wseas Trans on Heat Mass Transfer** (2014); Volume 9, p. 01–08.

2. **Rout, S.K.**, Choudhury B.K., Sahoo, R.K. and Sarangi, S.K., "Multi-objective parametric optimization of Inertance type pulse tube refrigerator using response surface methodology and non-dominated sorting genetic algorithm". **Cryogenics** (2014); Volume 62, p. 71-83.

3. **Rout, S.K.**, Mukare, R., Choudhury B.K., Sahoo, R.K. and Sarangi, S.K., CFD Simulation to Optimise Single Stage Pulse Tube Refrigerator Temperature Below 6oK. **Procedia Engineering**, (2012); Volume 38, p. 1524-1530.

4. **Rout, S.K.**, A.K. Gupta, Choudhury B.K., Sahoo, R.K. and Sarangi, S.K., Influence of Porosity on the Performance of a Pulse Tube Refrigerator: A CFD Study. **Procedia Engineering**, (2013); Volume 51:, p. 609-616.

5. **Rout, S.K**., R. Mukare, Sahoo, R.K. and Sarangi, S.K.,, A thermally non-equilibrium approach for CFD simulation of a pulse tube refrigerator. ***International Conference on Engineering Technology and Management***, 7-8, September 2012, Tirupati, India: p. 21-25.

6. **Rout, S.K.**,A.K. Gupta, Sahoo, R.K. and Sarangi , S.K., Application of FUZZY logic for optimization in pulse tube cryocooler, ***Proceedings of the 24th National Symposium on Cryogenics***, January 22-24, 2013., IPR, Ahmedabad, India.

7. Gupta, A.K., **Rout, S.K**., R.K. Sahoo, S.K. Sarangi, Losses due to ineffectiveness of regenerator in a pulse tube refrigerator. ***An International Conference on Applications of Fluid Engineering*** September 20-22, 2012 Greater Noida, India.

8. **Rout, S.K**., Sahoo, R.K. and Sarangi, S.K., "Numerical analysis of a modified type pulse tube refrigerator". ***NUICONE-2013*** 28 - 30 November, 2013 - Organized by Institute of Technology Nirma University, Ahmedabad.

9. **Rout, S.K**., R.K. Sahoo, S.K. Sarangi, "Modelling and optimization of designing parameters for orifice pulse tube refrigerator using the response surface methodology" **Proceedings of the 25th National Symposium on Cryogenics**, December 8-10, 2014, Hyderabad, India.

Communicated

1. **Rout, S.K.**, Sahoo, R.K. and Sarangi, S.K., **"**Research on optimal design of orifice pulse tube refrigerator based on response surface and genetic algorithm**". (Under Review HVAC&R Research)**

APPENDIX 1

Genetic algorithms

Genetic algorithms have been successfully applied to various optimization problems. It is essentially a searching method based on the Darwinian principles of biological evolution. Genetic algorithm is a stochastic optimization algorithm which employs a population of chromosomes, each of them represents a possible solution. By applying genetic operators, each successive incremental improvement in a chromosome becomes the basis for the next generation. The process continues until the desired number of generations has been completed or the pre-defined fitness value has been reached.

The genetic algorithms differ from other methods of search and optimization in a number of ways. (a) Genetic algorithms search from a population of possible solutions instead of a single one. (b) The fitness or cost function used to resolve the redundancy has no requirement for continuity in the derivatives, so virtually "any" fitness function can be selected for optimizing. (c) Genetic algorithms use random operators throughout the process including reproduction, crossover, and mutation. (d) Genetic algorithms are blind since no specified information about the intended problem is needed to obtain the final solution. Basically, a genetic algorithm is a randomized search technique to simulate the nature evolution. It operates on a finite population of chromosomes. The chromosome is formed from genes. The fundamental characteristics of the chromosome are the values and the positions of the genes. Each chromosome has its own fitness measure based on the value and position. The new offspring of chromosomes is provided through genetic operations, i.e. selection, crossover and mutation, which provide a powerful global search mechanism. Typically binary coding is used in classic genetic algorithm, where each solution is encoded as a chromosome of binary digits. Each member of the population represents an encoded solution in the classic genetic algorithm. For many problems, this kind of coding is not nature. Generally, a genetic algorithm consists of the following steps that are repeated until the optimum solution is found.

(1) Initialization means the creation of the initial population. Many adaptive search methods work from point to point, using local information to decide which point to explore next. By contrast, the genetic algorithms use a set of population which consist many points to start the search simultaneously. The initial population is generated randomly and the population size is kept constant throughout the process.

(2) Evaluation of the fitness functions of chromosomes in the population. The fitness function is in most cases the objective function that should be maximized (or minimized) in the optimization problems. The fitness function is defined as the sum of squared differences between the randomly generated guess values and the exact solutions.

(3) Selection is the survival of the fittest within the genetic algorithm and it is based on the fitness functions of chromosomes to produce a new pool of population for the subsequent genetic operations. There are many ways to achieve effective selection. One of them is proportionate selection with ranking. The fitness function is normalized with the average value, so the chromosomes with above average fitness will be kept for the next steps. That is at each generation relatively good chromosomes are reproduced, the relatively bad chromosomes die out. This step directs the search towards the best.

(4) Crossover is a mating operator to allow production of new offspring through combination of parts of chromosomes with the purpose of constructing a better solution. The simplest way is called the one-point crossover. It is done by choosing randomly a pair of the chromosomes and swapping parts of these chromosomes to form a new pair of chromosomes.

(5) Mutation is the occasional (with small probability) random alteration of the genes of chromosome. The mutation operator arbitrarily alters one or more genes of a selected chromosome, which increase the variability of the population and against the loss of important genetic genes at a particular position. Each bit position of each chromosome in the new population undergoes a random change with equal probability.

After mutation, the offspring are including into the pool of population to repeat the process.

The computational procedure of a genetic algorithm is as follows:

Step 1. Generate at random an initial population of chromosomes.

Step 2. Evaluate the fitness of each chromosome in the population.

Step 3. Select the best chromosomes, based on the fitness function, for reproduction.

Step 4. Choose at random pairs of chromosomes for mating. Exchange bit genes with crossover to create new pairs of chromosomes.

Step 5. Process the new chromosomes by the mutation operator. Put the resulting chromosomes into the population.

Step 6. Repeat Step 2 to Step 5, until the fitness function is convergent or less than a predefined value (here 1000).

- To solve an equation in Genetic algorithm, first we have to generate chromosomes and population
- Gene – a single encoding of part of the solution space, i.e. either single bits or short blocks of adjacent bits that encode an element of the candidate solution

- Chromosomes mean a string of genes that represent solution.

- String of genes means number of variables in an equation. (eg. In equation 5.2 there are 4 variables so the chromosome size is 4.
- It is generated randomly within the range of variable.
- Initially we set a number of chromosomes which is known as population.

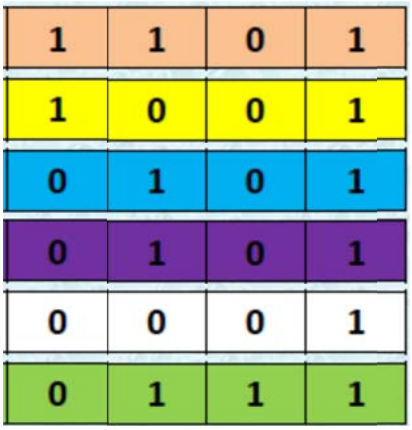

- Generally the population size 10, 20, 30, 40, or 50.. depending upon user and it is called initialize population.

- Satisfy conditions gen>1000. It is the stop criteria chosen for present case. GA runs for minimum 1000 generation.

Selection

Crossover

Choose a random point

•Split parents at this crossover point

•Create children by exchanging tails

•Probability of crossover is typically in range (0.6, 0.9)

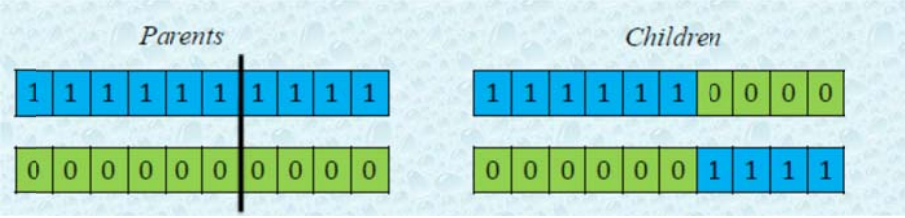

Mutation

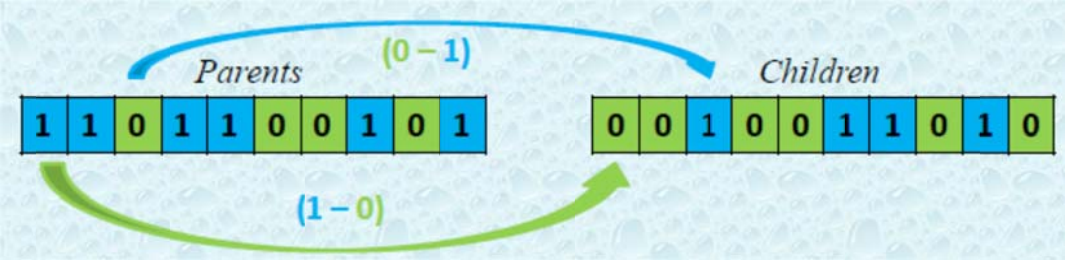

APPENDIX 2

DESIGN OF EXPERIMENTS

In many engineering problems there are more than one variable are related, and it is of attention to model and explore this relationship.

In general, suppose that there is a single dependent variable or response y that depends on 'k' independent or regressor variables, for example, x_1, x_2,. .., x_k. The relationship between these variables is characterized by a mathematical model called a regression model. The regression model is fit to a set of sample data. In some instances, the investigator knows the exact form of the true functional relationship between y and x_1, x_2,..., x, say $y = Ø(x_1, x_2,.. ., x_j)$. However, in most cases, the true functional relationship is unknown, and the investigator chooses an appropriate function to approximate. Low-order polynomial models are widely used as approximating functions [230].

LINEAR REGRESSION MODELS

The focus is here to fitting linear regression models. To illustrate, suppose an empirical model relating the viscosity of a polymer to the temperature and the catalyst feed rate. A model that might describe this relationship is

$$y = \beta_0 + \beta_1 x_1 + \beta_2 x_2 + \varepsilon \qquad \text{A2-1}$$

where y represents the viscosity, x_1 represents the temperature, and x_2 represents the catalyst feed rate. This is a multiple linear regression model with two independent variables. This is generally called the independent variables predictor variables or regressors.

The term linear is used because Equation A2.1 is a linear function of the unknown parameters β_0, β_1, and β_2. The model describes a plane in the two-dimensional x_1, x_2 space. The parameter β_0 defines the intercept of the plane. β_1, and β_2 are the partial regression coefficients, because β_1 measures the expected change in y per unit change in x_1 when x_2 is held constant, and β_2 measures the expected change in y per unit change in x_2 when x_1 is held constant. In general, the response variable y may be related to k regressor variables.

$$y = \beta_0 + \beta_1 x_1 + \beta_2 x_2 + ... + \beta_k x_k + \varepsilon \qquad \text{A2-2}$$

The model is called a multiple linear regression model with k regressor variables. The parameters β_j, j= 0, 1,... , k, are called the regression coefficients. This model describes a hyper plane in the k-dimensional space of the regressor variables $\{x_j\}$. The parameter β_j represents the expected changes in response Y per unit change in x_j when all the remaining independent variables $x_i (i \neq j)$ are kept constant.

For the second-order response surface model in two variables:

$$y = \beta_0 + \beta_1 x_1 + \beta_2 x_2 + \beta_{11} x_1^2 + \beta_{22} x_2^2 .... + \beta_{12} x_1 x_2 + \varepsilon \qquad \text{A2-3}$$

If we let $x_3=x_1^2, x_4=x_2^2, x_5=x_1x_2, \beta_3=\beta_{11}, \beta_4=\beta_{22}$ and $\beta_5=\beta_{12}$ then this becomes

$$y = \beta_0 + \beta_1 x_1 + \beta_2 x_2 + \beta_3 x_3 + \beta_4 x_4 + \beta_5 x_5 + \varepsilon \qquad \text{A2-4}$$

which is a linear regression model. In general, any regression model that is linear in the parameters (the β values) is a linear regression model, regardless of the shape of the response surface that it generates. Methods for estimating the parameters in multiple linear regression models is often called model fitting.

The method of least squares is typically used to estimate the regression coefficients in a multiple linear regression model. Suppose that n > k observations on the response variable are available, say y_1, y_2, y_3. . y_n. Along with each observed response y, we will have an observation on each regressor variable and let X_{ij} denote the i^{th} observation or level of variable x_i. The data will appear as in Table A2 1.

The model equation (EquationA2.2) in terms of the observation in Table 1 as

$$\begin{aligned} y_i &= \beta_0 + \beta_1 x_{i1} + \beta_2 x_{i2} .....{}_4 + \beta_k x_{ik} + \varepsilon_i \\ &= \beta_0 + \sum_{j=1}^{k} x_{ij} + \varepsilon_i \quad \text{i=1,2,....,n} \end{aligned} \qquad \text{A2-5}$$

Table A2 1 Data for Multiple Linear Regression

y	x_1	x_2	$\cdots$	x_k
y_1	x_{11}	x_{12}	$\cdots$	x_{1k}
y_2	x_{21}	x_{22}	$\cdots$	x_{2k}
$\vdots$	$\vdots$	$\vdots$		$\vdots$
y_n	x_{n1}	x_{n2}	$\cdots$	x_{nk}

The method of least squares chooses the β's in Equation A2.5 so that the sum of the squares of the errors, ε is minimized. The least squares function is

$$L = \beta_0 + \sum_{i=1}^{n} \varepsilon_i^2 = \sum_{i=1}^{n} \left(y_i - \beta_0 - \sum_{j=1}^{k} \beta_j x_{ij} \right)^2 \qquad \text{A2-6}$$

Th function L is to be minimized with respect to β_0 β_1**.....,** β_k. The least squares estimators, say $\hat{\beta}_0, \hat{\beta}_1, ..., \hat{\beta}_k$, must satisfy

$$\left.\frac{\partial L}{\partial \beta_0}\right|_{\hat{\beta}_0, \hat{\beta}_1, ..., \hat{\beta}_k} = 0 \quad \text{and} \quad \left.\frac{\partial L}{\partial \beta_j}\right|_{\hat{\beta}_0, \hat{\beta}_1, ..., \hat{\beta}_k} = 0 \qquad j = 1, 2, 3....., k \qquad \text{A2-7}$$

These equations are called the least squares normal equations. Note that there are p = k + 1 normal equations, one for each of the unknown regression coefficients. The solution to the normal equations will be the least squares estimators of the regression coefficients

$\hat{\beta}_0, \hat{\beta}_1, ..., \hat{\beta}_k$.

It is simpler to solve the normal equations if they are expressed in matrix notation. Generating a matrix development of the normal equations that parallels the development of Equation A2.7. The model in terms of the observations, Equation A2.5, as

$$y = x\beta + \varepsilon \qquad \text{A2-8}$$

$$\mathbf{y} = \begin{bmatrix} y_1 \\ y_2 \\ \vdots \\ y_n \end{bmatrix}, \qquad \mathbf{X} = \begin{bmatrix} 1 & x_{11} & x_{12} & \cdots & x_{1k} \\ 1 & x_{21} & x_{22} & \cdots & x_{2k} \\ \vdots & \vdots & \vdots & & \vdots \\ 1 & x_{n1} & x_{n2} & \cdots & x_{nk} \end{bmatrix}$$

$$\boldsymbol{\beta} = \begin{bmatrix} \beta_0 \\ \beta_1 \\ \vdots \\ \beta_k \end{bmatrix} \quad \text{and} \quad \boldsymbol{\epsilon} = \begin{bmatrix} \epsilon_1 \\ \epsilon_2 \\ \vdots \\ \epsilon_n \end{bmatrix}$$

In general, y is an (n × 1) vector of the observations, where n=number of observations, X = a design matrix (n × p) in canonical form of the variables, β = (p × 1) vector of the regression coefficients, and ε = an (n × 1) vector of random errors.

The least squares estimator of β is

$$\hat{\beta} = \left(X'X\right)^{-1}X'y \qquad \text{A2-9}$$

$$\begin{bmatrix} n & \sum_{i=1}^{n} x_{i1} & \sum_{i=1}^{n} x_{i2} & \cdots & \sum_{i=1}^{n} x_{ik} \\ \sum_{i=1}^{n} x_{i1} & \sum_{i=1}^{n} x_{i1}^2 & \sum_{i=1}^{n} x_{i1}x_{i2} & \cdots & \sum_{i=1}^{n} x_{i1}x_{ik} \\ \vdots & \vdots & \vdots & & \vdots \\ \sum_{i=1}^{n} x_{ik} & \sum_{i=1}^{n} x_{ik}x_{i1} & \sum_{i=1}^{n} x_{ik}x_{i2} & \cdots & \sum_{i=1}^{n} x_{ik}^2 \end{bmatrix} \begin{bmatrix} \hat{\beta}_0 \\ \hat{\beta}_1 \\ \vdots \\ \hat{\beta}_k \end{bmatrix} = \begin{bmatrix} \sum_{i=1}^{n} y_i \\ \sum_{i=1}^{n} x_{i1}y_i \\ \vdots \\ \sum_{i=1}^{n} x_{ik}y_i \end{bmatrix}$$

Design matrix X: The design matrix has n rows and several blocks of columns, corresponding to the terms in the model. The fitted regression model is

$$\hat{y} = X\hat{\beta} \qquad \text{A2-10}$$

In scalar notation, the fitted model is

$$\hat{y}_i = \hat{\beta}_0 + \sum_{j=1}^{k} \hat{\beta}_j x_{ij} \qquad \text{i=1,2,.....,n} \qquad \text{A2-11}$$

The difference between the actual observation y_i and corresponding fitted value $\hat{y}_i$ is the residual; say $e_i = y_i - \hat{y}_i$.

Standardized or studentized residuals: z_i: The residual e_i scaled by its standard deviation. The observations having more than ±2 standardized residual are identified as outliers with 95% confidence. The formula is:

$$z_i = \frac{e_i}{\sqrt{\left[MSE\left(1 - h_i\right)\right]}}$$

where MSE = mean square error and h_i = leverage. The denominator is an estimator of the standard deviation of e_i.

Standard error of fitted value (SE fit): The estimated standard deviation of the fitted value at a given predictor point $X'_0 = [1, x_{1,0}, \ldots, x_{m,0}]$ is given formula as

$$\sqrt{s^2\left[X_O^{'}\left(X'X\right)^{-1}X_0\right]}$$

where s^2 = MS Error.

Confidence interval: The range in which the estimated mean response for a given set of predictor values is expected to fall. The interval is defined by lower and upper limits, which is calculated from the confidence level and the standard error of the fits. The formula is:

$$\hat{y}_0 \pm t\left(1 - \alpha / 2; n - p\right) \times s\left(\hat{y}_0\right)$$

where α = chosen risk value, n = number of observations, p = number of predictors, and

$$s\left(\hat{y}_0\right) = \sqrt{s^2\left[X_O^{'}\left(X'X\right)^{-1}X_0\right]}$$

where s^2 = mean square error.

Leverages: This statistic indicate whether an observation has unusual predictor values compared to the rest of the data. An observation with large leverage value will exert significant influence on the fitted value as well as on the regression model.

The leverage of the i^{th} observation, h_i is the i^{th} diagonal element of the hat matrix **H**, which is a (n × n) projection matrix specified as: $H = X(X'X)^{-1}X'$.

Its value falls between 0 and 1 and the observations with considerable large leverage should be examined.

Estimating σ^2

It is also usually necessary to estimate σ^2. To develop an estimator of this parameter, consider the sum of squares of the residuals, say

$$SS_E = \sum_{i=1}^{n}(y_i - \hat{y}_i)^2 = \sum_{i=1}^{n} e_i^2 = e'e \qquad \text{A2-12}$$

$$SS_E = y'y - \hat{\beta}'X'y \qquad \text{A2-13}$$

Equation A2.13 is called the error or residual sum of squares, and it has n-p degrees of freedom associated with it.

So an unbiased estimator of σ^2 is given by

$$\sigma^2 = \frac{SS_E}{n-p} \qquad \text{A2-14}$$

Regression model fitting is almost always done using a statistical software packages. We used *Design-Expert® version 7*.1 software packages for present investigation.

The Box-Behnken Design

Box and Behnken have proposed some three-level designs for fitting response surfaces. These designs are formed by combining 2^k factorials with incomplete block designs. The resulting designs are usually very efficient in terms of the number of required runs, and they are either rotatable or nearly rotatable.

The Box—Behnken design is shown geometrically in Figure A2 1. Notice that the Box—Behnken design is a spherical design, with all points lying on a sphere of radius $\sqrt{2}$. Also, this design does not contain any points at the vertices of the cubic region created by the upper and lower limits for each variable. This could be advantageous when the points on the corners of the cube represent factor-level combinations that are prohibitively expensive or impossible to test because of physical process constraints.

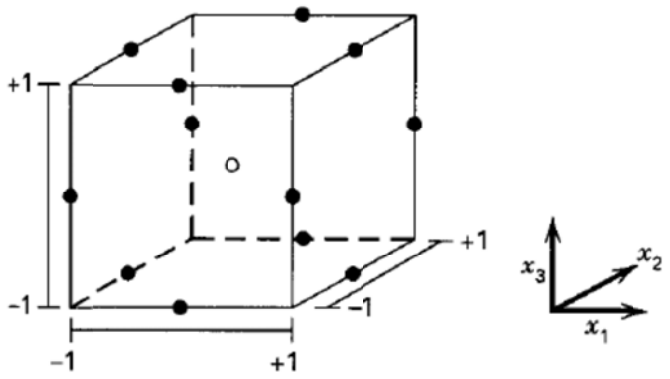

Figure A2 1 Box—Behnken design for three factors

Analysis of Variance (ANOVA)

Experimental factors will influence the response and so will be due to unknown causes or errors, there exists some variability. Every data set is most likely to shown certain variability, but whether such change is due to inputs factors or due to random factors is to be answered by ANOVA. The method tries to carry out the following.

• Decomposes the deviation of the input data in relation to possible sources; the source may be from the main effect, from the interaction, or may be from error.

• Measures the magnitude of variation due to all sources.

• Recognize the main and interactions effects which have significant effects on variation of data.

Sum of Squares (SS)

The distance between any point in a set of data and the mean of the data is the deviation. Sum of Squares is the sum of all such squared deviations. SS_{Total} is the total variation in the data. $SS_{Regression}$ is the portion of the variation explained by the model, while SS_{Error} is the portion not explained by the model and is attributed to error. The calculations are:

$$SS_{Total} = \sum_{i}^{n}\sum_{j}^{r}\left(y_{ij} - \bar{y}\right)^2 \qquad \text{A2-15}$$

$$SS_{Error} = \sum_{i}^{n}\sum_{j}^{r}\left(y_{ij} - \bar{y}_i\right)^2 \qquad \text{A2-16}$$

$$SS_{\text{Re gression}} = SS_{Total} - SS_{Error} \quad \text{A2-17}$$

Where y_{ij}=i^{th} observed response of jth replicate $\hat{y}_i = i^{th}$ fitted response, and $\bar{y}_I$ = mean of all (nXr) observations.

The sum of squares for r set of replicates are calculated and added together to create the pure error sum of squares (SS_{PE}). Sum of square error SS_{Error} is the sum of pure error sum of squares SS_{PE} and sum of squares lack of fit SS_{LOF} .

$$SS_{PE} = \sum_{i}^{n}\left[\sum_{j}^{r}\left(y_{ij} - \bar{y}_i\right)^2\right] \quad \text{A2-18}$$

$$SS_{LOF} = SS_E - SS_{PE} \quad \text{A2-19}$$

Where $\bar{y}_I$ = mean of r replicates of i^{th} observed response.

Degree of Freedom

It depicts the number of independent variables needed to calculate the sum of squares the response data. The degrees of freedom for each component of the model are:

$DF_{Regression}$=t-1

DF_{Error}=n-t

DF_{Total}=n-1

DF_{ABl}=(A-1)(B-1)

DF_{PE}=n-m

where n = number of observations, t = number of terms in the model, a, b = number of levels of factors A and B, respectively. DOF of pure error DF_{PE} is (n – m), where n = number of observations and m = the number of distinct x-values.

Mean Square

In an ANOVA, the term Mean Square refers to an estimate of the population variance based on the variability among a given set of measures. The calculation for the mean square for the model terms is:

$$MS_{Term} = \frac{AdjSS_{Term}}{DF_{Term}} \quad \text{A2-20}$$

F-value: F-value is the measurement of distance between individual distributions. More the F-value, less is the P-value. F is a test to determine whether the interaction and

main effects are significant. The formula for the model terms is:

$$MS_{Term} = \frac{MS_{Term}}{Ms_{Error}} \qquad \text{A2-21}$$

Larger values of F support rejecting the null hypothesis that there is not a significant Effect.

P-value: P-value is used in hypothesis tests helps to decide whether to reject or fail to reject a null hypothesis. The p-value is the probability of obtaining a test statistic that is at least as extreme as the actual calculated value, if the null hypothesis is true.

Model Adequacy Check

The adequacy of the underlying model can be checked from ANOVA as follows: It is always necessary to examine the fitted model to ensure that it provides an adequate approximation to the true system.

R^2: Coefficient of determination; indicates how much variation in the response is explained by the model. The higher the R^2, the better the model fits the data. The formula is:

$$R^2 = 1 - \frac{SS_{Error}}{SS_{Total}} \qquad \text{A2-22}$$

Adjusted R^2 (Adj R^2): Adjusted R^2accounts for the number of factors in the model. The formula is:

$$R^2 = 1 - \frac{MS_{Error}}{SS_{Total} \,/\, DF_{Total}} \qquad \text{A2-23}$$

Lack-of-fit test: This test checks the straight line fit of the model. To calculate the pure error lack-of-fit test:

1. Calculate the pure error mean square:

$$MS_{PE} = \frac{SS_{PE}}{DF_{PE}}$$

2. Calculate the lack-of-fit mean square:

$$MS_{LOF} = \frac{SS_{LOF}}{DF_{SSE} - DF_{PE}} \qquad \text{A2-24}$$

3. Calculate the F-statistic = MS_{LOF} /MS_{PE} and corresponding p-value. Large F-values and small p-values suggest that the model is inadequate.